LINEAR AND NONLINEAR FLUCTUATIONS IN ELECTRON-POSITRON PLASMAS

by

Ian Joseph Lazarus

Submitted in partial fulfilment of the requirements for the Degree of Doctor of Philosophy in the School of Physics of the University of KwaZulu-Natal.

Durban

December 2009.

As the candidate's Supervisor I agree/do not agree to the submission of this thesis.

Supervisor: Prof. S R Pillay

Student: I J Lazarus

Preface

The work described in this thesis was conducted in the School of Physics, University of University of KwaZulu-Natal, from January 2003 to December 2009, under the supervision of Professor Ramesh Bharuthram and Professor Sadha Pillay.

DECLARATION 1

I **Ian Joseph Lazarus** declare that

(i) The research reported in this dissertation, except where indicated, is my original work.

(ii) This dissertation has not been submitted for any degree or examination at any other university.

(iii) This dissertation does not contain other persons' data, pictures, graphs or other information, unless specifically acknowledged as being sourced from other persons.

(iv) This dissertation does not contain other persons' writing, unless specifically acknowledged as being sourced from other researchers. Where other written sources have been quoted, then:

(a) their words have been re-written but the general information attributed to them has been referenced.

(b) where their exact words have been used, their writing has been placed inside quotation marks, and referenced.

(v) Where I have reproduced a publication of which I am an author, co-author or editor, I have indicated in detail which part of the publication was actually written by myself alone and have fully referenced such publications.

(vi) This dissertation does not contain text, graphics or tables copied and pasted from the Internet, unless specifically acknowledged, and the source being detailed in the dissertation and in the References sections.

Signed:

DECLARATION 2

PUBLICATION

- Lazarus I J, Bharuthram R, Hellberg M A 2008 *'Modified Korteweg-de Vries-Zakharov-Kuznetsov solitons in symmetric two-temperature electron-positron plasmas'*, *J. Plasma Physics* **74**, 519.

PUBLICATIONS IN PREPARATION

- Lazarus I J, Bharuthram R, Pillay S R, Singh S V and Lakhina G S *'Linear Waves in an Electron-Positron Plasma'*
- Lazarus I J, Moolla S, Bharuthram R, Singh S V and Lakhina G S *'Nonlinear Electrostatic Solitary Waves in Electron-Positron Plasmas'*
- Lazarus I J, Bharuthram R and Singh S V *'Arbitrary Amplitude Solitary Waves in a Relativistic Electron-Positron Plasma'*
- Singh S V, Lakhina G S, Lazarus I J and Bharuthram R *'Small Amplitude Solitons in Relativistic Electron-Positron Plasmas'*

CONFERENCE PROCEEDINGS

- Lazarus I J, Bharuthram R, Hellberg M A *'Modified Korteweg-de Vries-Zakharov-Kuznetsov solitons in symmetric two-temperature electron-positron plasmas'*, 51^{st} Annual Conference of the South African Institute of Physics, University of the Western Cape, 3-7 July 2006.

- Lazarus I J, Bharuthram R, Hellberg M A *'Modified Korteweg-de Vries-Zakharov-Kuznetsov solitons in symmetric two-temperature electron-positron plasmas'*, 3^{rd} Flemish-South African Workshop on Space Plasma Physics, Ghent (Belgium), 27-29^{th} September 2006.

- Lazarus I J, Bharuthram R, Singh S V and Pillay S R *'Solitary Waves in Relativistic Electron-Positron Plasmas'*, 52^{nd} Annual conference of the South African Institute of Physics, University of the Witwatersrand, 3-6 July 2007.

Signed:

Acknowledgements

To the following persons, I extend my gratitude for your invaluable guidance, assistance and support during my research study.

The Physics Experts

- My principal supervisor, Professor Ramesh Bharuthram, for mentoring my research development with patience and expert guidance.
- My co-supervisor Professor Sadha Pillay for your contributions to the relevant sections of this thesis.
- Professor Manfred Hellberg for your collaborative assistance in one of the topics studied.
- Dr. Suleman Moolla for the numerous discussions and selfless support.
- Professor G.S Lakhina and Dr. S. V Singh from the Indian Institute of Geomagnetism, Mumbai, India, for your collaborative involvement.
- Dr. Shimul Maharaj from the Hermanus Magnetic Observatory for your input.

My Family

- My loving wife Casandra for your support, understanding and patience.
- My darling daughter Erin Maree (my Bhughims) for adding light and laughter to my days.

- To my parents, the late Joseph and Theresa Lazarus. Thank you for always instilling in me the importance of a good education, religious teachings and being a witness to Jesus Christ Our Lord.

- My siblings, Hugh, Marianne, Noelene and Graeme and their families. I may have been the pet but thank you all for your unconditional love, concern and support.

- My family inlaw, Uncle Errol, Aunty Devi, Richard, Sharon and Mama Daya. Thank you for your encouragement and availability to support my family.

- My dear friends, Denise, Julianna, the late Derek, Warren and Jeandré for your concern, love and support.

- My colleagues, especially Deepak Singh, in the Physics Division at the Durban University of Technology.

Funders

- The Durban University of Technology.

- The National Research Foundation.

God my maker and master, I give thanks to you for being my daily reference and guiding me with the strength, the knowledge and the understanding to complete this study.

This thesis is dedicated to my late dad, Joseph (Jos) Lazarus, an acclaimed biology educator, who encouraged me to pursue and complete this study.

ABSTRACT

The behaviour of both small amplitude and arbitrary amplitude nonlinear electrostatic fluctuations are studied in electron-positron plasmas. The propagation characteristics of associated linear modes are also examined for selected plasma models. In the case of the four component, two-temperature, electron-positron plasma, three particular features are investigated. The first investigates existence conditions of the range of possible electrostatic linear waves that can propagate in a two-temperature electron-positron plasma, the study being particularly relevant to both astrophysical situations and laser-induced fusion experiments. The second includes the development and investigation of the mKdV-ZK equation governing the three dimensional propagation of solitary waves in a magnetized plasma. The third application is the investigation of nonlinear electrostatic solitary waves structures, similar to those found in the broadband electrostatic noise observed in various regions of the earth's magnetosphere. The study ends by considering relativistic effects on solitary waves in an electron-positron plasma.

Contents

List of Figures

Chapter 1

Introduction

Electron-positron plasmas play a significant role in the understanding of the early universe (Misner *et al.*, 1980; Weinberg, 1972; Rees, 1983; Gibbons *et al.*, 1983; Peebles, 1993), active galactic nuclei (Miller and Witta, 1987), gamma ray bursts (GRBs) (Piran, 2005), pulsar magnetospheres (Goldreich and Julian, 1969; Michel, 1982) and the solar atmosphere (Tandberg and Emslie, 1988).

In the early stages of the Universe, at an extremely short time after the 'Big Bang', all matter was in a plasma state. This plasma consisted of extremely high-energy photons and charged elementary particles. When these photons combined to produce an electron, another particle with a positive charge (positron) had to be created for the electric charge to be conserved. During these early stages, the Universe was so hot with very energetic photons, that these pairs of particles and antiparticles were created easily via the radia-

tion that was present. Most of the plasma was hence made up of electrons, positrons, neutrinos and antineutrinos, with a lesser abundance of protons and neutrons.

An electron-positron plasma, which is a typical example of a particle-antiparticle system, is also important in understanding extremely dense stars such as white dwarfs and pulsars, which are thought to be rotating neutron stars. The existence of these plasmas in neutron stars and in the pulsar magnetosphere are well documented (Beskin *et al.*, 1983). In the case of pulsars with curvilinear magnetic fields, particles that are accelerated by the longitudinal electric field, and which possess sufficient energy, emit high-energy curvature photons. These photons are radiated along the pulsar magnetic field and produces electron-positron pairs. The positrons travel away from the star, while the electrons becomes accelerated by the electric field in the opposite direction. The emitted curvature photons produced by the accelerated electrons then produce electron-positron pairs near the star's surface. The newly formed positrons then begin to accelerate away from the star and the pair production is repeated, resulting in a chain reaction of gamma-ray quanta being produced and the generation of new electron-positron pairs being formed near the neutron star (Beskin *et al.*, 1993).

Another source of electron-positron plasmas are gamma-ray bursts (GRBs), which are short, random bursts of gamma-ray emissions (photons). They have been detected ubiquitously across the sky since the 1960's (Klebesadel

et al., 1973; Fishman *et al.*, 1986). These GRBs are the most energetic and electromagnetically luminous forms of light that presently occur in our universe. Typically, a GRB event occurs due to the collapse of the core of a rapidly rotating massive star into a black hole, a theory called the collapsar model (Woosley, 1993; MacFadyen and Woosley, 1999; Woosley and Zhang, 2004). Matter from this star around the core first forms a high-density accretion disk which causes the core to become unstable, forming a black hole. Relativistic shock waves are created due to a pair of jets accelerating towards the surface of the star. These shock waves breaks out into space, releasing energy in the form of gamma-rays. Another possibility is that they are caused by the merger of two neutron stars or a neutron star and a black hole (Lattimer and Schramm, 1976). Physically, over time the two objects in the binary system spiral towards one another and eventually merge into a single black hole, resulting in the release of large amounts of energy. Due the process of 'internal shocks', energy from the newly formed black hole together with some material from the collapsed star is ejected outward in several shells. These shells collide, producing gamma-rays. Recent satellite and ground-based observations have led astronomers to believe that gamma-ray bursts can originate near the furthest edges of our observable universe and at cosmological distances (Metzger *et al.*, 1997; Hurley *et al.*, 1998). A GRB lasts typically from about a few seconds to about a few minutes. Its initial burst is followed by a longer lived 'afterglow' of progressively less energetic photons and emission of X-rays, ultraviolet, optical, infrared and radio waves. The characteristics and existence of electron-positron pairs

in gamma-ray bursts can be explained through the relativistic expansion of the electron-positron plasma using 'The Fireball Model' (Piran, 1999). The relativistic fireball model is the release of large amounts of energy within a small volume and in a short time frame from a compact source, resulting in afterglow radiation. This generic 'fireball' model has also been confirmed by afterglow observations (Paradijs, 1998). Due to inverse Compton scattering, large amounts of high energy gamma-ray photons are produced via synchrotron photons. These photons interact with lower energy photons to produce electron-positron pairs due to the relativistic flow of the emitting region. Goodman (1986) and Paczyński (1986) have shown that the sudden release of these high-energy gamma-ray photons into a compact region can lead to a relativistic fireball due to the production of the electron-positron pairs. It must be noted that electron-positron pairs can also be produced via the neutrino-antineutrino process $\nu + \bar{\nu} \rightarrow e^+ + \ e^-$, (Eichler *et al.*, 1989).

Electron-positron plasmas also exist in active galactic nuclei (AGN), like quasars and blazars (which are brighter objects than quasars). These are the compact regions that appear as point-like sources of radiation at the center of galaxies. They are seen at cosmological distances and are believed to be supermassive black holes accreting nearby matter. The production and annihilation of electron-positron pairs play an important role in the gamma-ray region of these active galactic nuclei. Henri *et al.* (1993), pointed out that the gamma-ray emission from AGN can be interpreted as a signature of electron-positron beams. Hartman *et al.* (2001), in their study of the spec-

tral variability of the Blazar, 3C279, also concluded that electron-positron jets are a possible origin of the observed radiation. A feature of AGN is the production of a continuum spectrum of relativistic electrons via synchrotron or inverse Compton radiation. This radiation is generated as high-energy gamma-rays, thereby producing electron-positron pairs. Collisions from the above radiation processes can also produce the electron-positron pairs.

The presence of electron-positron plasmas in the solar atmosphere during solar flares has been confirmed by the observation of the 511 keV gamma-ray electron-positron annihilation line (Share *et al.*, 2004). Solar flares are sudden and rapid releases of enormous amounts of energy when magnetic energy that has built up in the solar atmosphere is suddenly released. They take place in the solar corona and in active regions around sunspots, heating plasmas and accelerating particles like electrons, protons and ions to near the speed of light. From the annihilation of the electron-positron pair, two gamma-ray quanta are emitted. This means that positrons (which need to interact with the electrons) had to be produced in and near the flare region, before the onset of the solar flares. The positrons are produced from the positive pion decay in the solar atmosphere where a large number of these pions are produced from collisions between accelerated particles and background atoms (Sakurai *et al.*, 1988). Szgipel *et al.* (2007), in their study of the energy spectrum in electron-positron plasmas in a Drell-Yan process, indicated that these pairs are produced from proton-proton collisions in the solar atmosphere.

Many of the investigations into electron-positron plasma behaviour have focussed on the relativistic regime. However, it is plausible that non-relativistic astrophysical electron-positron plasmas may exist, given the effect of cooling by cyclotron emission (Bhattacharyya *et al.*, 2003). Electron-positron laboratory plasmas are useful for simulating astrophysical plasmas and studying fundamental electron-positron behaviour. Due to the progress in pure positron production and trapping techniques using Penning traps (Greaves *et al.*, 1994) and the magnetic mirror configuration (Boehmer, 1994), it is now possible to perform experiments on a variety of electron-positron pair plasmas (Greaves and Surko, 1995; Liang *et al.*, 1998; Wilks *et al.*, 2005). Penning traps accumulate large numbers of positrons from radioactive sources which are cooled down to room temperature by collisions with a buffer gas. The magnetic mirror and Paul traps (Paul, 1990) are useful trapping techniques since they are able to trap both signs of charge simultaneously for the formation of electron-positron plasmas.

New generation laser-plasma systems, where lasers can reach much higher intensities, also make it possible to model astrophysical plasma conditions in a laboratory environment (Remington, 2005). These laser-plasma systems have been suggested as sources of high intensity radiation, where particles are accelerated to relativistic velocities. Such systems could therefore form the basis for electron-positron pair creation (Alkofer *et al.*, 2001; Ringwald, 2001; Roberts *et al.*, 2002). Since such plasmas give rise to radio-wave emission, with large energy scales, pulsar atmospheres are likely to host other

quantum electrodynamical effects as well, such as vacuum non-linearities in the form of photon-photon scattering (Marklund and Shukla, 2006).

Electron-positron plasmas belong to the family of pair-plasmas (Oohara *et al.*, 2005; Kourakis *et al.*, 2006). Pair-plasmas are characterized as fully ionized gases with particles of equal and opposite charge and having equal mass. The equality in masses means that only one frequency scale exists and hence due to the symmetry, the analysis is simplified. The equal charge to mass ratio for the oppositely charged species allows for different physical phenomena than in conventional electron-ion plasmas. Another example of a pair-plasma is a fullerene plasma. Recently, laboratory experiments have been carried out on fullerene pair-plasmas (Oohara *et al.*, 2005). Fullerenes are large molecules that are composed entirely of carbon, the most common one being C_{60} (known as 'buckyballs'). Fullerenes can be used as candidates for the ion source to produce pair-ion plasmas since the interaction between electrons and fullerenes can easily result in positively or negatively charged ions. Hence fullerene-ion plasmas can be used to study various pair-plasma phenomena as they can mimic electron-positron plasma behaviour. Fullerene plasmas have the advantage of a longer lifetime in comparison to electron-positron plasmas due to pair annihilation in the latter.

With regard to fluctuation phenomena, linear and nonlinear waves in electron-positron plasmas have attracted considerable interest. The understanding of these wave fluctuations which arise from plasma instabilities are important in

space and astrophysical environments. Although space plasma systems are assumed to be in stable equilibrium, evidence has shown that these systems are often unstable (e.g solar flames and auroras). Instabilities that occur in plasma systems are generally classified into two groups, viz, configurational instability (macroinstability) and velocity space instability (microinstablity) and involves the growth of electrostatic and electromagnetic waves. These plasma instabilities are caused by perturbations and possess free energy. Due to its instability, the plasma then discharges its free energy in order to reach thermodynamic equilibrium, and in doing so gives rise to a growing wave mode. Investigations conducted have focussed on modulational instabilities and wave localization (Stenflo *et al.*, 1985), envelope solitons (Mofiz *et al.*, 1985), multidimensional effects (Yu *et al.*, 1986), soliton existence and electrostatic nonlinear potential structures (Pillay and Bharuthram, 1992; Verheest *et al.*, 1996). Zank and Greaves (1995) examined linear and nonlinear modes using the two-fluid model with a single temperature in an electron-positron plasma. More recently Shukla N and Shukla P K (2007) showed that the dispersion relation in a strongly magnetized nonuniform electron-positron plasma admits a new purely growing instability for generating electrostatic fluctuations.

Within the context detailed above, an outline of the studies undertaken in this thesis is presented. Chapter 2 investigates the linear behaviour of electrostatic modes in a two-temperature, four component electron-positron plasma in the presence of a magnetic field using the fluid model. We note that our

model is an extension of Zank and Greaves (1995) single temperature two component electron-positron model. The effect of plasma parameters such as the propagation angle, cool to hot temperature and density ratios and the magnetic field strength on the waves are also examined. The fluid theory results are compared with the solutions of the kinetic dispersion relation.

A theoretical study on solitary waves in a two-temperature electron-positron plasma propagating at oblique angles to an ambient magnetic field is presented in chapter 3. In particular we explore the nonlinear behaviour of these solitary waves as a function of plasma parameters such as propagation angle, soliton velocity, cool to hot density ratios and cool to hot temperature ratios.

In chapter 4, an approach used by several authors (Reddy *et al.*, 2002; Moolla *et al.*, 2007) is used to explore the generation of electrostatic solitary waves characterized by their spiky bipolar structures in an electron-positron plasma. In this regard the work of Reddy *et al.* (2002) and Moolla *et al.* (2007) are important for the broadband electrostatic noise (BEN) observed in the earth's magnetosphere. Satellite measurements using high-time resolution equipment aboard spacecrafts S3-3 (Mozer *et al.*, 1977), Viking (Andre *et al.*, 1987), Geotail (Matsumoto *et al.*, 1994), Polar (Franz *et al.*, 1998), and Fast (Ergun *et al.*, 1998) have indicated the presence of BEN in the auroral magnetosphere at altitudes between 3000 km to 8000 km and beyond. Observations from these satellites show the detection of electrostatic solitary waves (ESWs), which are characterized by their spiky bipolar pulses. In this

study, the nonlinear propagation of these electrostatic waves in three different magnetized four component electron-positron plasma models is examined. In particular, the spiky nature of the electrostatic potential structures and the effects of the propagation angle, cold and hot drift velocities, cool to hot density and temperature ratios and Mach number on the ESWs are examined. Our findings could serve as a pointer for observing such ESWs in electron-positron plasmas.

Whilst the primary focus in the previous chapters has been largely around the behaviour of the four component electron-positron plasma in non-relativistic plasmas, chapter 5 examines solitary wave structures in a two component unmagnetized plasma having relativistic electrons and positrons. The existence conditions of soliton structures are studied using both small amplitude and arbitrary amplitude theory. The nonlinear solitary wave structures are examined as a function of the plasma parameters.

Finally, chapter 6 presents an overall summary of the results and conclusions are drawn.

Chapter 2

Linear Electrostatic Waves in Electron-Positron Plasmas

2.1 Literature Review

Theoretical studies on linear waves in electron-positron plasmas have largely focussed on the relativistic regime relevant to astrophysical contexts, for example, (Yu *et al.*, 1984; Lakhina and Verheest, 1997; Lontano *et al.*, 2001; Fonseca *et al.*, 2003; Matsukiyo *et al.*, 2003; Machabeli *et al.*, 2005; Nishikawa *et al.*, 2006). This is largely due to the fact that the production of these electron-positron pairs require high-energy processes which are more common in astrophysical conditions such as those which exist in the environments of pulsars, active galactic nuclei, gamma-ray bursts, solar flares and black holes. The majority of the reported studies have been primarily limited to single temperature electron-positron plasmas.

More recent studies have now focussed on the nonrelativitic regime, given the cooling by cyclotron emission of the electron-positron plasmas (Bhattacharyya *et al.*, 2003). Stewart and Laing (1992) researched the dispersion properties of linear waves in equal-mass plasmas and found that due to the special symmetry of such plasmas, well known phenomena such as Faraday rotation and whistler wave modes disappear. Iwamoto (1993) studied the collective modes in nonrelativistic electron-positron plasmas using the kinetic approach. The author found that the dispersion relations for the longitudinal modes in the electron-positron plasma for both unmagnetized and magnetized electron-positron plasmas were similar to the modes in one-component electron or electron-ion plasmas. The transverse modes for the unmagnetized case were also found to be similar. However, the transverse modes in the presence of a magnetic field were found to be different from those in electron-ion plasmas. In an electron-ion plasma the extraordinary wave is known to have two cutoff frequencies. However the mode is found to have just one in an electron-positron plasma. Moreover, the hybrid resonances present in the former are not found in an electron-positron plasma.

A study of wave propagation in electron-positron plasmas highlights the role played by the equal mass of the electrons and positrons. For example, the low frequency ion acoustic wave, a feature of electron-ion plasmas due to the significantly different masses of the electrons and ions, has no counterpart in an electron-positron plasma. The phenomena of Faraday rotation is absent in such plasmas (Zank and Greaves, 1995). In one such study, using the two-

fluid model with a single temperature, Zank and Greaves (1995) investigated linear and nonlinear longitudinal and transverse electrostatic and electromagnetic waves in a nonrelativistic electron-positron plasma in the absence and presence of an external magnetic field. They found that several of the modes present in electron-ion plasmas also existed in electron-positron plasmas, but in a modified form, due to the symmetry derived from the common mass of the electrons and positrons. On the other hand, it is noted that the whistler and lower hybrid modes are nonexistent in electron-positron plasmas. A study of the two-stream instability yielded similar results to the electron-ion case, except that the growth rate was now substantially larger due to the equality in masses of the electrons and positrons. In their nonlinear analysis, solitary waves are found to exist in the subsonic regime, and the width of the soliton was found to be proportional to the wave speed, while in electron-ion plasmas, the amplitude is related to the wave speed. Esfandyari-Kalejahi *et al.* (2006) studied oblique modulation of electrostatic modes and envelope excitations in pair-ion and electron-positron plasmas. Their investigation showed the existence of two distinct linear electrostatic modes, namely an acoustic lower mode and a Langmuir-type, optic-type upper mode. They also showed that the conditions for modulational depend on the angle between the propagation and modulation direction, the carrier wave number and the positron to electron temperature ratio. Shukla N and Shukla P K (2007) in their strongly magnetized nonuniform electron-positron plasma derived a new dispersion relation for low-frequency electrostatic waves. They showed that the dispersion relation admits a new purely growing instability

in the presence of the equilibrium density and magnetic field inhomogeneties.

In this chapter, we extend the work of Zank and Greaves (1995) in a magnetized two-component electron-positron plasma to a magnetized four component, two-temperature plasma, having hot electrons and positrons and cool electrons and positrons. Both fluid and kinetic approaches are used to investigate the linear waves of the system.

2.2 Fluid Theory Approach

2.2.1 Basic Theory

The model considered is a homogeneous magnetized, four component electron-positron plasma, consisting of cool electrons and cool positrons with equal temperatures and equilibrium densities denoted by T_c and n_{0c}, respectively, and hot electrons and hot positrons with equal temperatures and equilibrium densities denoted by T_h and n_{0h}, respectively. Here, temperatures are expressed in energy units and wave propagation is taken in the x-direction at an angle θ to the ambient magnetic field $\mathbf{B_0}$, which is assumed to be in the x-z plane.

The hot isothermal species are assumed to have a Boltzmann distribution.

Their densities are, respectively

$$n_{eh} = n_{0h} \exp\left(\frac{e\phi}{T_h}\right) \tag{2.1}$$

and

$$n_{ph} = n_{0h} \exp\left(\frac{-e\phi}{T_h}\right) , \tag{2.2}$$

where n_{eh} (n_{ph}) is the density of the hot electrons (positrons) and ϕ is the electrostatic potential.

The dynamics of the cooler species are governed by the fluid equations, namely,
the continuity equations,

$$\frac{\partial n_{jc}}{\partial t} + \nabla.(n_{jc}\mathbf{v}_{jc}) = 0 , \tag{2.3}$$

the equations of motion,

$$\frac{\partial \mathbf{v}_{jc}}{\partial t} + \mathbf{v}_{jc}.\nabla\mathbf{v}_{jc} = -\epsilon_j\frac{e}{m}\nabla\phi + \epsilon_j\frac{e}{m}(\mathbf{v}_{jc}\times\mathbf{B}_0) - \frac{\gamma T_c}{n_{jc}m}\nabla n_{jc} , \tag{2.4}$$

where the adiabatic equation of state is used, ϵ_j=+1(-1) for positrons (electrons), $j = e(p)$ for the electrons (positrons) and γ is the ratio of the specific heats.

The system is closed by the Poisson equation

$$\varepsilon_0 \frac{\partial^2 \phi}{\partial x^2} = -e(n_{pc} - n_{ec} + n_{ph} - n_{eh}) \ . \tag{2.5}$$

In the above equations, n_j and $\mathbf{v}_j$ are the densities and fluid velocities respectively, of the j^{th} species.

It must be noted that the chosen plasma model is an extension of that used by Zank and Greaves (1995). Here the two additional hot species having Boltzmann density distributions have been included.

To determine the linear dispersion relation, equations (2.3) – (2.5) are linearized. For perturbations varying as $\exp(i(kx - \omega t))$, $\partial/\partial t$ is replaced with $-i\omega$ and $\partial/\partial x$ with ik. Hence linearization of the continuity equation (2.3) and dropping the '1' for the first order perturbed quantities yields,

$$-i\omega n_{ec} + ikn_{0c}v_{ecx} = 0 \ , \tag{2.6}$$

for which

$$n_{ec} = \frac{kn_{0c}v_{ecx}}{\omega} \ . \tag{2.7}$$

Linearizing the equations of motion, one obtains for the velocity components for the electrons,

$$v_{ecx} = \frac{3kv_{tc}^2}{\omega}\left(\frac{n_{ec}}{n_{0c}}\right) - \frac{ek\phi}{m\omega} - i\frac{\Omega}{\omega}v_{ecy}\sin\theta \ , \tag{2.8}$$

$$v_{ecy} = -i\frac{\Omega}{\omega}\left(v_{ecz}\cos\theta - v_{ecx}\sin\theta\right) , \tag{2.9}$$

$$v_{ecz} = i\frac{\Omega}{\omega}v_{ecy}\cos\theta , \tag{2.10}$$

where, $v_{tc} = (T_c/m)^{1/2}$ is the thermal velocity of the cool species and $\Omega_j = \epsilon_j eB_o/m = \epsilon_j\Omega$ is the gyrofrequency of the electrons and positrons with $\Omega = eB_o/m$.

Upon elimination of v_{ecz} from equations (2.9) and (2.10),

$$v_{ecy} = i\frac{\omega\Omega v_{ecx}\sin\theta}{\omega^2 - \Omega^2\cos^2\theta} . \tag{2.11}$$

Substituting for v_{ecy} from equation (2.11) into equation (2.8) and using equation (2.7), v_{ecx} becomes,

$$v_{ecx} = -\frac{\omega^2(\omega^2 - \Omega^2\cos^2\theta)\left(\frac{ek\phi}{m\omega}\right)}{\omega^4 - \omega^2(3k^2v_{tc}^2 + \Omega^2) + 3k^2v_{tc}^2\Omega^2\cos^2\theta} . \tag{2.12}$$

Substituting the above into equation (2.7), the perturbed density of the electrons is determined to be,

$$n_{ec} = -\left(\frac{n_{0c}ek^2\phi}{m}\right)\left(\frac{\omega^2 - \Omega^2\cos^2\theta}{\omega^4 - \omega^2(3k^2v_{tc}^2 + \Omega^2) + 3k^2v_{tc}^2\Omega^2\cos^2\theta}\right) . \tag{2.13}$$

Similarly, and by symmetry, the perturbed density of the positrons becomes,

$$n_{pc} = \left(\frac{n_{0c} e k^2 \phi}{m}\right)\left(\frac{\omega^2 - \Omega^2 \cos^2\theta}{\omega^4 - \omega^2(3k^2 v_{tc}^2 + \Omega^2) + 3k^2 v_{tc}^2 \Omega^2 \cos^2\theta}\right) . \tag{2.14}$$

From equations (2.1) and (2.2), the perturbed densities for the hot species are given by,

$$n_{eh} = n_{oh}\frac{e\phi}{T_h} \tag{2.15}$$

and

$$n_{ph} = -n_{oh}\frac{e\phi}{T_h} . \tag{2.16}$$

Substituting equations (2.13), (2.14), (2.15) and (2.16), into Poisson's equation (2.5), the general dispersion relation for the two temperature electron-positron plasma is found to be

$$\omega^4 - \omega^2(3k^2 v_{tc}^2 + \Omega^2) + 3k^2 v_{tc}^2 \Omega^2 \cos^2\theta = \frac{k^2 v_{ea}^2(\omega^2 - \Omega^2\cos^2\theta)}{1 + \frac{1}{2}k^2\lambda_{Dh}^2} , \tag{2.17}$$

which may be rewritten as,

$$\omega^4 - \omega^2\left(\Omega^2 + 3k^2 v_{tc}^2 + \frac{k^2 v_{ea}^2}{1 + \frac{1}{2}k^2\lambda_{Dh}^2}\right) + \Omega^2\cos^2\theta\left(3k^2 v_{tc}^2 + \frac{k^2 v_{ea}^2}{1 + \frac{1}{2}k^2\lambda_{Dh}^2}\right) = 0 , \tag{2.18}$$

where $v_{ea} = (n_{0c}/n_{0h})^{1/2} v_{th}$ is the acoustic speed of the electron-positron plasma, analogous in form to the electron acoustic speed in an electron-ion

plasma (Gary and Tokar, 1985). Here, $v_{th} = (T_h/m)^{1/2}$ is the thermal velocity of the hot species and $\lambda_{Dh} = (\varepsilon_0 T_h/n_{0h}e^2)^{1/2}$ is the Debye length of the hot species.

For a single species electron-positron plasma, with temperature T_c, equation (2.18) reduces to,

$$\omega^4 - \omega^2(\Omega^2 + 3k^2 v_{tc}^2) + 3k^2 v_{tc}^2 \Omega^2 \cos^2\theta = 0 \ . \tag{2.19}$$

This is identical in form to the dispersion relation (equation (13)) of Zank and Greaves (1995) for electrostatic modes in their single temperature electron-positron model.

Rearranging the general dispersion relation equation (2.18) we have

$$\omega^2(\omega^2 - \Omega^2) - 3k^2 v_{tc}^2(\omega^2 - \Omega^2\cos^2\theta) - \frac{k^2\ v_{ea}^2}{1 + \frac{1}{2}k^2\lambda_{Dh}^2}(\omega^2 - \Omega^2\cos^2\theta) = 0 \tag{2.20}$$

For wavefrequencies much lower than the gyrofrequency, satisfying $\omega \ll \Omega\cos\theta$, one obtains for the associated acoustic mode,

$$\omega^2 = \frac{k^2 v_{ea}^2 \cos^2\theta}{1 + \frac{1}{2}k^2\lambda_{Dh}^2} + 3k^2 v_{tc}^2 \cos^2\theta \ . \tag{2.21}$$

In the short wavelength limit ($k^2\lambda_{Dh}^2 \gg 1$), the dispersion relation equation (2.20) reduces to,

$$\omega^4 - \omega^2(\Omega^2 + 3k^2 v_{tc}^2 + 2\omega_{pc}^2) + 3k^2 v_{tc}^2 \Omega^2 \cos^2\theta + 2\omega_{pc}^2\Omega^2\cos^2\theta = 0 \tag{2.22}$$

The above equation may be rewritten as

$$\omega^4 - \omega^2(3k^2v_{tc}^2 + \omega_{UH}^2) + (3k^2v_{tc}^2 + 2\omega_{pc}^2)\Omega^2\cos^2\theta = 0 \ , \tag{2.23}$$

where

$$\omega_{UH}^2 = \Omega^2 + 2\omega_{pc}^2 \tag{2.24}$$

is the upper hybrid frequency associated with the cooler species (Zank and Greaves, 1995), with $\omega_{pc} = (n_{oc}e^2/\varepsilon_0 m)^{1/2}$ as the plasma frequency of the cooler species.

Solving equation (2.23), which is a quadratic equation in ω^2, in the limit $(3k^2v_{tc}^2 + \omega_{UH}^2)^2 \gg 4(3k^2v_{tc}^2\Omega^2\cos^2\theta + 2\omega_{pc}^2\Omega^2\cos^2\theta)$, one obtains for the positive square root,

$$\omega_+^2 = (3k^2v_{tc}^2 + \omega_{UH}^2) - \frac{(3k^2v_{tc}^2 + 2\omega_{pc}^2)\Omega^2\cos^2\theta}{3k^2v_{tc}^2 + \omega_{UH}^2} \ , \tag{2.25}$$

which is the dispersion relation for the upper hybrid mode.

Taking the negative square root of equation (2.23) yields

$$\omega_-^2 = \frac{(3k^2v_{tc}^2 + 2\omega_{pc}^2)\Omega^2\cos^2\theta}{3k^2v_{tc}^2 + \omega_{UH}^2} \ , \tag{2.26}$$

It is noted that for perpendicular propagation ($\cos\theta = 0$), $\omega_+^2 = \omega_{UH}^2 + 3k^2v_{tc}^2$ and $\omega_-^2 = 0$, the results of which are discussed in the next section.

In order to gain physical insight into the solution space of the dispersion relation, the two extreme limits of equation (2.20) will now be considered, viz. pure perpendicular and pure parallel propagations.

Case I: Pure Perpendicular Propagation

Considering the pure perpendicular ($\theta = 90^o$) limit, the general dispersion relation (2.20), reduces to:

$$\omega^4 - \omega^2 \left(\Omega^2 + 3k^2 v_{tc}^2 + \frac{k^2 v_{ea}^2}{1 + \frac{1}{2} k^2 \lambda_{Dh}^2} \right) = 0 \ . \tag{2.27}$$

Hence the normal mode frequencies are,

$$\omega = 0 \ , \tag{2.28}$$

which is a non-propagating mode and is consistent with that found by Zank and Greaves (1995, Table 1), and

$$\omega^2 = \Omega^2 + 3k^2 v_{tc}^2 + \frac{k^2 v_{ea}^2}{1 + \frac{1}{2} k^2 \lambda_{Dh}^2} \ . \tag{2.29}$$

Taking the short wavelength limit ($k^2 \lambda_{Dh}^2 \gg 1$) of the above relationship, one obtains,

$$\omega^2 = \Omega^2 + 3k^2 v_{tc}^2 + \frac{2 v_{ea}^2}{\lambda_{Dh}^2} \ . \tag{2.30}$$

Now:

$$\begin{aligned} \frac{v_{ea}^2}{\lambda_{Dh}^2} &= \frac{n_{0c}}{n_{0h}}\frac{T_h}{m} \times \frac{n_{0h}e^2}{\epsilon_0 T_h} \\ &= \frac{n_{0c}e^2}{\varepsilon_0 m} \\ &= \omega_{pc}^2 \ . \end{aligned} \tag{2.31}$$

Thus for the perpendicular case, in the short wavelength limit, the dispersion relation for the linear wave is,

$$\omega^2 = \Omega^2 + 3k^2 v_{tc}^2 + 2\omega_{pc}^2 \ , \tag{2.32}$$

which may be written in the form,

$$\omega^2 = \omega_{UH}^2 + 3k^2 v_{tc}^2 \ . \tag{2.33}$$

It is noted that this result can also be derived from (2.23) and is consistent with the findings of Zank and Greaves (1995, Table 1) for their upper hybrid mode. Further, it is noted that it is the cooler species that contribute to the dispersion of the waves. The short wavelength ($k^2\lambda_{Dh}^2 \gg 1$) approximation in arriving at (2.33) eliminates the contribution of the hot species.

In the (opposite) long wavelength limit ($k^2\lambda_{Dh}^2 \ll 1$) of the dispersion relation for perpendicular propagation, equation (2.29) reduces to

$$\omega^2 = \Omega^2 + k^2 3v_{tc}^2 + k^2 v_{ea}^2 \ . \tag{2.34}$$

This is the cyclotron mode for the electron-positron plasma with contributions from both the thermal motion of the adiabatic cooler species and the

acoustic motion due to the two species of different temperatures. It is noted that equation (2.34) differs from the cyclotron mode found by Zank and Greaves (1995, Table 1). Due to the introduction of the second species having a different temperature in our model, there is now a contribution to wave dispersion of the acoustic motion. To try and understand the physical implications, the above expression for the dispersion relation can be written as,

$$\omega^2 = \Omega^2 + k^2 v_{ea}^2 \left(1 + 3\frac{T_c}{T_h}\frac{n_{0h}}{n_{0c}}\right) \ . \tag{2.35}$$

For plasma parameters such that $T_c/T_h \ll n_{0c}/n_{0h}$ ($\Rightarrow 3\frac{T_c}{T_h}\frac{n_{0h}}{n_{0c}} \ll 1$), $\omega^2 = \Omega^2 + k^2 v_{ea}^2$ and the contribution to wave dispersion of the acoustic motion of the two temperature electron-positron plasma dominates over the contribution of the thermal motion of the cooler species.

Case II: Pure Parallel Propagation

Considering the limit of parallel propagation ($\theta = 0^o$), the general dispersion relation (2.20) reduces to,

$$\omega^4 - \omega^2 \left(\Omega^2 + 3k^2 v_{tc}^2 + \frac{k^2 v_{ea}^2}{1 + \frac{1}{2}k^2\lambda_{Dh}^2}\right) + \Omega^2 \left(3k^2 v_{tc}^2 + \frac{k^2 v_{ea}^2}{1 + \frac{1}{2}k^2\lambda_{Dh}^2}\right) = 0 \ , \tag{2.36}$$

from which it can be shown without any approximations that

$$\omega^2 = \frac{1}{2}\left[\Omega^2 + 3k^2v_{tc}^2 + \frac{k^2v_{ea}^2}{1+\frac{1}{2}k^2\lambda_{Dh}^2} \pm \left(\Omega^2 - 3k^2v_{tc}^2 - \frac{k^2v_{ea}^2}{1+\frac{1}{2}k^2\lambda_{Dh}^2}\right)\right] . \tag{2.37}$$

There exists two possible solutions. Taking the positive sign of the relevant term in equation (2.37) as the first option yields,

$$\omega_+^2 = \Omega^2, \tag{2.38}$$

which is a constant frequency, non-propagating cyclotron oscillation also found by Zank and Greaves (1995, Table 1).

Taking the negative sign of the term in equation (2.37) yields the normal mode frequency

$$\omega_-^2 = 3k^2v_{tc}^2 + \frac{k^2v_{ea}^2}{1+\frac{1}{2}k^2\lambda_{Dh}^2} , \tag{2.39}$$

which may be written for $k^2\lambda_{Dh}^2 \ll 1$ as

$$\omega_-^2 = k^2v_{ea}^2\left(1 + 3\frac{T_c}{T_h}\frac{n_{0h}}{n_{0c}}\right) , \tag{2.40}$$

which is identified fundamentally, as the acoustic mode, with a correction term to its phase velocity due to the thermal motion of the cooler species. We note that equation (2.39) differs from the acoustic mode found by Zank

and Greaves (1995, Table 1), where once again there is a contribution of the acoustic motion due to the inclusion of a second species having a different temperature in our model .

In the limit $k^2\lambda_{Dh}^2 \gg 1$, one obtains

$$\omega_-^2 = 3k^2 v_{tc}^2 + 2\omega_{pc}^2 \ , \tag{2.41}$$

which is the well known expression for the Langmuir wave in an electron-positron plasma (Zank and Greaves, 1995, Figure 1 and Table 1).

Equating equations (2.38) and (2.41) in the limit $k^2\lambda_{Dh}^2 \gg 1$, the critical k value for which the two modes may couple is determined to be,

$$(k\lambda_D)_{crit} = \left(\frac{T_h}{3T_c}\right)^{1/2} \left(\frac{\Omega^2}{\omega_p^2} - 2\frac{n_{0c}}{n_0}\right)^{1/2} \ , \tag{2.42}$$

which provides a feel for the parameter range within which we may explore in more detail the coupling between the lower (ω_-) and upper (ω_+) modes. Such a coupling can produce instabilities, for example, the parametric instability (Chen, 1984, p309).

We now proceed to solving the dispersion relation (2.18) fully.

2.2.2 Numerical Results

Normalizing the fluid speeds by the thermal velocity $v_{th} = (T_h/m)^{1/2}$, the particle density by the total equilibrium plasma density $n_0 = n_{0c} + n_{0h}$, the temperatures by T_h, the spatial length by $\lambda_D = (\varepsilon_0 T_h/n_0 e^2)^{1/2}$, and the time by $\omega_p^{-1} = (n_0 e^2/\varepsilon_0 m)^{-1/2}$ in equation (2.18), yields the normalized general dispersion relation,

$$\omega'^4 - \omega'^2\left(\frac{1}{R^2} + 3k'^2\frac{T_c}{T_h} + \frac{k'^2 n'_{0c}}{n'_{0h} + \frac{1}{2}k'^2}\right) + \frac{\cos^2\theta}{R^2}\left(3k'^2\frac{T_c}{T_h} + \frac{k'^2 n'_{0c}}{n'_{0h} + \frac{1}{2}k'^2}\right) = 0 \ , \tag{2.43}$$

where $\omega' = \omega/\omega_p$, $k' = k\lambda_D$, $n'_{0h} = n_{0h}/n_0$, $n'_{0c} = n_{0c}/n_0$ and $R = \omega_p/\Omega$ is a measure of the plasma densities and the strength of the magnetic field. Numerical solutions of the normalized dispersion relation (2.43) are presented in figures (2.1)-(2.9) for a fixed value of $R = 0.333$. The value of $R = 0.333$ is chosen for easy comparison with Zank and Greaves (1995). For completeness, we explore larger values of R in figures $2.10 - 2.12$. The analysis focusses on the effects of the density and temperature ratios of the hot and cool electrons and positrons, as this is novel in the sense that such a plasma has not been considered before.

The investigation begins by focussing on waves that propagate perpendicular to the magnetic field. Figures 2.1 and 2.2 shows the normalized real frequency as a function of the normalized wavenumber for perpendicular propagation for various density and temperature ratios, respectively. Since

$k\lambda_{Dh} = k\lambda_D(n_0/n_{0h})^{1/2}$, for $n_{0c}/n_{0h} = 1/9$ we have $n_0/n_{0h} = 10/9$ and hence $k\lambda_{Dh} \approx k\lambda_D$. Hence in the short wavelength limit, i.e. large $k\lambda_D$ (and therefore large $k\lambda_{Dh}$) the modes in figure 2.1 correspond to the dispersion relation (2.33), satisfying the linear relation $\omega = \sqrt{3}kv_{tc}$ for $k^2v_{tc}^2 \gg \omega_{UH}^2$. In this regard, since the temperatures are normalized relative to T_h, in the normalized form one has $\omega/\omega_p = \sqrt{3}k\lambda_D(T_c/T_h)^{1/2}$, which for $T_c/T_h = 0.01$ could explain why for large $k' = k\lambda_D$, the linear portions of the curves in figure 2.1 have a smaller slope than the corresponding curves for the single temperature two component plasma in figure 2(a) of Zank and Greaves (1995). In the opposite limit, $k^2\lambda_{Dh}^2$ (and $k^2\lambda_D^2$) $\ll 1$ the relevant dispersion relation is (2.34), from which when $k = 0$, $\omega = \Omega$, which in normalized form corresponds to $\omega/\omega_p = \Omega/\omega_p = 1/R$. For the fixed parameter of $R = 0.333$ this implies that $\omega = 1/R = 3.0$. This explains why the curves in figures 2.1 and 2.2 start off with $\omega/\omega_p = 3.0$ at $k\lambda_D = 0$. For small values of $k\lambda_D$ and with a fixed value of $T_c/T_h = 0.01$ there is a sharp rise in the frequency curves in figure 2.1. This is a feature of our four component two temperature electron-positron model since the term involving n_{oc} disappears for $n_{oc} = 0$. Consequently this behaviour is not present in the results of Zank and Greaves (1995) in their two component model (see their figure 2(a)). In figure 2.2 the (solid) curve corresponding to $T_c/T_h = 0$ is introduced. The fact that the slope of this curve is different to those corresponding to $T_c/T_h \neq 0$ can be understood from the dispersion relation (2.33) valid for $k^2\lambda_D^2 \gg 1$. Setting $T_c = 0$ yields $\omega = \omega_{UH}$. This explains the frequency of the (solid) curve in figure 2.2 reaching a constant value for large values of $k\lambda_D$ at the normalized

value of $\omega_{UH} = \sqrt{9.2} = 3.03$. The increase in the slope of the frequency curves with increasing values of T_c/T_h for larger values of $k\lambda_D$ is in keeping with the dispersion relation $\omega/\omega_p = \sqrt{3}k\lambda_D(T_c/T_h)^{1/2}$. It must be emphasized that the behaviour of the curves in figure 2.2 is a characteristic of a four component two temperature electron-positron plasma and has not been reported in the literature before.

Figures 2.3 and 2.4 shows the normalized real frequency as a function of the normalized wavenumber for parallel propagation for various density and temperature ratios respectively. The figures show the constant frequency ($\omega = \Omega$) non-propagating oscillation and the acoustic mode (equation (2.39)), for which both the density ratios and temperature ratios contribute to the wave dynamics. For $k^2\lambda_{Dh}^2$ (and $k^2\lambda_D^2$) $\ll 1$, the curves satisfy the dispersion relation (2.40), which in normalized form corresponds to $\omega/\omega_p = k\lambda_D(3T_c/T_h + n_{oc}/n_{oh})^{1/2}$. For a fixed T_c/T_h value, it is noted that the slope of the curves in figure 2.3 increases sharply when n_{oc}/n_{oh} is increased. This is once again a feature of the four component two temperature electron-positron plasma and is due to the contribution of the second species. In the opposite limit, i.e $k^2\lambda_{Dh}^2$ (and $k^2\lambda_D^2$) $\gg 1$, the curves satisfy the dispersion relation (2.41). It is noted that the behaviour of the curves for both large and small values of $k\lambda_D$ as well as the variations of n_{oc}/n_{oh} and T_c/T_h are similar to those for perpendicular propagation. As before, the patterns can be understood by an examination of the relevant dispersion relations.

Having looked at perpendicular and parallel propagation, we now look at oblique propagation. Figure 2.5 is a plot of the normalized real frequency as a function of the normalized wavenumber, showing the acoustic and cyclotron branches, for a range of propagation angles. It is noted that the slope of the curves are much smaller as compared to the single temperature electron-positron model of Zank and Greaves (1995) for the reasons outlined above. It is seen that the acoustic mode vanishes for $\theta = 90^o$. This can be understood from equation (2.21) where $\omega = 0$ for $\cos\theta = 0$.

Figure 2.6 (a)-(c) shows the normalized real frequency as a function of the normalized wavenumber for increasing cool to hot density ratios. As pointed out earlier, as the mode initially begins (small values of $k\lambda_D$), the steepness of the slope of the curves increase when the density ratio is increased. It is also observed that for a fixed T_c/T_h value, the $k\lambda_D$ value at which decoupling of the acoustic and cyclotron modes takes place decreases when the density n_{oc} of the cool species increases, which can be deduced from equation (2.42). Curves (a)-(c) in figure 2.7 shows increasing cool to hot temperature ratios for the normalized real frequency. The critical $k\lambda_D$ value at which the decoupling takes place is calculated from equation (2.42). As an illustration, for the parameters corresponding to figures 2.7 (a)-(c), equation (2.42) yields $(k\lambda_D)_{crit} = 17.1, 5.4$ and 2.3, respectively, which agrees very well with the values in the curves, noting that $(k\lambda_D)_{crit}$ (and therefore $k\lambda_{Dh}$) is not much larger than 1 for figure 2.7 (c). It is noted that for a fixed n_{oc}/n_{oh} density ratio value, the $k\lambda_D$ value for which the two modes decouple decreases when

T_c/T_h is increased. This effect can be seen in equation (2.42). Also as T_c/T_h is increased, the acoustic mode reaches a constant frequency at a smaller $k\lambda_D$ value.

Curves (a)-(c) in figures 2.8 and 2.9 show the normalized real frequency for various propagation angles for different density and temperature ratios respectively. As you move to larger propagation angles, the separation between the modes become more distinct, with the acoustic mode eventually disappearing as you go to perpendicular propagation, as shown in figures 2.1 and 2.2, and which can be deduced from equation (2.21).

Up to now the value of $R = \omega_p/\Omega$ has been kept fixed at 0.333 for direct comparison with the two species, single temperature model of Zank and Greaves (1995). Next we examine the effect of varying R in figures 2.10$-$2.12. It is seen that as the magnetic field strength becomes weaker ($R = \omega_p/\Omega$ increasing), the frequency gap between the acoustic and cyclotron modes decreases for small wavenumbers, with the frequency for the acoustic mode becoming a constant at a smaller wavenumber.

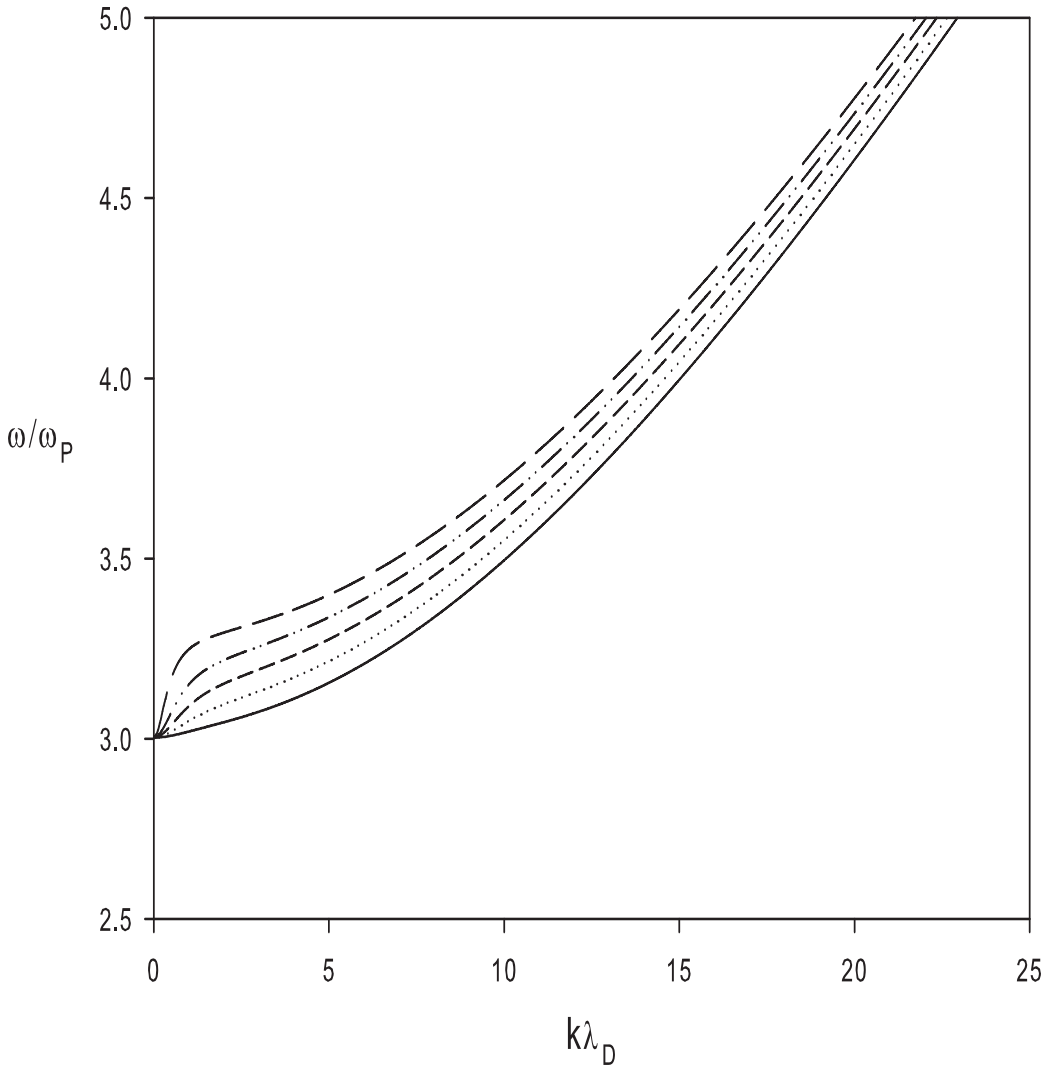

Figure 2.1: Normalized real frequency as a function of the normalized wavenumber. The fixed parameters are $R = 0.333$, $T_c/T_h = 0.01$ and $\theta = 90^o$. The curves represent different values of the equilibrium density ratio $n_{0c}/n_{0h} = 0.11$ (solid), 0.43 (dotted), 1.0 (broken), 2.33 (dashddot) and 9.0 (longbroken).

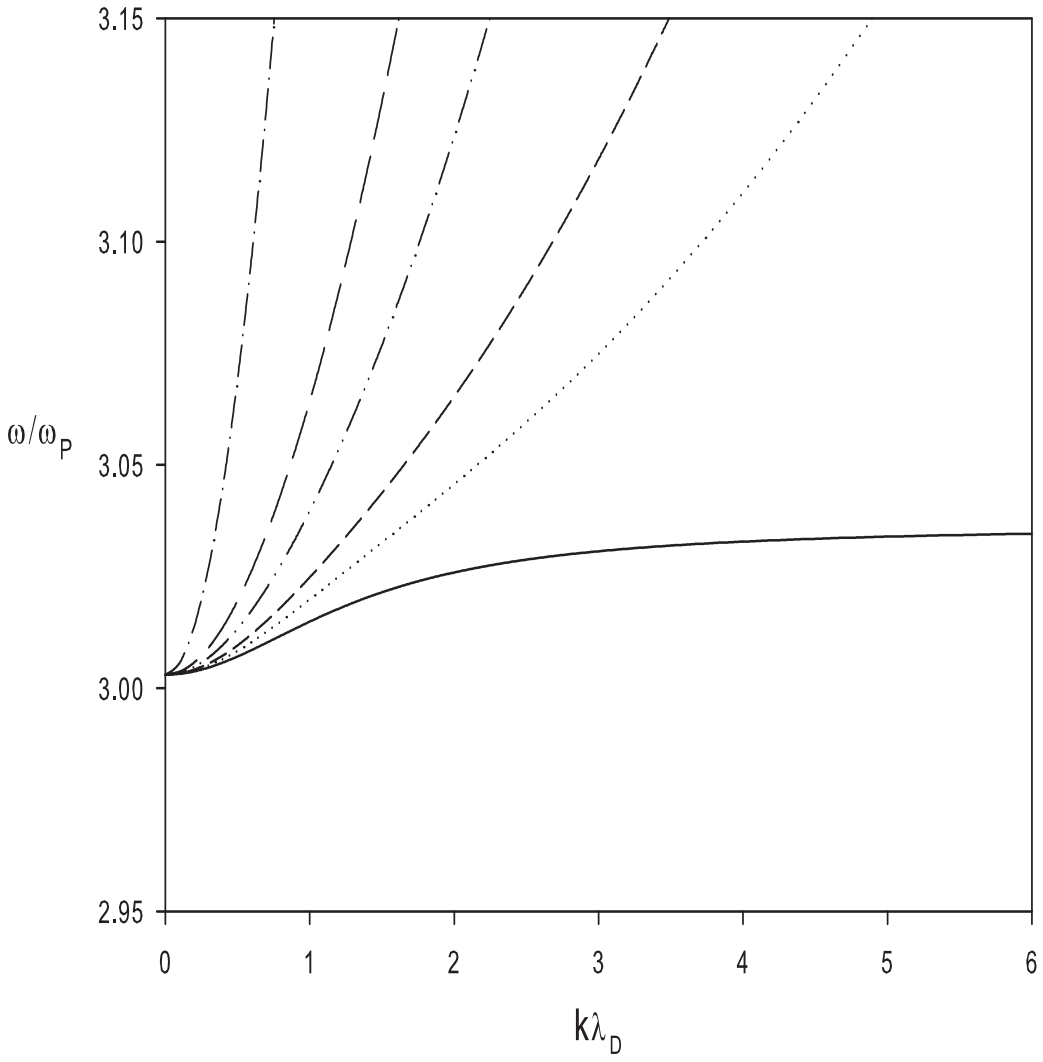

Figure 2.2: Normalized real frequency as a function of the normalized wavenumber. The fixed plasma parameters are $R = 0.333$, $n_{0c}/n_{0h} = 0.11$ and $\theta = 90^o$. The curves represent different values of the temperature ratio $T_c/T_h = 0.0$ (solid), 0.01 (dotted), 0.02 (broken), 0.05 (dashddot), 0.1 (longbroken) and 0.5 (dashdot).

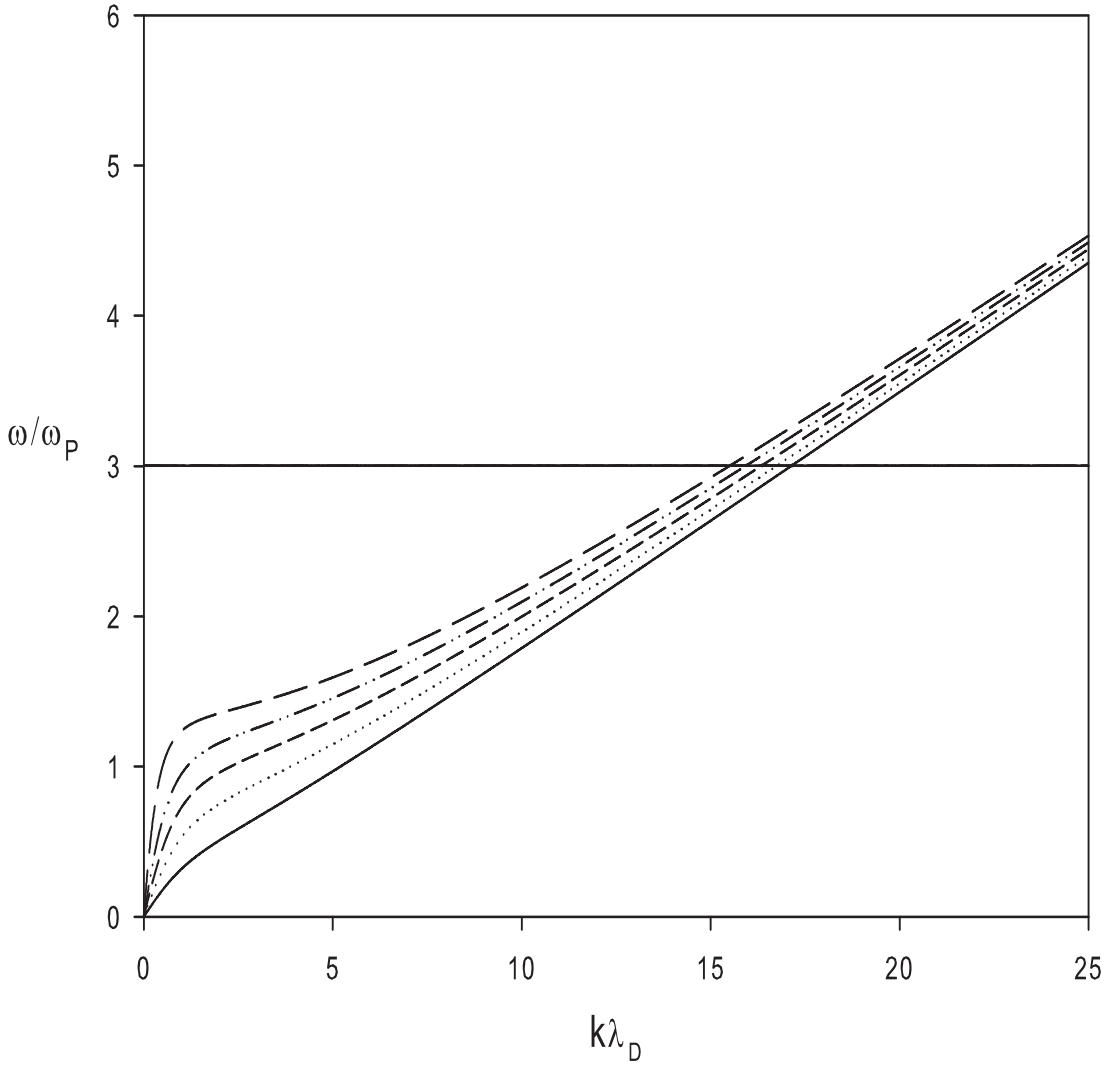

Figure 2.3: Normalized real frequency as a function of the normalized wavenumber. The fixed parameters are $R = 0.333$, $T_c/T_h = 0.01$ and $\theta = 0^o$. The curves represent different values of the equilibrium density ratio $n_{0c}/n_{0h} = 0.11$ (solid), 0.43 (dotted), 1.0 (broken), 2.33 (dashddot) and 9.0 (longbroken).

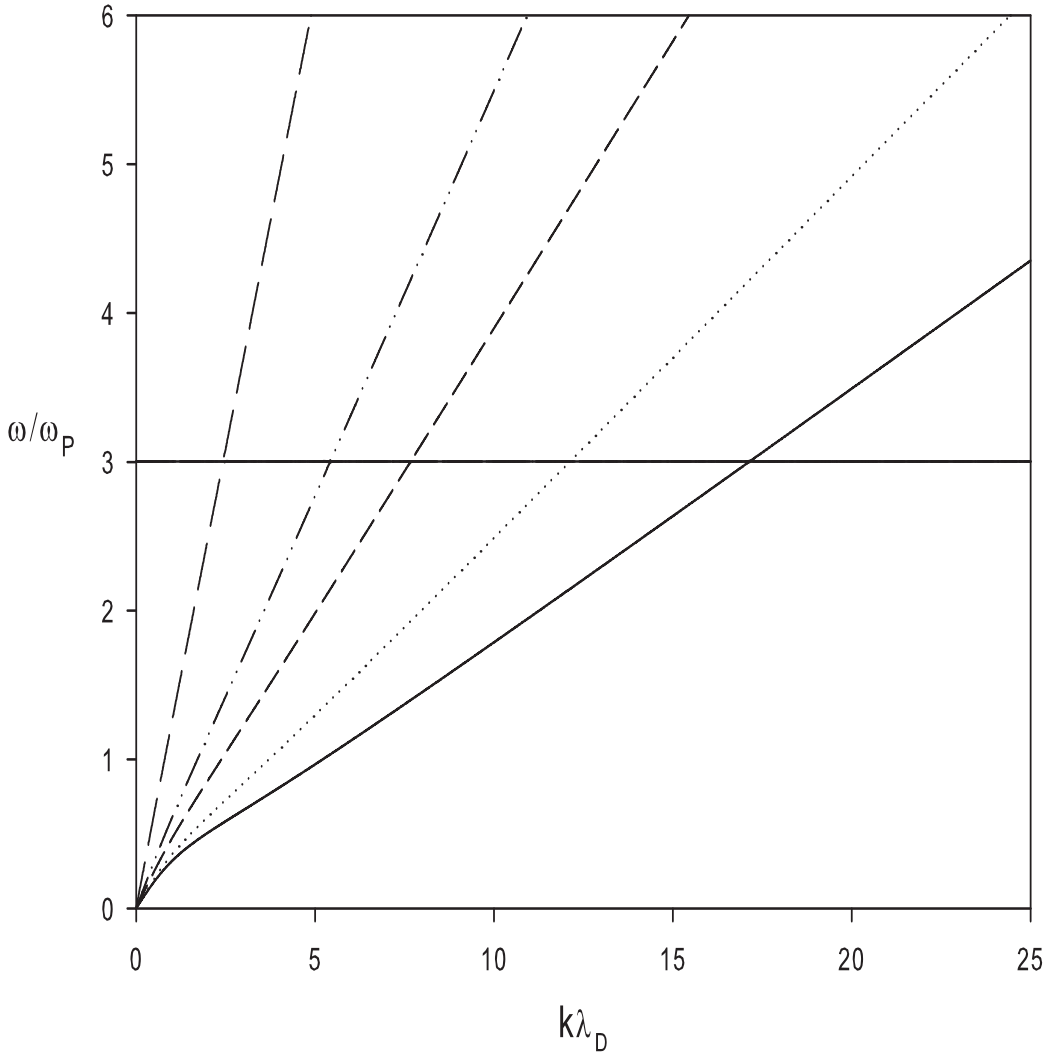

Figure 2.4: Normalized real frequency as a function of the normalized wavenumber. The fixed plasma parameters are $R = 0.333$, $n_{0c}/n_{0h} = 0.11$ and $\theta = 0^o$. The curves represent different values of the temperature ratio $T_c/T_h = 0.01$ (solid), 0.02 (dotted), 0.05 (broken), 0.1 (dashddot) and 0.5 (longbroken).

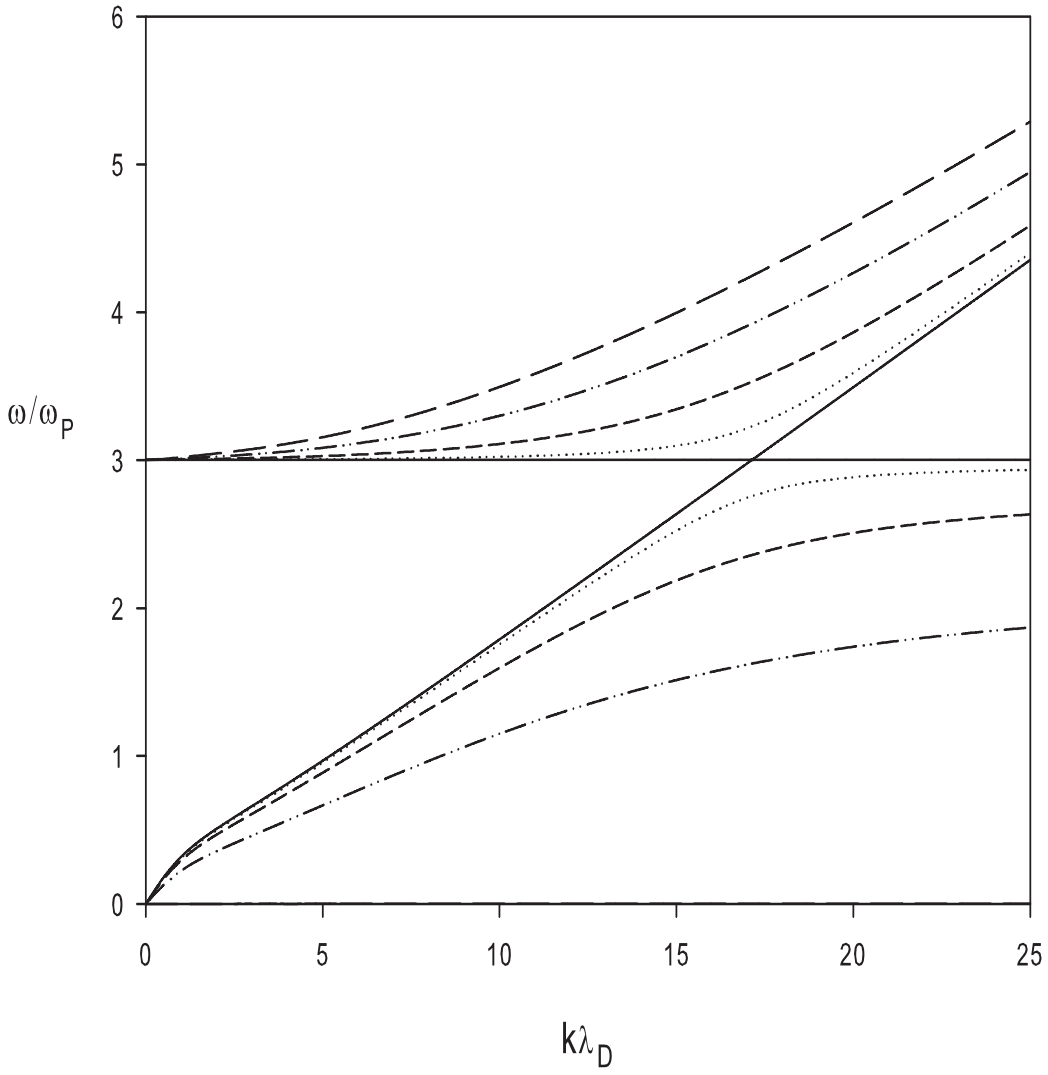

Figure 2.5: Normalized real frequency as a function of the normalized wavenumber showing the acoustic and cyclotron branches for various angles of propagation $\theta = 0^o$ (solid), 9^o (dotted), 22.5^o (broken), 45^o (dashddot) and 90^o (longbroken). The fixed plasma parameters are $R = 0.333$, $T_c/T_h = 0.01$ and $n_{0c}/n_{0h} = 0.11$.

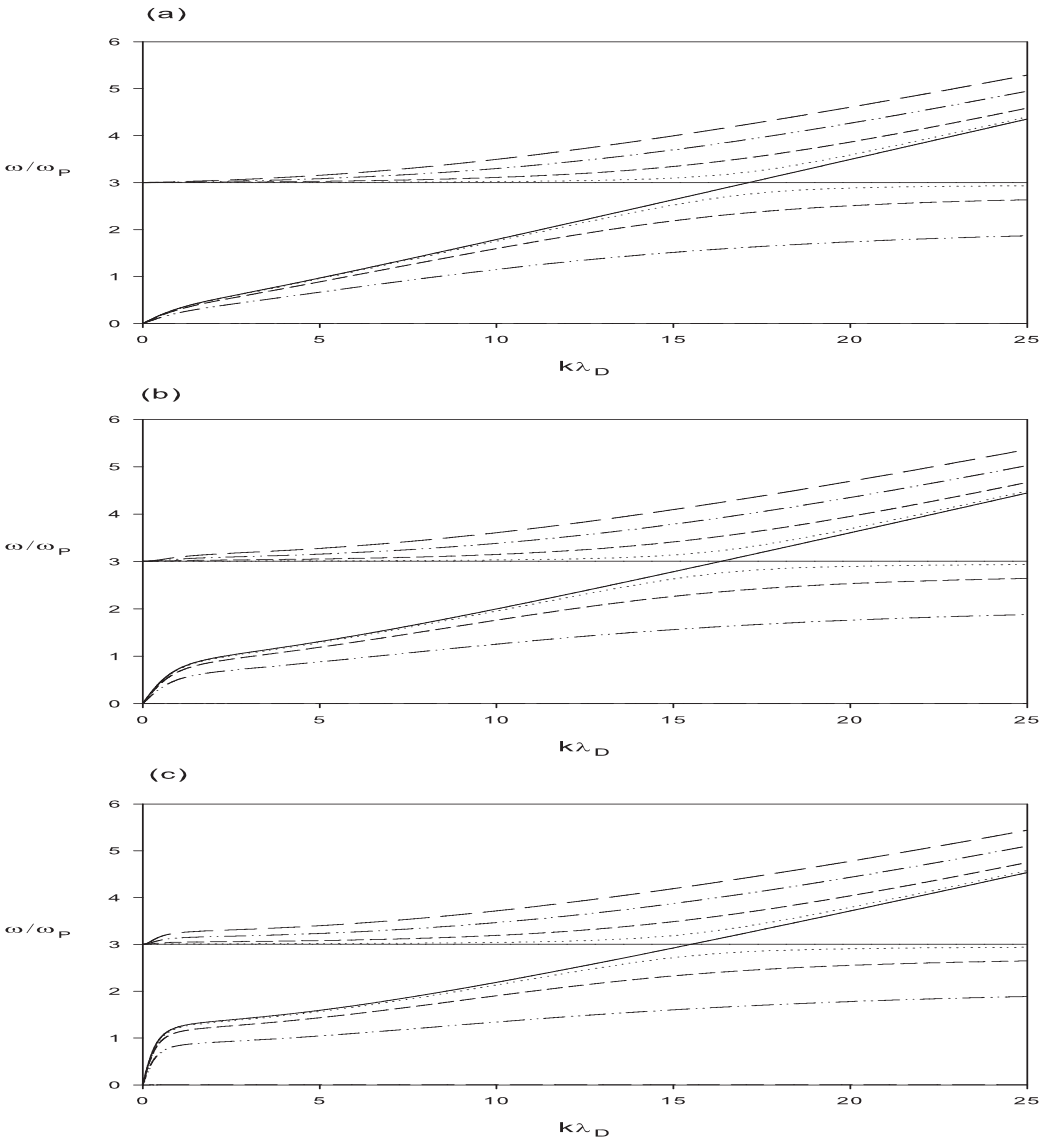

Figure 2.6: Normalized real frequency as a function of the normalized wavenumber for various density ratios n_{0c}/n_{0h} = (a) 0.11, (b) 1.0 and (c) 9.0. The fixed parameters are $R = 0.333$ and $T_c/T_h = 0.01$. The curves represent different values of the propagation angles $\theta = 0^o$ (solid), 9^o (dotted), 22.5^o (broken), 45^o (dashddot) and 90^o (longbroken).

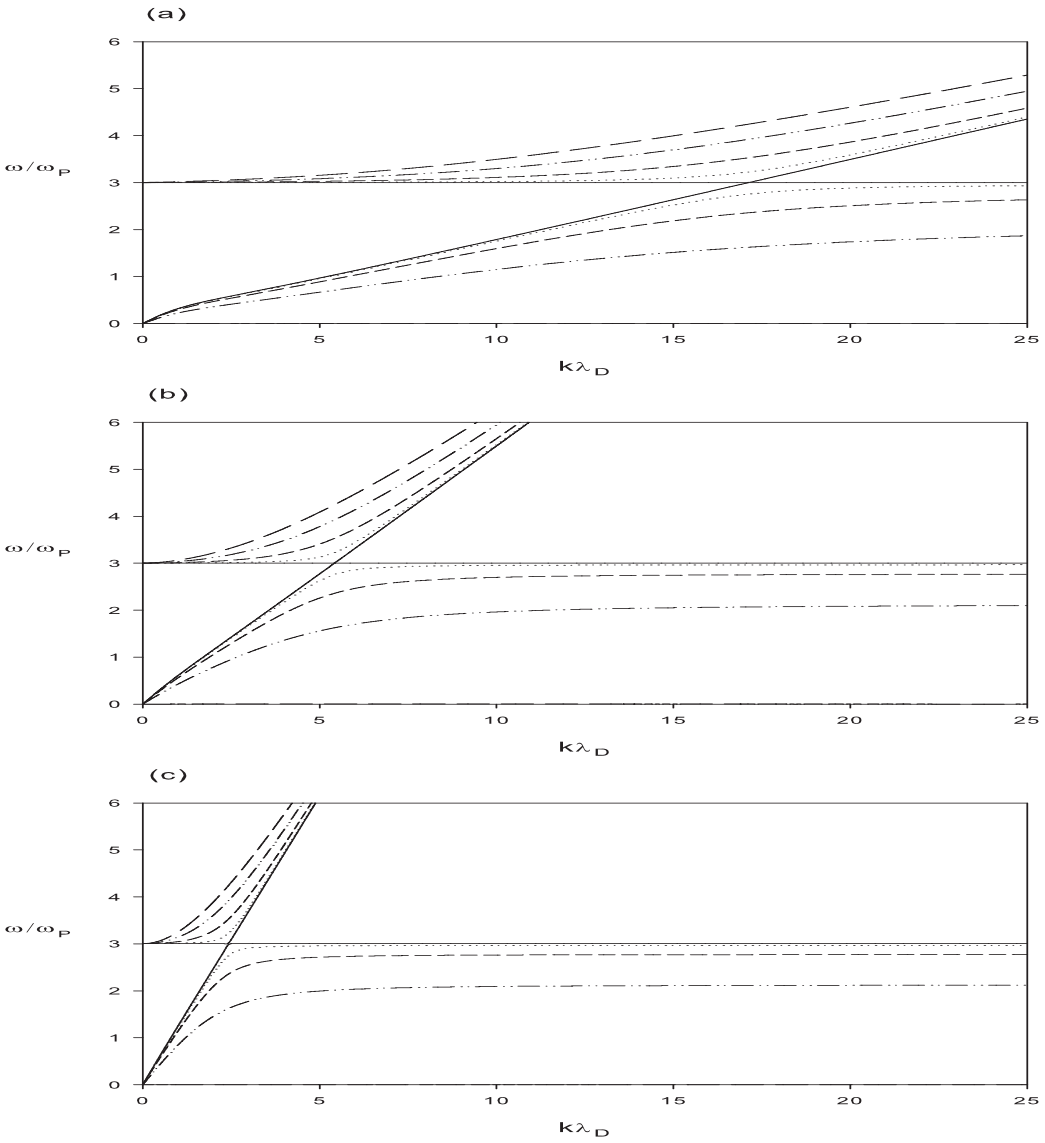

Figure 2.7: Normalized real frequency as a function of the normalized wavenumber for various temperature ratios T_c/T_h = (a) 0.01, (b) 0.1 and (c) 0.5. The fixed parameters are $R = 0.333$ and $n_{0c}/n_{0h} = 0.11$. The curves represent different values of the propagation angles $\theta = 0^o$ (solid), 9^o (dotted), 22.5^o (broken), 45^o (dashddot) and 90^o (longbroken).

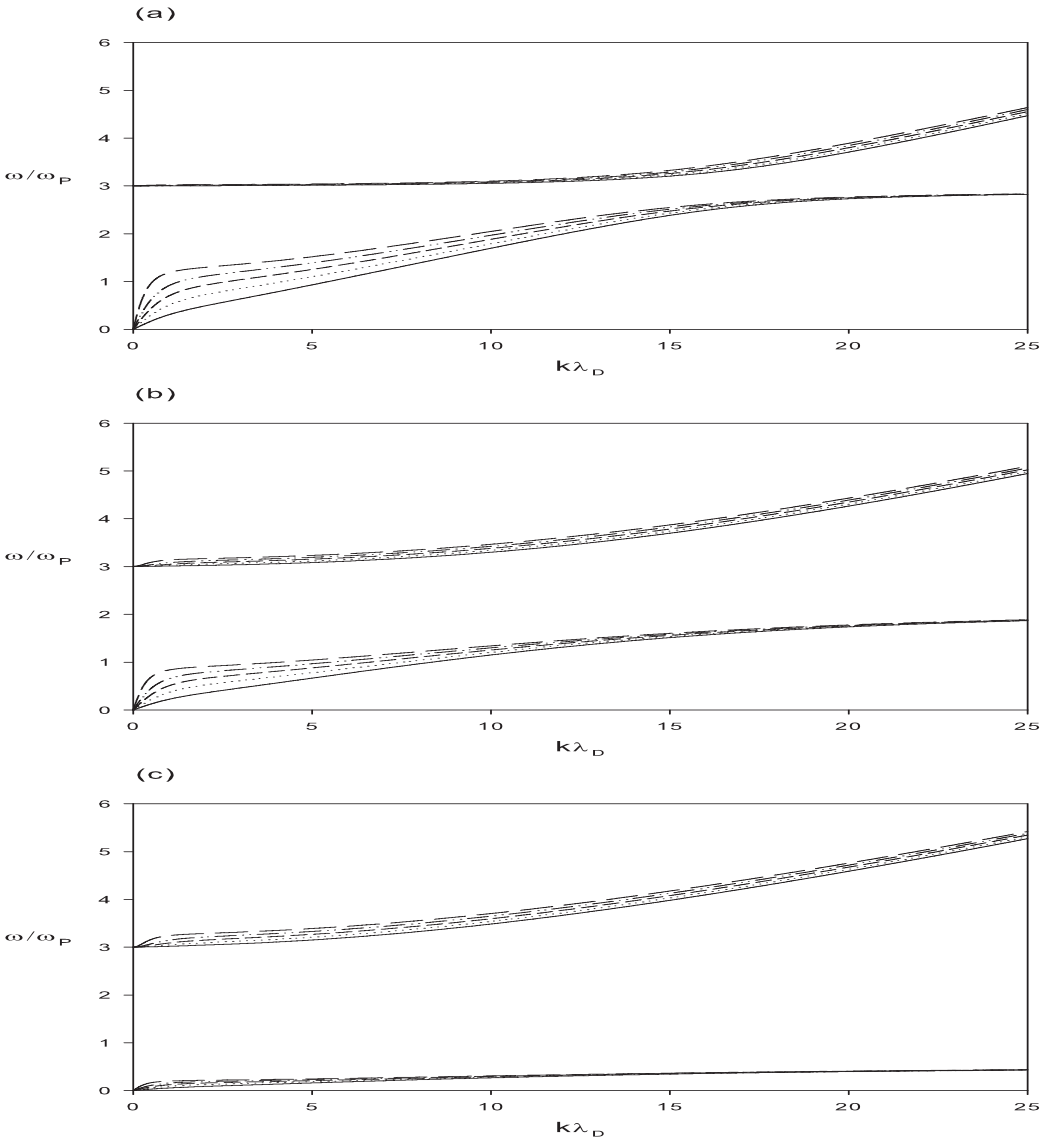

Figure 2.8: Normalized real frequency as a function of the normalized wavenumber for various propagation angles θ = (a) 15^o, (b) 45^o and (c) 80^o. The fixed parameters are $R = 0.333$ and $T_c/T_h = 0.01$. The curves represent different values of the equilibrium density ratio $n_{0c}/n_{0h} = 0.11$ (solid), 0.43 (dotted), 1.0 (broken), 2.33 (dashddot) and 9.0 (longbroken).

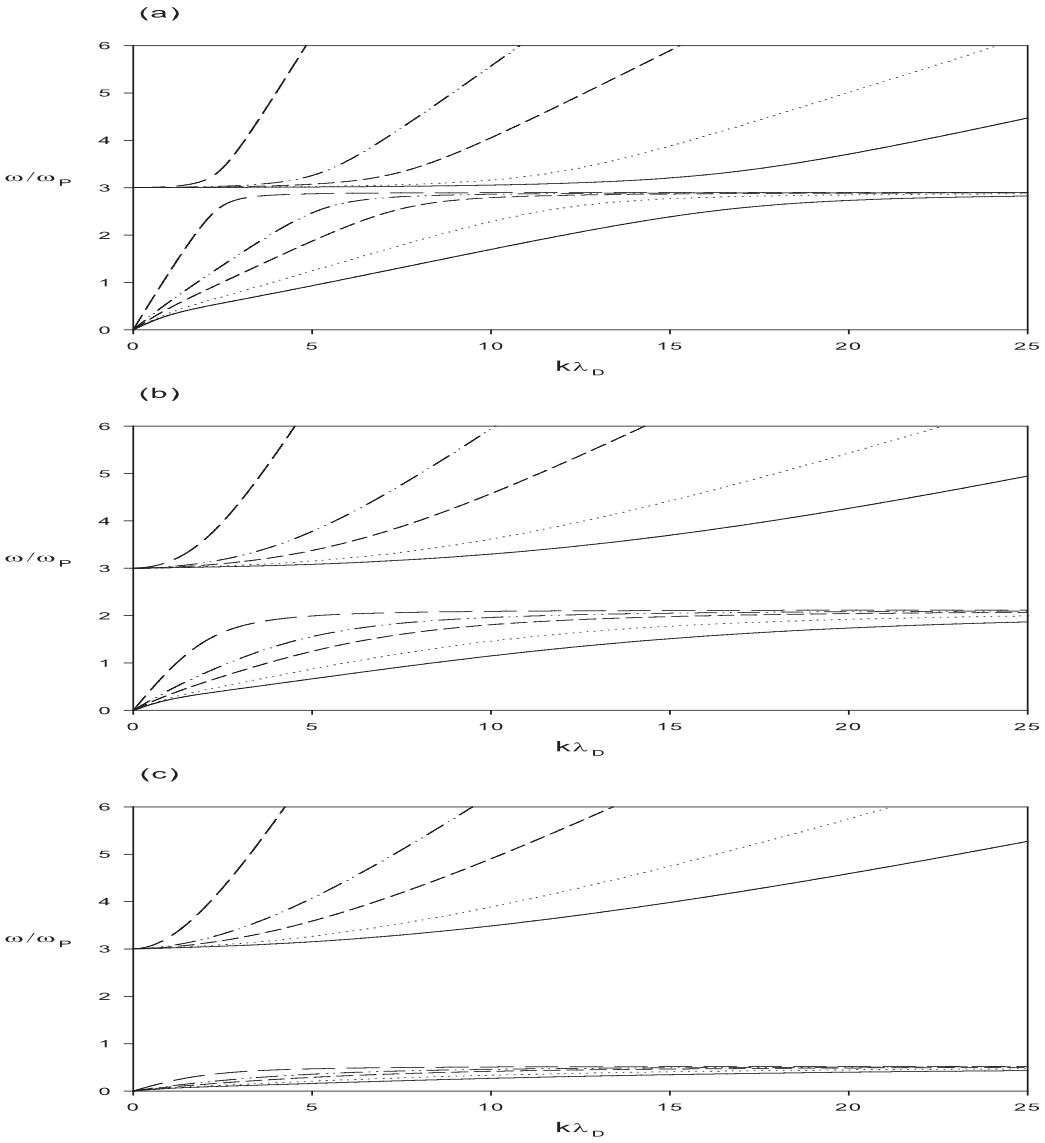

Figure 2.9: Normalized real frequency as a function of the normalized wavenumber for various propagation angles θ = (a) 15^o, (b) 45^o and (c) 80^o. The fixed parameters are $R = 0.333$ and $n_{0c}/n_{0h} = 0.11$. The curves represent different values of the temperature ratio $T_c/T_h = 0.01$ (solid), 0.02 (dotted), 0.05 (broken), 0.1 (dashddot) and 0.5 (longbroken).

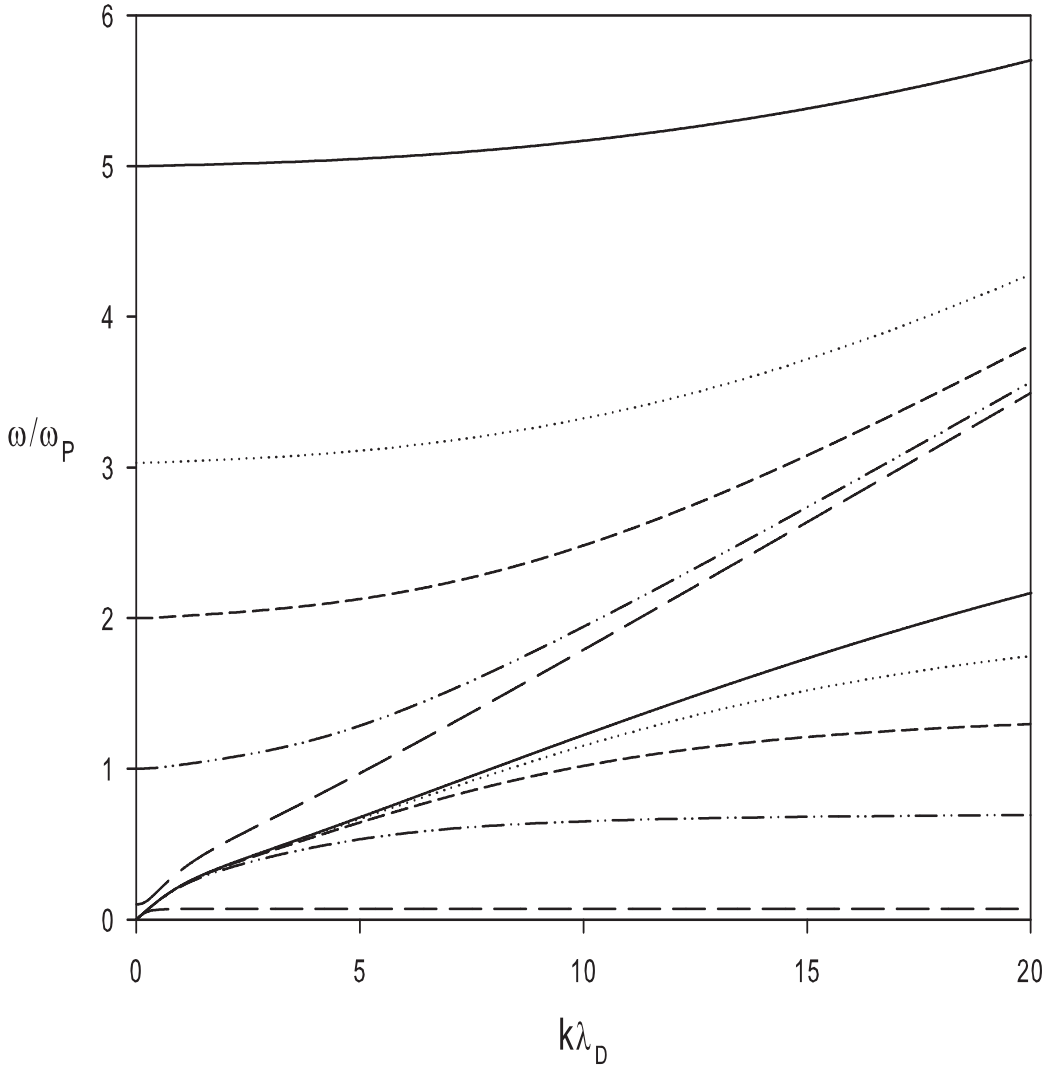

Figure 2.10: Normalized real frequency as a function of the normalized wavenumber. The fixed plasma parameters are $T_c/T_h = 0.01$, $n_{0c}/n_{0h} = 0.11$ and $\theta = 45^o$. The curves represent values for $R = 0.2$ (solid), 0.33 (dotted), 0.5 (broken), 1.0 (dashddot) and 10.0 (longbroken).

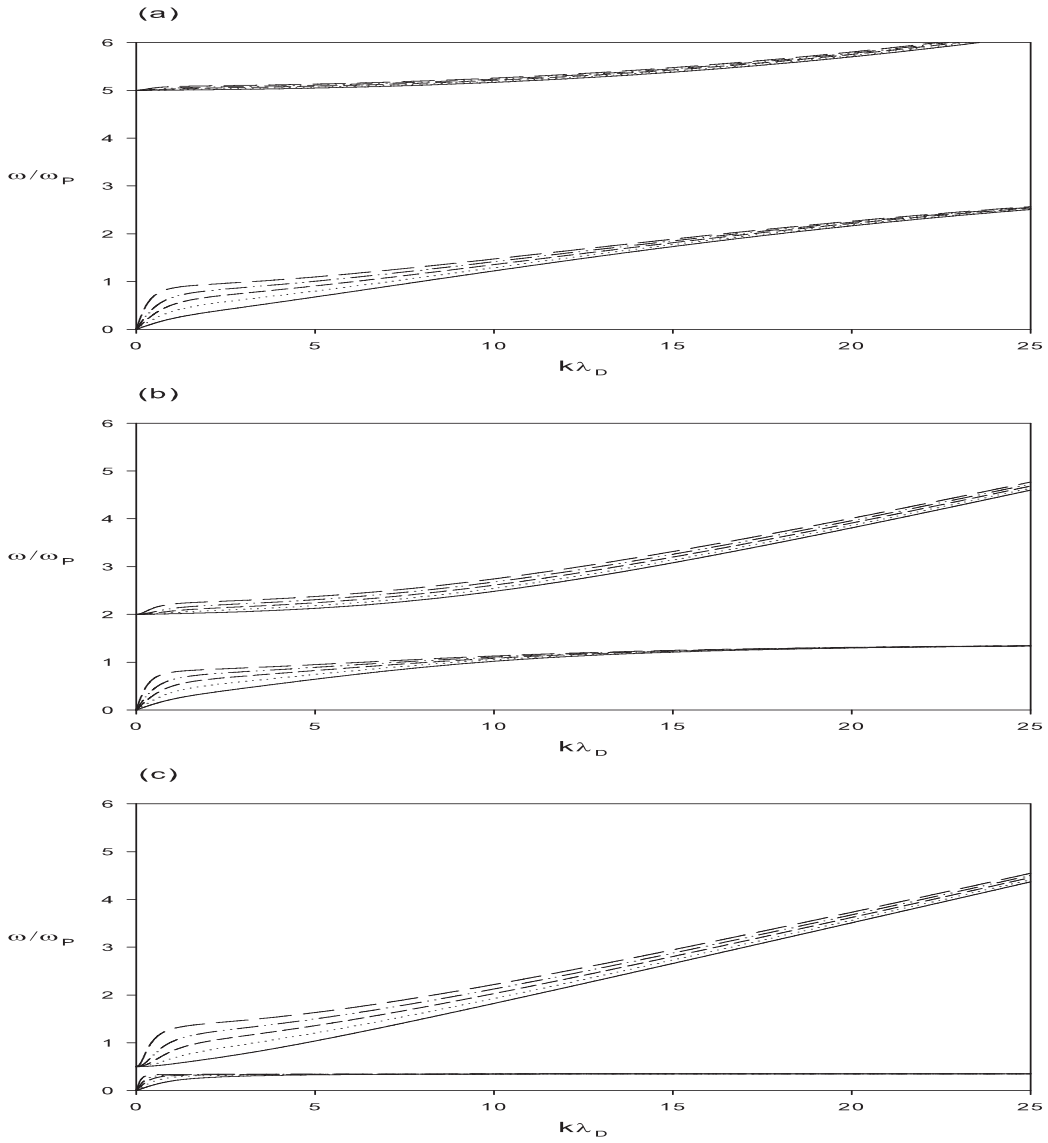

Figure 2.11: Normalized real frequency as a function of the normalized wavenumber for various values of R = (a) 0.2, (b) 0.5 and (c) 2.0. The fixed parameters are $\theta = 45^o$ and $T_c/T_h = 0.01$. The curves represent different values of the equilibrium density ratio $n_{0c}/n_{0h} = 0.11$ (solid), 0.43 (dotted), 1.0 (broken), 2.33 (dashddot) and 9.0 (longbroken).

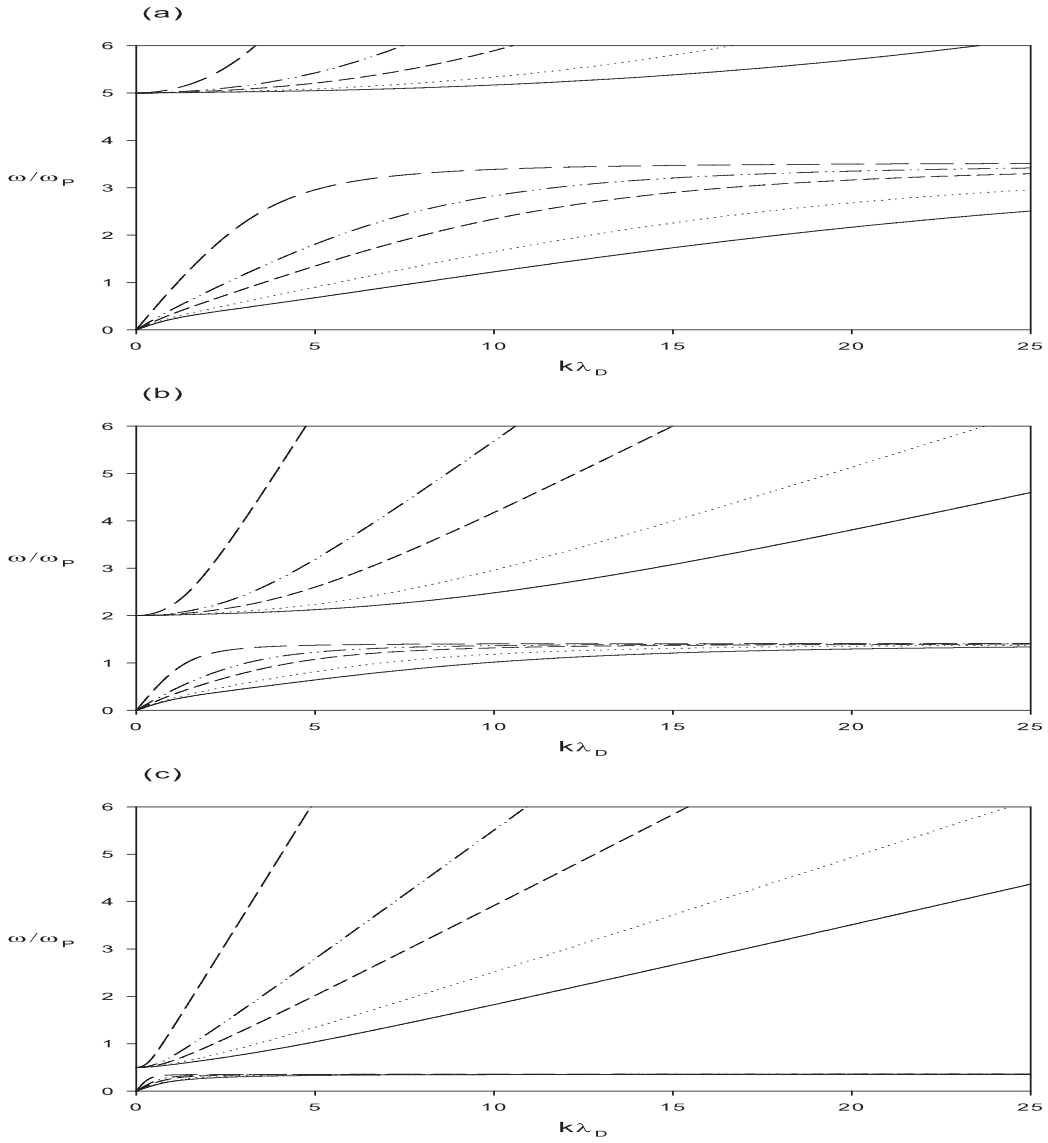

Figure 2.12: Normalized real frequency as a function of the normalized wavenumber for various values of R = (a) 0.2, (b) 0.5 and (c) 2.0. The fixed parameters are $\theta = 45^o$ and $n_{0c}/n_{0h} = 0.11$. The curves represent different values of the temperature ratio T_c/T_h = 0.01 (solid), 0.02 (dotted), 0.05 (broken), 0.1 (dashddot) and 0.5 (longbroken).

2.3 The Kinetic Dispersion Relation

In this section kinetic theory is used to study the acoustic mode that was investigated with fluid theory in the previous section. The focus is on this mode since it is a micro-instability arising from resonances in velocity space. This instability is kinetic in nature and the growth rate of the wave is a function of the slope of the velocity distribution function. When the wave phase velocity along $\mathbf{B_0}$ sees a negative slope of the velocity distribution ($\partial f_0/\partial V_\parallel < 0$), the particles on average will gain energy from the wave, consequently the wave losses energy and becomes damped, an effect known as Landau damping. The wave mode is hence subjected to Landau damping and wave enhancement. Therefore the focus in this section is primarily on the effect of the temperatures of the plasma species.

The same plasma model as in section 2.3 is considered, i.e a four component magnetized electron-positron plasma, consisting of cool electrons and cool positrons with equal temperatures and equilibrium densities denoted by T_c and n_{0c} respectively, and hot electrons and hot positrons with equal temperatures and equilibrium densities denoted by T_h and n_{0h}, respectively.

We begin by deriving the general dispersion relation (see details in Appendix A) where each species j has an isotropic, drifting Maxwellian velocity distribution with temperatures T_j drifting parallel to the magnetic field $\mathbf{B_0} = B_0\hat{z}$, with drift velocities V_{oj} (figure 2.3(a)).

Hence, the equilibrium velocity distribution for the electron and positron species is chosen to be,

$$f_{\alpha 0} = \frac{n_{\alpha 0}}{(2\pi v_{tj}^2)^{\frac{3}{2}}} \exp\left\{ \frac{-[V_x^2 + V_y^2 + (V_z - V_{oj})^2]}{2v_{tj}^2} \right\}, \tag{2.44}$$

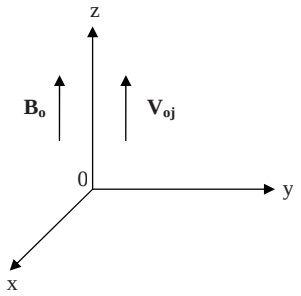

Figure 2.3(a)

The Vlasov equations are,

$$\frac{\partial f_\alpha}{\partial t} + \mathbf{V}.\nabla f_\alpha + \frac{q_\alpha}{m}(\mathbf{E} + \mathbf{V} \times \mathbf{B}).\frac{\partial f_\alpha}{\partial \mathbf{V}} = 0 \ , \tag{2.45}$$

and the equations of motion for the electrons and positrons is given by,

$$m\frac{d\mathbf{V}}{dt} = q_\alpha \left\{ \mathbf{E} + \mathbf{V} \times \mathbf{B} \right\}, \tag{2.46}$$

where $j = c(h)$ for the cool (hot) species and $\alpha = ec, pc, eh$ and ph for the

cool electrons, cool positrons, hot electrons and hot positrons respectively, and $v_{tj} = (T_j/m)^{1/2}$ is the thermal velocity of the j^{th} species.

Following standard techniques for electron-ion plasmas (see for example Bharuthram and Pather, 1996), the general kinetic dispersion relation for the four component, two temperature electron-positron plasma is given by (see Appendix A),

$$\begin{aligned} k^2 \; + \; & \frac{2}{\lambda_{Dc}^2}\left[1 + \frac{\omega - \mathbf{k}.\mathbf{V_{oc}}}{\sqrt{2}k_{\parallel}v_{tc}} \sum_{p=-\infty}^{\infty} Z(z_{pc})\Gamma_{pc}\right] \\ & + \frac{2}{\lambda_{Dh}^2}\left[1 + \frac{\omega - \mathbf{k}.\mathbf{V_{oh}}}{\sqrt{2}k_{\parallel}v_{th}} \sum_{p=-\infty}^{\infty} Z(z_{ph})\Gamma_{ph}\right] = 0 \; , \end{aligned} \tag{2.47}$$

where $\lambda_{Dc,h} = (\varepsilon_0 T_h/n_{0c,h}e^2)^{1/2}$ is the Debye length for the cool (hot) species and z_{pj} is the argument of the plasma dispersion function or Z-function (Fried and Conte, 1961) and is given by,

$$z_{pj} = \frac{\omega - \mathbf{k}.\mathbf{V_{oj}} - p\Omega_j}{\sqrt{2}k_{\parallel}v_{tj}} \; , \tag{2.48}$$

where,

$$\Gamma_{pj} = e^{-\alpha_j} I_p(\alpha_j) \; , \tag{2.49}$$

and

$$\alpha_j = \frac{k_{\perp}^2 v_{tj}^2}{\Omega_j^2} \; , \tag{2.50}$$

where I_p is the modified Bessel function of order p. The components of $\mathbf{k}$ parallel (perpendicular) to $\mathbf{B_0}$ are given by $k_{\parallel}$ ($k_{\perp}$) respectively, while $\mathbf{V_{oc}}$ and $\mathbf{V_{oh}}$ are the drift velocities of the cool (hot) species, respectively.

2.3.1 Approximate Solutions of the Kinetic Dispersion Relation

The general dispersion relation (2.47) can be numerically solved without any approximations. However, to get some insight into the solutions, here, approximate expansions of the plasma dispersion function are used to obtain analytical expressions for the frequency and growth rate of the acoustic mode.

In proceeding, for the temperatures it is assumed that $T_h \gg T_c(\sim 0)$. In addition low frequency modes satisfying $|\omega| \ll \Omega$ are considered. The series expansion of the Z-function(Fried and Conte, 1961) is given by

$$Z(z) \;=\; i\sqrt{\pi}e^{-z^2} - 2z\left[1 - \frac{2z^2}{3} + \frac{4z^4}{15} - ...\right] \text{ for } |z| \ll 1 \text{ and} \tag{2.51}$$

$$Z(z) \;=\; i\sqrt{\pi}\delta e^{-z^2} - \frac{1}{z}\left[1 + \frac{1}{2z^2} + \frac{3}{4z^4} + ...\right] \text{ for } |z| \gg 1\ . \tag{2.52}$$

where for $\mid z \mid \gg 1$, $\qquad \delta = \begin{cases} 0, & \mathrm{Im}(z) > 0 \\ 1, & \mathrm{Im}(z) = 0 \\ 2, & \mathrm{Im}(z) < 0 \end{cases}$

Assuming the drift of the electrons and positrons to be weak (i.e small V_{oc} and V_{oh}) (Rosenberg, 1993) and $|\omega| \ll \Omega$,

$$z_{pc} = \frac{\omega - \mathbf{k}.\mathbf{V_{oc}} - p\Omega}{\sqrt{2}k_\parallel v_{tc}} \approx \frac{-p\Omega}{\sqrt{2}k_\parallel v_{tc}} \quad \text{for } p \neq 0 \tag{2.53}$$

and

$$z_{ph} = \frac{\omega - \mathbf{k}.\mathbf{V_{oh}} - p\Omega}{\sqrt{2}k_\parallel v_{th}} \approx \frac{-p\Omega}{\sqrt{2}k_\parallel v_{th}} \quad \text{for } p \neq 0\ . \tag{2.54}$$

Then for the cool species,

$$\sum_{p=-\infty}^{\infty} Z(z_{pc})\Gamma_{pc} \approx Z\left(\frac{\omega - \mathbf{k}.\mathbf{V_{oc}}}{\sqrt{2}k_{\parallel}v_{tc}}\right)\Gamma_{oc} + \sum_{\mathrm{p}=1}^{\infty}\left\{Z\left(\frac{p\Omega}{\sqrt{2}k_{\parallel}v_{tc}}\right) + Z\left(\frac{-p\Omega}{\sqrt{2}k_{\parallel}v_{tc}}\right)\right\}\Gamma_{pc} \,. \tag{2.55}$$

From the definition of the Z-function, $Z(\xi) + Z(-\xi) = 0$, hence

$$\sum_{p=-\infty}^{\infty} Z(z_{pc})\Gamma_{pc} \approx \; Z(z_{oc})\Gamma_{oc} \,. \tag{2.56}$$

In proceeding, we take the cooler species to be stationary. Therefore V_{oc} is set to zero, allowing only for the drift of the hot species. Then,

$$z_{oc} \;=\; \frac{\omega}{\sqrt{2}k_{\parallel}v_{tc}} \,. \tag{2.57}$$

For modes satisfying $\omega/k_{\parallel} \gg v_{tc}$, one may assume $|z_{oc}| \gg 1$, i.e. the wave phase speed along $\mathbf{B_o}$ is much larger than the cool electron thermal speed. For an instability (i.e. a growing wave with $\mathrm{Im}(z) > 0$), δ is set equal to zero in equation (2.52). Hence using the series expansion equation (2.52), equation (2.55) becomes

$$\sum_{p=-\infty}^{\infty} Z(z_{pc})\Gamma_{pc} \approx \; \left[-\frac{1}{z_{oc}} - \frac{1}{2z_{oc}^3} - \frac{3}{4z_{oc}^5}\right]\Gamma_{oc} \,. \tag{2.58}$$

For the hot species, we have

$$\sum_{p=-\infty}^{\infty} Z(z_{ph})\Gamma_{ph} \approx Z\left(\frac{\omega - \mathbf{k}.\mathbf{V_{oh}}}{\sqrt{2}k_{\parallel}v_{th}}\right)\Gamma_{oh} + \sum_{p=1}^{\infty}\left\{Z\left(\frac{p\Omega}{\sqrt{2}k_{\parallel}v_{th}}\right) + Z\left(\frac{-p\Omega}{\sqrt{2}k_{\parallel}v_{th}}\right)\right\}\Gamma_{ph}\ . \tag{2.59}$$

Again using the definition of the Z-function, $Z(\xi) + Z(-\xi) = 0$

and

$$z_{oh} \ = \ \frac{\omega - \mathbf{k}.\mathbf{V_{oh}}}{\sqrt{2}k_{\parallel}v_{th}}\ . \tag{2.60}$$

Hence

$$\sum_{p=-\infty}^{\infty} Z(z_{ph})\Gamma_{ph} \approx \ Z(z_{oh})\Gamma_{oh}. \tag{2.61}$$

For relatively high temperature T_h, the thermal velocity of the hot species is much larger than the wave phase velocity. Hence, for large T_h, one may assume that $|z_{oh}| \ll 1$. Hence using the series expansion equation (2.51) (where $e^{-z_{oh}^2} \approx 1$ for $|z_{oh}| \ll 1$), equation (2.61) becomes

$$\sum_{p=-\infty}^{\infty} Z(z_{ph})\Gamma_{ph} \approx \ (i\sqrt{\pi} - 2z_{oh} + \frac{4z_{oh}^3}{3})\Gamma_{oh}\ . \tag{2.62}$$

Substituting (2.58) and (2.62) into the dispersion relation (2.47) and multiplying by λ_D^2, where as before $\lambda_D = (\varepsilon_0 T_h/n_0 e^2)^{1/2}$, gives

$$k^2\lambda_D^2 + 2\frac{\lambda_D^2}{\lambda_{Dc}^2}\left[1 + z_{oc}\left(-\frac{1}{z_{oc}} - \frac{1}{2z_{oc}^3} - \frac{3}{4z_{oc}^5}\right)\Gamma_{oc}\right] + 2\frac{\lambda_D^2}{\lambda_{Dh}^2}\left[1 + z_{oh}(i\sqrt{\pi} - 2z_{oh} + \frac{4z_{oh}^3}{3})\Gamma_{oh}\right] \ = \ 0\,. \tag{2.63}$$

Substituting for λ_D, λ_{Dc} and λ_{Dh}, the above equation becomes

$$
\begin{aligned}
k^2\lambda_D^2 \;+\; 2\frac{\frac{n_{0c}}{n_0}}{\frac{T_c}{T_h}}\left[1+z_{oc}\left(i\sqrt{\pi}e^{-z_{oc}^2}-\frac{1}{z_{oc}}-\frac{1}{2z_{oc}^3}-\frac{3}{4z_{oc}^5}\right)\Gamma_{oc}\right] \\
+\; 2\frac{n_{0h}}{n_0}\left[1+z_{oh}(i\sqrt{\pi}-2z_{oh}+\frac{4z_{oh}^3}{3})\Gamma_{oh}\right] \;=\; 0\ .
\end{aligned}
\tag{2.64}
$$

For the cool species we assume $|\alpha_c| = |k_\perp^2 v_{tc}^2/\Omega^2| = k^2\rho_c^2 \ll 1$ (where ρ_c is the gyroradius of the cool species), i.e long wavelength fluctuations in comparison to ρ_c. Since in general for $|x| \ll 1$ we can write $\Gamma_p(x) = e^{-x}I_p(x) \approx (x/2)^p(1/p!)(1-x)$, hence we have

$$
\Gamma_{oc} \approx 1\ . \tag{2.65}
$$

In (2.64) the second and higher order terms in z_{oh} are neglected since we have assumed $|z_{oh}| \ll 1$. The equation then reduces to

$$
k^2\lambda_D^2 \;+\; 2\frac{\frac{n_{0c}}{n_0}}{\frac{T_c}{T_h}}\left[i\sqrt{\pi}z_{oc}e^{-z_{oc}^2}-\frac{1}{2z_{oc}^2}-\frac{3}{4z_{oc}^4}\right] \;+\; 2\frac{n_{0h}}{n_0}\left[1+i\sqrt{\pi}z_{oh}\Gamma_{oh}\right] \;=\; 0\ . \tag{2.66}
$$

Setting $\omega = \omega_r + i\gamma$ and assuming $\gamma/\omega_r \ll 1$ we may write

$$
\begin{aligned}
\frac{1}{\omega^2} &= \frac{1}{\omega_r^2 + 2i\gamma\omega_r - \gamma^2} \\
&= \frac{1}{\omega_r^2\left(1+\dfrac{2i\gamma}{\omega_r}-\dfrac{\gamma^2}{\omega_r^2}\right)} \\
&\approx \frac{1}{\omega_r^2}\left(1-\frac{2i\gamma}{\omega_r}\right)\ .
\end{aligned}
\tag{2.67}
$$

Using the above manipulation, equation (2.66) becomes

$$k^2\lambda_D^2 \;+\; 2\frac{\frac{n_{0c}}{n_0}}{\frac{T_c}{T_h}}\left[i\sqrt{\pi}\left(\frac{\omega_r+i\gamma}{\sqrt{2}k_\parallel v_{tc}}\right)e^{-z_{oc}^2}-\frac{k_\parallel^2 v_{tc}^2}{\omega_r^2}\left(1-\frac{2i\gamma}{\omega_r}\right)-\frac{3k_\parallel^4 v_{tc}^4}{\omega_r^4}\left(1-\frac{2i\gamma}{\omega_r}\right)^2\right]$$
$$+\; 2\frac{n_{0h}}{n_0}\left[1+i\sqrt{\pi}\left(\frac{\omega_r+i\gamma-\mathbf{k}.\mathbf{V_{oh}}}{\sqrt{2}k_\parallel v_{th}}\right)\Gamma_{oh}\right] \;=\; 0\ . \tag{2.68}$$

Taking the real part of equation (2.68) gives

$$k^2\lambda_D^2 \;+\; 2\frac{\frac{n_{0c}}{n_0}}{\frac{T_c}{T_h}}\left(\frac{-k_\parallel^2 v_{tc}^2}{\omega_r^2}-\frac{3k_\parallel^4 v_{tc}^4}{\omega_r^4}\right) \;+\; 2\frac{n_{0h}}{n_0} \;=\; 0\ . \tag{2.69}$$

Rearranging the above yields,

$$\omega_r^4\left(k^2\lambda_D^2+2\frac{n_{oh}}{n_o}\right)-2\frac{\frac{n_{0c}}{n_0}}{\frac{T_c}{T_h}}k_\parallel^2 v_{tc}^2\omega_r^2-6\frac{\frac{n_{0c}}{n_0}}{\frac{T_c}{T_h}}k_\parallel^4 v_{tc}^4=0\ . \tag{2.70}$$

With the charge neutrality condition

$$\frac{n_{0c}}{n_0}+\frac{n_{0h}}{n_0}=1, \tag{2.71}$$

equation (2.70), which is quadratic in ω^2 is solved as follows. Equation (2.70) can be written as $A\omega_r^2+B\omega_r+C=0$, where $A=k^2\lambda_D^2+2\frac{n_{oh}}{n_o}$, $B=-2\frac{\frac{n_{0c}}{n_0}}{\frac{T_c}{T_h}}k_\parallel^2 v_{tc}^2$ and $C=-6\frac{\frac{n_{0c}}{n_0}}{\frac{T_c}{T_h}}k_\parallel^4 v_{tc}^4$.

with solutions

$$\omega_r^2=\frac{-B\pm\sqrt{B^2-4AC}}{2A}$$

For $B^2 \gg 4AC$ this approximates to

$$\begin{aligned} \omega_r^2 = & \frac{-B \pm B(1-\frac{4AC}{B^2})^{1/2}}{2A} \\ \approx & \frac{-B \pm B(1-\frac{2AC}{B^2})}{2A} \end{aligned}$$

Taking the positive root the real frequency becomes

$$\omega_r^2 = \frac{2\frac{n_{0c}}{n_0}k_\parallel^2\frac{T_h}{m}}{2(1-\frac{n_{0c}}{n_0})+k^2\lambda_D^2} + 3k_\parallel^2\frac{T_c}{m} \ , \tag{2.72}$$

which may be rewritten as

$$\omega_r^2 = \frac{k^2 v_{ea}^2\cos^2\theta}{1+\frac{1}{2}k^2\lambda_{Dh}^2} + 3k^2 v_{tc}^2\cos^2\theta \ , \tag{2.73}$$

where $\cos\theta = k_\parallel/k$ and $v_{ea} = (n_{0c}/n_{0h})^{1/2}v_{th}$ is the acoustic speed of the electron-positron plasma. It is noted that equation (2.73) is consistent with the expression (2.21) obtained from fluid theory.

In order to derive the approximate solution of the growth rate, we consider the imaginary part of equation (2.68), which yields

$$\begin{aligned} & 2\frac{\frac{n_{0c}}{n_0}}{\frac{T_c}{T_h}}\left[\left(\frac{\pi}{2}\right)^{1/2}\left(\frac{m}{T_c}\right)^{1/2}\frac{\omega_r}{k_\parallel}e^{-z_{oc}^2} + \frac{2k_\parallel^2\frac{T_c}{m}\gamma}{\omega_r^3} + \frac{12k_\parallel^4\frac{T_c^2}{m^2}\gamma}{\omega_r^5}\right] \\ & + 2\frac{n_{0h}}{n_0}\left[\left(\frac{\pi}{2}\right)^{1/2}\left(\frac{m}{T_h}\right)^{1/2}\left(\frac{\omega_r - \mathbf{k}.\mathbf{V_{oh}}}{k_\parallel}\right)\Gamma_{oh}\right] = 0 \ . \end{aligned} \tag{2.74}$$

The above equation is simplified as

$$\left[\frac{2k_{\parallel}^2\frac{T_c}{m}}{\omega_r^3}+\frac{12k_{\parallel}^4\frac{T_c^2}{m^2}}{\omega_r^5}\right]\gamma = -\left(\frac{\pi}{2}\right)^{1/2}\left(\frac{m}{T_c}\right)^{1/2}\frac{\omega_r}{k_{\parallel}}e^{-z_{oc}^2} + \frac{n_{0h}}{n_{0c}}\frac{T_c}{T_h}\left(\frac{\pi}{2}\right)^{1/2}\left(\frac{m}{T_h}\right)^{1/2}\frac{\omega_r}{k_{\parallel}}\left(\frac{\mathbf{k}.\mathbf{V_{oh}}}{\omega_r}-1\right)\Gamma_{oh}\ . \tag{2.75}$$

Solving for γ, one finds

$$\gamma = \frac{\frac{\omega_r^4}{k_{\parallel}^3}\left(\frac{\pi}{8}\right)^{1/2}\left(\frac{m}{T_h}\right)^{3/2}\left[-\left(\frac{T_h}{T_c}\right)^{3/2}e^{-z_{oc}^2}+\left(\frac{n_{0h}}{n_{0c}}\right)\left(\frac{\mathbf{k}.\mathbf{V_{oh}}}{\omega_r}-1\right)\Gamma_{oh}\right]}{\left[1+\frac{6k_{\parallel}^2\frac{T_c}{m}}{\omega_r^2}\right]}\ . \tag{2.76}$$

We note that in equation (2.76), it is the cooler species that provides the Landau damping, i.e. the velocity distribution function sees a negative slope ($\partial f_0/\partial V_{\parallel} < 0$). It is also seen from equation (2.76) that for an unstable mode ($\gamma > 0$), it is necessary that $V_{0h} > \omega_r/k_{\parallel}$, i.e the drift velocity of the hot species has to be larger than the parallel (to $\mathbf{B_0}$) phase velocity to overcome the damping terms.

Normalizing the fluid speeds by the thermal velocity $v_{th} = (T_h/m)^{1/2}$ of the hot species, the particle density by the total equilibrium plasma density $n_0 = n_{0c} + n_{0h}$, the temperatures by T_h, the spatial length by $\lambda_D = (\frac{\varepsilon_0 T_h}{n_0 e^2})^{1/2}$, and the time by $\omega_p^{-1} = (\frac{n_0 e^2}{\varepsilon_0 m})^{-1/2}$, the general kinetic dispersion relation

(2.47) becomes,

$$k'^2 \; + \; 2\frac{n'_{0c}}{\frac{T_c}{T_h}}\left[1+\frac{\omega'-k'_\parallel V'_{oc}}{\sqrt{2}k'_\parallel\sqrt{\frac{T_c}{T_h}}}\sum_{p=-\infty}^{\infty}Z(z'_{pc})\Gamma'_{pc}\right] + 2n'_{0h}\left[1+\frac{\omega'-k'_\parallel V'_{oh}}{\sqrt{2}k'_\parallel}\sum_{p=-\infty}^{\infty}Z(z'_{ph})\Gamma'_{ph}\right]=0\ , \tag{2.77}$$

with the normalized Z-functions given by,

$$z'_{pc}=\frac{\omega'-p\dfrac{\Omega}{\omega_p}}{\sqrt{2}k'_\parallel\sqrt{\frac{T_c}{T_h}}} \tag{2.78}$$

and

$$z'_{ph}=\frac{\omega'-k'_\parallel V'_{oh}-p\dfrac{\Omega}{\omega_p}}{\sqrt{2}k'_\parallel}\ . \tag{2.79}$$

Also

$$\alpha'_c=\frac{{k'_\perp}^2\frac{T_c}{T_h}}{\frac{\Omega^2}{\omega_p^2}} \tag{2.80}$$

and

$$\alpha'_h=\frac{{k'_\perp}^2}{\frac{\Omega^2}{\omega_p^2}}\ . \tag{2.81}$$

where $\omega'=\omega/\omega_p$, $k'=k\lambda_D$, $k'_\parallel=k_\parallel\lambda_D$, $k'_\perp=k_\perp\lambda_D$, $n'_{0c}=n_{0c}/n_0$ and $n'_{0h}=n_{0h}/n_0$.

From equation (2.72), the normalized real frequency is given by,

$$\omega_r'^2 \;=\; \frac{2n'_{0c}k'^2_{\parallel}}{2n'_{0h}+k'^2} + 3k'^2_{\parallel}\frac{T_c}{T_h}\;, \tag{2.82}$$

and using equation (2.76), the normalized approximate expression for the growth rate is given by,

$$\gamma' \;=\; \frac{\dfrac{\omega_r'^4}{k'^3_{\parallel}}\left(\dfrac{\pi}{8}\right)^{1/2}\left[-\left(\dfrac{T_h}{T_c}\right)^{3/2}e^{-z'^2_{oc}} + \left(\dfrac{n'_{0h}}{n'_{0c}}\right)\left(\dfrac{\mathbf{k}.\mathbf{V_{oh}}}{\omega'_r}-1\right)\Gamma_{oh}\right]}{\left[1+\dfrac{6k'^2_{\parallel}\frac{T_c}{T_h}}{\omega_r'^2}\right]} \tag{2.83}$$

where $\gamma' = \gamma/\omega_p$ and

$$z^2_{oc} \;=\; \left(\frac{\omega}{\sqrt{2}k_{\parallel}v_{tc}}\right)^2 \;=\; \frac{\omega_r^2\left(1+\frac{2\imath\gamma}{\omega_r}-\frac{\gamma^2}{\omega_r^2}\right)}{2k^2_{\parallel}\frac{T_c}{m}}\;. \tag{2.84}$$

Substituting from equation (2.82) for ω'_r one obtains

$$\begin{aligned} z'^2_{0c} \;&\approx\; \frac{\left(\frac{2n'_{0c}k'^2_{\parallel}\frac{T_h}{T_c}}{2n'_{0h}+k'^2}+3k'^2_{\parallel}\right)}{2k'^2_{\parallel}} \\ &=\; \frac{n'_{0c}\frac{T_h}{T_c}}{2n'_{0h}+k'^2}+\frac{3}{2}\;. \end{aligned} \tag{2.85}$$

Terms involving γ/ω_r have been neglected as $|\gamma/\omega_r| \ll 1$ has been assumed.

2.3.2 Numerical Results

The MATHEMATICA program was used to determine the real and imaginary roots of the general dispersion relation (equation (2.77)), which has the form $D(k, \omega) = 0$. An initial guess value was first obtained from the approximate expressions (2.82) and (2.83). Figure (2.13) shows the real frequency for the acoustic mode, where fixed plasma parameters are chosen in order to compare directly with fluid theory results. For completeness, also shown is the solution for the upper hybrid mode which satisfies the dispersion relation (2.20). It is seen from a comparison with fluid theory results, that the real frequencies for the acoustic mode are in very good agreement with that from kinetic theory results.

We now explore the behaviour of the growth rate of the (kinetic) acoustic instability. Figure (2.14) (a) and (b) shows the behaviour of the normalized real frequency ω_r/ω_p and the normalized growth rate γ/ω_p, respectively, for a normalized drift velocity of $V_{oh} = 0.5$. The curves are shown to be in good agreement with the approximate analytical expressions (2.82) and (2.83). For large values of $k\lambda_D$ the difference between the growth rates in the curves increases. This could be due to the fact that Landau damping, which is neglected in fluid theory, becomes stronger as $k\lambda_D$ increases, as can be seen from equations (2.83) and (2.85). In figure (2.15) the normalized growth rate is plotted for different values of V_{0h}. The fixed parameters are $T_c/T_h = 0.01$ and $n_{oc} = 0.1$. As V_{0h} increases there is an increase in the growth rate of

the instability which is associated with the increase in free energy (of the drifting hot species) to drive the instability. For the fixed set of parameters corresponding to this curve, it is found that a minimum value of $V_{oh} = 0.5$ is required to drive the instability. The $k\lambda_D$ value for maximum growth rate also increases with V_{0h}. Figure (2.16) displays the normalized growth rate as a function of the normalized wavenumber for varying cool to hot species temperature ratios T_c/T_h. It is noted that as the T_c/T_h decreases, the growth rate increases, implying that the instability is more easily excited with lower temperature ratios. A possible reason for this is as follows. As T_c increases, the velocity distribution function of the cooler species changes in a way that the wave sees a larger (negative) slope of the distribution function, resulting in an enhanced Landau damping ($\gamma \propto \partial f_0/\partial V_\parallel$) which reduces the net growth rate. It is noted that a cutoff $k\lambda_D$ value is reached beyond which the mode is damped (Bharuthram and Pather, 1996), which could be the crossover point at which Landau damping dominates over contribution of the free energy of the drifting hot species. The normalized growth rate as a function of the normalized wavenumber for various cool to hot density values is plotted in figure (2.17). The fixed parameters are $T_c/T_h = 0.01$ and $V_{oh} = 0.8$. A simple plot of the maximum γ/ω_p of each of the curves shown in figure (2.17) against the corresponding n_{oc}/n_0 values is shown in figure (2.18). For the chosen set of parameters, the curve peaks at $n_{oc}/n_0 = 0.2$. The normalized growth rate for oblique angles of propagation are shown in Figure (2.19). It is seen that as θ increases the growth rate decreases. This behaviour may be explained as follows. In the analytical expressions (2.73) and (2.76) it is seen that

both $\omega_r^4/k_\parallel^3$ and $\mathbf{k}.\mathbf{V_{0h}} = k_\parallel V_{0h}$ decreases with $k_\parallel$. As the propagation angle θ relative to $\mathbf{B_o}$ increases, $k_\parallel$ decreases, thereby resulting in a reduction in growth rate. In figure (2.20) are shown shows the normalized growth rate for different magnetic field strengths for a fixed plasma density. As the magnetic field strength increases (R decreasing), the growth rate is found to increase. A possible explanation has been offered by (Bharuthram and Pather, 1996). As $|\mathbf{B_0}|$ increases, the electrons and positrons become more strongly tied to the field lines. Hence it becomes more difficult for them to move obliquely to the field line to neutralize the electrostatic fluctuations, thereby resulting in an enhancement of the growth rate.

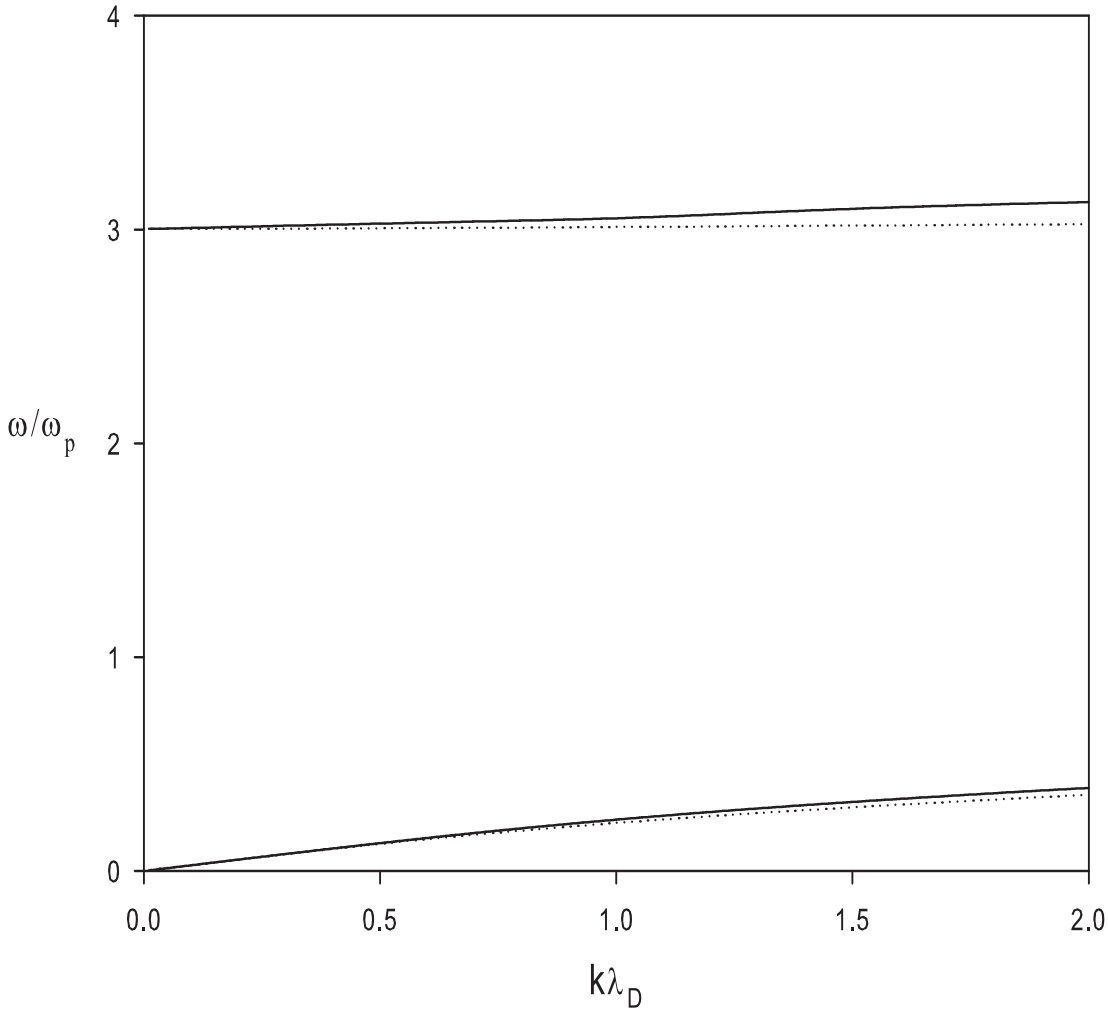

Figure 2.13: Normalized real frequency as a function of the normalized wavenumber using the fluid theory approach (solid line) and kinetic theory approach (broken line). The fixed parameters are $R = 0.333$, $T_c/T_h = 0.01$, $V_{oh} = 0.5$, $n_{0c} = 0.1$ and $\theta = 45^o$.

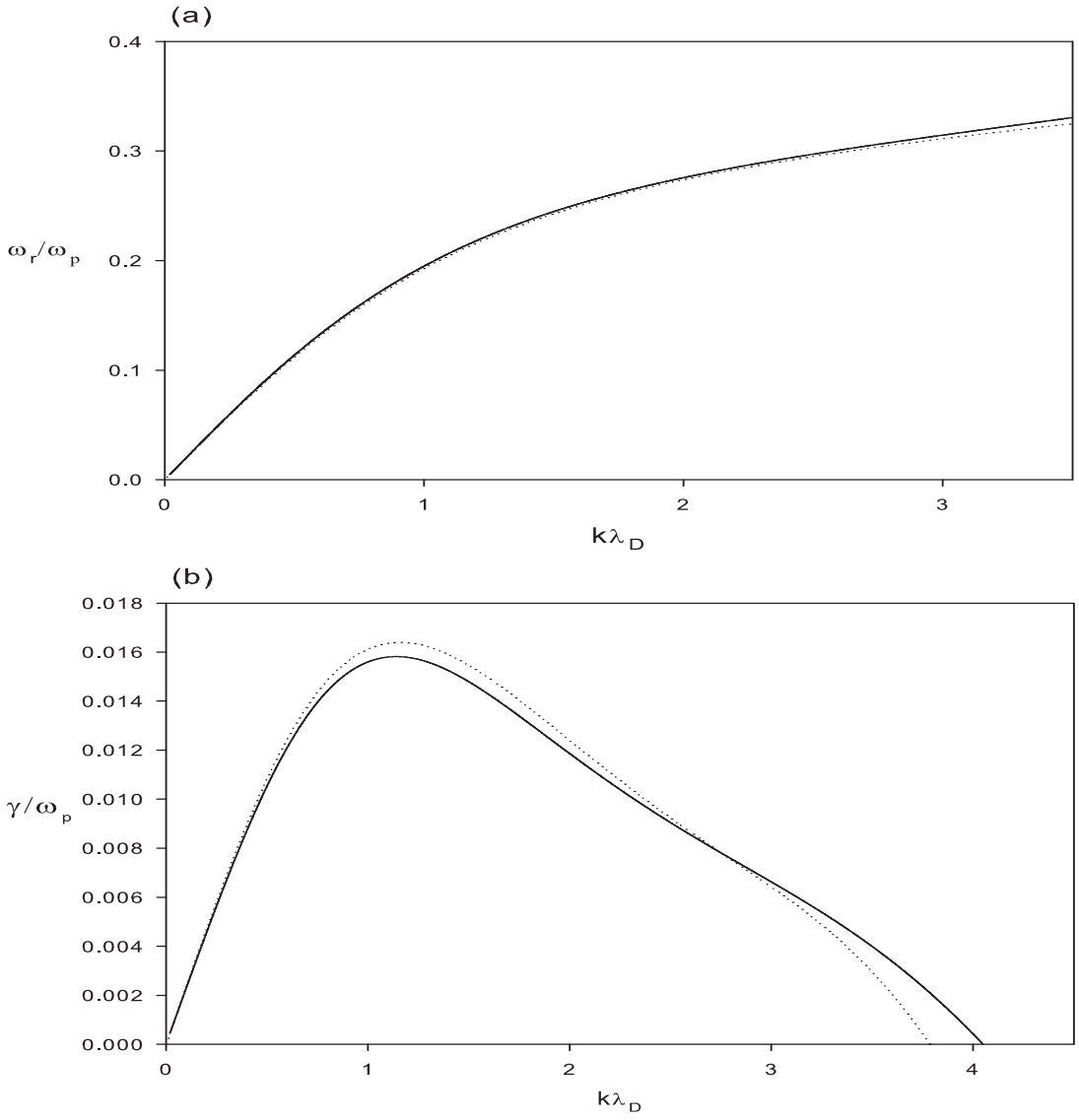

Figure 2.14: Normalized real frequency (a) and normalized growth rate (b) as a function of the normalized wavenumber for the general dispersion relation (solid line) and from the approximate expression (broken line). The fixed parameters are $R = 0.333$, $T_c/T_h = 0.001$, $V_{oh} = 0.5$, $n_{0c} = 0.1$ and $\theta = 45^o$.

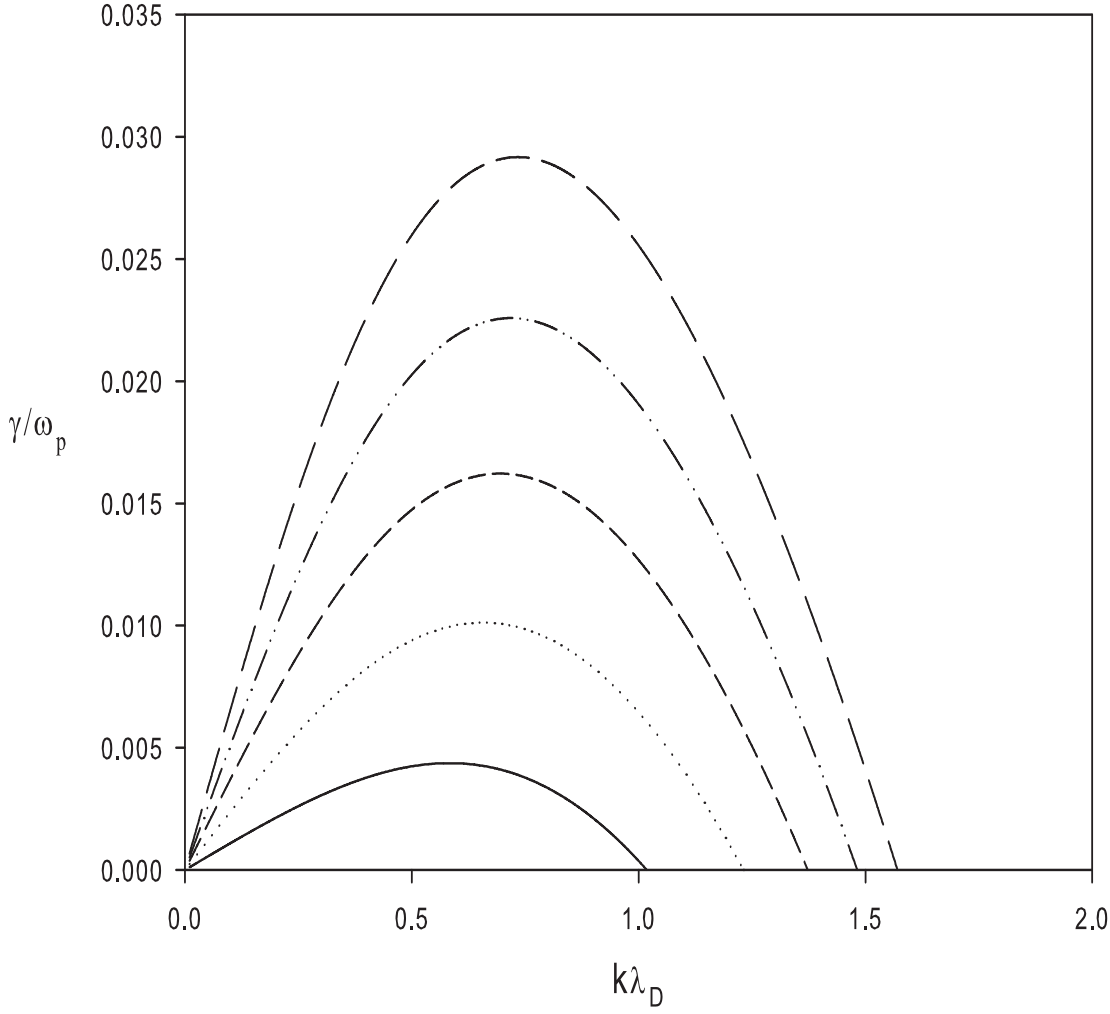

Figure 2.15: Normalized real frequency as a function of the normalized wavenumber. The fixed parameters are $R = 0.333$, $T_c/T_h = 0.01$, $n_{0c} = 0.1$ and $\theta = 45^o$. The curves represent different values of the hot drift velocity $V_{oh} = 0.5$ (solid), 0.6 (dotted), 0.7 (broken), 0.8 (dashddot) and 0.9 (long-broken).

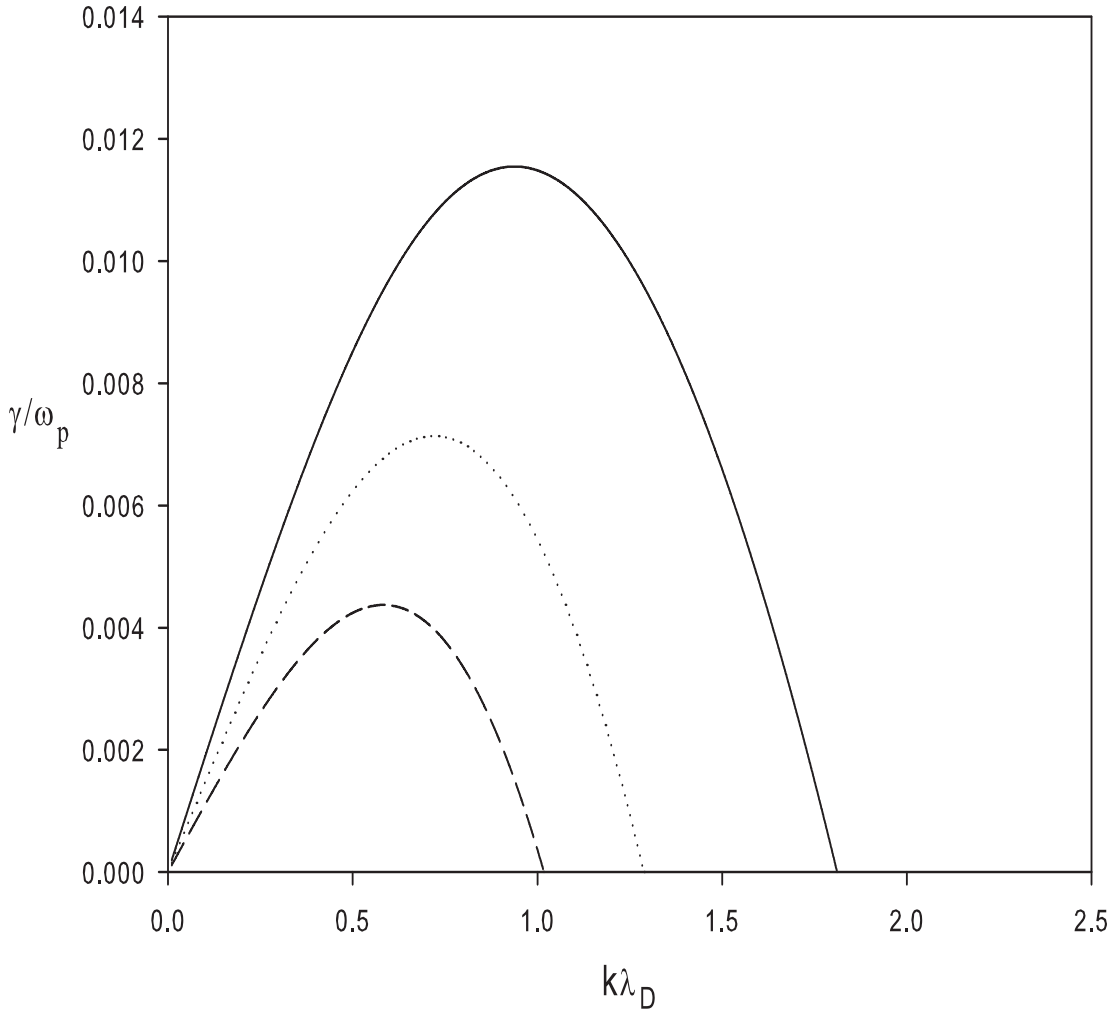

Figure 2.16: Normalized growth rate as a function of the normalized wavenumber. The fixed parameters are $R = 0.333$, $V_{oh} = 0.5$, $n_{0c} = 0.1$ and $\theta = 45^o$. The curves represent different values of the cool to hot temperature ratio $T_c/T_h = 0.005$ (solid), 0.008 (dotted), and 0.01 (broken).

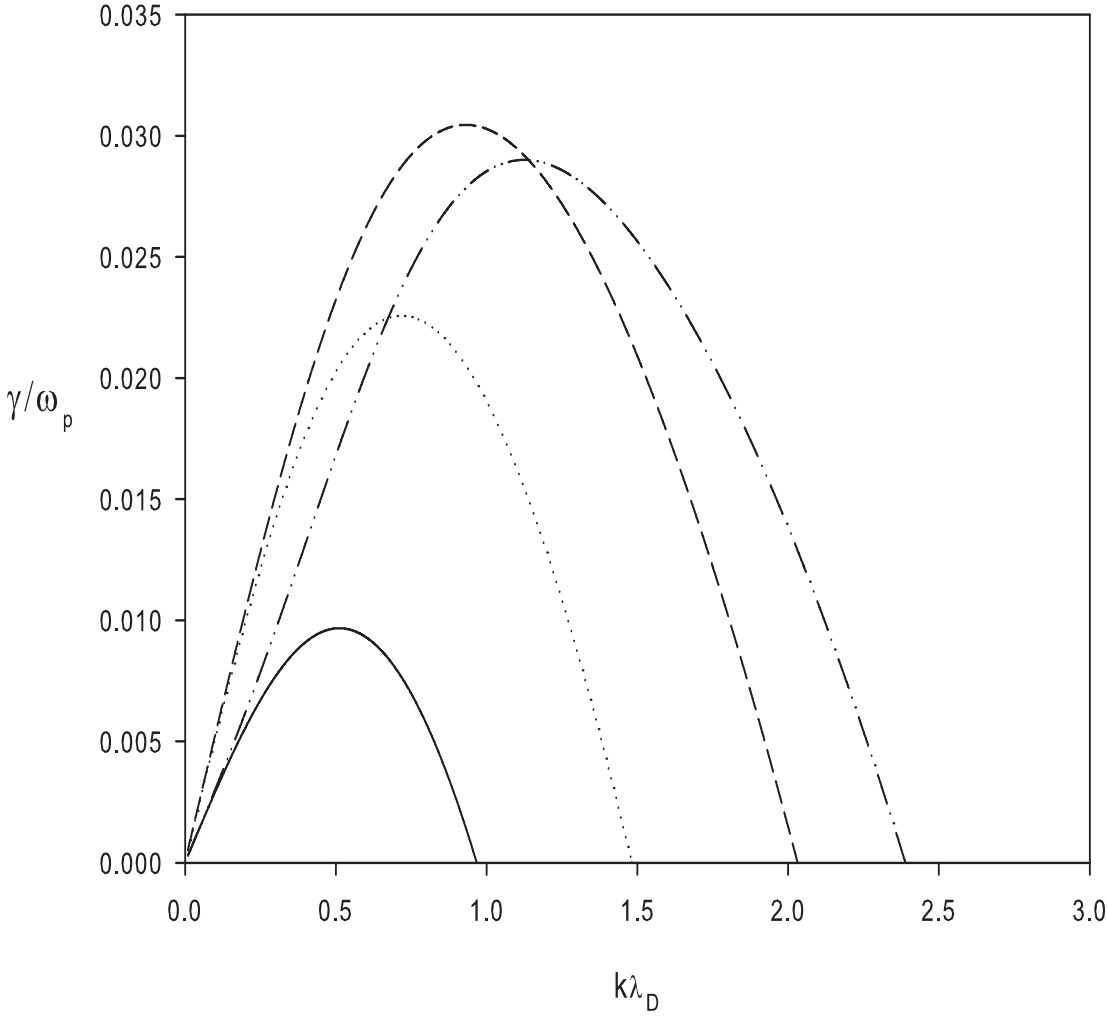

Figure 2.17: Normalized growth rate as a function of the normalized wavenumber. The fixed parameters are $R = 0.333$, $T_c/T_h = 0.01$, $V_{oh} = 0.8$ and $\theta = 45^o$. The curves represent different values of the cool electron and positron densities $n_{0c} = 0.05$ (solid), 0.1 (dotted), 0.2 (broken) and 0.3 (dashddot).

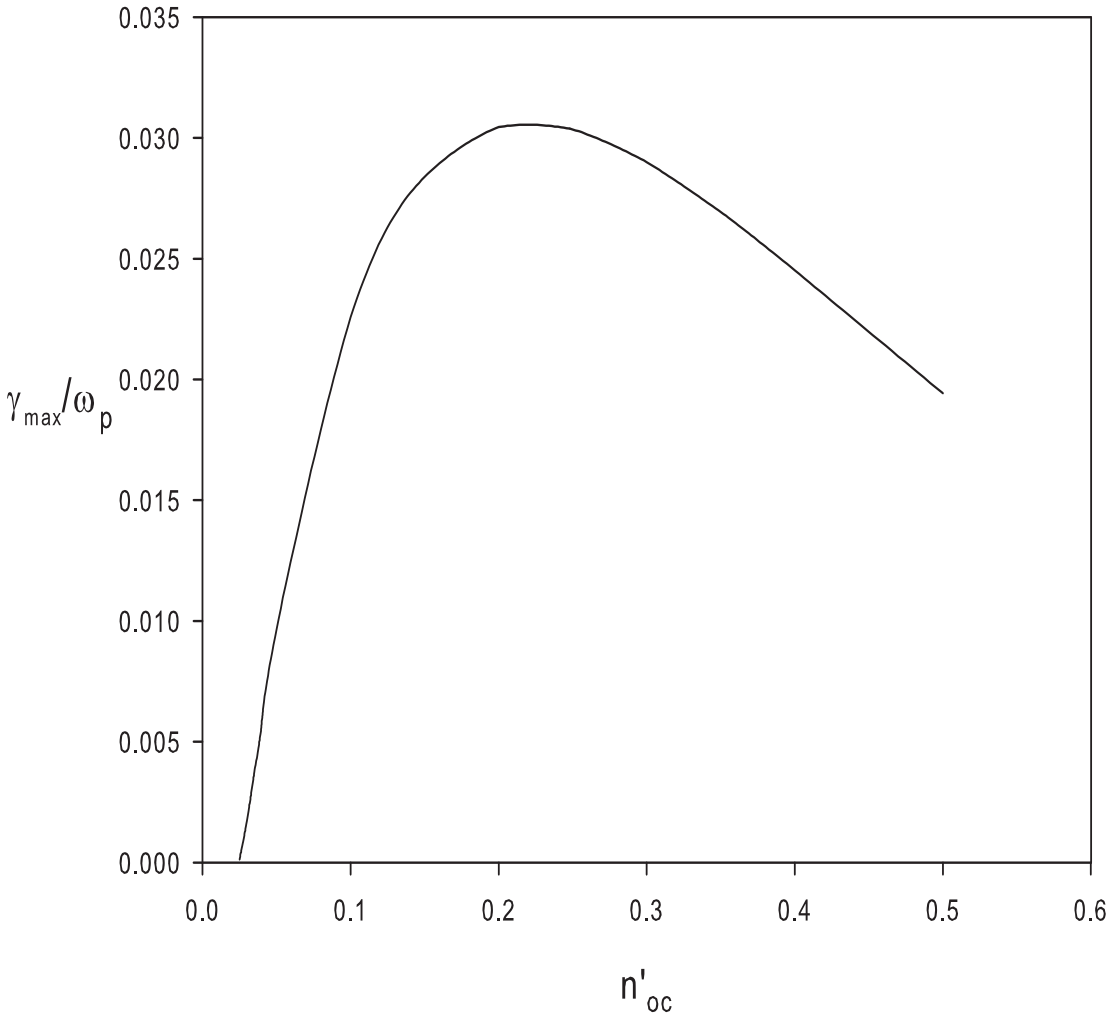

Figure 2.18: Maximum growth rate as a function of the cool densities n_{0c}. The fixed parameters are $R = 0.333$, $T_c/T_h = 0.01$, $V_{oh} = 0.8$ and $\theta = 45^o$.

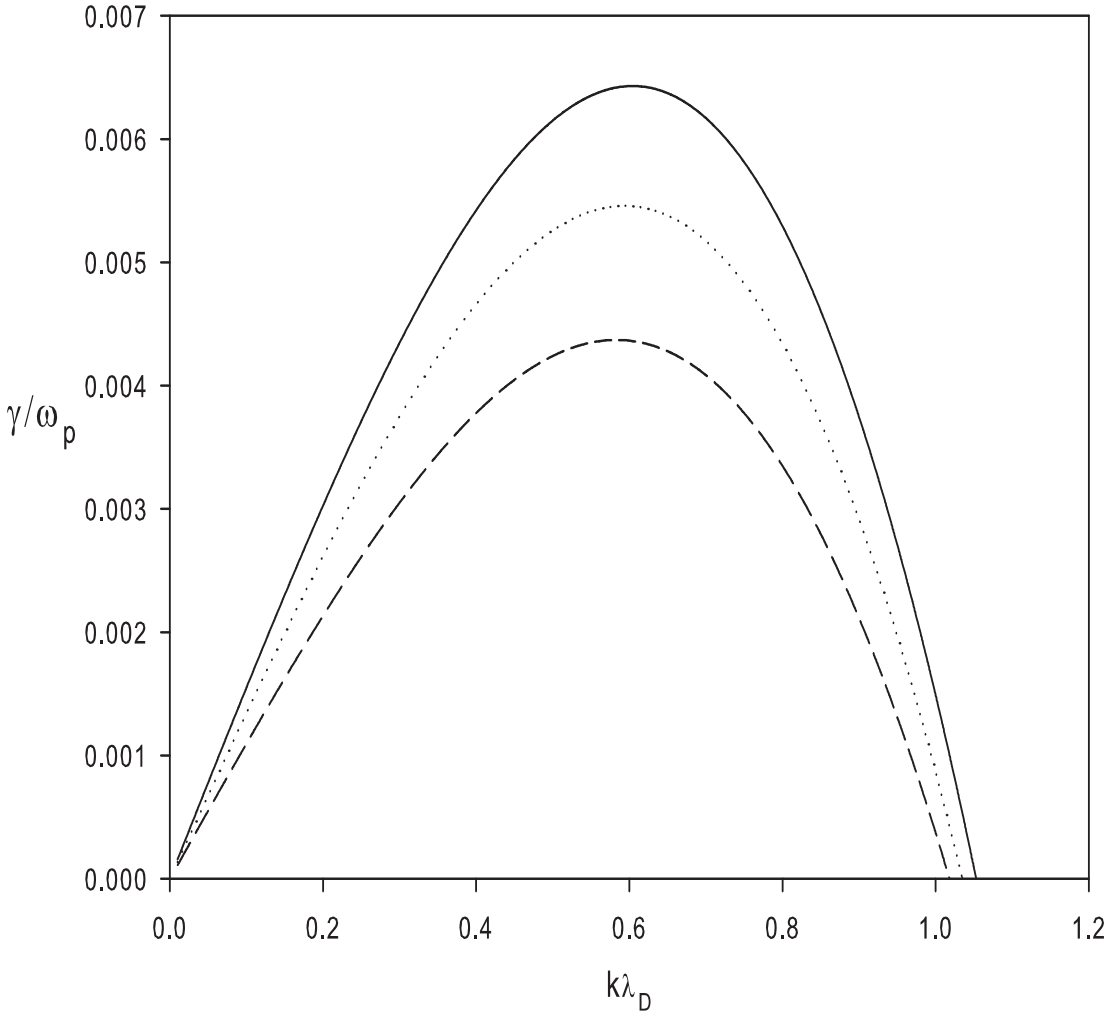

Figure 2.19: Normalized growth rate as a function of the normalized wavenumber. The fixed parameters are $T_c/T_h = 0.01$, $V_{oh} = 0.5$ and $n_{0c} = 0.1$. The curves represent different values of the propagation angle $\theta = 0^o$ (solid), 30^o (dotted) and 45^o (broken).

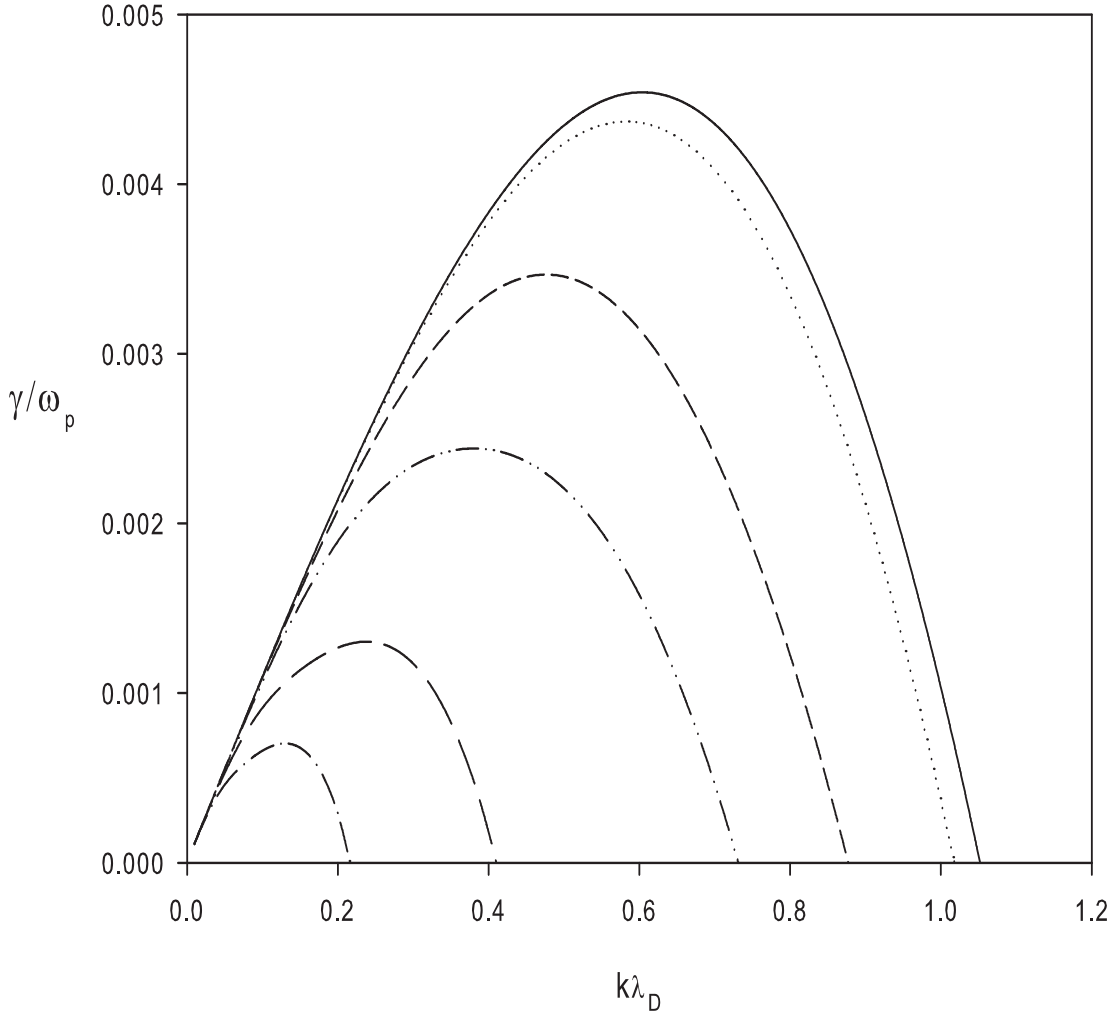

Figure 2.20: Normalized growth rate as a function of the normalized wavenumber for various magnetic field strengths. The fixed parameters are $T_c/T_h = 0.01$, $V_{oh} = 0.5$, $n_{0c} = 0.1$ and $\theta = 45^o$. The curves represent different values of $R = \omega_p/\Omega = 0.05$ (solid), 0.333 (dotted), 1.0 (broken), 2.0 (dashddot), 5.0 (longbroken) and 10.0 (dashdot).

2.4 Discussion

In this chapter, linear waves in a magnetized four component two-temperature electron-positron plasma have been initially investigated, with the hot species having a Boltzmann density distribution and the dynamics of the cooler species governed by the fluid equations. Solutions of the corresponding dispersion relation yield two primary modes, the associated acoustic and cyclotron branches, which were explored as a function of several plasma parameters.

The behavior for perpendicular wave propagation shows only the existence of the cyclotron mode, with the acoustic mode vanishing ($\omega = 0$). Moreover, in the short wavelength limit, only the cooler species contributes to the wave dynamics, whilst in the long wavelength limit, both the cooler adiabatic species and the hot species contribute, with the hot species dominating for $T_c \ll T_h$, and hence influencing the dispersive properties of the wave. On the other hand, for parallel propagation, the solutions display the dominant acoustic mode and a constant frequency ($\omega = \Omega$) non-propagating oscillation. For the two-temperature electron-positron model presented here, it is noted that the linear portions of the dispersion curves (i.e large $k\lambda_D$ values in figure 2.3) have a smaller slope when compared to the corresponding curves of Zank and Greaves (1995) for their single temperature electron-positron model. This is due to the contribution of the second species, which has a different temperature and hence resulting in enhanced wave dispersion. Moreover, in the

large wavelength limit (small $k\lambda_D$ values in figure 2.3) the dispersion curves display a sharp rise, which is a feature of our four component two temperature electron-positron model and differs from the results of Zank and Greaves (1995) for their single temperature electron-positron model. An increase in the cool to hot temperature ratio results in a decrease of the critical $k\lambda_D$ value at which the acoustic and cyclotron branches separate. As the propagation angle increases, the separation between the two modes widens.

A kinetic theory analysis is then used to study the acoustic mode, in particular the effect of Laudau damping, which for the parameter regime considered is due to the cooler species. Consequently, it is found that as the temperature ratio T_c/T_h increases (for fixed T_h) Landau damping increases and the overall growth rate decreases. The results show that a large enough drift velocity (V_{oh}) is required to produce wave growth. It is also noted that when the propagation angle relative to $\mathbf{B_0}$ is decreased, the growth rate is enhanced, while an increase in the magnetic field strength results in an increase in the growth rate.

Chapter 3

Small Amplitude Solitons in a Multispecies Electron-Positron Plasma

3.1 Literature Review

As pointed out in the introductory chapter, electron-positron plasmas have been suggested to appear in the magnetosphere of pulsars (Beskin *et al.*, 1983; Lominade *et al.*, 1983; Gurevich and Istomin, 1985) and near the polar cap of a rotating neutron star (Sturrock 1971, Ruderman and Sutherland, 1975). Electron-positron plasmas are generated due to the acceleration of particles to very high energies along the pulsar magnetic fields. The nonlinear wave phenomena in such plasmas have been considered to play an important role in understanding the physics of electrostatic soliton potential structures. The

nonlinear behaviour of waves propagating in electron-positron plasmas has been investigated in a number of studies. For instance, Gedalin *et al.* (1985) investigated nonlinear wave conversions in electron-positron plasmas in a very strong magnetic field. They showed that the nonlinear Landau damping phenomena related to Čerenkov resonances as well as cyclotron resonances, causes large-frequency shifts. Stenflo *et al.* (1985) studied the nonlinear propagation of field-aligned circularly polarized electromagnetic waves in an electron-positron plasma. They discussed the modulational instability and wave localization and showed that a new class of cusped solitons are possible. Due to multidimensional effects, Yu *et al.* (1986) showed that a new class of nonlinear structures, namely the travelling Alfvén vortex, can also exist in strongly magnetized electron-positron plasmas. Bharuthram (1992) investigated the existence of double layers in an unmagnetized electron-positron plasma. This asymmetric model consisted of hot and cool electrons and hot positrons, all of which were assumed to be Boltzmann-distributed, while the cold positrons, treated as very cold, were described by the fluid equations. Pillay and Bharuthram (1992) then investigated the possibility of large amplitude solitons where both the cold electrons and positrons, which are strictly cold, were described by the fluid equations. Verheest *et al.* (1996), considered an unmagnetized symmetric two-temperature electron-positron plasma with equal electron and positron densities of the cool species at temperature T_c, and similarly equal densities of the two hot species at temperature T_h. They described the two hot species by the Boltzmann distribution and treated the two cool species as fluid. The Sagdeev potential method was used to explore

the existence and properties of non-linear, arbitrary amplitude electrostatic potential structures. The Boltzmann assumption was shown to impose upper limits on the density and temperature of the cool species, and hence only small amplitude soliton structures were found to be possible. Misra and Chowdhury (2003), investigated the nonlinear interaction of electromagnetic pulses in an electron-positron plasma and showed that the electromagnetic wave envelope is governed by a coupled Schrodinger equation which also possesses solitary wave like solutions.

Nonlinear low frequency structures have also been studied in electron-ion plasmas. For instance, in one of the earlier studies, Shukla and Yu (1978) investigated a two component magnetized electron-ion plasma. They found that finite amplitude ion acoustic solitary waves propagate obliquely to an external magnetic field. More recently, these structures have been studied in three component plasmas consisting of electrons, ions and positrons. Popel *et al.* (1995) showed that the presence of positrons in an unmagnetized plasma, in the supersonic region, decreased the amplitude of the usual ion acoustic soliton in electron-ion plasmas. It is interesting to note that in a magnetized electron-positron-ion plasma, and in the subsonic region, the presence of positrons increased the ion-acoustic soliton amplitude (Mahmood *et al.*, 2003).

In this chapter, the properties of nonlinear electron-positron solitons in a magnetized, two-temperature, electron-positron plasma, allowing for propa-

gation at oblique angles to the magnetic field are investigated. The symmetric four component, two-temperature pair plasma formed by the mixing of two simple pair plasmas with different temperatures, could exist on a timescale shorter than the thermalization time. Using the reductive-perturbation technique, a modified Korteweg-de Vries-Zakharov-Kuznetsov (mKdV-ZK) equation for solitary structures is derived. The structures are then studied as a function of the plasma parameters. The results presented in the following sections has already been published in the Journal of Plasma Physics (Lazarus *et al.*, 2008)(see Appendix E).

3.2 Theory

The model considered is a homogeneous magnetized, four component electron-positron plasma, consisting of cool electrons and positrons with equal temperatures and equilibrium densities denoted by T_c and N_c, respectively, and hot electrons and positrons with equal temperatures and equilibrium densities denoted by T_h and N_h, respectively. Note that the electron distribution function may be made up of a number of distribution functions with different characteristics, e.g. having different values of $n_\alpha(\mathbf{x}, t)$, $\mathbf{v}_\alpha(\mathbf{x}, t)$, $T_\alpha(\mathbf{x}, t)$, etc. Thus, for instance, the electrons may be made up of two 'subspecies' of electrons, primary and secondary, generated by different mechanisms, and with different temperatures. On a timescale short compared to the electron thermalization time, the distribution function could then be bi-Maxwellian, with two different temperatures. Wave propagation is at an angle θ to the

ambient magnetic field $\mathbf{B}_o$, which is taken in the x-direction.

Charge neutrality at equilibrium requires for each species that

$$N_c + N_h = N_0 \ . \tag{3.1}$$

In this model the hot isothermal species have a Boltzmann distribution given by,

$$n_{eh} = N_h \exp\left(\frac{e\phi}{T_h}\right) \tag{3.2}$$

and

$$n_{ph} = N_h \exp\left(\frac{-e\phi}{T_h}\right), \tag{3.3}$$

where n_{eh} (n_{ph}) is the density of the hot electrons (positrons) and ϕ is the electrostatic potential.

The dynamics of the cooler adiabatic species, denoted by the running subscript α are governed by the fluid equations, namely,

the continuity equations,

$$\frac{\partial n_\alpha}{\partial t} + \nabla.(n_\alpha \mathbf{v}_\alpha) = 0 \ , \tag{3.4}$$

the equations of motion,

$$\frac{\partial \mathbf{v}_\alpha}{\partial t} + \mathbf{v}_\alpha.\nabla \mathbf{v}_\alpha + \frac{1}{n_\alpha m_\alpha}\nabla p_\alpha = -\frac{q_\alpha}{m_\alpha}\nabla\phi + \Omega_\alpha \mathbf{v}_\alpha \times \mathbf{e}_x \ , \tag{3.5}$$

and the adiabatic pressure equations,

$$\frac{\partial p_\alpha}{\partial t} + \mathbf{v}_\alpha.\nabla p_\alpha + \gamma_\alpha p_\alpha \nabla.\mathbf{v}_\alpha = 0 \ . \tag{3.6}$$

The system is closed by the Poisson equation

$$\varepsilon_0 \nabla^2 \phi + \sum_\alpha n_\alpha q_\alpha + \sum_\beta N_\beta q_\beta \exp\left[\frac{-q_\beta \phi}{T_\beta}\right] = 0 \ , \tag{3.7}$$

where n_α, $\mathbf{v}_\alpha$ and p_α are the densities, fluid velocities and pressures, respectively, of the cooler species. Here q_α (q_β) = -e +(e) for electrons (positrons), are the charges of the cool (hot) species and $m = m_e = m_p$ is the common mass of the electrons and the positrons. The adiabatic compression indices are denoted by γ_α and the gyrofrequencies by $\Omega_\alpha = q_\alpha B_o/m$.

The dispersion relation for linear waves for electron-positron plasmas is found by linearizing equations (3.2) − (3.7), where the spatio-temporal variations are assumed to be $\propto \exp[i(\mathbf{k}.\mathbf{x} - \omega t)]$. From the continuity equation (3.4), one finds

$$n_{1\alpha} = \frac{N_\alpha}{\left(\omega - k_\parallel V_\alpha\right)} \left[k_\parallel v_{1\alpha x} + k_\perp v_{1\alpha y}\right] \ , \tag{3.8}$$

and from the pressure equation (3.6),

$$p_{1\alpha} = \frac{\gamma_\alpha P_\alpha n_{1\alpha}}{N_\alpha} \ , \tag{3.9}$$

where V_α is defined as the equilibrium drift of the α-species along the external magnetic field, P_α the equilibrium pressure, $k_\parallel$ and $k_\perp$ are the components of the wavenumber parallel and perpendicular to the direction of the static magnetic field respectively, $v_{1\alpha x}$ and $v_{1\alpha y}$ are the perturbed velocities in the x and y directions respectively, $n_{1\alpha}$ is the perturbed density, and $p_{1\alpha}$ is the perturbed pressure.

Linearization of the equations of motion (3.5) in the x, y and z directions, yields,

$$v_{1\alpha x} = \frac{\dfrac{q_\alpha}{m_\alpha} k_\parallel \phi + v_{t\alpha}^2 \dfrac{n_{1\alpha}}{N_\alpha} k_\parallel}{\left(\omega - k_\parallel V_\alpha\right)} \ , \tag{3.10}$$

$$v_{1\alpha y} = \frac{\dfrac{q_\alpha}{m_\alpha} k_\perp \phi + v_{t\alpha}^2 \dfrac{n_{1\alpha}}{N_\alpha} k_\perp}{\dfrac{\left(\omega - k_\parallel V_\alpha\right)^2 - \Omega_\alpha^2}{\left(\omega - k_\parallel V_\alpha\right)}} \ , \tag{3.11}$$

and

$$v_{1\alpha z} = \frac{\Omega_\alpha}{i\left(\omega - k_\parallel V_\alpha\right)} v_{1\alpha y} \ . \tag{3.12}$$

Hence, the perturbed density becomes,

$$n_{1\alpha} = \frac{\dfrac{\varepsilon_0}{q_\alpha} \omega_{p\alpha}^2 \left(k^2 \hat{\omega}_\alpha^2 - k_\parallel^2 \Omega_\alpha^2\right)}{\hat{\omega}_\alpha^4 - \hat{\omega}_\alpha^2 \left(k^2 v_{t\alpha}^2 + \Omega_\alpha^2\right) + k_\parallel^2 v_{t\alpha}^2 \Omega_\alpha^2} \ . \tag{3.13}$$

Substituting the above into Poisson's equation (3.7), yields the linear dispersion relation for an electron-positron plasma,

$$\sum_\alpha \frac{\omega_{p\alpha}^2 \left(k^2 \hat{\omega}_\alpha^2 - k_\parallel^2 \Omega_\alpha^2\right)}{\hat{\omega}_\alpha^4 - \hat{\omega}_\alpha^2 \left(k^2 v_{t\alpha}^2 + \Omega_\alpha^2\right) + k_\parallel^2 v_{t\alpha}^2 \Omega_\alpha^2} = k^2 + \sum_\beta \frac{1}{\lambda_{D\beta}^2} \ . \tag{3.14}$$

It is noted that this is similar in form to the dispersion relation for linear modes obtained by Verheest *et al.*, (2002) for multi-fluid plasmas. Here, the plasma frequencies $\omega_{p\alpha}$, the Debye lengths $\lambda_{D\beta}$ and thermal velocities $v_{t\alpha}$

for the species α are defined as $\omega_{p\alpha}^2 = N_\alpha q_\alpha^2/\varepsilon_0 m$, $\lambda_{D\beta}^2 = \varepsilon_0 T_\beta/N_\beta q_\beta^2$ and $v_{t\alpha}^2 = \gamma_\alpha P_\alpha/N_\alpha m$, respectively. The Doppler-shifted wave frequencies are defined as $\widehat{\omega}_\alpha = \omega - k_\parallel V_\alpha$.

For the electron-positron plasma, equation (3.14) reduces to

$$\frac{\omega_{pc}^2 \lambda_{Dh}^2 \left(k^2\omega^2 - k^2\Omega^2 \cos^2\theta\right)}{\omega^4 - \omega^2\left(k^2 v_{tc}^2 + \Omega^2\right) + k^2\Omega^2 \cos^2\theta v_{tc}^2} = 1 + \frac{1}{2}k^2\lambda_{Dh}^2, \tag{3.15}$$

which may be written as

$$\omega^4 - \omega^2\left(\Omega^2 + k^2 v_{tc}^2 + \frac{k^2 v_{ea}^2}{1 + \frac{1}{2}k^2\lambda_{Dh}^2}\right) + \Omega^2\cos^2\theta\left(k^2 v_{tc}^2 + \frac{k^2 v_{ea}^2}{1 + \frac{1}{2}k^2\lambda_{Dh}^2}\right) = 0\ , \tag{3.16}$$

where $v_{ea} = (n_{0c}/n_{0h})^{1/2} v_{th}$ is the acoustic speed. In arriving at equation (3.16) we have for simplicity set $V_\alpha = 0$. This expression for the dispersion relation is the same as equation (2.18) obtained in chapter 2, where the γ=3 factor has been incorporated into the definition of v_{tc}.

Now assuming strongly magnetized particles, and using $\omega^2 \ll (k_\parallel^2/k^2)\Omega^2$ and $\Omega \gg \omega \gg k v_{tc}$, we obtain from the general equation (3.14), the appropriate phase velocity for oblique propagation as

$$\frac{\omega}{k} = \frac{k_\parallel}{k}\left[\left(\frac{N_c}{N_h}\right)\left(\frac{\kappa T_h}{m}\right)\right]^{\frac{1}{2}}. \tag{3.17}$$

This expression is analogous in form to that of the electron-acoustic wave in an unmagnetized electron-ion plasma (Gary and Tokar, 1985) with the $(k_{\parallel}/k)$ factor reflecting the effect of the magnetic field. At parallel propagation the dispersion relation (3.14) reduces to

$$\sum_{\alpha} \frac{\omega_{p\alpha}^2}{\hat{\omega}_{\alpha}^2 - k^2 v_{t\alpha}^2} = 1 + \sum_{\beta} \frac{1}{k^2 \lambda_{D\beta}^2} = 1 + \frac{2}{k^2 \lambda_{Dh}^2} \ , \tag{3.18}$$

where $\lambda_{Dh} = (\varepsilon_0 T_h / N_h e^2)^{1/2}$, is the Debye length for the hot species. Equation (3.18) may be written as

$$\omega^2 = k^2 v_{tc}^2 + \frac{k^2 v_{ea}^2}{1 + \frac{1}{2} k^2 \lambda_{Dh}^2} \ .$$

The above expression is the same as equation (2.39) obtained in chapter 2, where the γ=3 factor has been incorporated into the definition of v_{tc}.

3.3 Nonlinear modes

We follow the method outlined by Verheest *et al.* (2002) introducing the usual KdV streched co-ordinates,

$$\rho = \epsilon^{\frac{1}{2}}(x - Vt), \qquad \eta = \epsilon^{\frac{1}{2}} y, \qquad \zeta = \epsilon^{\frac{1}{2}} z, \qquad \tau = \epsilon^{\frac{3}{2}} t, \tag{3.19}$$

and expand the fluid velocity, density, pressure and the potential by the smallness parameter ϵ as follows

$$\begin{aligned} v_{\alpha x} &= V_{\alpha 0} + \epsilon^{\frac{1}{2}} v_{1\alpha x} + \epsilon v_{2\alpha x} + \epsilon^{\frac{3}{2}} v_{3\alpha x} + ... \\ v_{\alpha y} &= \epsilon v_{1\alpha y} + \epsilon^{\frac{3}{2}} v_{2\alpha y} + \epsilon^2 v_{3\alpha y} + ... \\ v_{\alpha z} &= \epsilon v_{1\alpha z} + \epsilon^{\frac{3}{2}} v_{2\alpha z} + \epsilon^2 v_{3\alpha z} + ... \\ n_\alpha &= N_{\alpha 0} + \epsilon^{\frac{1}{2}} n_{1\alpha} + \epsilon n_{2\alpha} + \epsilon^{\frac{3}{2}} n_{3\alpha} + ... \\ p_\alpha &= P_{\alpha 0} + \epsilon^{\frac{1}{2}} p_{1\alpha} + \epsilon p_{2\alpha} + \epsilon^{\frac{3}{2}} p_{3\alpha} + ... \\ \phi &= \epsilon^{\frac{1}{2}} \phi_1 + \epsilon \phi_2 + \epsilon^{\frac{3}{2}} \phi_3 + ... \end{aligned} \tag{3.20}$$

Using equations (3.19) and (3.20) and taking equation (3.7) to order $\epsilon^{\frac{1}{2}}$ and equations $(3.4) - (3.6)$ to order ϵ and solving, yields

$$n_{1\alpha} = \left(\frac{N_{\alpha 0}^2 q_\alpha}{m N_{\alpha 0} (V - V_{\alpha 0})^2 - \gamma_\alpha P_{\alpha 0}} \right) \phi_1 \tag{3.21}$$

and

$$p_{1\alpha} = \frac{N_{\alpha 0} q_\alpha v_{t\alpha}^2}{\left[(V - V_{\alpha 0})^2 - v_{t\alpha}^2 \right]} \phi_1. \tag{3.22}$$

Substituting for $n_{1\alpha}$ into (3.7), yields

$$\sum_\alpha \frac{\omega_{p\alpha}^2}{(V - V_{\alpha 0})^2 - v_{t\alpha}^2} - \sum_\beta \frac{1}{\lambda_{D\beta}^2} = 0. \tag{3.23}$$

From the above equation, the phase velocity V can be determined.

Taking equation (3.7) to order ϵ and equations (3.4) – (3.6) to order $\epsilon^{\frac{3}{2}}$ one gets

$$p_{2\alpha} = \frac{q_\alpha N_{\alpha 0} v_{t\alpha}^2 \left(1+\gamma_\alpha\right)}{2m[(V-V_{\alpha 0})^2 - v_{t\alpha}^2]}\phi_1^2 - \frac{\gamma_\alpha P_{\alpha 0}}{(V-V_{\alpha 0})} v_{2\alpha x}, \tag{3.24}$$

$$v_{2\alpha x} = \frac{-q_\alpha (V-V_{\alpha 0})}{m[(V-V_{\alpha 0})^2 - v_{t\alpha}^2]}\phi_2 - \frac{q_\alpha^2 (V-V_{\alpha 0})\left[[(V-V_{\alpha 0})^2 - v_{t\alpha}^2] + v_{t\alpha}^2\left(1+\gamma_\alpha\right)\right]}{2m^2[(V-V_{\alpha 0})^2 - v_{t\alpha}^2]^3}\phi_1^2, \tag{3.25}$$

and

$$n_{2\alpha} = \frac{q_\alpha N_{\alpha 0}}{m[(V-V_{\alpha 0})^2 - v_{t\alpha}^2]}\phi_2 + \frac{q_\alpha^2 N_{\alpha 0}\left[3[(V-V_{\alpha 0})^2 - v_{t\alpha}^2] + v_{t\alpha}^2\left(1+\gamma_\alpha\right)\right]}{2m^2[(V-V_{\alpha 0})^2 - v_{t\alpha}^2]^3}\phi_1^2. \tag{3.26}$$

Substituting for $n_{2\alpha}$ into Poisson's equation, results in

$$\mathcal{D}\phi_2 + B\phi_1^2 = 0 \tag{3.27}$$

where

$$\mathcal{D} = \sum_\alpha \frac{\omega_{p\alpha}^2}{[(V-V_{\alpha 0})^2 - v_{t\alpha}^2]} - \sum_\beta \frac{1}{\lambda_{D\beta}^2} \tag{3.28}$$

and

$$B = \sum_\alpha \frac{\omega_{p\alpha}^2 q_\alpha [3(V-V_{\alpha 0})^2 + (\gamma_\alpha - 2)v_{t\alpha}^2]}{2m[(V-V_{\alpha 0})^2 - v_{t\alpha}^2]^3} + \frac{1}{2}\sum_\beta \frac{q_\beta}{\lambda_{D\beta}^2 T_\beta}. \tag{3.29}$$

This expression for B differs slightly from that of Verheest *et al.* (2002). In fact, having carried out the calculation *ab initio*, equation (3.29) is highlighted as a correction of the equivalent equation given by Verheest *et al.*

(2002) (equation (18)). The factor '2' in the denominator of the first term and the '$\frac{1}{2}$' in the second term of equation (3.29) was omitted in their equation. Using (3.23) implies $\mathcal{D} = 0$, hence the first term in (3.27) vanishes, which means either $B = 0$ or $\phi_1 = 0$. For the electron-positron model, one can easily show that $B = 0$ if the cool electrons and positrons have equal drifts. Then $\phi_1 \neq 0$, which will naturally lead to a modified KdV-ZK type of equation for ϕ_1.

Taking Poisson's equation to order $\epsilon^{\frac{3}{2}}$ and the continuity, momentum and pressure equations to order ϵ^2, and solving simultaneously, the following mKdV-ZK equation is obtained (Verheest *et al.*, 2002),

$$\frac{\partial \phi_1}{\partial \tau} + a\,\frac{\partial^3 \phi_1}{\partial \rho^3} + c\,\phi_1^2 \frac{\partial \phi_1}{\partial \rho} + d\,\frac{\partial}{\partial \rho}\left(\frac{\partial^2 \phi_1}{\partial \eta^2} + \frac{\partial^2 \phi_1}{\partial \zeta^2}\right) = 0. \tag{3.30}$$

where the coefficients a, c and d are given by

$a = \frac{1}{A}$, $\qquad c = \frac{C}{A}$, $\qquad d = \frac{D}{A}$,

with

$$A = 2\sum_{\alpha} \frac{\omega_{p\alpha}^2 (V - V_{\alpha 0})}{\left[(V - V_{\alpha 0})^2 - v_{t\alpha}^2\right]^2}\ , \tag{3.31}$$

$$C = \frac{1}{2}\sum_{\alpha} \frac{\omega_{p\alpha}^2 q_\alpha^2 \left[15(V - V_{\alpha 0})^4 + E_1 (V - V_{\alpha 0})^2 v_{t\alpha}^2 + E_2 v_{t\alpha}^4\right]}{m^2 \left[(V - V_{\alpha 0})^2 - v_{t\alpha}^2\right]^5} - \frac{1}{2}\sum_{\beta} \frac{q_\beta}{\lambda_{D\beta}^2 T_\beta^2}\ , \tag{3.32}$$

and

$$D = 1 + \sum_{\alpha} \frac{\omega_{p\alpha}^2 (V - V_{\alpha 0})^4}{\Omega_{\alpha}^2 [(V - V_{\alpha 0})^2 - v_{t\alpha}^2]^2} \ , \tag{3.33}$$

where $E_1 = {\gamma_\alpha}^2 + 13\gamma_\alpha - 18$ and $E_2 = 2{\gamma_\alpha}^2 - 7\gamma_\alpha + 6$.

We look for a one-soliton planar solution propagating at an angle θ to the static magnetic field. The running phase argument for stationary non-linear solutions is

$$\sigma = \rho \ \cos\theta + \eta \ \sin\theta\cos\psi + \zeta \ \sin\theta\sin\psi - M\tau \ , \tag{3.34}$$

where ψ is the second angle in spherical co-ordinates and M is the soliton velocity.

Then the mKdV-ZK equation reduces to

$$(c \ \cos\theta \ \phi_1^2 - M)\frac{\partial\phi_1}{\partial\sigma} + \alpha\frac{\partial^3\phi_1}{\partial\sigma^3} = 0, \tag{3.35}$$

where $\alpha = (a \ \cos^2\theta + d \ \sin^2\theta)\cos\theta$.

Using the standard technique (Nicholson, 1983) to solve (3.35), yields,

$$\phi_1 = \sqrt{\frac{6M}{c \ \cos\theta}}\mathrm{sech}(\mu\sigma) \ , \tag{3.36}$$

where

$$\mu^2 = \frac{M}{(a \ \cos^2\theta + d \ \sin^2\theta)\cos\theta} \ .$$

We now adopt the following normalizations, the electrostatic potential ϕ by T_h/e, the fluid speeds v_α by the thermal velocity $v_{th} = (T_h/m)^{1/2}$, the particle density by the equilibrium plasma density N_0, the spatial length by $\lambda_{Dh} = (\frac{\varepsilon_0 T_h}{N_h e^2})^{1/2}$ and the time by $\omega_{ph}^{-1} = (\frac{N_h e^2}{\varepsilon_0 m})^{-1/2}$.

Using $\widehat{\ }$to indicate normalized variables, it follows that the normalized electrostatic potential, (3.36) becomes

$$\widehat{\phi} = \phi_m \text{sech}(\widehat{\mu}\ \widehat{\sigma})\ , \tag{3.37}$$

where the normalized soliton amplitude is given explicitly by

$$\phi_m = \left[\frac{6\left(\frac{N_c}{N_h}\right)^{\frac{7}{2}} \left[1 + \left(\frac{T_c}{T_h}\right)\left(\frac{N_c}{N_h}\right)^{-1}\right]^{\frac{1}{2}} \widehat{M}}{\left[F + E_2\left(\frac{T_c}{T_h}\right)^2 - \left(\frac{N_c}{N_h}\right)^4\right]\cos\theta} \right]^{\frac{1}{2}}\ , \tag{3.38}$$

and

$$\mu^2 = \left[\frac{\widehat{M}}{\left(\left[\left(\frac{N_c}{N_h}\right) + \left(\frac{T_c}{T_h}\right)\left(\frac{N_c}{N_h}\right)^{-2}\right]^{-\frac{1}{2}} + \left(\frac{2}{\Lambda^2}\right)\left[\frac{N_c}{N_h} + \frac{T_c}{T_h}\right]^{\frac{3}{2}} \sin^2\theta \right)\cos\theta} \right]\ , \tag{3.39}$$

where

$$F = 15\left(\frac{N_c}{N_h}\right)^2 \left[1 + \left(\frac{T_c}{T_h}\right)\left(\frac{N_c}{N_h}\right)^{-1}\right]^2 + E_1\left(\frac{T_c}{T_h}\right)\left(\frac{N_c}{N_h}\right)\left[1 + \left(\frac{T_c}{T_h}\right)\left(\frac{N_c}{N_h}\right)^{-1}\right]$$

and

$$\Lambda^2 = \frac{\Omega^2}{\omega_{ph}^2} \ .$$

3.4 Numerical Results and Limitations

3.4.1 Limitations of the Model

The calculations in the previous section are based on a reductive perturbation expansion, and thus are valid only for small normalized soliton amplitude, where the 'natural' normalization energy is associated with $T_{eff} = N_0 T_c T_h/(N_c T_h + N_h T_c)$. The hot species are assumed to have a Boltzmann distribution, and the cool species behave adiabatically and are governed by the fluid equations. This implies that there are two further limits imposed on our model. For the cool species, we ensure that the thermal velocity is much less than the phase velocity of the fluctuation, i.e. $v_{tc} \ll v_{ph}$, and the Boltzmann assumption requires that the thermal velocity of the hot species is much larger than the phase velocity, i.e. $v_{ph} \ll v_{th}$. Hence the model can only be applied if $v_{tc} \ll v_{ph} \ll v_{th}$. Using expression (3.17) for v_{ph} this becomes,

$$\sqrt{\frac{T_c}{T_h}} \ll \frac{k_\parallel}{k}\sqrt{\frac{N_c}{N_h}} \ll 1 \ . \tag{3.40}$$

This means that upper limits are imposed on both the temperature ratio (T_c/T_h) and the particle density ratio (N_c/N_h).

3.4.2 Numerical Results

In this section a parametric study of the soliton dependence on plasma variables is undertaken, as some of the features are not transparent from equations $(3.37) - (3.39)$. Figure 3.1 shows the typical soliton potential profile as a function of the propagation angle θ. For simplicity we set $V_{\alpha 0} = 0$ for all species. For each angle θ, the profile has a maximum at $\sigma = 0$ (as may be seen also from equation (3.37). As θ is increased, the amplitude increases and the half-width decreases, the effect being more significant for larger propagation angles. The former follows from the $1/\sqrt{\cos\theta}$ dependence of (3.38), the latter from the $1/[(G + H\sin^2\theta)\cos\theta]$ behaviour of (3.39). Here G and H are functions of the density ratio, the temperature ratio and the gyrofrequency. Figure 3.2 is a plot of the soliton amplitude as a function of θ. The graph shows that the soliton amplitude increases monotonically with θ, as may also be deduced from the behaviour observed in figure 3.1. It is noted that the approximation used in the derivation may restrict validity to $k_\parallel < k_\perp$, which implies that the results are more relevant for larger angles of propagation (small $k_\parallel$). Figure 3.3 shows the variation of the soliton amplitude with the equilibrium density ratio N_c/N_h, for various temperature ratios T_c/T_h. N_c (N_h) are the equilibrium densities of the cool (hot) electron and positron species. It is seen that as the ratio of the cool to hot equilibrium densities is increased, the soliton amplitude increases. Although a large range of solitons is shown to be possible, the limits imposed by this model demand that $k_\parallel/k\sqrt{N_c/N_h} \ll 1$, i.e. $N_c/N_h < 0.25$ for $\theta = 15^o$. This is similar to the

results of Verheest *et al.* (1996), where solitons were found to be possible for low values of the density ratio and are of small amplitude ($\phi_m < 0.2$). For a fixed N_c/N_h, the amplitude ϕ_m is larger for smaller values of the ratio of the cool to hot temperatures. This is clearer in figure 3.4, where it is seen that ϕ_m decreases as the temperature ratio increases for a chosen density ratio. It is also noted that as the temperature ratio decreases, the plasma moves further away from a state of thermodynamic equilibrium, thereby making it easier to generate nonlinear soliton structures with a correspondingly larger amplitude. Figure 3.5 shows the maximum soliton amplitude as a function of the soliton velocity for a cut off value of $N_c/N_h = 0.25$. The fixed parameters are $\theta = 15^o$ and $\gamma_\alpha = 3$. The soliton amplitude increases as the temperature ratio T_c/T_h tends to zero.

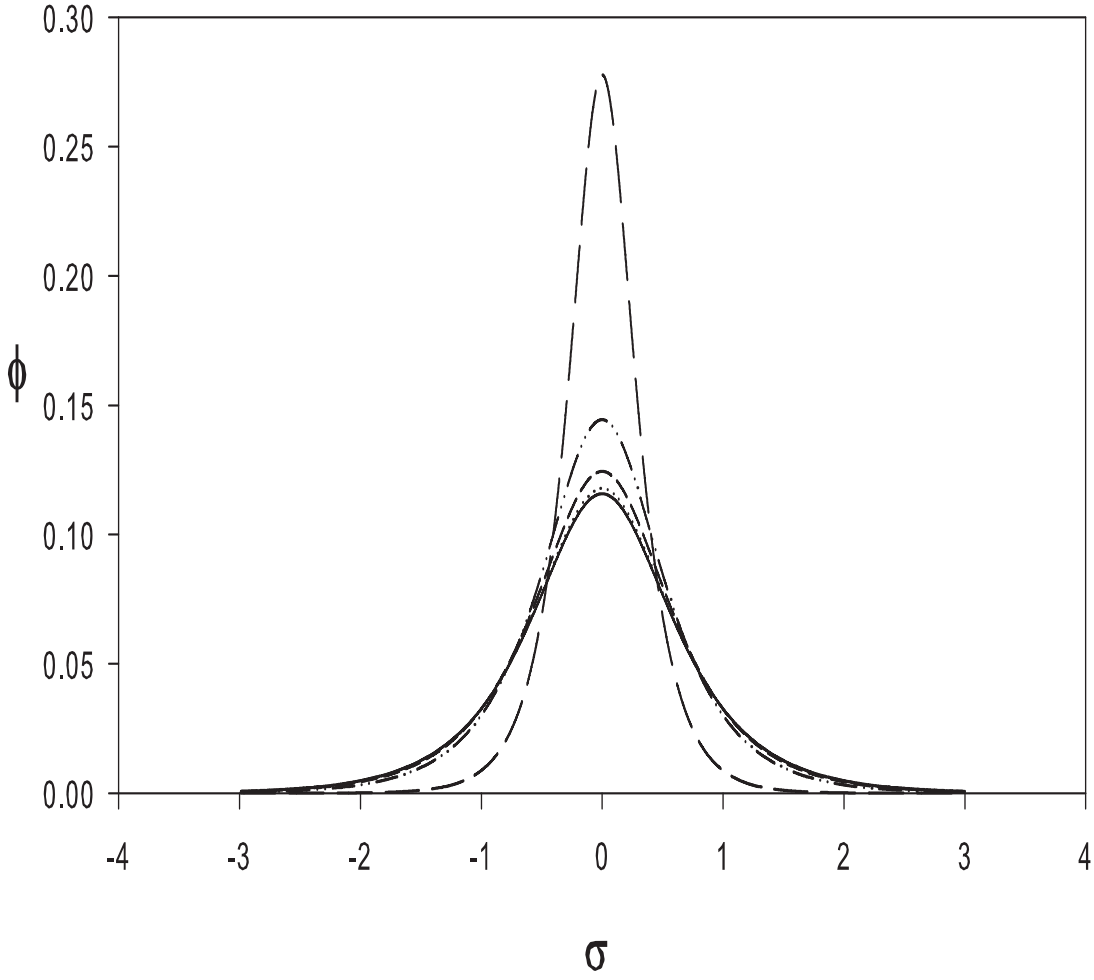

Figure 3.1: The soliton profile ϕ for different angles of propagation θ. The curves correspond to $\theta = 0^o$ (solid), 15^o (dotted), 30^o (broken), 50^o (dashddot) and 80^o (longbroken). The fixed plasma parameters are $M = 1.2$, $T_c/T_h = 0.01$, $N_c/N_h = 1/9$ and $\gamma_\alpha = 3$.

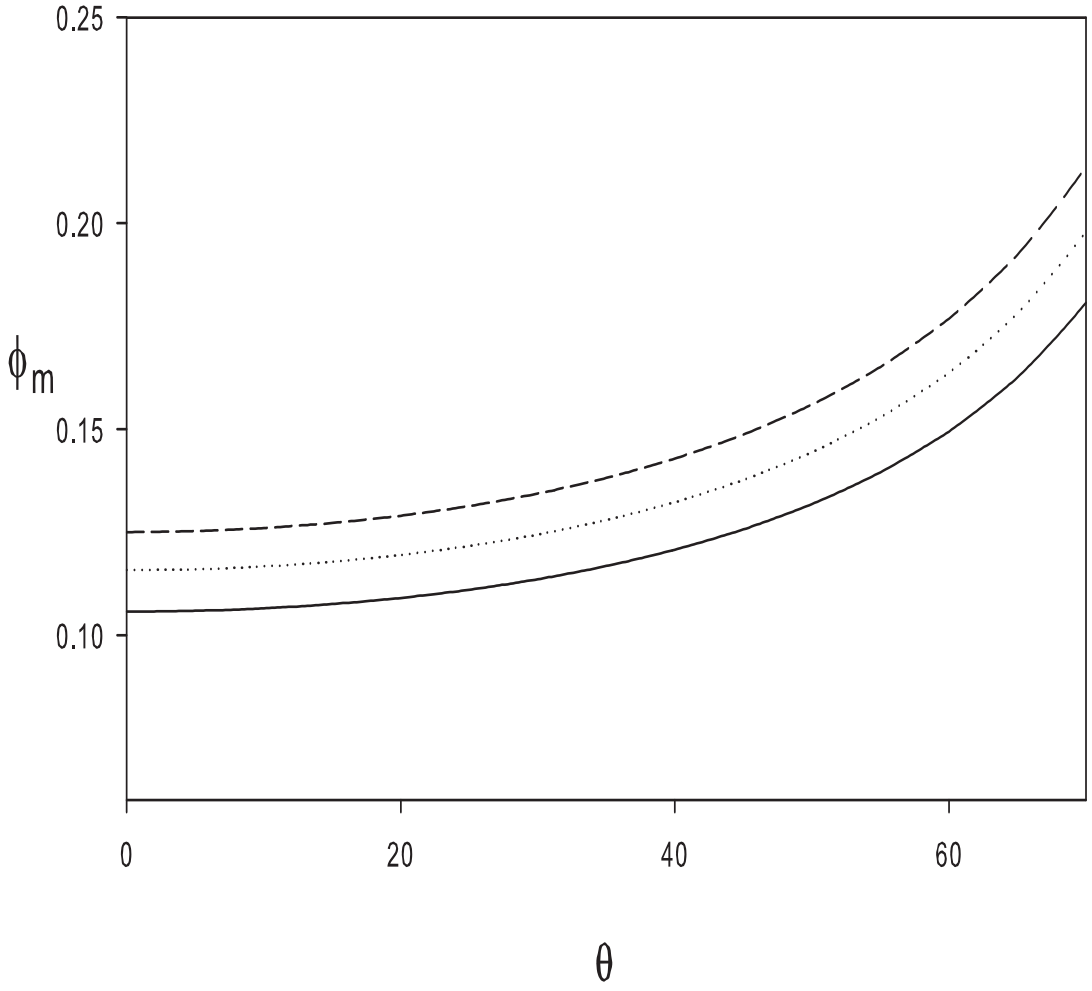

Figure 3.2: The variation of the soliton amplitude ϕ_m as a function of the propagation angle θ for different normalized soliton velocities $M = 1.0$ (solid), 1.2 (dotted) and 1.4 (broken). The fixed plasma parameters are $N_c/N_h = 1/9$, $T_c/T_h = 0.01$ and $\gamma_\alpha = 3$.

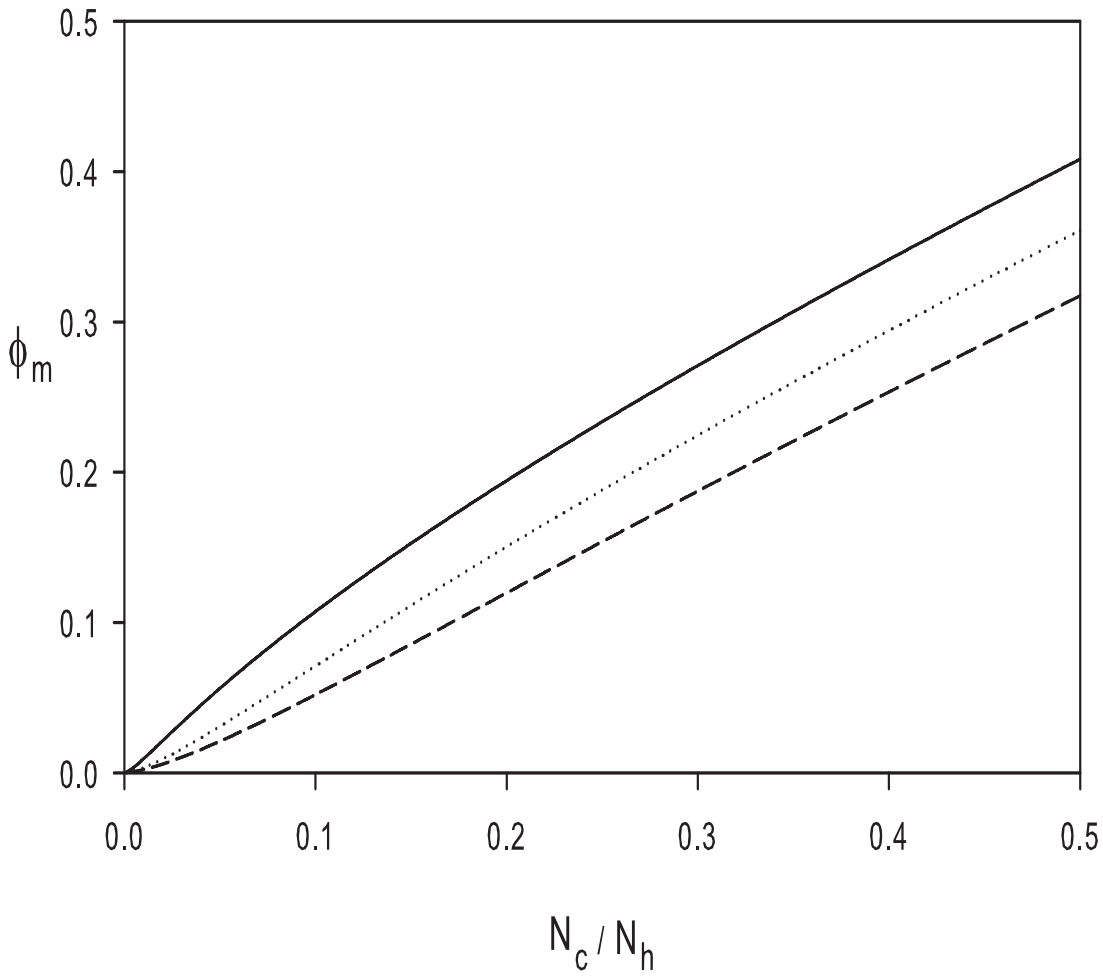

Figure 3.3: The variation of the soliton amplitude ϕ_m as a function of N_c/N_h. The curves correspond to the temperature ratio $T_c/T_h = 0.01$ (solid) , 0.05 (dotted) and 0.1 (broken). The fixed plasma parameters are $M = 1.2$, $\theta = 15^o$ and $\gamma_\alpha = 3$.

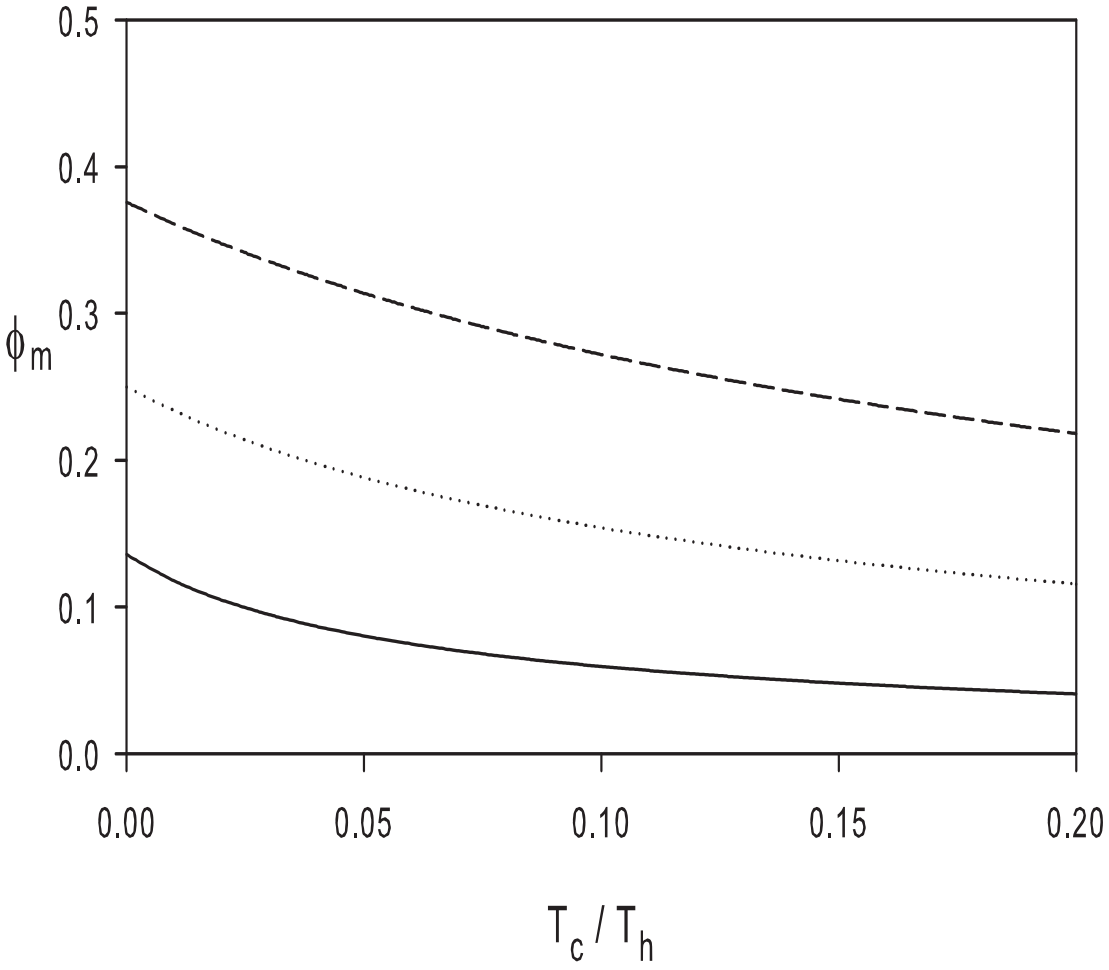

Figure 3.4: The variation of the soliton amplitude ϕ_m as a function of T_c/T_h. The curves correspond to $N_c/N_h = 0.11$ (solid), 0.25 (dotted), 0.43 (broken). The fixed plasma parameters are $M = 1.2$, $\theta = 15^o$ and $\gamma_\alpha = 3$.

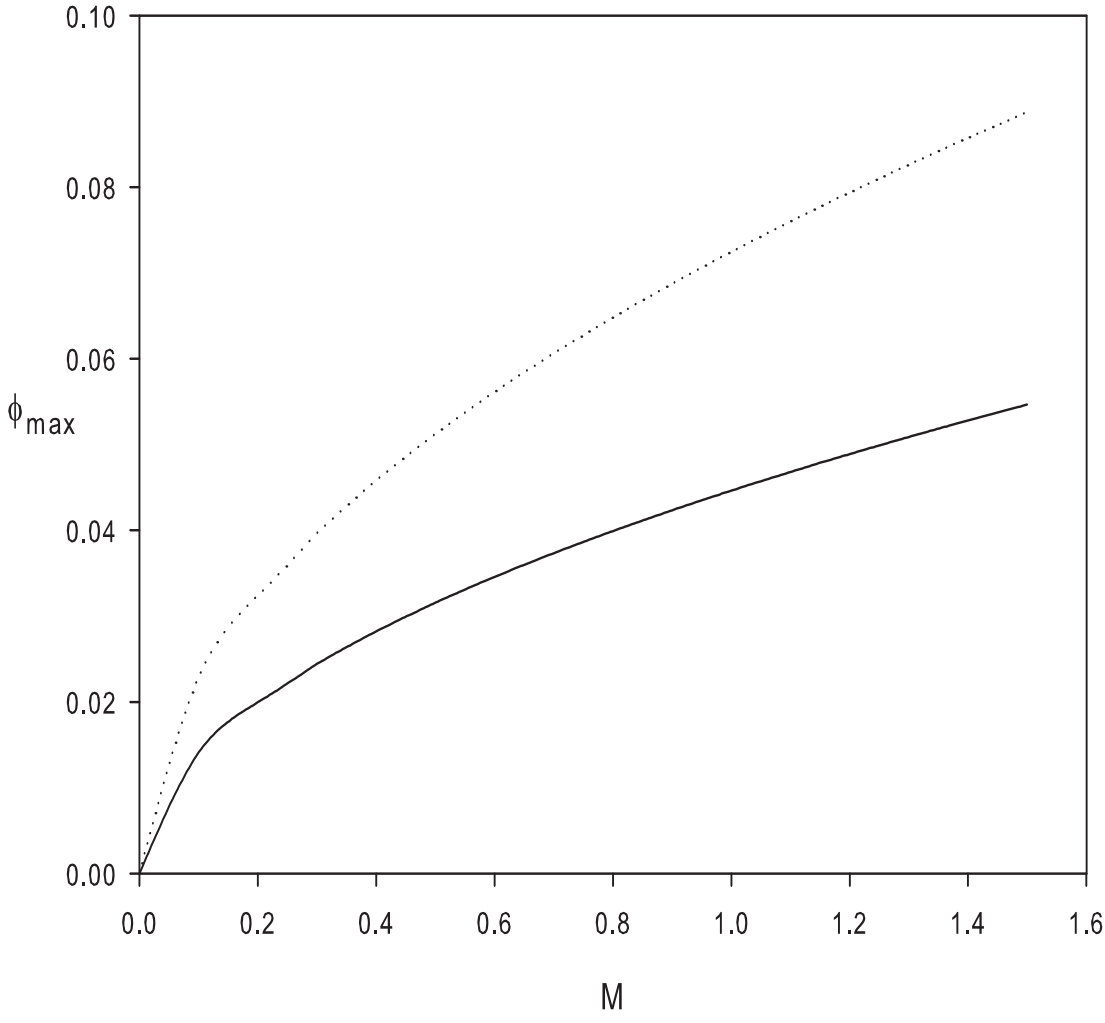

Figure 3.5: The maximum soliton amplitude ϕ_m as a function of M for $N_c/N_h = 0.25$. The curves correspond to $T_c/T_h = 0.1$ (solid) and 0.01 (dotted). The fixed parameters are $\theta = 15^o$ and $\gamma_\alpha = 3$.

3.5 Discussion

In this chapter the existence of solitary waves in a magnetized four component two-temperature electron-positron plasma propagating obliquely to the ambient magnetic field $\mathbf{B}_o$ is investigated. This model is a symmetric one with equal equilibrium densities N_h and N_c, and temperatures T_h and T_c, for the hot and cool electrons and positrons respectively. The hot species are described by the Boltzmann density distribution and the cooler species by the fluid equations with finite temperatures. The reductive perturbation technique was used to derive the modified KdV-ZK (mKdV-ZK) equation for nonlinear electrostatic modes. An exact analytical solution was determined for the soliton potential structures. Due to the symmetry of the model, double layers are not possible. Double layers can only be found if there is an asymmetry in the system. Numerical results are presented showing that the soliton amplitudes are functions of plasma parameters such as the propagation angle θ, N_c/N_h and T_c/T_h. Due to the use of the reductive perturbation approach and the limitations imposed by the model, i.e. $v_{tc} \ll \omega/k \ll v_{th}$, only small amplitude solitons can be considered. Propagation at larger angles to $\mathbf{B}_o$ are found to enhance the soliton amplitude. As N_c/N_h, the ratio of the cool to hot species was increased, the soliton amplitude increased. The soliton amplitude also increases as the plasma moves away from a state of thermal equilibrium, i.e. as T_c/T_h is decreased. Given that a non-relativistic analysis is presented, the results could be of relevance to astrophysical electron-positron plasmas produced through cooling by cyclotron emission, and in

laboratory experiments, arising from pair production by ultra-intense laser pulses (Liang *et al.*, 1998) or in beam generated electron-positron plasmas (Greaves and Surko, 1995). Finally, cognisance should be taken of the difference between the work presented here and that of Verheest *et al.*, (2002). The latter paper sets up a general formalism, which is in principle applicable to acoustic solitons in a wide variety of multi-species plasmas. They then apply it to a number of examples of KdV-ZK cases, but do not consider an electron-positron plasma, nor do they discuss examples of mKdV-ZK solitons. The results of the work done in this chapter have been published in the Journal of Plasma Physics (Lazarus *et al.*, 2008)(see Appendix E) and are consistent with those reported by several authors in their independent studies (Choi *et al.*, 2005; Tagare *et al.*, 2004; Ghosh and Lakhina, 2004; Farid *et al.*, 2001).

Chapter 4

Arbitrary Amplitude Electrostatic Solitary Waves in a Four Component Electron-Positron Plasma

4.1 Literature Review

Various spacecraft observations have established the presence of a class of broadband electrostatic noise (BEN) in several regions of the earth's magnetosphere. The broadband electrostatic noise has been detected in the magnetopause region (Matsumoto *et al.*, 1994; Cattell *et al.*, 2002), the plasma sheet boundary (Frantz *et al.*, 1998; Matsumoto *et al.*, 1999; Cattell *et al.*, 1999), foreshock region (Scarf *et al.*, 1970; Greenstadt and Fedricks, 1979),

bow shock (Matsumoto *et al.*, 1997; Bale *et al.*, 1998), auroral acceleration region (Teremin *et al.*, 1982; Mozer *et al.*, 1997; Ergun *et al.*, 1998; Bounds *et al.*, 1999), the polar cap boundary (Tsurutani *et al.*, 1998), within the solar wind (Magenay *et al.*, 1999) and at high altitude cusp injections (Cattell *et al.*, 2001b).

Many theoretical models have been studied in order to explain the broad-band electrostatic noise (BEN) observed in the earths magnetosphere. The first theoretical study of BEN in the geomagnetic tail was presented by Huba *et al.* (1978). Although the lower-hybrid drift instability in their study produced frequencies ranging up to the lower-hybrid frequency, they could not account for BEN, especially the high frequency component. Ion-beam generated electrostatic instabilities in the plasma sheet boundary layer were studied by Grabbe and Eastman (1984), Grabbe (1985), Omidi *et al.* (1985) and Ashour-Abdalla and Okuda (1986a). They found that a broad range of ESWs could be excited with an upper limit near the electron plasma frequency. Later Schriver and Ashour-Abdalla (1987) included the cold electron component in their model and found that the electron-acoustic instability became excited, hence addressing the high frequency component of BEN. Schriver and Ashour-Abdalla (1989) then investigated cold electron-beam driven electrostatic waves with hot background electrons. The low frequency component of the wave was found to be driven by the ion-acoustic wave and the high frequency component by the electron-acoustic wave. Singh *et al.* (2001), examined a four-component unmagnetized plasma consisting of stationary

cold and hot electrons, a drifting electron beam and ions. They solved the electrostatic linear dispersion relation for electron-acoustic waves and used their results to explain BEN observations below the total electron plasma frequencies in the dayside auroral zone and other regions of the magnetosphere. Earlier Bharuthram and Shukla (1988) examined the nonlinear properties of low-frequency electron-acoustic waves in a three-component magnetized plasma having hot electrons, hot ions and a cold electron component. They found that the spectrum cascade process by three-wave interactions within the electron-acoustic wave turbulence can extend the low-frequency range as well as account for the high-frequency component of BEN.

Satellite observations have also shown the existence of ESWs as part of BEN in different regions of the earth's magnetosphere. These ESWs have been observed by spacecrafts GEOTAIL (Matsumoto *et al.*, 1994, 1997; Kojima *et al.*, 1999; Deng *et al.*, 2006), POLAR (Frantz *et al.*, 1998; Cattell *et al.*, 2003) and FAST (Ergun *et al.*,1998). These ESWs are characterized by their solitary bipolar pulses and consist of small scale, large amplitude parallel electric fields (component of electric field parallel to the background magnetic field). They have been identified to have frequencies up to and higher that of the electron plasma and cyclotron frequencies. These large amplitude spiky structures have been interpreted in terms of either solitons (Temerin *et al.*, 1982) or isolated electron holes in the phase space corresponding to positive electrostatic potential (Omura *et al.*, 1994).

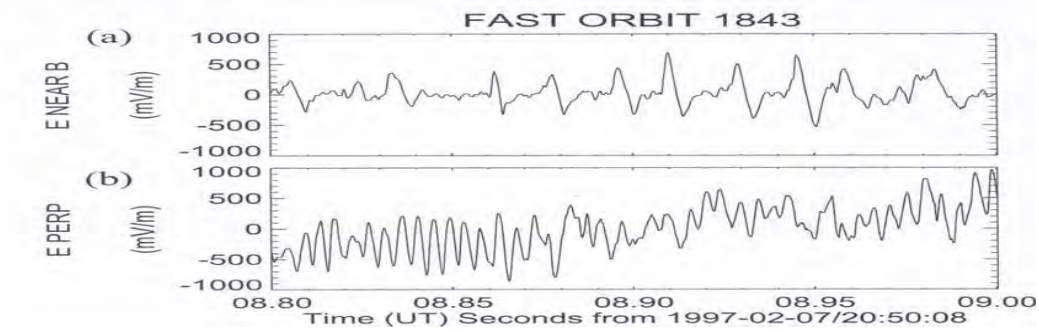

Parallel and perpendicular electric field structures observed by the FAST satellite (Ergun *et al.*, 1998).

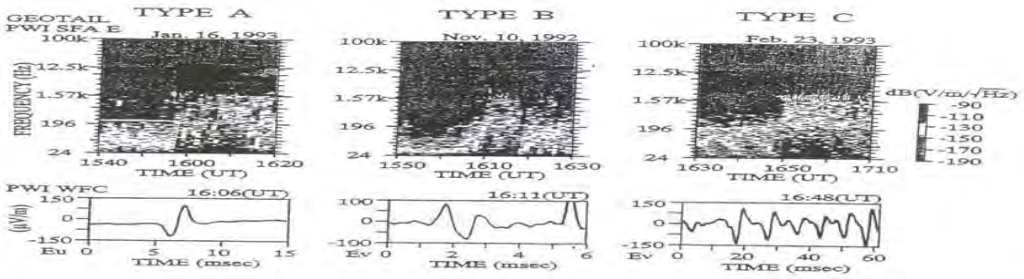

Three types of BEN wave forms and their corresponding dynamic spectra. TYPE A is the most frequently observed (Matsumoto *et al.*, 1994).

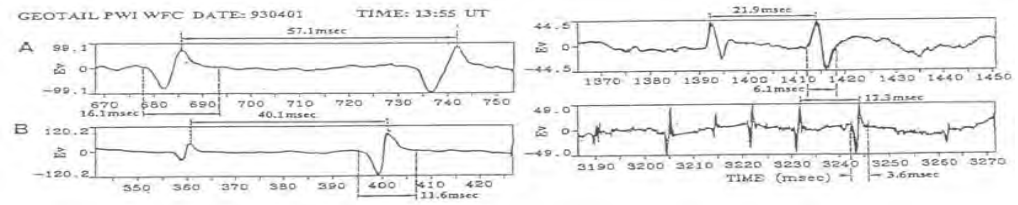

Figure showing the pulse widths and repetition periods, in particular the *w/T* ratio obtained by (Kojima *et al.*, 1994).

Figure 4a. Typical waveforms from FAST and GEOTAIL satellite observations (Taken from Ergun *et al.*, 1998; Matsumoto *et al.*, 1994; Kojima *et al.*, 1994).

Figure 4a shows typical bipolar signatures from FAST and GEOTAIL satellite observations (Ergun *et al.*, 1998; Matsumoto *et al.*, 1994; Kojima *et al.*, 1994).

In a recent study, Reddy *et al.* (2002) examined a possible source for the nonlinear, spiky electric field structures. They considered a magnetized electron-ion plasma consisting of fluid ions and warm electrons described by the Boltzmann distribution. They closed their system by the quasi-neutrality condition, hence concentrating on the low frequency regime and derived a nonlinear wave equation in the rest frame of the propagating wave. They showed that the nonlinear coupling of the ion-acoustic mode and ion-cyclotron oscillations led to the generation of parallel electric fields which were highly spiky with periods ranging from ion-cyclotron to ion-acoustic. The shape of the waveform was found to have a strong dependence on the initial driving electric field and the Mach number. Their results were in good agreement with observations of Ergun *et al.* (1998). Later Bharuthram *et al.* (2002) included the finite ion temperature to study the effect on the parallel electric field structures. They found that for the ion-cyclotron wave, an increase in the ion temperature resulted in a decrease in the periodicity of the oscillations, and the nonlinearity of the wave was suppressed due to the enhanced dispersive effects. For the ion-acoustic wave, the behaviour was opposite, where the period increased with an ion temperature increase. Reddy *et al.* (2005, 2006) further extended their earlier work for the low frequency domain to a three-component plasma by including an oxygen ion beam in the system and

having hot Boltzmann electrons and protons. They found that the inclusion of the oxygen ion beam significantly affected the evolution of the nonlinear electric field structures. The ion-cyclotron oscillations were found to be only possible for very high oxygen ion densities while the driven ion-acoustic mode existed for only very small oxygen ion densities.

Moolla *et al.* (2003) extended the work of Reddy *et al.* (2002) to the high frequency domain by including the Poisson equation and thereby neglecting the quasi-neutrality condition, assuming only point quasi-neutrality (i.e quasi-neutrality at s=0). Their model was a three component plasma consisting of hot electrons, cold electrons and a cold ion species, where all species were described by the fluid equations. They showed that the nonlinear coupling between the high frequency electron-cyclotron and electron-acoustic modes could explain the spiky structures in the high frequency region of the broadband electrostatic noise. Later, Moolla *et al.* (2007) extended their previous high frequency study, but now having all species with finite temperatures. Included in their studied was an investigation of the pulse widths and periods of the waves, as well as effects of the propagation angle on the electric field structures. They found that the ratio of the pulse widths to the periods of the ESWs is a constant. They also showed that with the inclusion of a finite cool electron temperature, the waves broadened and the nonlinearity increased. As the propagation angle of the wave relative to the ambient magnetic field increased, they observed that the nonlinear electric field structures transformed from a uniform BEN TYPE A waveform to a

more distorted double-humped BEN TYPE C waveform.

Given that electron-positron plasmas are increasingly observed in astrophysical environments, as well as in laboratory experiments, the above mentioned satellite observations lead us to explore if such nonlinear structures are also possible in electron-positron plasmas. In this chapter three different symmetric four-component electron-positron plasma models are used to explore the existence of nonlinear electric field structures in the form of solitary waves. Model 1 consists of a cold electron and a cold positron species and a hot electron and a hot positron species. The hot species are described by the Boltzmann distribution and the dynamics of the cold species determined by the fluid equations. By virtue of the chosen symmetry, the cold (hot) electrons and positrons have equal density at equilibrium. Model 2 is an extension of Model 1 whereby all species (cold and hot) are described by the fluid equations. Then in Model 3, finite, non-zero temperatures are considered for all species, allowing for a cool component (temperature $T_c \neq 0$) and a hot component (temperature T_h) for both electrons and positrons.

4.2 MODEL 1: Plasma with cold fluid electrons and positrons ($\mathbf{T_c = 0}$) and hot Boltzmann electrons and positrons

4.2.1 Basic Equations

The model considered is a homogeneous magnetized, four component electron-positron plasma, consisting of cold electrons and positrons with temperatures ($T_c = 0$) and equilibrium densities denoted by n_{ec0} and n_{pc0} respectively, and hot electrons and positrons with equal temperatures denoted by T_h and equilibrium densities denoted by n_{eh0} and n_{ph0} respectively. Wave propagation is in the x-direction at an angle θ to the ambient magnetic field $\mathbf{B_0}$, which is assumed to be in the x-z plane.

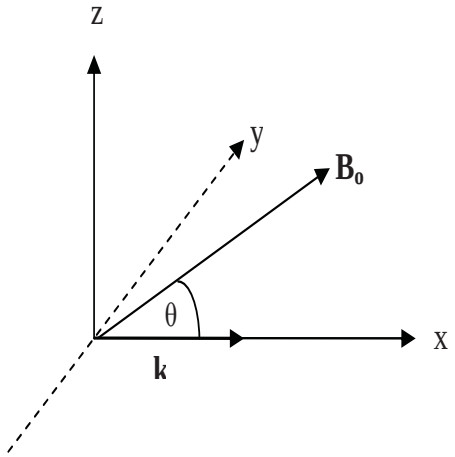

The hot isothermal species have a Boltzmann distribution given by,

$$n_{eh} = n_{eh0} \exp\left(\frac{e\phi}{T_h}\right) \tag{4.1}$$

and

$$n_{ph} = n_{ph0} \exp\left(\frac{-e\phi}{T_h}\right) , \tag{4.2}$$

where n_{eh} (n_{ph}) is the density of the hot electrons (positrons) and ϕ is the electrostatic potential.

The continuity and momentum equations for the cold isothermal species are given by

$$\frac{\partial n_j}{\partial t} + \frac{\partial (n_j v_{jcx})}{\partial x} = 0 , \tag{4.3}$$

$$\frac{\partial v_{jcx}}{\partial t} + v_{jcx}\frac{\partial v_{jcx}}{\partial x} = -\frac{\epsilon_j e}{m}\frac{\partial \phi}{\partial x} + \epsilon_j \Omega v_{jcy} \sin\theta , \tag{4.4}$$

$$\frac{\partial v_{jcy}}{\partial t} + v_{jcx}\frac{\partial v_{jcy}}{\partial x} = \epsilon_j \Omega v_{jcz} \cos\theta - \epsilon_j \Omega v_{jcx} \sin\theta , \tag{4.5}$$

$$\frac{\partial v_{jcz}}{\partial t} + v_{jcx}\frac{\partial v_{jcz}}{\partial x} = -\epsilon_j \Omega v_{jcy} \cos\theta , \tag{4.6}$$

where ϵ_j=+1(-1) for positrons (electrons), and $j = e(p)$ for the electrons (positrons) respectively.

The system is closed by the Poisson equation

$$\varepsilon_0 \frac{\partial^2 \phi}{\partial x^2} = -e(n_{pc} - n_{ec} + n_{ph} - n_{eh}) . \tag{4.7}$$

In the above equations, n_j and $\mathbf{v}_j$ are the densities and fluid velocities respectively, of the j^{th} species. $\Omega = \Omega_e = \Omega_p = eB_0/m$ is the cyclotron frequency.

Here $m = m_e = m_p$ is the common mass of the electrons and the positrons. To determine the linear dispersion relation, equations $(4.3) - (4.7)$ are linearized. Hence for perturbations varying as $\exp(i(kx - \omega t))$, $\partial/\partial t$ is replaced with $-i\omega$ and $\partial/\partial x$ with ik in equations $(4.3) - (4.7)$. Neglecting the higher order terms and eliminating v_{jcy} and v_{jcz} for each species, yields

$$v_{ecx} = \frac{-\dfrac{ek\phi}{m\omega}}{1 + \dfrac{\Omega^2 \sin^2\theta}{\Omega^2 \cos^2\theta - \omega^2}} \tag{4.8}$$

and

$$v_{pcx} = \frac{\dfrac{ek\phi}{m\omega}}{1 + \dfrac{\Omega^2 \sin^2\theta}{\Omega^2 \cos^2\theta - \omega^2}} \ . \tag{4.9}$$

Substituting these velocities into the respective continuity equations and in turn, substituting the densities into the Poisson's equation, the following dispersion relation is derived,

$$\omega^4 - \omega^2\left(\Omega^2 + \frac{k^2 v_{ea}^2}{1 + \frac{1}{2}k^2\lambda_{Dh}^2}\right) + \Omega^2 \cos^2\theta\left(\frac{k^2 v_{ea}^2}{1 + \frac{1}{2}k^2\lambda_{Dh}^2}\right) = 0 \ , \tag{4.10}$$

which is the dispersion relation (2.18) in chapter 2, but with no contribution from the cold species since $v_{tc} = 0$ for $T_c = 0$.

From equation (4.10),

$$\omega^2 = \frac{1}{2}\left(\Omega^2 + \frac{k^2 v_{ea}^2}{1 + \frac{1}{2}k^2\lambda_{Dh}^2}\right)\left[1 \pm \sqrt{1 - \frac{4\Omega^2 \cos^2\theta(\frac{k^2 v_{ea}^2}{1+\frac{1}{2}k^2\lambda_{Dh}^2})}{(\Omega^2 + \frac{k^2 v_{ea}^2}{1+\frac{1}{2}k^2\lambda_{Dh}^2})^2}}\right] \ , \tag{4.11}$$

where $v_{ea} = (n_{0c}/n_{0h})^{1/2} v_{th}$ is the acoustic speed and $\lambda_{Dh} = (\varepsilon_0 T_h / n_{0h} e^2)^{1/2}$ is the Debye length of the hot species as defined in chapter 2.

Taking the positive square in (4.11) and following the technique used in chapter 2 (in arriving at equation (2.72)), in the limit $(4\Omega^2 \cos^2\theta \frac{k^2 v_{ea}^2}{1+\frac{1}{2}k^2\lambda_{Dh}^2}) \ll (\Omega^2 + \frac{k^2 v_{ea}^2}{1+\frac{1}{2}k^2\lambda_{Dh}^2})^2$, one obtains

$$\omega_+^2 = \left(\Omega^2 + \frac{k^2 v_{ea}^2}{1+\frac{1}{2}k^2\lambda_{Dh}^2}\right) - \frac{\Omega^2 \cos^2\theta \frac{k^2 v_{ea}^2}{1+\frac{1}{2}k^2\lambda_{Dh}^2}}{\Omega^2 + \frac{k^2 v_{ea}^2}{1+\frac{1}{2}k^2\lambda_{Dh}^2}} \ . \tag{4.12}$$

The approximation used above restricts the mode to propagation angles satisfying $\cos\theta \ll \dfrac{\Omega^2 + \frac{k^2 v_{ea}^2}{1+\frac{1}{2}k^2\lambda_{Dh}^2}}{2\Omega(\frac{k^2 v_{ea}^2}{1+\frac{1}{2}k^2\lambda_{Dh}^2})^{\frac{1}{2}}}$.

Following Mace and Hellberg (1993), for small wavenumbers, $k\lambda_{Dh} \ll 1$ and in the limit $kv_{th} \ll \Omega$, this yields the dispersion relation for the cyclotron waves,

$$\omega_+ = \Omega + \frac{k^2 v_{ea}^2 \sin^2\theta}{2\Omega} \ , \tag{4.13}$$

as obtained by Mace and Hellberg (1993) for their electron cyclotron wave.

For the negative square root in (4.11), one obtains

$$\omega_-^2 = \frac{\Omega^2 \cos^2\theta \frac{k^2 v_{ea}^2}{1+\frac{1}{2}k^2\lambda_{Dh}^2}}{\Omega^2 + \frac{k^2 v_{ea}^2}{1+\frac{1}{2}k^2\lambda_{Dh}^2}} \ , \tag{4.14}$$

which in the limit $kv_{th} \ll \Omega$, yields

$$\omega_{-} = kv_{ea}\cos\theta \ , \tag{4.15}$$

as obtained by Mace and Hellberg (1993) for their electron acoustic wave.

4.2.2 Nonlinear Analysis

Given that we are adapting the approach adopted in an electron-ion plasma by Reddy *et al.* (2002) for low frequency phenomena and later by Moolla *et al.* (2003, 2007) for high frequency studies, it is important to present some discussion that contextualizes our work. In their work Reddy *et al.* (2002) used the quasineutral approximation to derive a single nonlinear equation for the wave potential. The equation provided periodic solutions for the wave electric field ranging from linear sinusoidal to nonlinear sawtooth to spiky bipolar in form, very similar to those generated by Temerin *et al.* (1979) (their figure 3) for nonlinear electrostatic cyclotron waves. Such an approach was also used by Lee and Kan *et al.* (1981) in studying nonlinear ion cyclotron and ion acoustic waves. It is noted that these simple solutions do not take into account the effect of higher order harmonics and other nonlinear effects. On the other hand in their study, Moolla *et al.* (2003, 2007) could not adopt the quasineutral approximation as they investigated the high frequency domain. As a result the system of nonlinear equations governing the dynamics of their plasma model could not be reduced to a single nonlinear equation, but had to be numerically solved as a coupled set. Their results

produced periodic nonlinear electron cyclotron and nonlinear electron acoustic waves. For our electron-positron plasma, given the single time-scale, the quasineutral approximation is also not valid. Hence one may anticipate the need to solve the governing set of equations numerically.

In the nonlinear regime, a transformation into a stationary frame $s = (x - Vt)(\Omega/V)$ is performed, and the normalizations of v, t, x and ϕ are with respect to v_{th}, Ω^{-1}, $\rho = v_{th}/\Omega$, and T_h/e, respectively. V is the phase velocity of the wave. In equations $(4.3) - (4.7)$, $\partial/\partial t$ is replaced by $-\Omega(\partial/\partial s)$ and $\partial/\partial x$ by $(\Omega/V)(\partial/\partial s)$.

Integrating equation (4.3) and using the initial conditions $n_{ec} = n_{ec0}$ and $v_{ecx} = v_{0c}$ at $s = 0$, yields the velocity for the cold electrons and positrons in the x-direction.

$$v_{ecx} = -\left(\frac{n_{ec0}}{n_{ec}}\right)(V - v_{0c}) + V \tag{4.16}$$

$$v_{pcx} = -\left(\frac{n_{pc0}}{n_{pc}}\right)(V - v_{0c}) + V \tag{4.17}$$

The dimensionless quantities $\psi = e\phi/T_h$, $M = V/v_{th}$ are introduced, and $\delta_c = v_{0c}/v_{th}$ where ψ is the normalized potential, M is the normalized Mach number, δ_c is the normalized drift velocity of the cold species and the driving electric field $E = -(\partial\psi/\partial s)$. Substituting equations (4.16) and (4.17) into equations $(4.4) - (4.7)$, the following set of nonlinear first-order differential

equations in the stationary frame are obtained.

$$\frac{\partial \psi}{\partial s} = -E \tag{4.18}$$

$$\frac{\partial E}{\partial s} = R^2 M^2 (n_{pcn} - n_{ecn} + \frac{n_{ph0}}{n_0} e^{-\psi} - \frac{n_{eh0}}{n_0} e^{\psi}) \tag{4.19}$$

$$\frac{\partial n_{ecn}}{\partial s} = \frac{n_{ecn}^3}{(M-\delta_c)^2} \left(\frac{n_0}{n_{ec0}}\right)^2 \left[E + M \sin\theta v_{ecyn}\right] \tag{4.20}$$

$$\frac{\partial v_{ecyn}}{\partial s} = \frac{M n_{ecn}}{(M-\delta_c)} \left(\frac{n_0}{n_{ec0}}\right) \left[-\left(M - \frac{(M-\delta_c)}{n_{ecn}} \left(\frac{n_{ec0}}{n_0}\right)\right) \sin\theta + v_{eczn} \cos\theta\right] \tag{4.21}$$

$$\frac{\partial v_{eczn}}{\partial s} = -\left(\frac{n_0}{n_{ec0}}\right) \frac{n_{ecn} v_{ecyn} M \cos\theta}{(M-\delta_c)} \tag{4.22}$$

$$\frac{\partial n_{pcn}}{\partial s} = \frac{n_{pcn}^3}{(M-\delta_c)^2} \left(\frac{n_0}{n_{pc0}}\right)^2 \left[-E - M \sin\theta v_{pcyn}\right] \tag{4.23}$$

$$\frac{\partial v_{pcyn}}{\partial s} = \frac{M n_{pcn}}{(M-\delta_c)} \left(\frac{n_0}{n_{pc0}}\right) \left[\left(M - \frac{(M-\delta_c)}{n_{pcn}} \left(\frac{n_{pc0}}{n_0}\right)\right) \sin\theta - v_{pczn} \cos\theta\right] \tag{4.24}$$

$$\frac{\partial v_{pczn}}{\partial s} = \left(\frac{n_0}{n_{pc0}}\right) \frac{n_{pcn} v_{pcyn} M \cos\theta}{(M-\delta_c)} \tag{4.25}$$

In equations (4.18) – (4.25) the equilibrium density of the cold (hot) electrons is n_{ec0} (n_{eh0}) and n_{pc0} (n_{ph0}) is the equilibrium density of the cold (hot) positrons, with $n_{ec0} + n_{eh0} = n_{pc0} + n_{ph0} = n_0$. $R = \omega_p/\Omega$, where $\omega_p = (n_0 e^2/\varepsilon_0 m)^{1/2}$ is the total plasma frequency and $\Omega = qB_o/m$ is the gyrofrequency. The additional subscript 'n' has been introduced to indicate normalized quantities. The normalized particle densities, e.g. n_{pcn}, are with respect to the total density n_0. As in chapter 2, the parameter R represents the strength of the magnetic field for fixed total plasma density. For a

strongly magnetized plasma, $R \ll 1$, while for a weakly magnetized plasma, $R \gg 1$.

4.2.3 Numerical Results

The system of nonlinear first-order differential equations $(4.18) - (4.25)$ are solved numerically using the Runge-Kutta (RK4) technique (Press *et al.*, 1996). The initial values were determined self consistently. Initial values are given to v_{ecyn} and v_{eczn}. Then v_{pcyn0} and v_{pczn0} are calculated self consistently (see Appendix B). All figures illustrate the actual normalized electric fields $E_{norm} = -(1/M)(\partial\psi/\partial s)$.

We recall that in this chapter, an attempt is made to explore in an electron-positron plasma the existence of electrostatic waves (ESWs) of the type found initially by Reddy *et al.* (2002) for electron-ion plasmas in their effort to explain satellite observations of such structures in the earth's magnetosphere. Hence a wide rage of parameters were investigated. Our examination showed that for this particular plasma model these ESWs were only possible for relatively large R-values, i.e in high density weakly magnetized plasmas. Consequently we set $R = 160$ as a typical value in our calculations. The exact reason for this behaviour is not understood. It is important to note however, that in an electron-positron plasma both the (equal mass) species are equally magnetized (having the same magnitude for the gyrofrequency). This is not the case for the electron-ion plasma models of Reddy *et al.* (2002) and other

authors used for studies in the magnetosphere. It maybe that the dynamics whereby both the electrons and the positrons are essentially tied to the field lines in a strongly magnetized plasma (low R-values) impedes the development to the spiky structures because then the assumption of Boltzmann density distributions for the hot species is not valid. This is confirmed to some extent in the following sections of this chapter in which the Boltzmann assumption is not made. Then nonlinear spiky structures are obtained for much lower R-values (e.g. $R = 10$ in section 4.2).

Noting that satellite observations of ESWs in the earth's magnetosphere were observed for angles of propagation in a narrow cone about the direction of the earth's magnetic field, Reddy *et al.* (2002), Moolla *et al.* (2003, 2007), and other authors set the angle of propagation to $\theta = 2^o$. In this investigation this value of θ is initially retained followed by a θ variation later on.

Effect of the driving amplitude E_0 on the waves

Figures $4.1 - 4.3$ shows the evolution of the system as the electric field amplitudes E_0 is increased. The fixed normalized parameters are $M = 1.6$, $R = 160$, $\theta = 2^o$, $\delta_c = 0.0$ and $n_{ec0}/n_0 = n_{pc0}/n_0 = 0.73$. Since $R = 160$, we have a very weakly magnetized plasma. Note that wave propagation is taken almost parallel to the ambient magnetic field $\mathbf{B_0}$, consistent with theoretical studies (Reddy *et al.*, 2002) and experimental observations for the earth's magnetosphere. As E_0 increases, the electric field structure evolves from a

linear sinusoidal waveform to a nonlinear sawtooth structure. For a higher E_0 value of 1.3, the structure is spiky bipolar in form. This is similar to a BEN TYPE A structure (see figure 4a). The change in electric field structure with increasing E_0 is similar to that found by Reddy *et al.* (2002) and studies in electron-ion plasmas that folloewd. As E_0 increases, the period of the wave increases and the frequency decreases. The period of oscillations is given by $\Delta S = (\Delta x - V\Delta t)(\Omega/V)$. Typically for $\Delta x = 0$, $\Delta S = |\Omega \Delta t|$. The period of the waves can be expressed in terms of the cyclotron period $\tau_c = 2\pi/\Omega$. This enables one to distinguish between the cyclotron mode ($T_w \leq 1.0\tau_c$) and the acoustic mode ($T_w > 1.0\tau_c$). Hence for the linear wave in figure 4.1, with a small driving amplitude of $E_0 = 0.05$, the period of the wave is calculated to be $T_w = 1.02\tau_c$ (frequency $f_w = 0.98 f_c$), which is associated with the cyclotron mode, where $\tau_c = 2\pi/\Omega$. Figure 4.2 shows a sawtooth waveform for $E_0 = 0.3$ with a period of $T_w = 1.05\tau_c$ (frequency $f_w = 0.95 f_c$) and for $E_0 = 1.3$ a spiky bipolar waveform is shown (figure 4.3), where the period of the wave $T_w = 1.08\tau_c$ (frequency $f_w = 0.93 f_c$). Thus as E_0 increases, the mode transforms from the cyclotron to the acoustic wave (dispersion relations (4.14) and (4.15)). We recall that a similar behaviour was found by Reddy *et al.* (2002) for an electron-ion plasma, with the mode transforming from the ion cyclotron to the ion acoustic mode as E_0 increases.

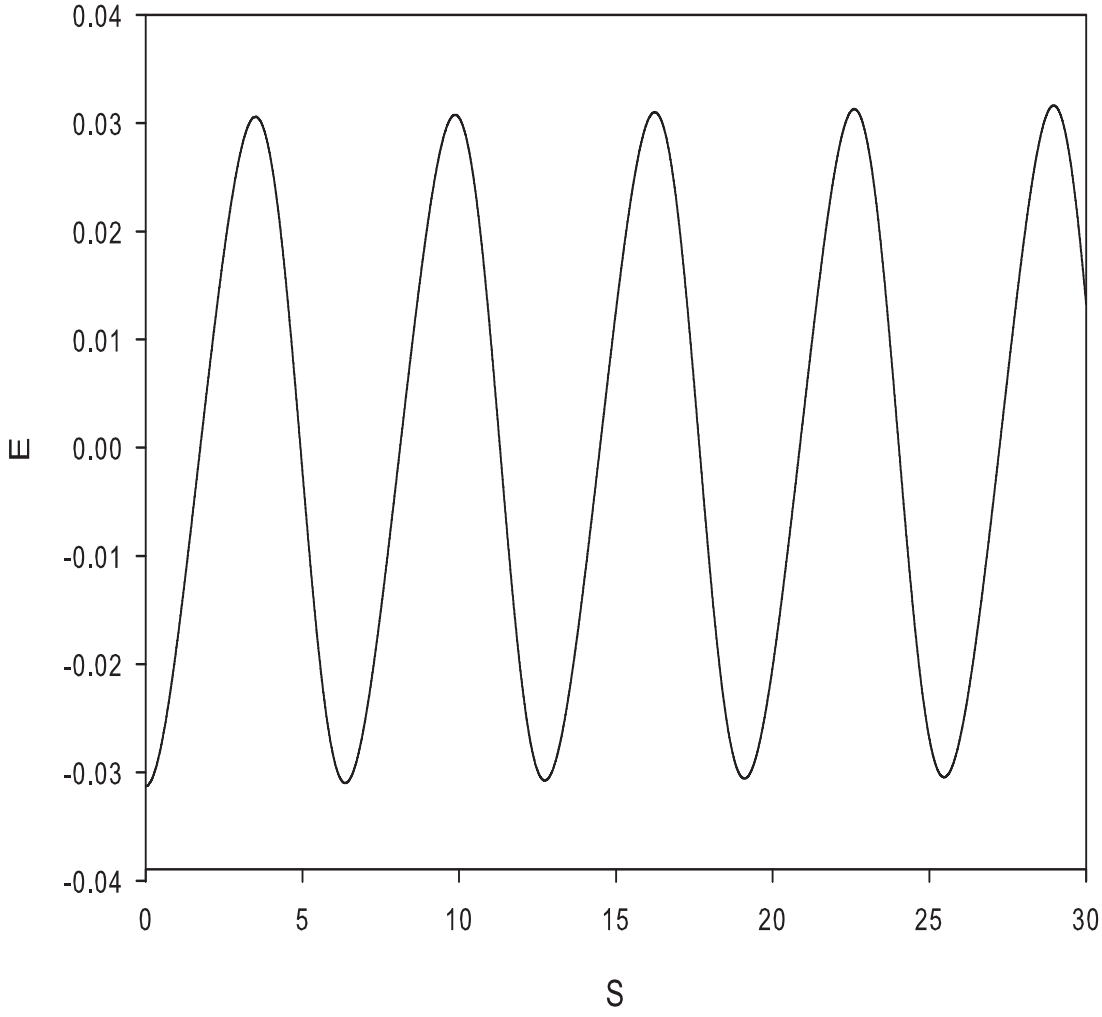

Figure 4.1: Numerical solution of the normalized electric field (sinusoidal waveform) for the parameters $M = 1.6$, $\theta = 2^o$, $R = 160$, $\delta_c = 0.0$, $n_{ec0}/n_0 = n_{pc0}/n_0 = 0.73$ and $E_0 = 0.05$. The period of the wave is $T_w = 1.02\tau_c$ (frequency $f_w = 0.98 f_c$).

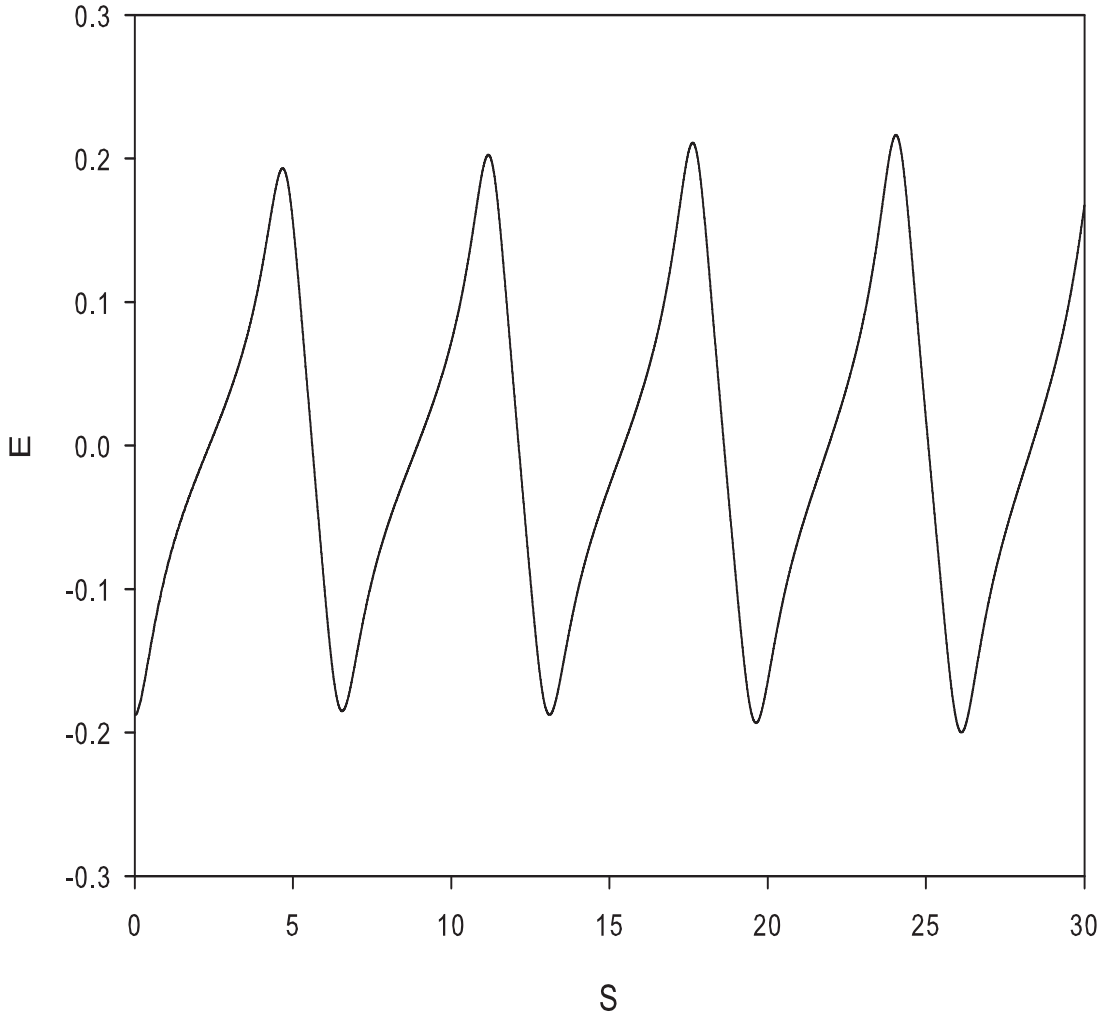

Figure 4.2: Numerical solution of the normalized electric field (sawtooth waveform) for the parameters $M = 1.6$, $\theta = 2^o$, $R = 160$, $\delta_c = 0.0$, $n_{ec0}/n_0 = n_{pc0}/n_0 = 0.73$ and $E_0 = 0.3$. the period of the wave is $T_w = 1.05\tau_c$ (frequency $f_w = 0.95 f_c$).

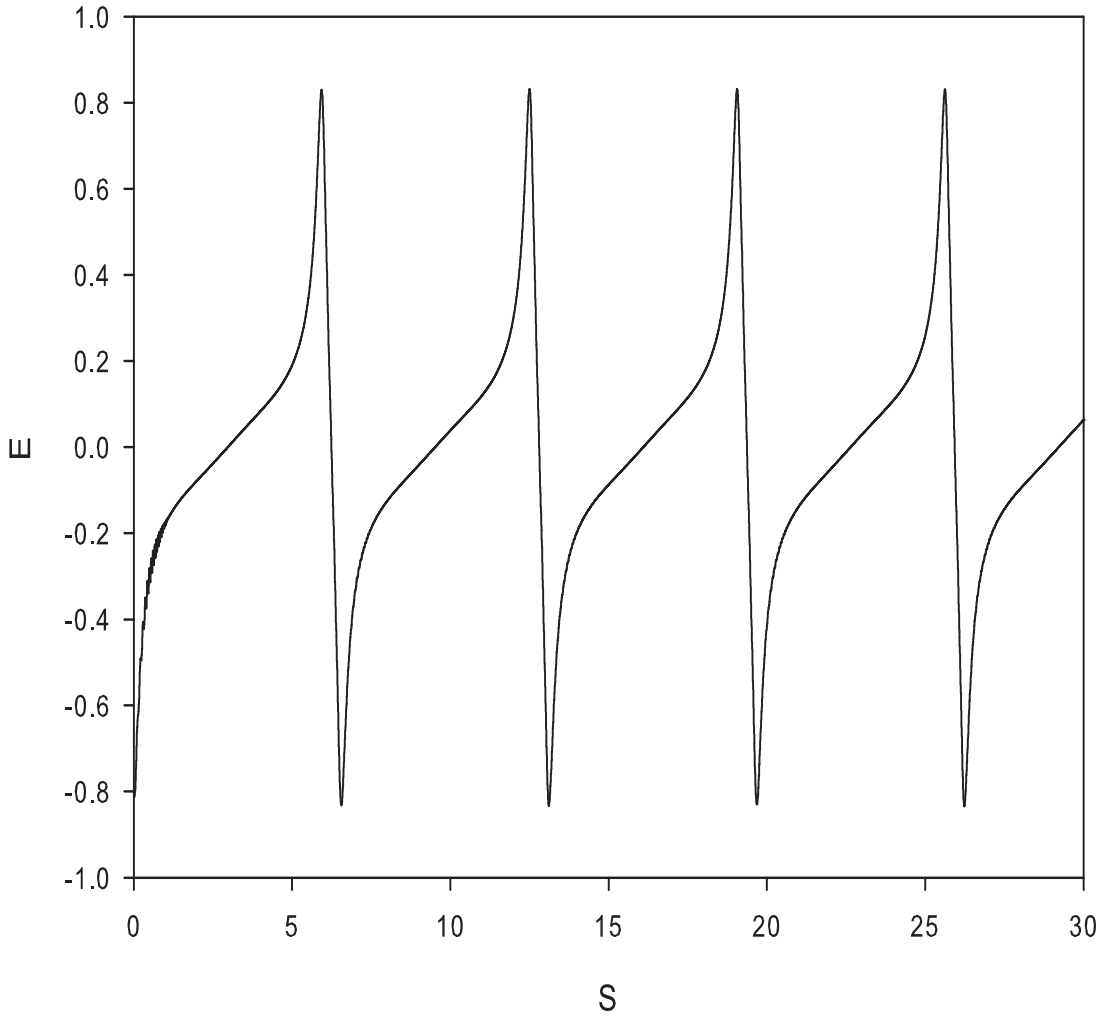

Figure 4.3: Numerical solution of the normalized electric field (bipolar waveform) for the parameters $M = 1.6$, $\theta = 2^o$, $R = 160$, $\delta_c = 0.0$, $n_{ec0}/n_0 = n_{pc0}/n_0 = 0.73$ and $E_0 = 1.3$. the period of the wave is $T_w = 1.08\tau_c$ (frequency $f_w = 0.93 f_c$).

Effect of the drift velocity of the cold species

In figures $4.4 - 4.8$, the effect of the drift velocity of the cold species from being anti-parallel to parallel to the external magnetic field is studied. The fixed parameters are $E_0 = 0.8$, $M = 1.6$, $R = 160$, $\theta = 2^o$ and $n_{ec0}/n_0 = n_{pc0}/n_0 = 0.73$. Here, it is observed that the period of the spiky structures decreases from $1.11\tau_c$ for $\delta_c = -0.02$ to $1.04\tau_c$ for $\delta_c = +0.02$), i.e, as the cold beam flow changes from anti-parallel to parallel to the ambient magnetic field. Therefore, one may conclude that the cold electron and positron flows anti-parallel (parallel) to $\mathbf{B_0}$ increases (decreases) the period of the spiky structure. These results are consistent with previous work done in electron-ion plasmas (Reddy *et al.*, 2002; Bharuthram *et al.*, 2002; Moolla *et al.*, 2003, 2007).

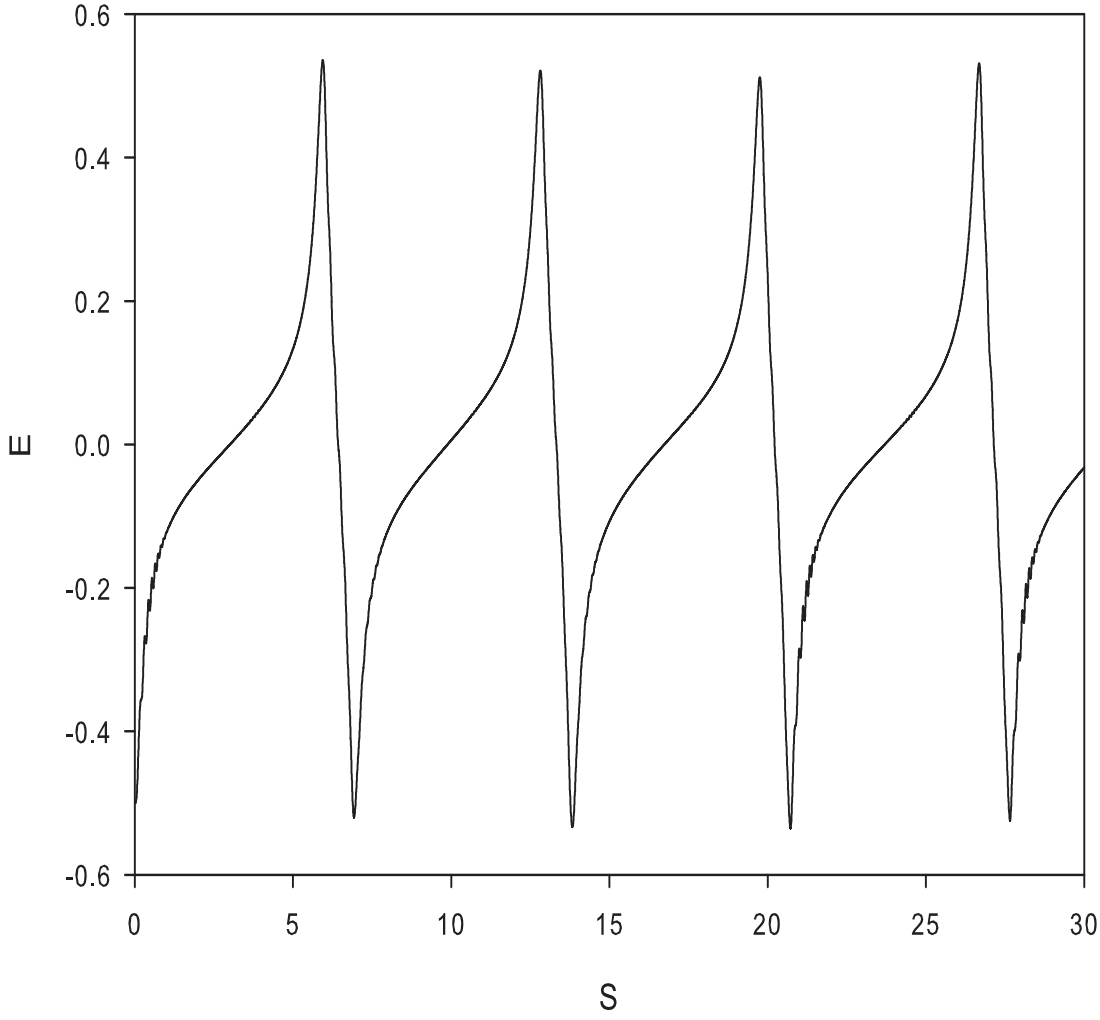

Figure 4.4: Numerical solution of the normalized electric field for the parameters $M = 1.6$, $E_0 = 0.8$, $R = 160$, $\theta = 2^o$, $n_{ec0}/n_0 = n_{pc0}/n_0 = 0.73$ and $\delta_c = -0.02$. The period of the wave is $T_w = 1.11\tau_c$ (frequency $f_w = 0.90 f_c$).

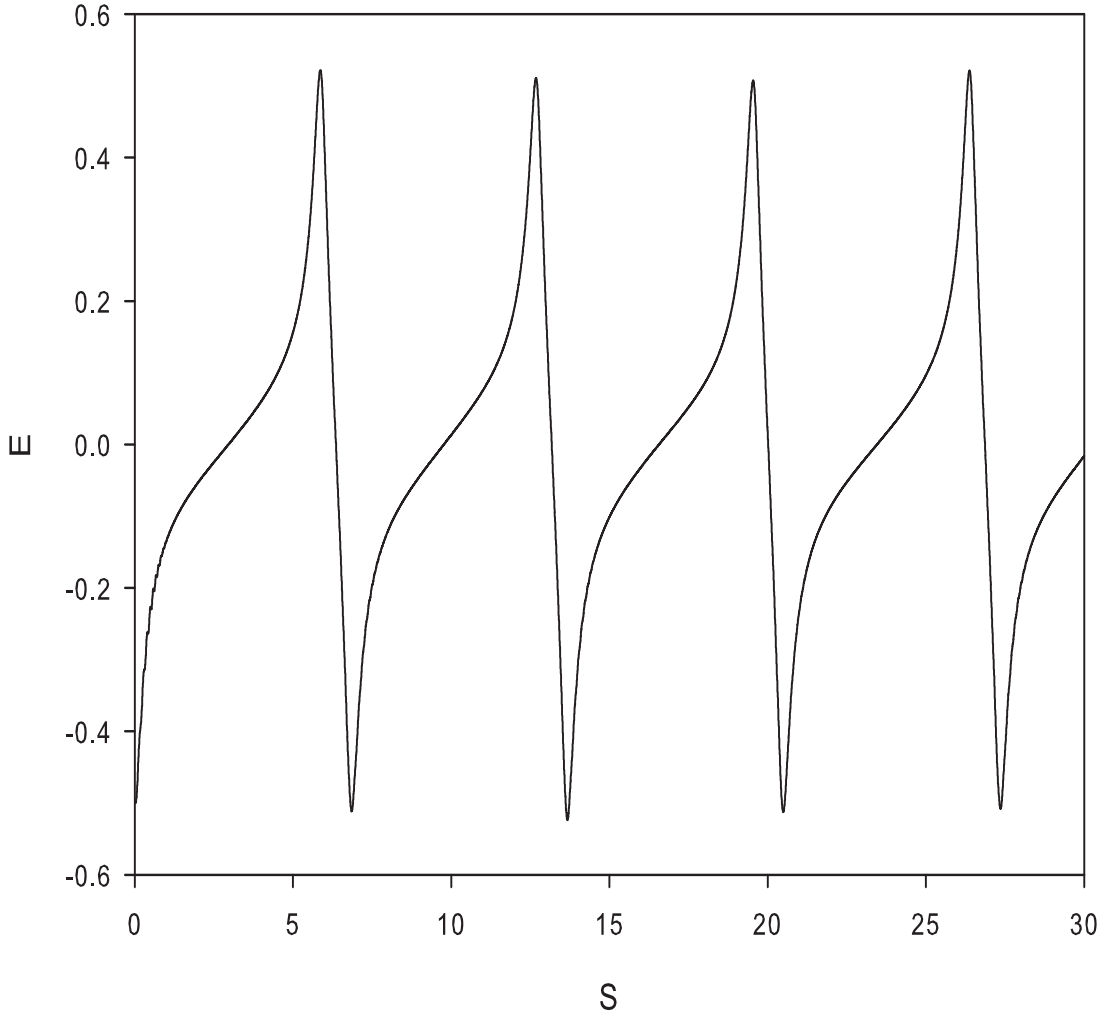

Figure 4.5: Numerical solution of the normalized electric field for the parameters $M = 1.6$, $E_0 = 0.8$, $R = 160$, $\theta = 2^o$, $n_{ec0}/n_0 = n_{pc0}/n_0 = 0.73$ and $\delta_c = -0.01$. The period of the wave is $T_w = 1.09\tau_c$ (frequency $f_w = 0.92 f_c$).

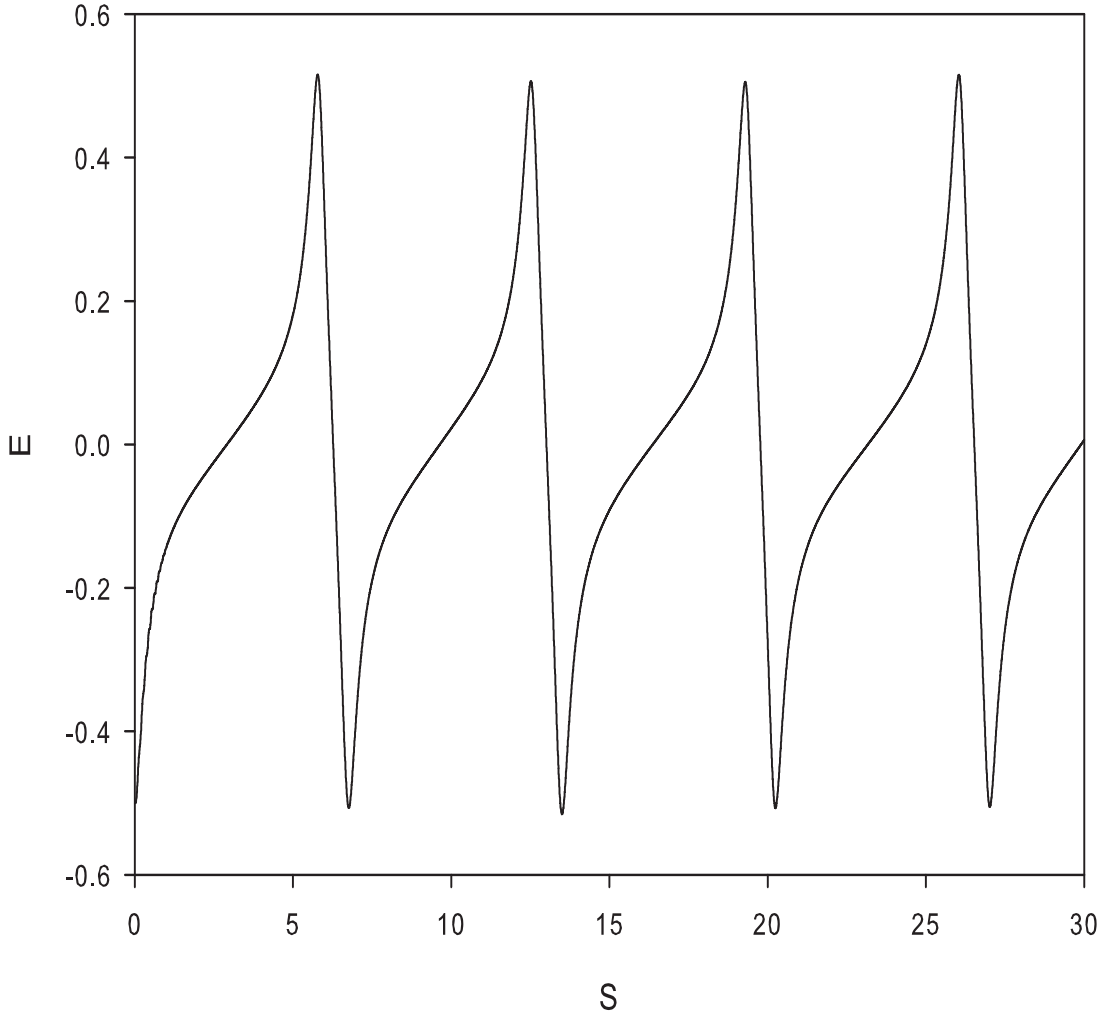

Figure 4.6: Numerical solution of the normalized electric field for the parameters $M = 1.6$, $E_0 = 0.8$, $R = 160$, $\theta = 2^o$, $n_{ec0}/n_0 = n_{pc0}/n_0 = 0.73$ and $\delta_c = 0.0$. The period of the wave is $T_w = 1.07\tau_c$ (frequency $f_w = 0.93 f_c$).

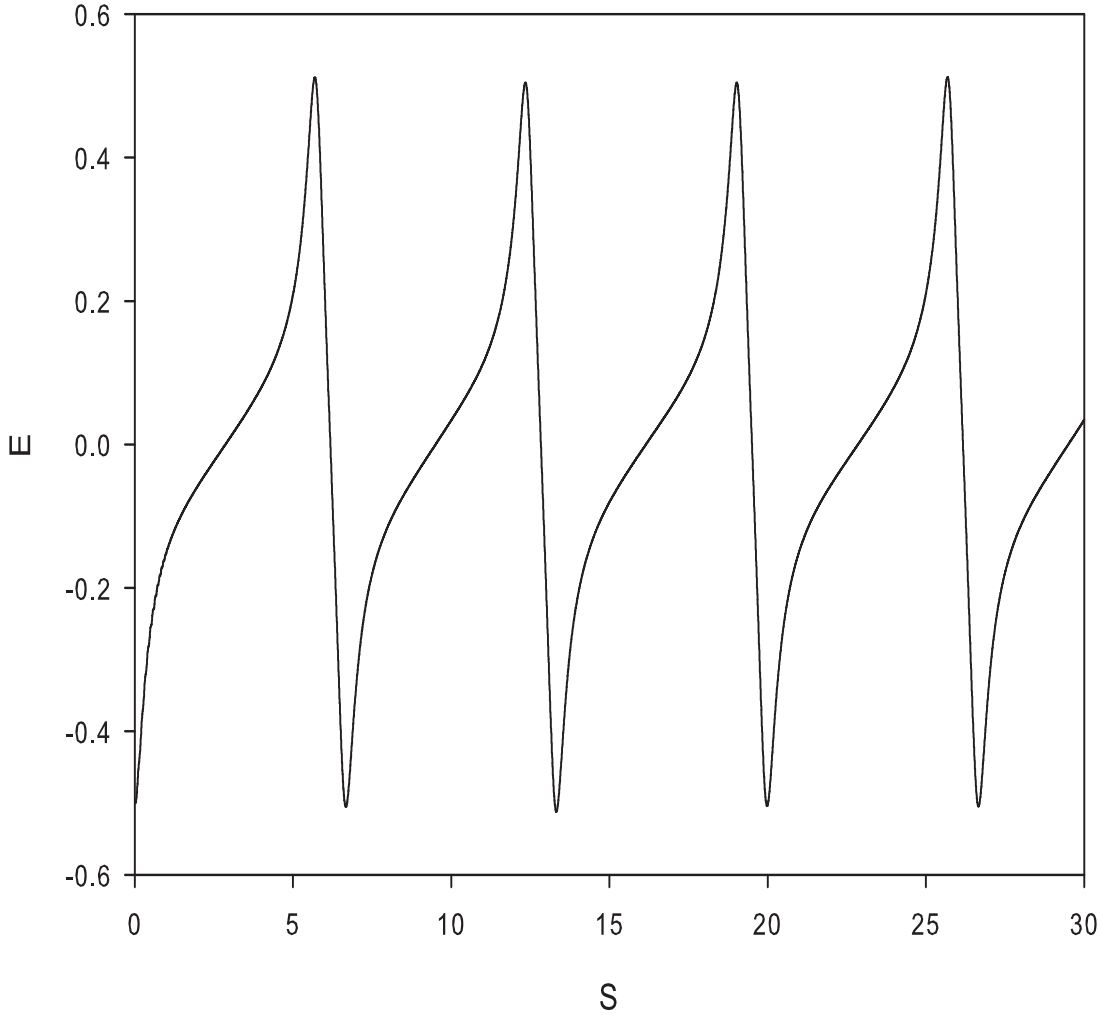

Figure 4.7: Numerical solution of the normalized electric field for the parameters $M = 1.6$, $E_0 = 0.8$, $R = 160$, $\theta = 2^o$, $n_{ec0}/n_0 = n_{pc0}/n_0 = 0.73$ and $\delta_c = 0.01$. The period of the wave is $T_w = 1.06\tau_c$ (frequency $f_w = 0.94 f_c$).

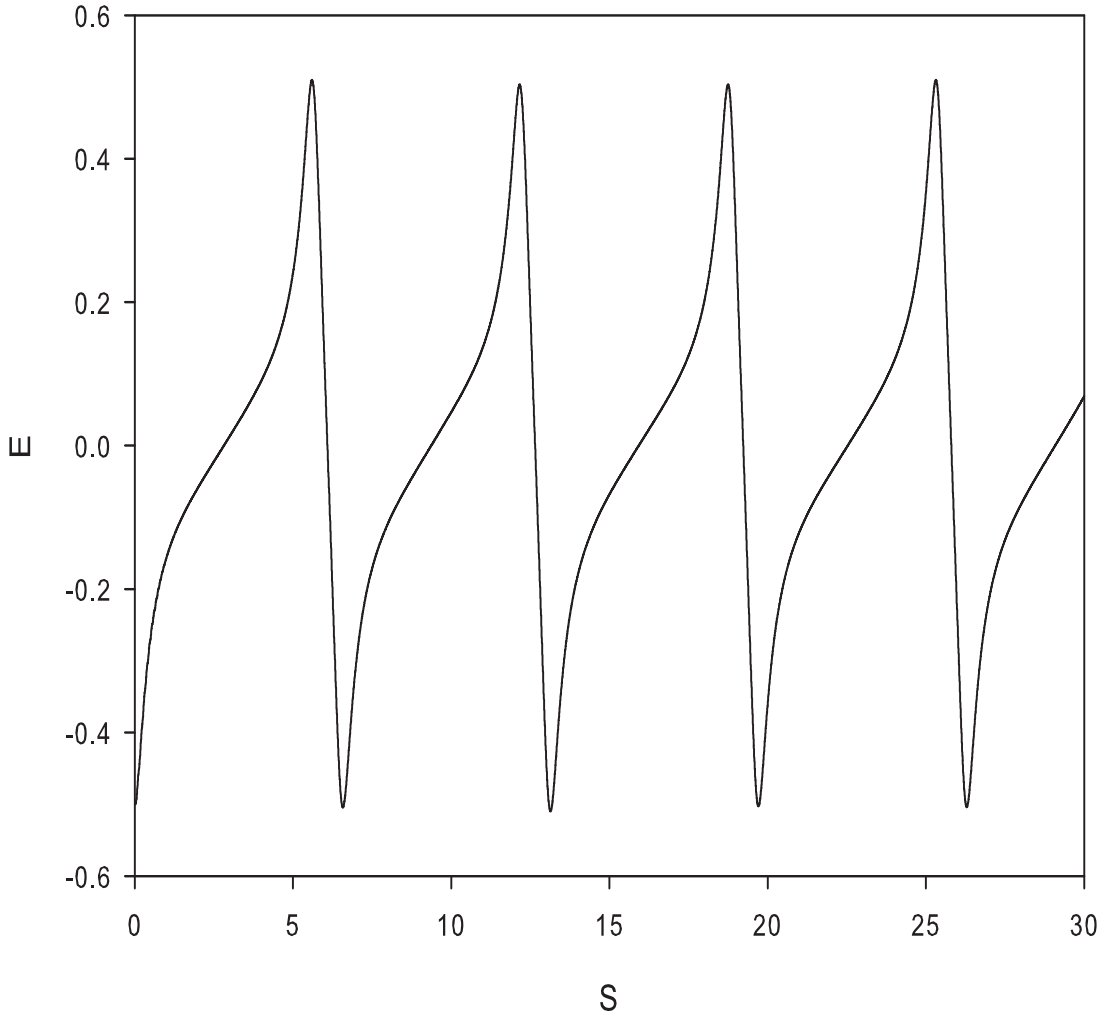

Figure 4.8: Numerical solution of the normalized electric field for the parameters $M = 1.6$, $E_0 = 0.8$, $R = 160$, $\theta = 2^o$, $n_{ec0}/n_0 = n_{pc0}/n_0 = 0.73$ and $\delta_c = 0.02$. The period of the wave is $T_w = 1.04\tau_c$ (frequency $f_w = 0.96 f_c$).

4.3 MODEL 2: Plasma with cold electrons and positrons ($\mathbf{T_c = 0}$) and hot electrons and positrons ($\mathbf{T_h \neq 0}$), including the full dynamics for all species

4.3.1 Basic Equations

Here, the model 1 in the previous section is extended to include the full dynamics of all species, thus the hot species no longer have Boltzmann density distributions. A homogeneous magnetized, four component, collisionless, electron-positron plasma, consisting of cold electrons (ec) and cold positrons (pc) with equilibrium densities ($n_{ec0} = n_{pc0}$), and hot electrons (eh) and hot positrons (ph) having equal temperatures T_h and equilibrium densities ($n_{eh0} = n_{ph0}$) is considered. Wave propagation is in the x-direction at an angle θ to the magnetic field $\mathbf{B_0}$, which is assumed to be in the x-z plane. The continuity and momentum equations for the four species are given by

$$\frac{\partial n_j}{\partial t} + \frac{\partial (n_j v_{jx})}{\partial x} = 0 \ , \tag{4.26}$$

$$\frac{\partial v_{jx}}{\partial t} + v_{jx}\frac{\partial v_{jx}}{\partial x} + \frac{\alpha_j}{n_j m}\frac{\partial p_j}{\partial x} = -\frac{\epsilon_j e}{m}\frac{\partial \phi}{\partial x} + \epsilon_j \Omega v_{jy}\sin\theta \ , \tag{4.27}$$

$$\frac{\partial v_{jy}}{\partial t} + v_{jx}\frac{\partial v_{jy}}{\partial x} = \epsilon_j \Omega v_{jz}\cos\theta - \epsilon_j \Omega v_{jx}\sin\theta \ , \tag{4.28}$$

$$\frac{\partial v_{jz}}{\partial t} + v_{jx}\frac{\partial v_{jz}}{\partial x} = -\epsilon_j \Omega v_{jy}\cos\theta \ , \tag{4.29}$$

where $\epsilon_j = +1(-1)$ for positrons (electrons), $\alpha_j = 0(1)$ for cold (hot) species and $j = ec, pc, eh, ph$ for the cold electrons, cold positrons, hot electrons,

and the hot positrons, respectively. As in section 4.2, the density of the cold electrons (positrons) is n_{ec} (n_{pc}), and that of the hot electrons (positrons) is n_{eh} (n_{ph}).

The general equation of state for the hot species is given by

$$\frac{\partial p_j}{\partial t} + v_{jx}\frac{\partial p_j}{\partial x} + 3p_j\frac{\partial v_{jx}}{\partial x} = 0 \ . \tag{4.30}$$

The system is closed by the Poisson equation

$$\varepsilon_0\frac{\partial^2\phi}{\partial x^2} = -e(n_{pc} - n_{ec} + n_{ph} - n_{eh}) \ . \tag{4.31}$$

In the above equations, one recalls that n_j, $\mathbf{v}_j$ and p_j are the densities, fluid velocities and pressures, respectively, of the j^{th} species. $\Omega = \Omega_e = \Omega_p = eB_0/m$ is the cyclotron frequency. Here $m = m_e = m_p$ is the common mass of the electrons and the positrons. Adiabatic compression ($\gamma = (2+N)/N$=3 is assumed, where N=1 implies one degree of freedom).

The linear dispersion relation for the model equations $(4.26) - (4.31)$ is obtained by linearizing as in section 4.2 for perturbations varying as $\exp(i(kx - \omega t))$. Neglecting the higher order terms and eliminating v_{jy} and v_{jz} for each species, results in

$$v_{ecx} = \frac{-\frac{ek\phi}{m\omega}(\omega^2 - \Omega^2\cos^2\theta)}{\omega^2 - \Omega^2} \ , \tag{4.32}$$

$$v_{pcx} = \frac{\frac{ek\phi}{m\omega}(\omega^2 - \Omega^2\cos^2\theta)}{\omega^2 - \Omega^2} \ , \tag{4.33}$$

$$v_{ehx} = \frac{-\frac{ek\phi}{m\omega}(\omega^2 - \Omega^2\cos^2\theta)}{\omega^2 - \Omega^2 - \frac{3k^2v_{th}^2}{\omega^2}(\omega^2 - \Omega^2\cos^2\theta)} \ , \tag{4.34}$$

and

$$v_{phx} = \frac{\frac{ek\phi}{m\omega}(\omega^2 - \Omega^2\cos^2\theta)}{\omega^2 - \Omega^2 - \frac{3k^2v_{th}^2}{\omega^2}(\omega^2 - \Omega^2\cos^2\theta)} \ . \tag{4.35}$$

Substituting these velocities into their respective continuity equations and in turn, substituting the densities into Poisson's equation, the following dispersion relation is obtained,

$$\omega^2 = \frac{2\omega_{pc}^2(\omega^2 - \Omega^2\cos^2\theta)}{\omega^2 - \Omega^2} + \frac{2\omega_{ph}^2(\omega^2 - \Omega^2\cos^2\theta)}{\omega^2 - \Omega^2 - \frac{3k^2v_{th}^2}{\omega^2}(\omega^2 - \Omega^2\cos^2\theta)} \ , \tag{4.36}$$

where $\omega_{pc,ph} = (n_{0j}e^2/\varepsilon_0 m)^{1/2}$ is the plasma frequencies of the cold and hot species respectively. In the limit $\omega/k \ll v_{th}$, i.e. wave speeds much smaller than the hot thermal velocity $v_{th} = (T_h/m)^{1/2}$, equation (4.36) becomes

$$\omega^4 - \omega^2(\Omega^2 + 2\omega_s^2) + 2\omega_s^2\Omega^2\cos^2\theta = 0 \ . \tag{4.37}$$

Following the technique in the previous section, equation (4.37) is solved for the normal modes. The positive square root yields

$$\omega_+^2 = (\Omega^2 + 2\omega_s^2) - \frac{2\omega_s^2\Omega^2\cos^2\theta}{\Omega^2 + 2\omega_s^2} \ , \tag{4.38}$$

where $\omega_s = \omega_{pc}/(1 + 2/3k^2\lambda_{Dh}^2)^{1/2}$ and $\lambda_{Dh} = (\varepsilon_0 T_h/n_{oh}e^2)^{1/2}$.

In the limit $\omega_s \ll \Omega$ and for small wavenumbers, $k\lambda_{Dh} \ll 1$, this yields the dispersion relation for the cyclotron waves

$$\omega_+ = \Omega + \frac{3k^2 v_{ea}^2 \sin^2\theta}{2\Omega} \ . \tag{4.39}$$

Taking the negative square root of equation (4.37) yields

$$\omega_-^2 = \frac{2\omega_s^2 \Omega^2 \cos^2\theta}{\Omega^2 + 2\omega_s^2} \ , \tag{4.40}$$

In the limit $\omega_s \ll \Omega$ and for small wavenumbers, $k\lambda_{Dh} \ll 1$ this yields the dispersion relation for the acoustic waves

$$\omega_- = \sqrt{3} k v_{ea} \cos\theta \ , \tag{4.41}$$

where $v_{ea} = (n_{0c}/n_{0h})^{1/2} v_{th}$ is the acoustic speed. The above modes are similar in form to those derived by Mace and Hellberg (1993) for an electron-ion plasma. A comparison of equations 4.39 and 4.41 with equations equations 4.13 and 4.15 shows the effect of the adiabatic compression of the hot species on the dispersion characteristics of the waves.

4.3.2 Nonlinear Analysis

In the nonlinear regime, as before a transformation to a stationary frame $s = (x - Vt)(\Omega/V)$ is performed, and v, t, x and ϕ are normalized with respect to v_{th}, Ω^{-1}, $\rho = v_{th}/\Omega$, and T_h/e, respectively. V is the phase velocity

of the wave. In equations $(4.26)-(4.30)$, $\partial/\partial t$ is replaced by $-\Omega(\partial/\partial s)$ and $\partial/\partial x$ by $(\Omega/V)(\partial/\partial s)$, and the driving electric field amplitude is defined as $E=-(\partial\psi/\partial s)$, where $\psi=e\phi/T_h$. Interestingly, here we find that nonlinear spiky electric field structures are possible for low values of R in comparison to the results in section 4.2. Hence, we typically set $R=10$, and hence consider a plasma that is much more strongly magnetized in comparison to section 4.2, where $R=160$ was used.

Integrating equation (4.26) and using the initial conditions $n_{ec}=n_{ec0}$ and $v_{ecx}=v_{0c}$ at $s=0$, yields the velocity for the cold electrons in the x-direction,

$$v_{ecx}=-\left(\frac{n_{ec0}}{n_{ec}}\right)(V-v_{0c})+V\ . \tag{4.42}$$

Similarly the cold positron, hot electron and hot positron velocities are determined, where $\delta_c=v_{0c}/v_{th}$ and $\delta_h=v_{0h}/v_{th}$.

Substituting these into equations $(4.26)-(4.31)$ gives the following set of nonlinear first-order differential equations in the stationary frame.

$$\frac{\partial\psi}{\partial s} = -E \tag{4.43}$$

$$\frac{\partial E}{\partial s} = R^2M^2(n_{pcn}-n_{ecn}+n_{phn}-n_{ehn}) \tag{4.44}$$

$$\frac{\partial n_{ecn}}{\partial s} = \frac{n_{ecn}^3}{(M-\delta_c)^2}\left(\frac{n_0}{n_{ec0}}\right)^2\left[E+M\sin\theta v_{ecyn}\right] \tag{4.45}$$

$$\frac{\partial v_{ecyn}}{\partial s} = \frac{Mn_{ecn}}{(M-\delta_c)}\left(\frac{n_0}{n_{ec0}}\right)\left[-\left(M-\frac{(M-\delta_c)}{n_{ecn}}\left(\frac{n_{ec0}}{n_0}\right)\right)\sin\theta+v_{eczn}\cos\theta\right] \tag{4.46}$$

$$\frac{\partial v_{eczn}}{\partial s} = -\left(\frac{n_0}{n_{ec0}}\right)\frac{n_{ecn}v_{ecyn}M\cos\theta}{(M-\delta_c)} \tag{4.47}$$

$$\frac{\partial n_{pcn}}{\partial s} = \frac{n_{pcn}^3}{(M-\delta_c)^2}\left(\frac{n_0}{n_{pc0}}\right)^2\left[-E - M\sin\theta v_{pcyn}\right] \tag{4.48}$$

$$\frac{\partial v_{pcyn}}{\partial s} = \frac{Mn_{pcn}}{(M-\delta_c)}\left(\frac{n_0}{n_{pc0}}\right)\left[\left(M - \frac{(M-\delta_c)}{n_{pcn}}\left(\frac{n_{pc0}}{n_0}\right)\right)\sin\theta - v_{pczn}\cos\theta\right] \tag{4.49}$$

$$\frac{\partial v_{pczn}}{\partial s} = \left(\frac{n_0}{n_{pc0}}\right)\frac{n_{pcn}v_{pcyn}M\cos\theta}{(M-\delta_c)} \tag{4.50}$$

$$\frac{\partial p_{phn}}{\partial s} = \frac{3p_{phn}n_{phn}^2\left[-E - M\sin\theta v_{phyn}\right]}{\left(\frac{n_{ph0}}{n_0}\right)^2(M-\delta_h)^2 - 3p_{phn}n_{phn}} \tag{4.51}$$

$$\frac{\partial n_{phn}}{\partial s} = \frac{n_{phn}^3\left[-E - M\sin\theta v_{phyn}\right]}{\left(\frac{n_{ph0}}{n_0}\right)^2(M-\delta_h)^2 - 3p_{phn}n_{phn}} \tag{4.52}$$

$$\frac{\partial v_{phyn}}{\partial s} = \frac{Mn_{phn}}{(M-\delta_h)}\left(\frac{n_0}{n_{ph0}}\right)\left[\left(M - \frac{(M-\delta_h)}{n_{phn}}\left(\frac{n_{ph0}}{n_0}\right)\right)\sin\theta - v_{phzn}\cos\theta\right] \tag{4.53}$$

$$\frac{\partial v_{phzn}}{\partial s} = \left(\frac{n_0}{n_{ph0}}\right)\frac{n_{phn}v_{phyn}M\cos\theta}{(M-\delta_h)} \tag{4.54}$$

$$\frac{\partial p_{ehn}}{\partial s} = \frac{3p_{ehn}n_{ehn}^2\left[E + M\sin\theta v_{ehyn}\right]}{\left(\frac{n_{eh0}}{n_0}\right)^2(M-\delta_h)^2 - 3p_{ehn}n_{ehn}} \tag{4.55}$$

$$\frac{\partial n_{ehn}}{\partial s} = \frac{n_{ehn}^3\left[E + M\sin\theta v_{ehyn}\right]}{\left(\frac{n_{eh0}}{n_0}\right)^2(M-\delta_h)^2 - 3p_{ehn}n_{ehn}} \tag{4.56}$$

$$\frac{\partial v_{ehyn}}{\partial s} = \frac{Mn_{ehn}}{(M-\delta_h)}\left(\frac{n_0}{n_{eh0}}\right)\left[-\left(M - \frac{(M-\delta_h)}{n_{ehn}}\left(\frac{n_{eh0}}{n_0}\right)\right)\sin\theta + v_{ehzn}\cos\theta\right] \tag{4.57}$$

$$\frac{\partial v_{ehzn}}{\partial s} = -\left(\frac{n_0}{n_{eh0}}\right)\frac{n_{ehn}v_{ehyn}M\cos\theta}{(M-\delta_h)} \tag{4.58}$$

In equations $(4.43)-(4.58)$, the velocities are normalized with respect to the thermal velocity $v_{th} = (T_h/m)^{1/2}$ of the hot species and the densities with respect to the total density n_0. We recall, the equilibrium density of the cold (hot) electrons is n_{ec0} (n_{eh0}), and that of the cold (hot) positrons is n_{pc0} (n_{ph0}), with $n_{ec0} + n_{eh0} = n_{pc0} + n_{ph0} = n_0$. $R = \omega_p/\Omega$, where $\omega_p = (n_0e^2/\varepsilon_0 m)^{1/2}$ is the total plasma frequency, $M = V/v_{th}$ is the normalized Mach number and $\delta_{c,h} = v_{0c,0h}/v_{th}$ is the normalized drift velocity of cold (hot) species at s=0. The additional subscript 'n' indicates the normalized quantities.

4.3.3 Numerical Results

The system of nonlinear first-order differential equations $(4.43) - (4.58)$ are once again solved numerically using the Runge-Kutta (RK4) technique (Press *et al.*, 1996). The initial values were determined self consistently. Initial values are given to v_{ecyn}, v_{eczn}, v_{pcyn}, v_{pczn}, v_{phyn}, and v_{phzn}. Then v_{ehyn0} and v_{ehzn0} are calculated self consistently (see Appendix C). From the quasi-neutrality condition at equilibrium we have for the normalized densities, $n_{ec0}+n_{eh0} = n_{pc0}+n_{ph0} = 1$. Hence for a given $n_{ec0} = n_{pc0}$ value, $n_{eh0} = n_{ph0}$ is calculated. All figures illustrate the actual normalized electric fields, where

$E_{norm} = -(1/M)(\partial\psi/\partial s)$.

Effect of the driving amplitude E_0 on the waves

Figures $4.9 - 4.11$ shows the evolution of the system for the various driving electric field amplitudes E_0. The fixed normalized parameters are $M = 3.5$, $R = 10.0$, $\theta = 2^o$, $\delta_c = \delta_h = 0.0$, $n_{ec0}/n_0 = n_{pc0}/n_0 = 0.5$ and $T_c/T_h = 0.0$. For the selected plasma parameters and a R value of 10, our investigations showed that the sought nonlinear structures were possible only for much higher values of M compared to the results in section 4.2. A typically value of $M = 3.5$ is used for curves $4.9 - 4.11$. Once again wave propagation is taken almost parallel to the ambient magnetic field $\mathbf{B_0}$. As E_0 increases, the electric field structure evolves from a linear sinusoidal waveform to a nonlinear sawtooth structure. For a higher E_0 value of 3.5, the structure displays a spiky bipolar pulse. Following the analysis in section 4.2.3, for the linear wave in figure 4.9, with a small driving amplitude of $E_0 = 0.05$, the period of the wave is calculated to be $T_w = 0.99\tau_c$ (frequency $f_w = 1.0f_c$), displaying the cyclotron oscillation, where $\tau_c = 2\pi/\Omega$. Figure 4.10 shows a sawtooth waveform for $E_0 = 1.5$, with the period of the wave being $T_w = 1.42\tau_c$ (frequency $f_w = 0.70f_c$). For $E_0 = 3.5$ (figure 4.11), a spiky bipolar waveform is shown, where the period of the wave is $T_w = 3.42\tau_c$ (frequency $f_w = 0.29f_c$). From a comparison of figures (4.11) and (4.3), it is seen that for the selected plasma parameters here a much stronger value of the driving electric field E_0 (=3.5) is required to generate the spiky bipolar structures.

It is also noted that the period of the spiky structure is about three and a half times the cyclotron period and hence deduce that the waveform is driven by the acoustic mode.

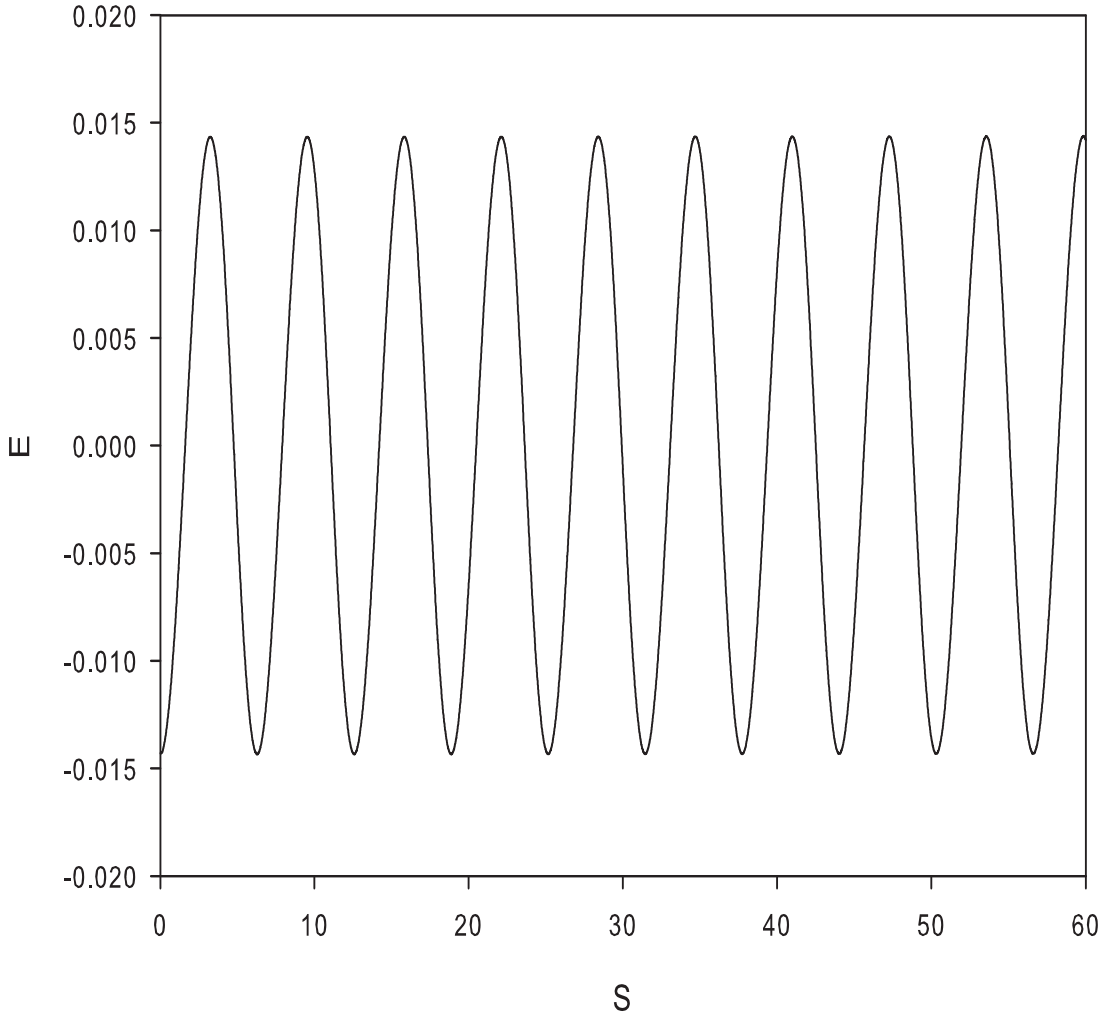

Figure 4.9: Numerical solution of the normalized electric field (sinusoidal waveform) for the parameters $M = 3.5$, $\theta = 2^o$, $R = 10.0$, $\delta_c = \delta_h = 0.0$, $n_{ec0}/n_0 = n_{pc0}/n_0 = 0.5$, $T_c/T_h = 0.0$, and $E_0 = 0.05$. The period of the wave is $T_w = 0.99\tau_c$ (frequency $f_w = 1.0 f_c$).

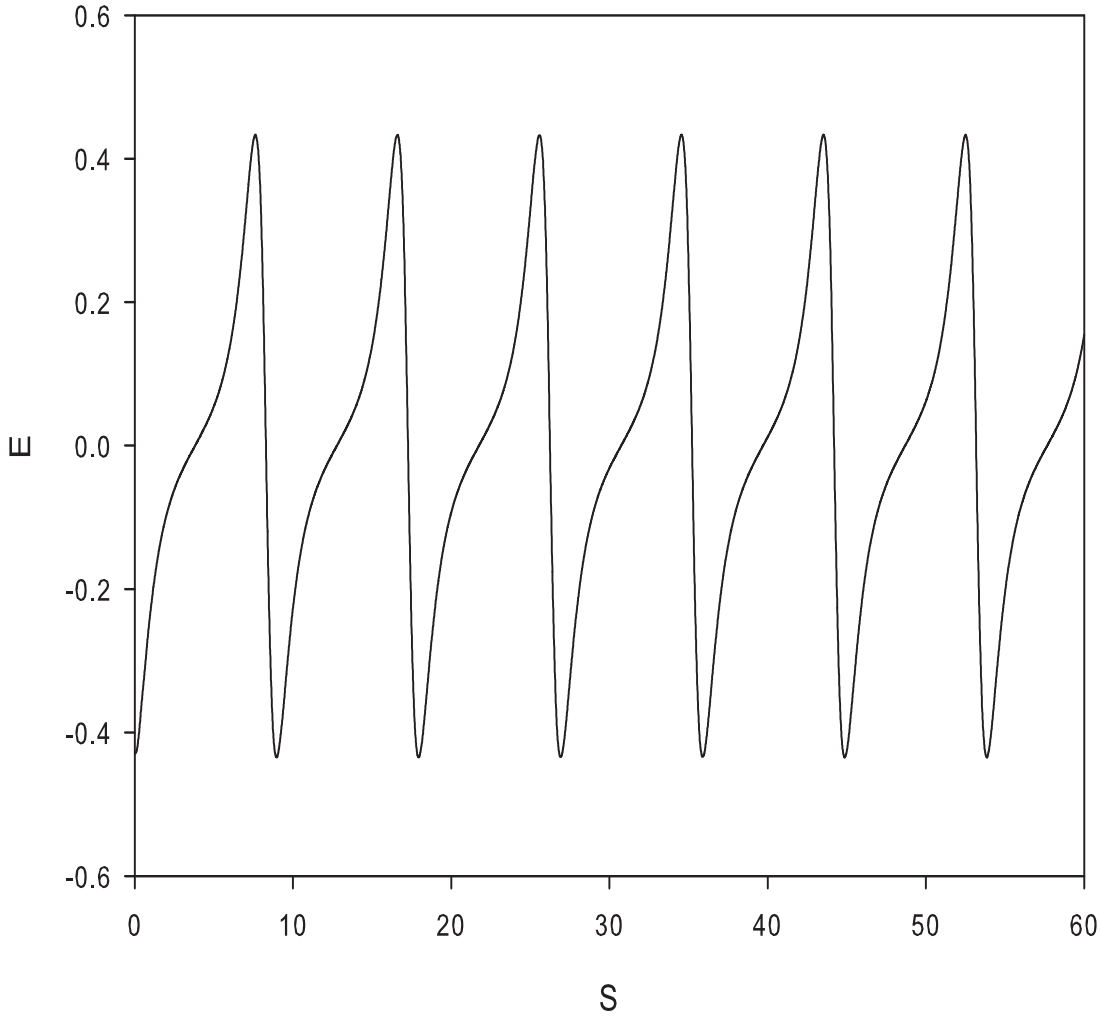

Figure 4.10: Numerical solution of the normalized electric field (sawtooth waveform) for the parameters $M = 3.5$, $\theta = 2^o$, $R = 10.0$, $\delta_c = \delta_h = 0.0$, $n_{ec0}/n_0 = n_{pc0}/n_0 = 0.5$, $T_c/T_h = 0.0$, and $E_0 = 1.5$. The period of the wave is $T_w = 1.42\tau_c$ (frequency $f_w = 0.70 f_c$).

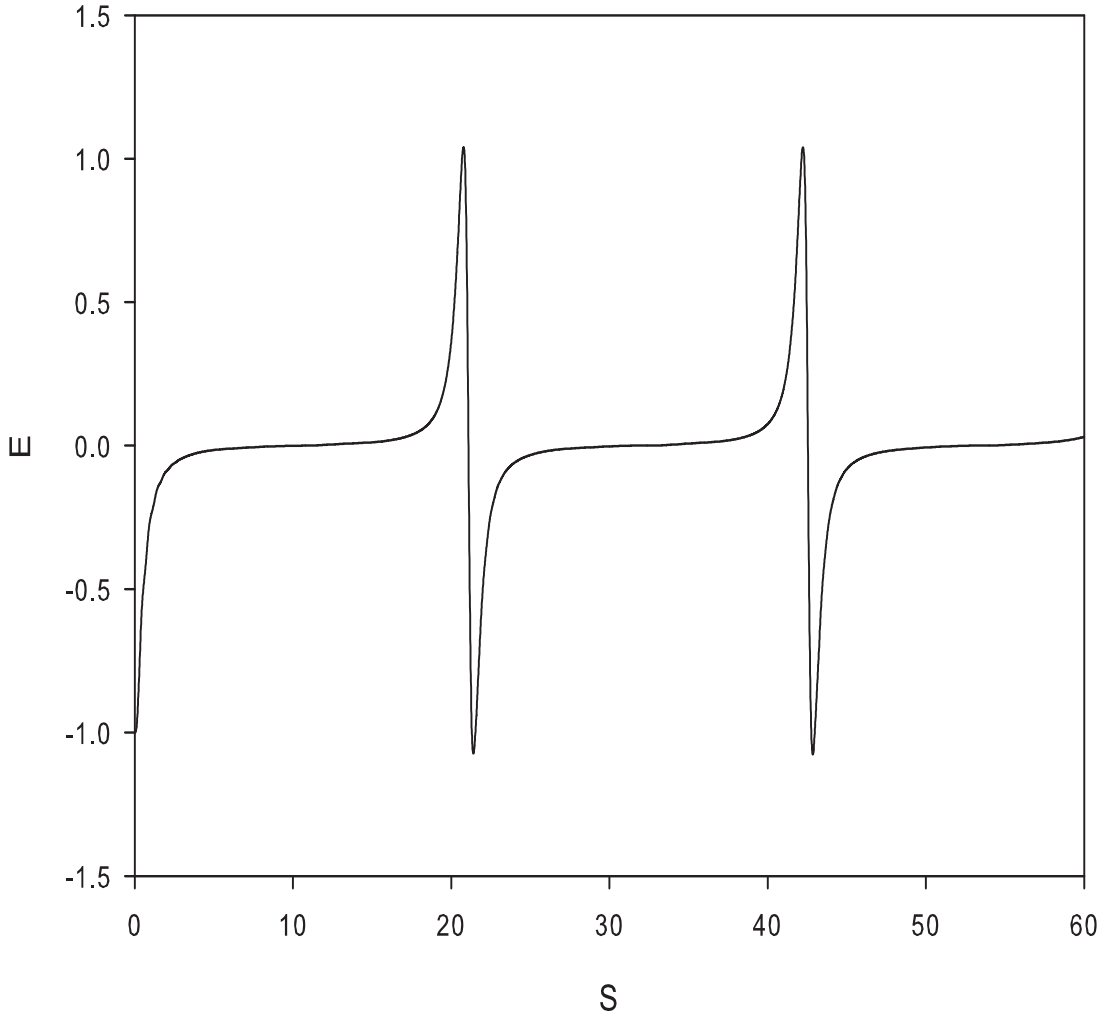

Figure 4.11: Numerical solution of the normalized electric field (bipolar waveform) for the parameters $M = 3.5$, $\theta = 2^o$, $R = 10.0$, $\delta_c = \delta_h = 0.0$, $n_{ec0}/n_0 = n_{pc0}/n_0 = 0.5$, $T_c/T_h = 0.0$, and $E_0 = 3.5$. The period of the wave is $T_w = 3.42\tau_c$ (frequency $f_w = 0.29 f_c$).

Effect of the Mach number M on the waves

Figures $4.12 - 4.14$ shows the effect of the Mach number on the electrostatic waves. Here M is varied from 3.0 to 5.0 with the fixed parameters, $E_0 = 2.0$, $R = 10.0$, $\theta = 2^o$, $\delta_c = \delta_h = 0.0$, $n_{ec0}/n_0 = n_{pc0}/n_0 = 0.5$ and $T_c/T_h = 0.0$. As the Mach number increases, the wave structure changes from a sharp spiky in form to more sawtooth-like. This indicates that the level of nonlinearity decreases with increasing M given the sequence observed when E_0 is increased in figures $4.9 - 4.11$. Hence for larger values of M, a stronger E_0 is required to generate the spiky structures. This effect was also observed by Reddy *et al.* (2002) and Moolla *et al.* (2003, 2007). Also noted is that the period of the wave decreases with an increase in the Mach number. For $M = 3.0$, which is the minimum value for which a waveform exists for the above fixed parameters, the wave has a period of $T_w = 2.62\tau_c$ (frequency $f_w = 0.38 f_c$), implying an associated driven acoustic mode. As the Mach number increases to 5.0, the period of the wave decreases to $1.15\tau_c$ (frequency $f_w = 0.87 f_c$), exhibiting a sawtooth type structure.

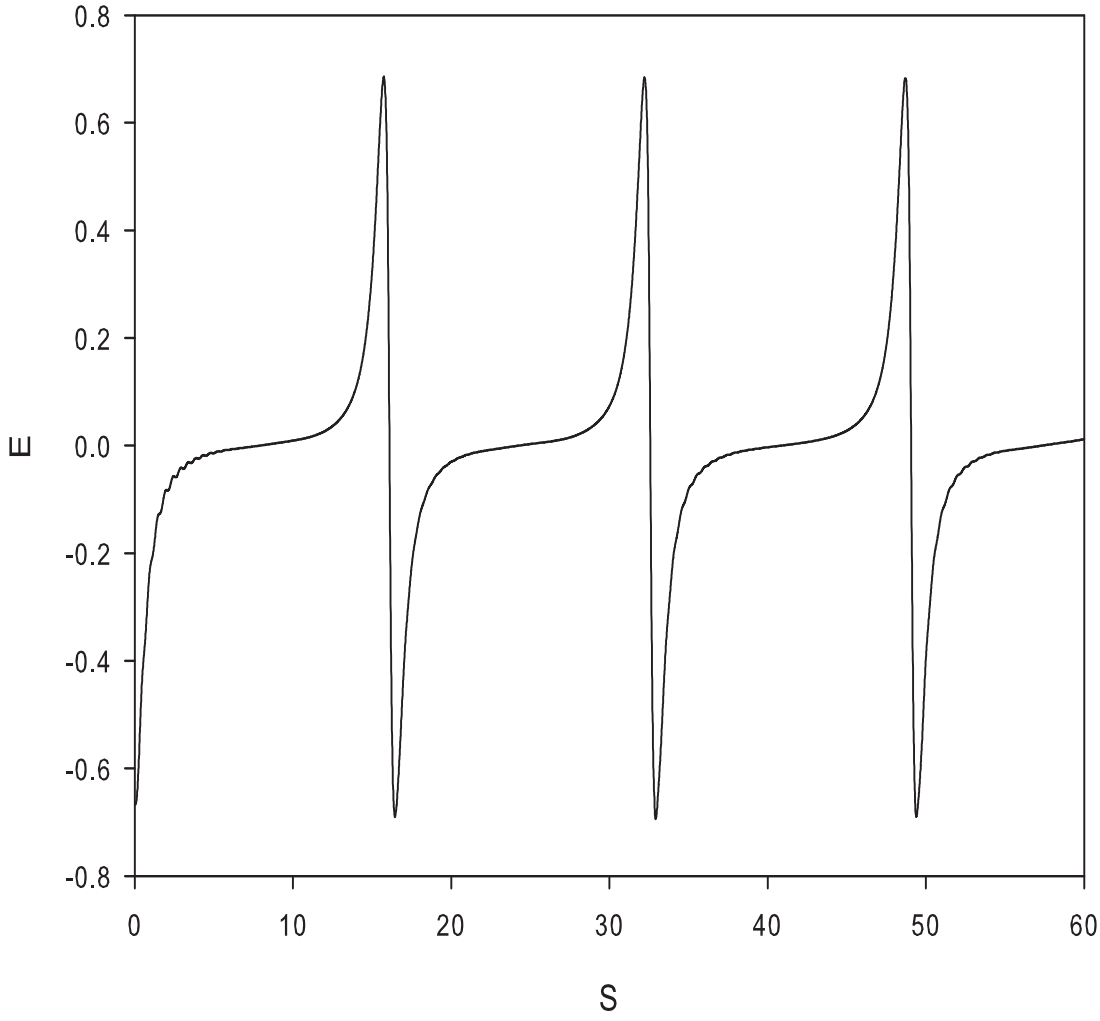

Figure 4.12: Numerical solution of the normalized electric field for the parameters $E_0 = 2.0$, $R = 10.0$, $\theta = 2^o$, $\delta_c = \delta_h = 0.0$, $n_{ec0}/n_0 = n_{pc0}/n_0 = 0.5$, $T_c/T_h = 0.0$, and $M = 3.0$. The period of the wave is $T_w = 2.62\tau_c$ (frequency $f_w = 0.38 f_c$).

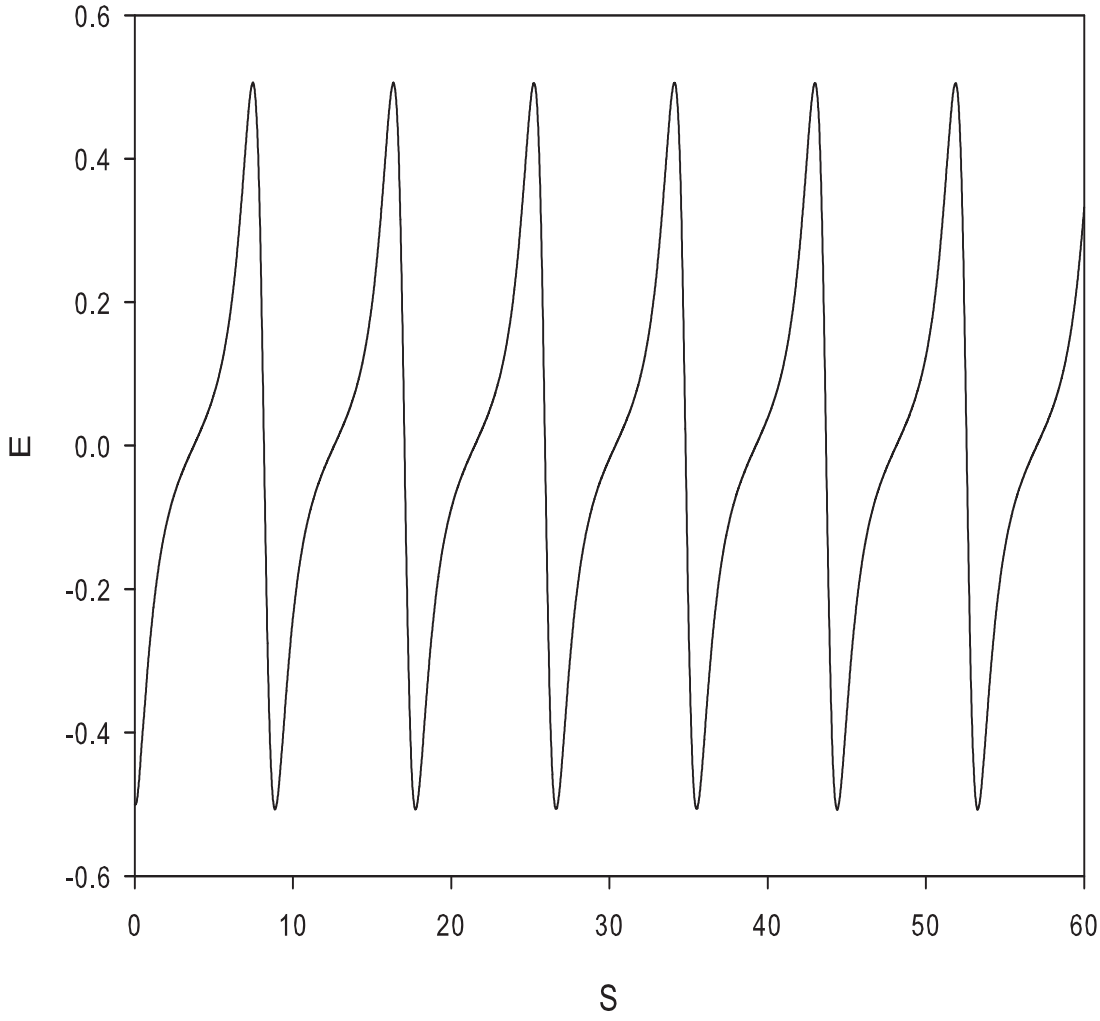

Figure 4.13: Numerical solution of the normalized electric field for the parameters $E_0 = 2.0$, $R = 10.0$, $\theta = 2^o$, $\delta_c = \delta_h = 0.0$, $n_{ec0}/n_0 = n_{pc0}/n_0 = 0.5$, $T_c/T_h = 0.0$, and $M = 4.0$. The period of the wave is $T_w = 1.42\tau_c$ (frequency $f_w = 0.70 f_c$).

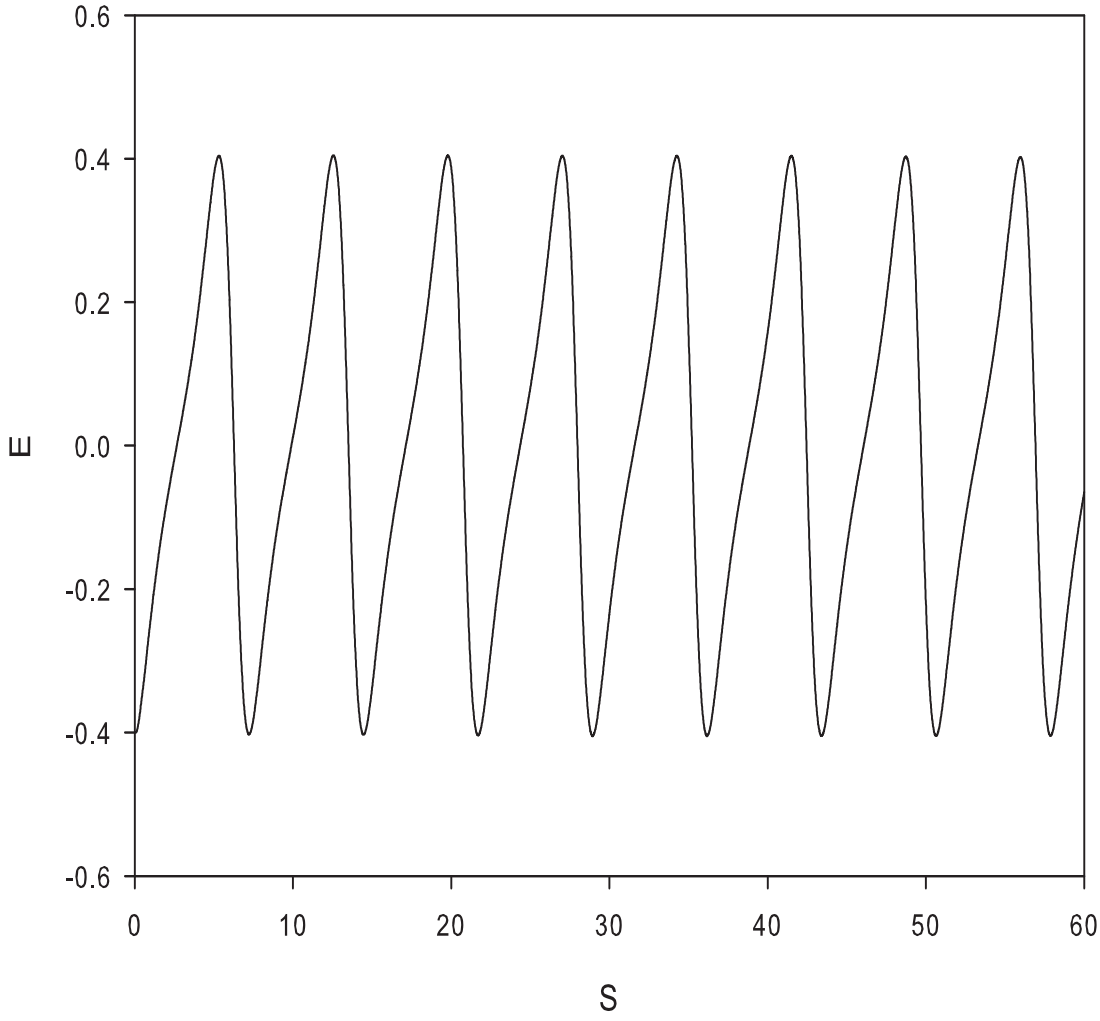

Figure 4.14: Numerical solution of the normalized electric field for the parameters $E_0 = 2.0$, $R = 10.0$, $\theta = 2^o$, $\delta_c = \delta_h = 0.0$, $n_{ec0}/n_0 = n_{pc0}/n_0 = 0.5$, $T_c/T_h = 0.0$, and $M = 5.0$. The period of the wave is $T_w = 1.15\tau_c$ (frequency $f_w = 0.87 f_c$).

Effect of the hot electron and positron drift velocity on the waves

Figures $4.15 - 4.19$ shows the variation of the the drift velocities for the hot electron and positron components. The fixed parameters are $E_0 = 3.5$, $M = 3.5$, $R = 10.0$, $\theta = 2^o$, $\delta_c = 0.0$, $n_{ec0}/n_0 = n_{pc0}/n_0 = 0.5$, and $T_c/T_h = 0.0$. The period of the spiky structures decreases from $3.83\tau_c$ for $\delta_h = -0.3$ (figure 4.15) to $3.08\tau_c$ for $\delta_h = +0.3$ (figure 4.19). As found in section 4.2 for the drift of the cold species, the hot electron and positron flow anti-parallel (parallel) to $\mathbf{B_0}$ increases (decreases) the period of the spiky structure. Previous studies by Reddy *et al.* (2002) and Moolla *et al.* (2003) on ion-electron plasmas showed a similar behaviour for the hot electron drift velocities.

For the ESWs observed in the earth's magnetosphere, Kojima *et al.* (1994) found that the period of the ESWs changed rapidly (see figure 4a). Given the above found dependence of the periodicity on the hot electron drift speed, Moolla *et al.* (2003) suggested that the observed rapid changes in the period of the ESWs could be due to electrons being accelerated in bursts. Our results show that a similar phenomenon could occur in an electron-positron plasma where due to the symmetry of the system both species (electrons and positrons) are drifting.

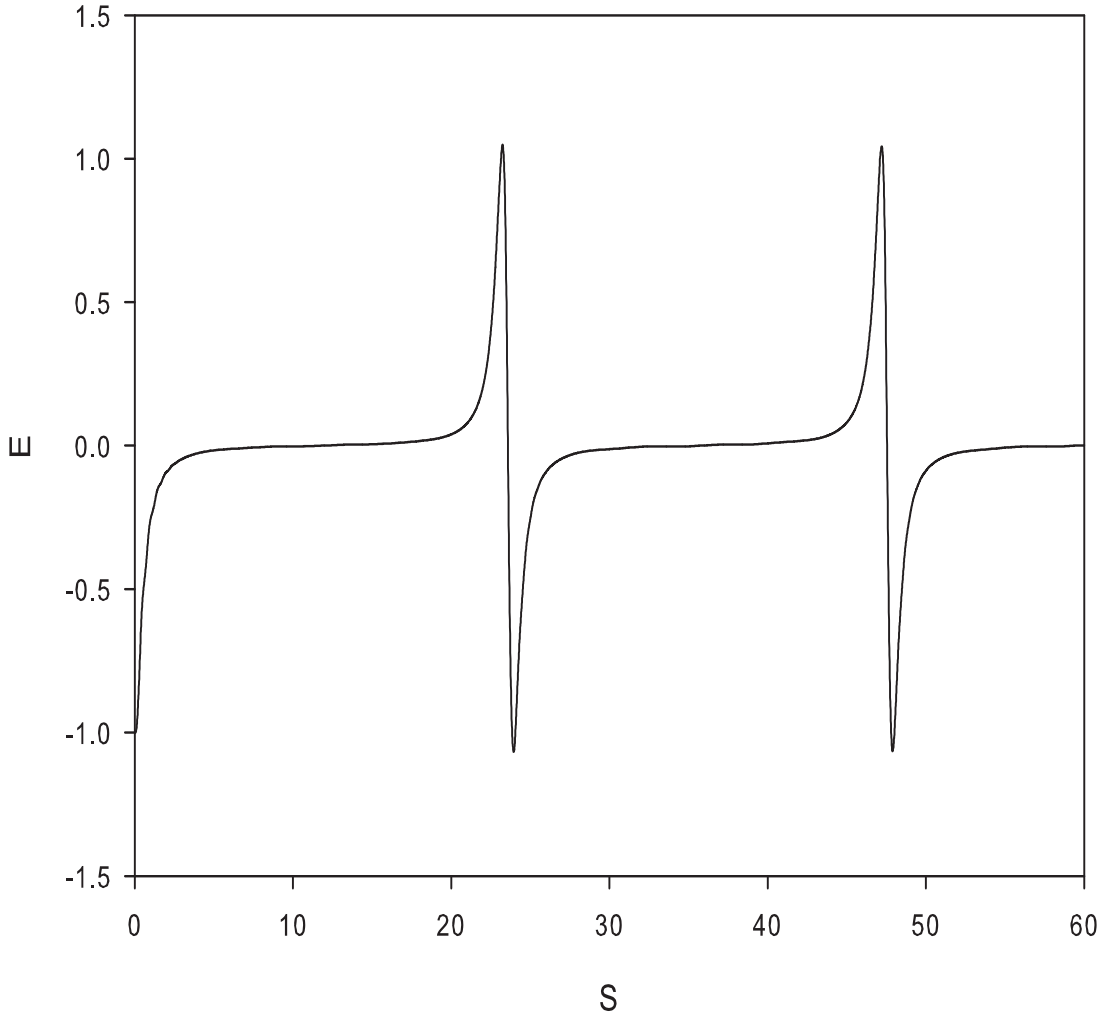

Figure 4.15: Numerical solution of the normalized electric field for the parameters $M = 3.5$, $E_0 = 3.5$, $R = 10.0$, $\theta = 2^o$, $n_{ec0}/n_0 = n_{pc0}/n_0 = 0.5$, $T_c/T_h = 0.0$, $\delta_c = 0$ and $\delta_h = -0.3$. The period of the wave is $T_w = 3.83\tau_c$ (frequency $f_w = 0.26 f_c$).

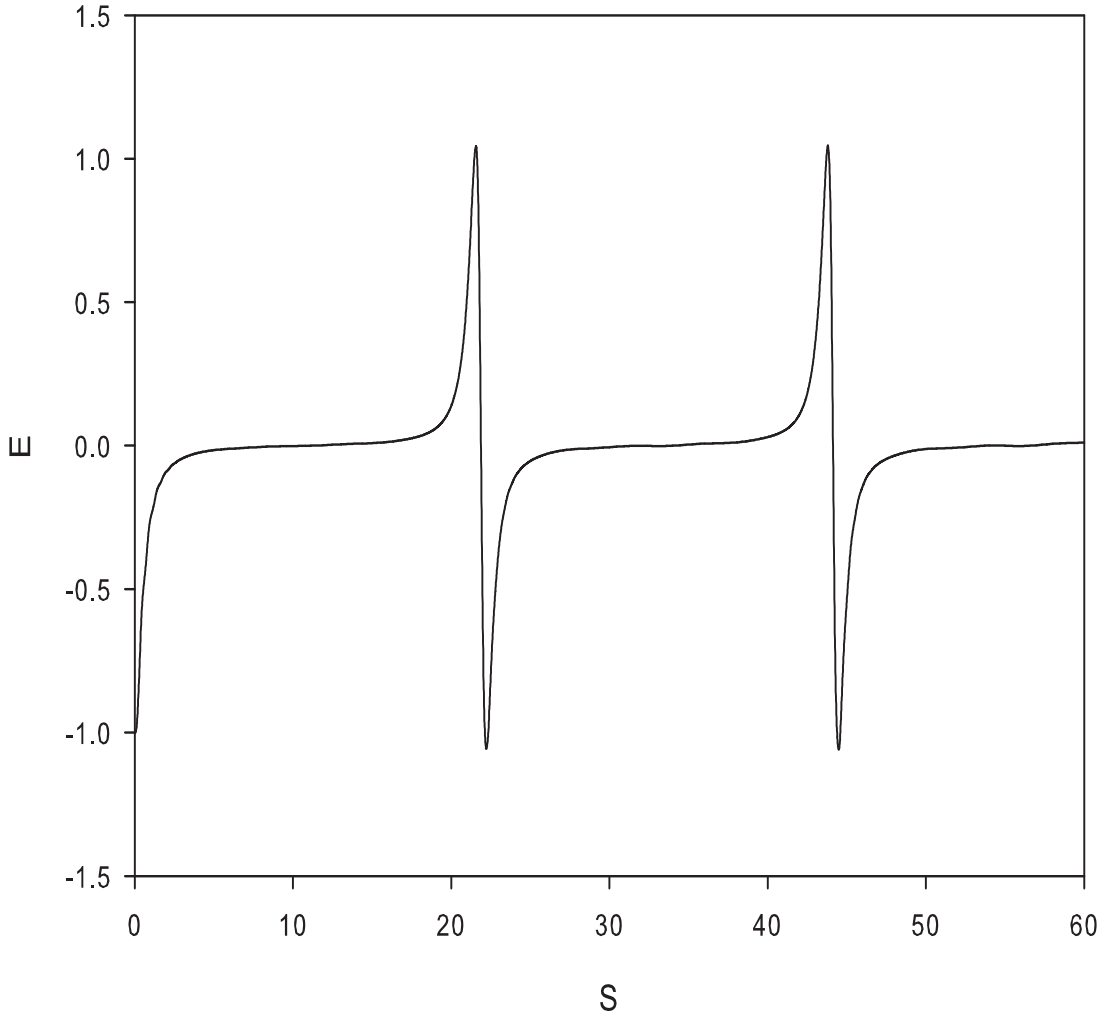

Figure 4.16: Numerical solution of the normalized electric field for the parameters $M = 3.5$, $E_0 = 3.5$, $R = 10.0$, $\theta = 2^o$, $n_{ec0}/n_0 = n_{pc0}/n_0 = 0.5$, $T_c/T_h = 0.0$, $\delta_c = 0$ and $\delta_h = -0.1$. The period of the wave is $T_w = 3.56\tau_c$ (frequency $f_w = 0.28 f_c$).

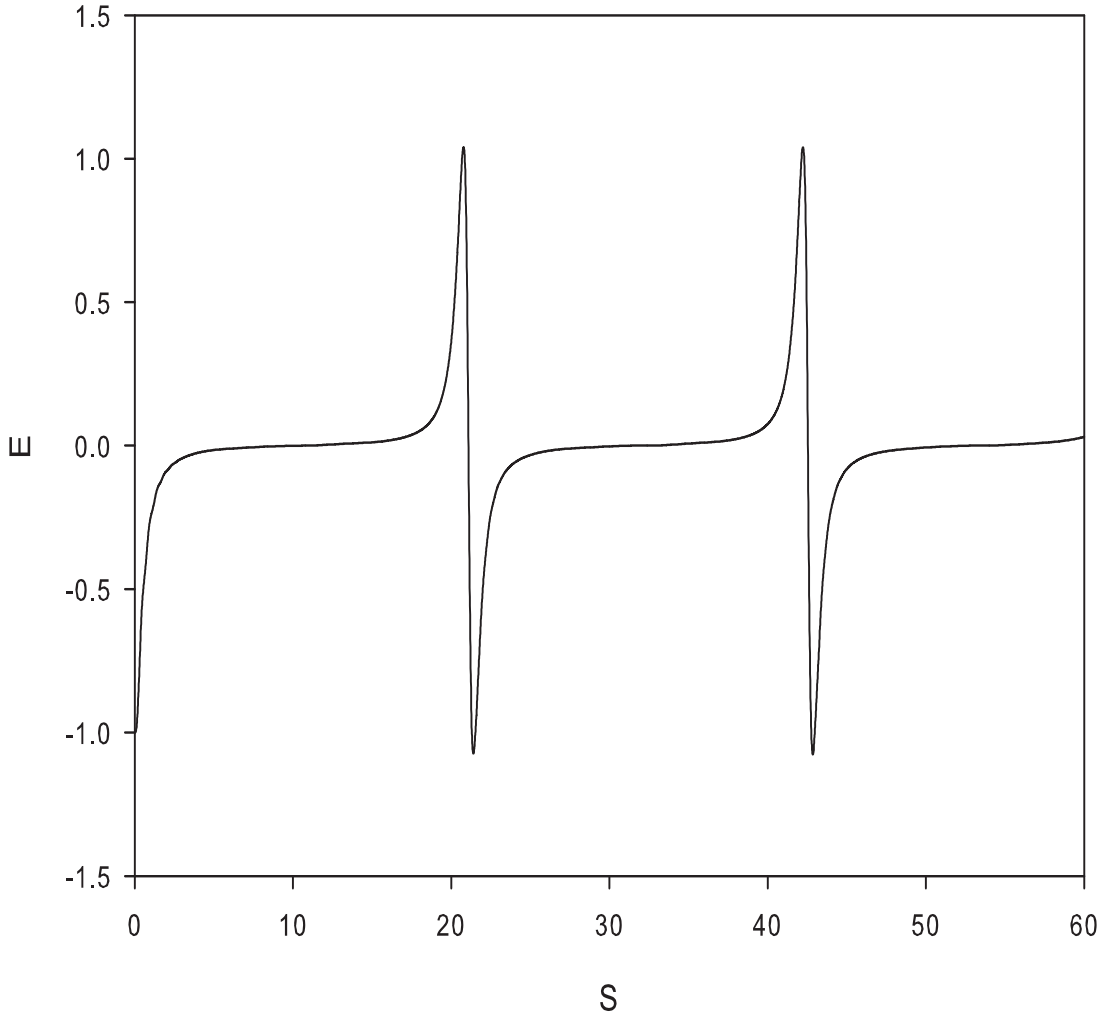

Figure 4.17: Numerical solution of the normalized electric field for the parameters $M = 3.5$, $E_0 = 3.5$, $R = 10.0$, $\theta = 2^o$, $n_{ec0}/n_0 = n_{pc0}/n_0 = 0.5$, $T_c/T_h = 0.0$, $\delta_c = 0$ and $\delta_h = 0.0$. The period of the wave is $T_w = 3.41\tau_c$ (frequency $f_w = 0.29 f_c$).

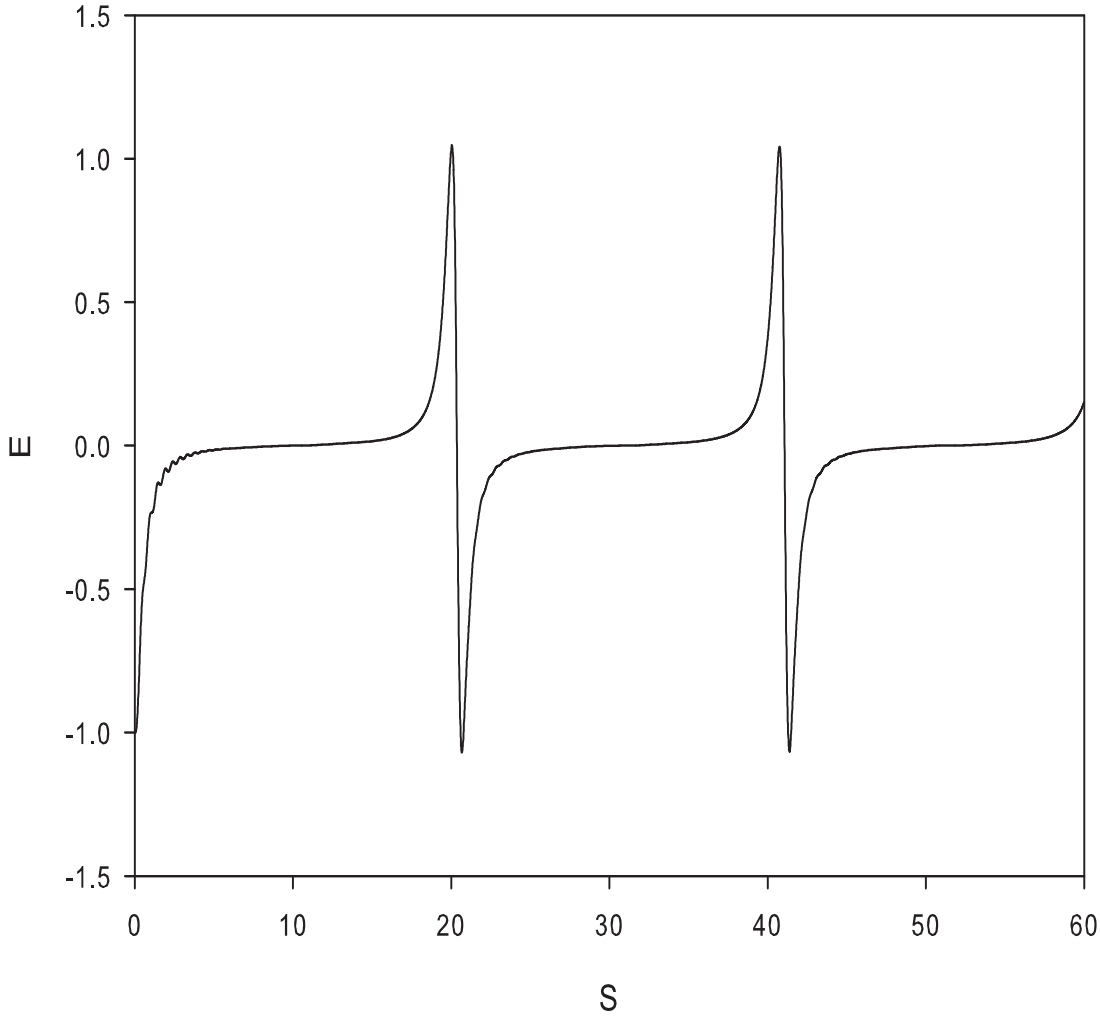

Figure 4.18: Numerical solution of the normalized electric field for the parameters $M = 3.5$, $E_0 = 3.5$, $R = 10.0$, $\theta = 2^o$, $n_{ec0}/n_0 = n_{pc0}/n_0 = 0.5$, $T_c/T_h = 0.0$, $\delta_c = 0$ and $\delta_h = 0.1$. The period of the wave is $T_w = 3.31\tau_c$ (frequency $f_w = 0.30 f_c$).

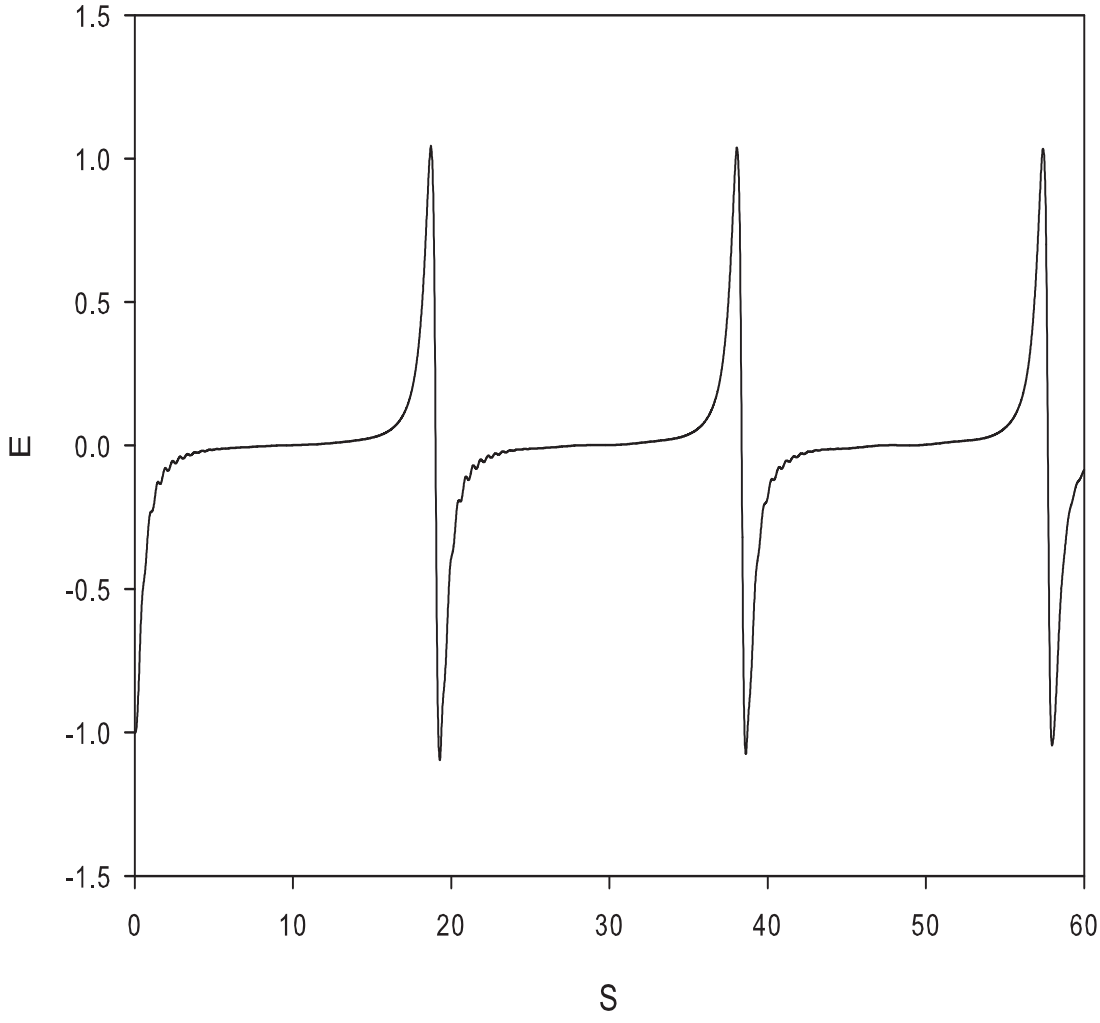

Figure 4.19: Numerical solution of the normalized electric field for the parameters $M = 3.5$, $E_0 = 3.5$, $R = 10.0$, $\theta = 2^o$, $n_{ec0}/n_0 = n_{pc0}/n_0 = 0.5$, $T_c/T_h = 0.0$, $\delta_c = 0$ and $\delta_h = 0.3$. The period of the wave is $T_w = 3.08\tau_c$ (frequency $f_w = 0.32f_c$).

Effect of the cold electron and positron drift velocity on the waves

The effect of the drift velocities for the cold electron and positron components are shown in Figures 4.20−4.24. The fixed parameters are $E_0 = 3.5$, $M = 3.5$, $R = 10.0$, $\theta = 2^o$, $\delta_h = 0.0$, $n_{ec0}/n_0 = n_{pc0}/n_0 = 0.5$, and $T_c/T_h = 0.0$. Here the period of the spiky structures are observed to increase from $2.89\tau_c$ for $\delta_c = -0.3$ (figure 4.20), to $4.17\tau_c$ for $\delta_c = +0.3$ (figure 4.24), i.e, as the cold beam flow becomes more parallel to the ambient magnetic field. Therefore, the cold electron and positron flow anti-parallel (parallel) to $\mathbf{B_0}$ decreases (increases) the period of the spiky structure. It is noted that the effect of the cold electron and positron drift on the ESWs is opposite to that of the hot electron and positron drift on the waves. Moolla *et al.* (2003), in their study of electron-ion plasmas found that the drift velocity of the cold ions had no effect on the period of the wave, but in their further study Moolla *et al.* (2007) found that the effect of the cold electron drift velocity increased the period of the waves as the flow moved from anti-parallel to parallel.

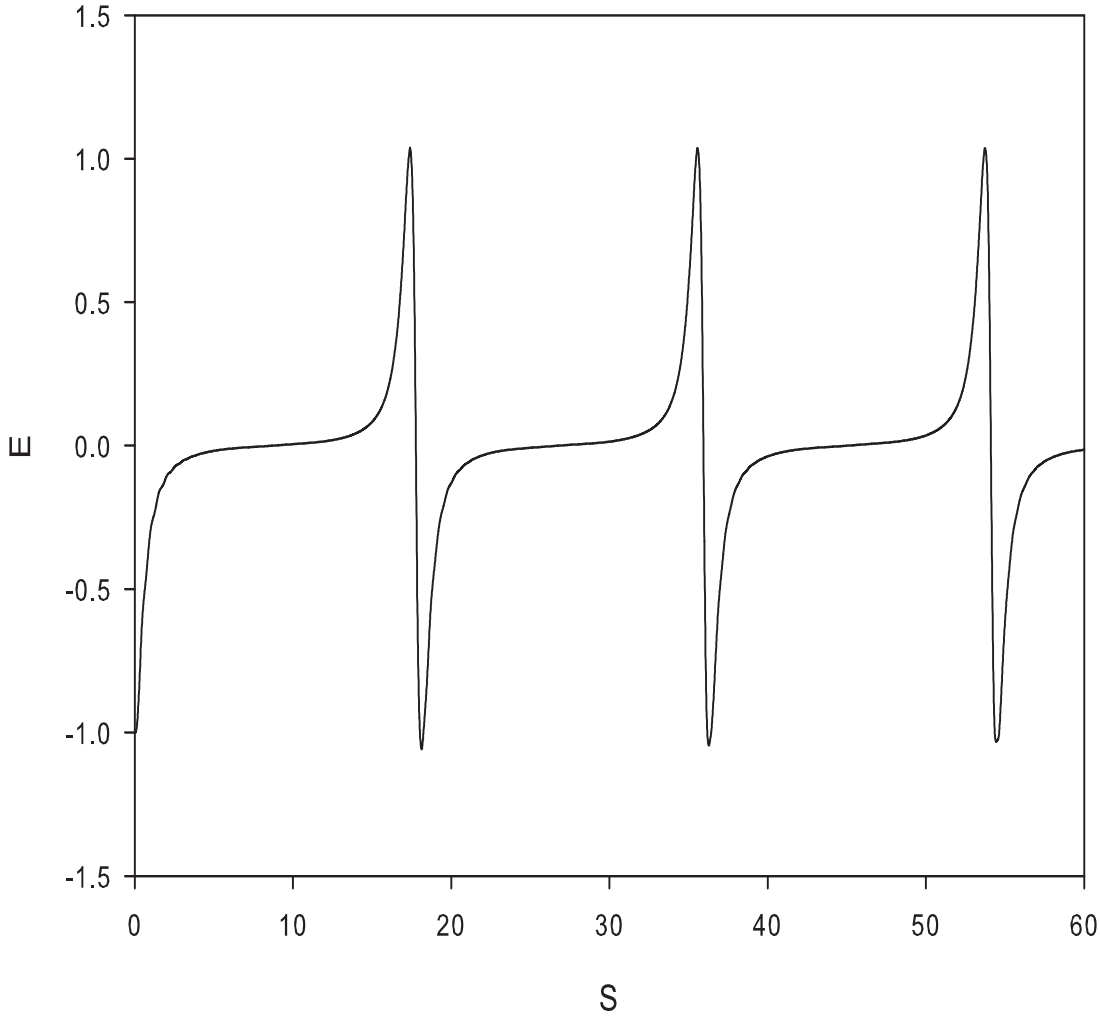

Figure 4.20: Numerical solution of the normalized electric field for the parameters $M = 3.5$, $E_0 = 3.5$, $R = 10.0$, $\theta = 2^o$, $n_{ec0}/n_0 = n_{pc0}/n_0 = 0.5$, $T_c/T_h = 0.0$, $\delta_h = 0$ and $\delta_c = -0.3$. The period of the wave is $T_w = 2.89\tau_c$ (frequency $f_w = 0.35 f_c$).

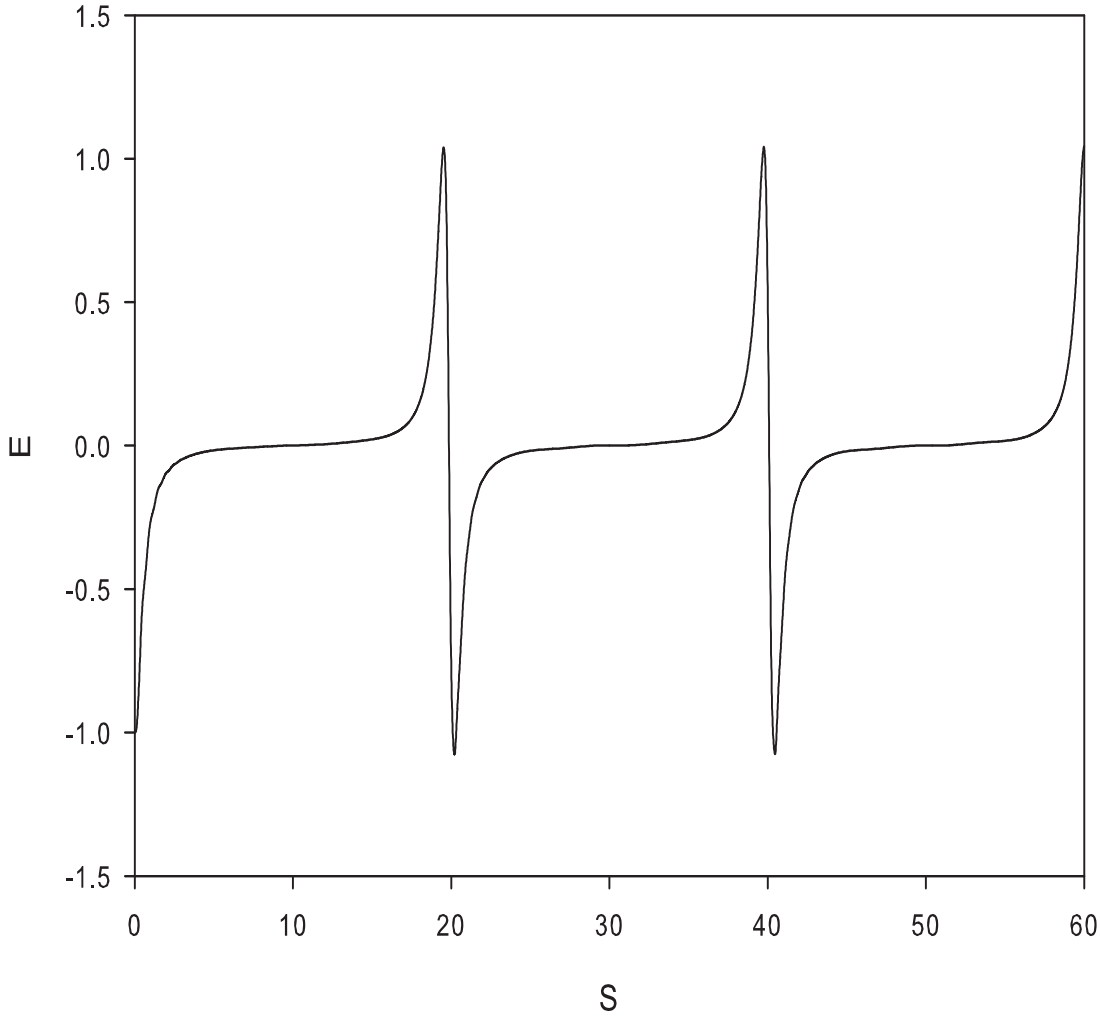

Figure 4.21: Numerical solution of the normalized electric field for the parameters $M = 3.5$, $E_0 = 3.5$, $R = 10.0$, $\theta = 2^o$, $n_{ec0}/n_0 = n_{pc0}/n_0 = 0.5$, $T_c/T_h = 0.0$, $\delta_h = 0$ and $\delta_c = -0.1$. The period of the wave is $T_w = 3.25\tau_c$ (frequency $f_w = 0.31 f_c$).

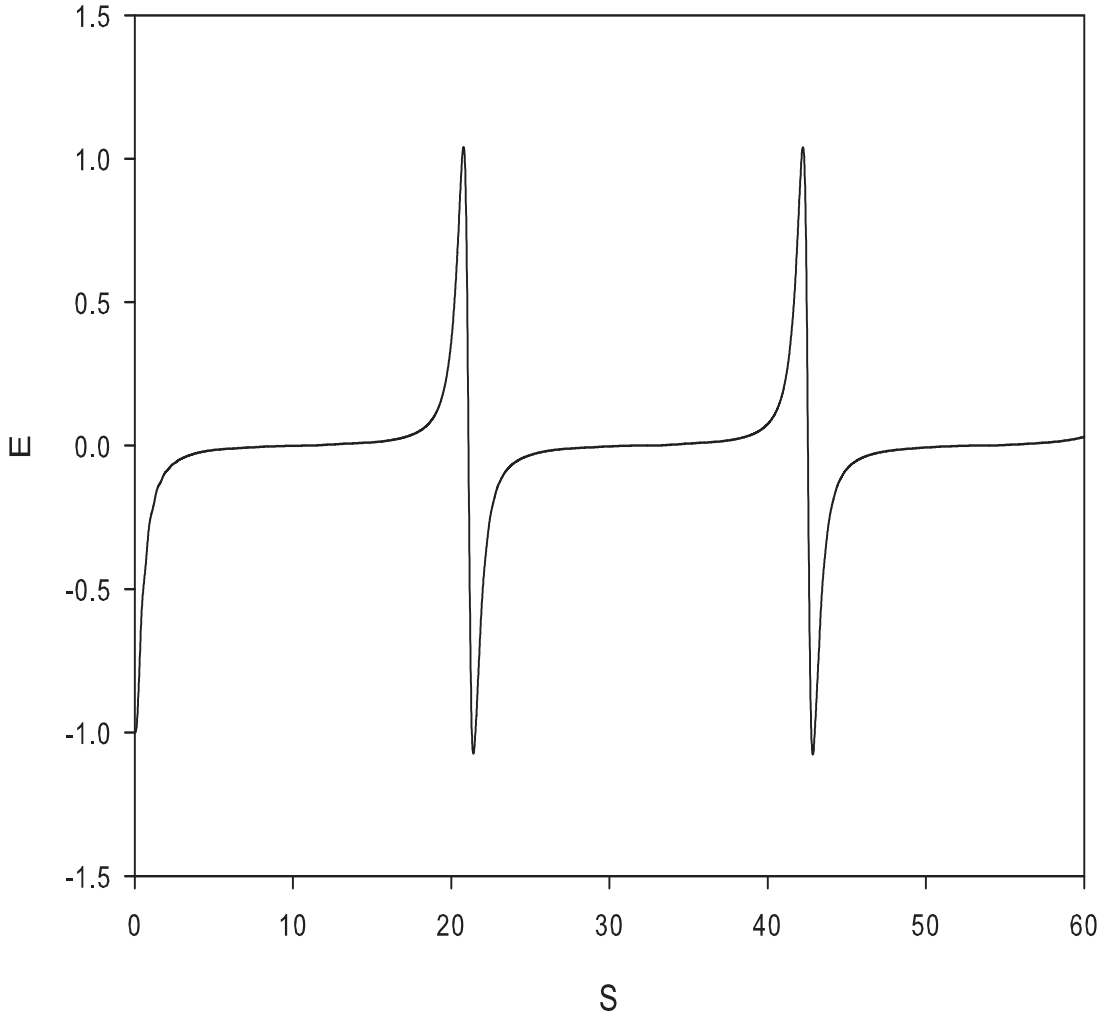

Figure 4.22: Numerical solution of the normalized electric field for the parameters $M = 3.5$, $E_0 = 3.5$, $R = 10.0$, $\theta = 2^o$, $n_{ec0}/n_0 = n_{pc0}/n_0 = 0.5$, $T_c/T_h = 0.0$, $\delta_h = 0$ and $\delta_c = 0.0$. The period of the wave is $T_w = 3.41\tau_c$ (frequency $f_w = 0.29 f_c$).

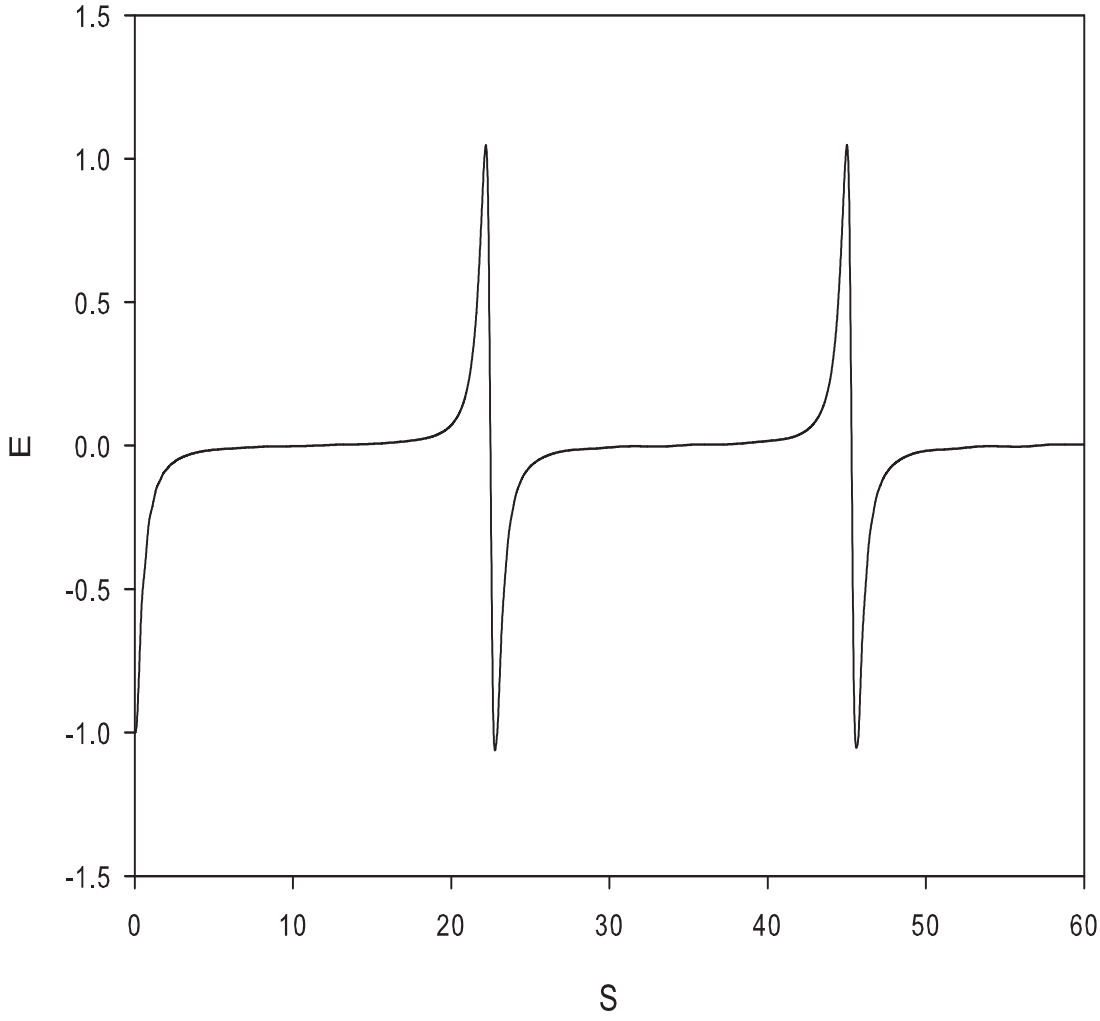

Figure 4.23: Numerical solution of the normalized electric field for the parameters $M = 3.5$, $E_0 = 3.5$, $R = 10.0$, $\theta = 2^o$, $n_{ec0}/n_0 = n_{pc0}/n_0 = 0.5$, $T_c/T_h = 0.0$, $\delta_h = 0$ and $\delta_c = 0.1$. The period of the wave is $T_w = 3.63\tau_c$ (frequency $f_w = 0.28 f_c$).

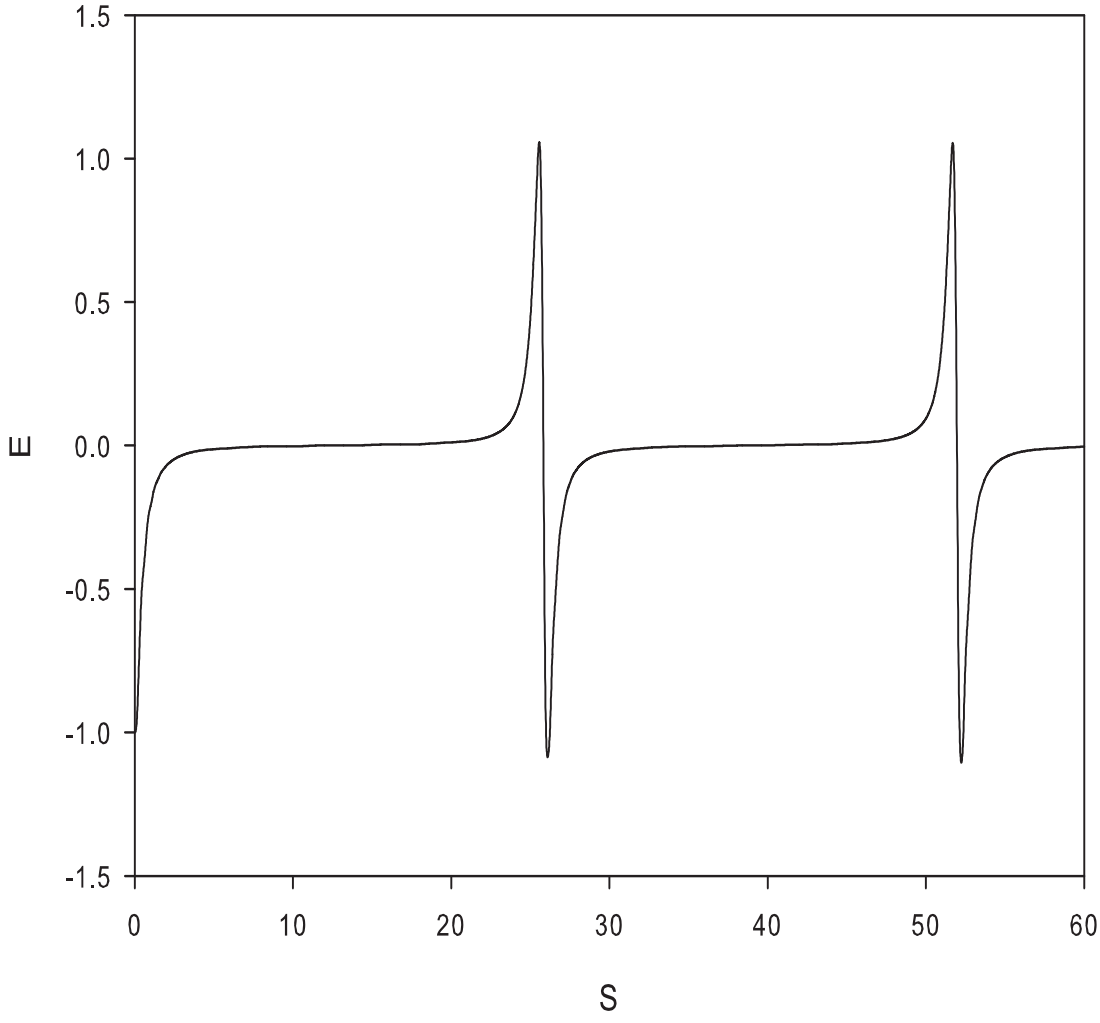

Figure 4.24: Numerical solution of the normalized electric field for the parameters $M = 3.5$, $E_0 = 3.5$, $R = 10.0$, $\theta = 2^o$, $n_{ec0}/n_0 = n_{pc0}/n_0 = 0.5$, $T_c/T_h = 0.0$, $\delta_h = 0$ and $\delta_c = 0.3$. The period of the wave is $T_w = 4.17\tau_c$ (frequency $f_w = 0.24 f_c$).

Effect of the density ratio of the species on the waves

Figures $4.25 - 4.27$ shows the effect of the electron and positron densities on the normalized electric field. The fixed parameters are, $E_0 = 1.5$, $M = 3.5$, $R = 10.0$, $\theta = 2^o$, $\delta_c = \delta_h = 0.0$ and $T_c/T_h = 0.0$. As the densities n_{ec0}/n_0 and n_{pc0}/n_0 increases, the oscillations becomes more nonlinear, with increasing periodicity. With $n_{ec0}/n_0 = n_{pc0}/n_0 = 0.1$ (figure 4.25), a linear waveform of period $1.0\tau_c$ (frequency f_w=$1.0f_c$) is observed. As the densities are increased ($n_{ec0}/n_0 = n_{pc0}/n_0 = 0.4$), the waveform tends to a sawtooth structure (figure 4.26) of period $1.22\tau_c$ (frequency f_w=$0.82f_c$). For even larger densities ($n_{ec0}/n_0 = n_{pc0}/n_0 = 0.7$), the electric field evolves into a spiky structure (figure 4.27) of period $2.66\tau_c$ (frequency f_w=$0.38f_c$). From a comparison of figure (4.27) with earlier results (e.g. figure 4.11), it is noted that a smaller driving electric field is required to drive the nonlinearity of the wave for larger density values. Since the periods of the waves are greater than $1.0\tau_c$, these waves are associated with the driven acoustic mode. The results indicate that the bipolar spiky structures are easier to excite in a two temperature electron-positron plasma for large values of the fractional density of the cold species.

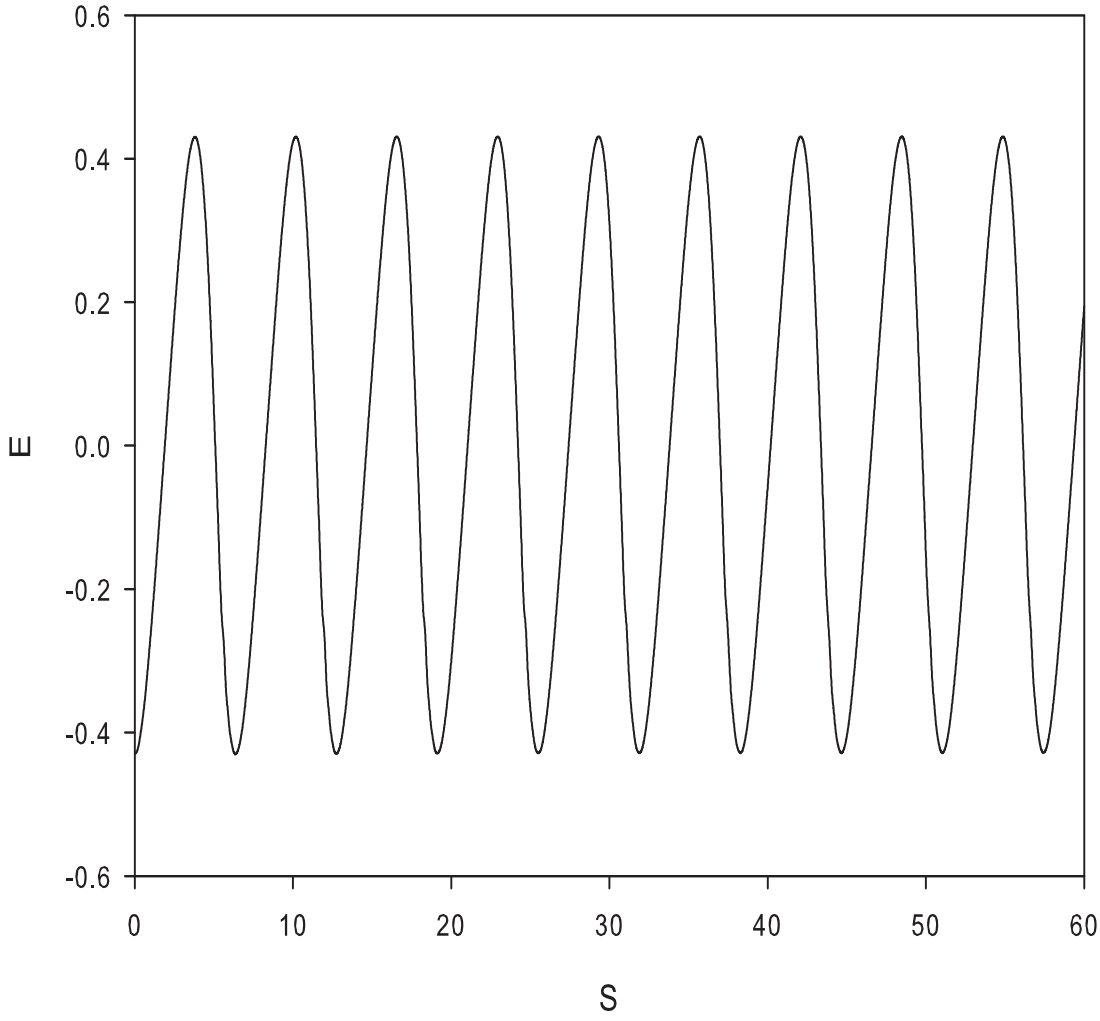

Figure 4.25: Numerical solution of normalized electric field for the parameters $M = 3.5$, $E_0 = 1.5$, $R = 10.0$, $\theta = 2^o$, $\delta_c = \delta_h = 0.0$, $T_c/T_h = 0.0$ and $n_{ec0}/n_0 = n_{pc0}/n_0 = 0.1$. The period of the wave is $T_w = 1.0\tau_c$ (frequency $f_w = 1.0f_c$).

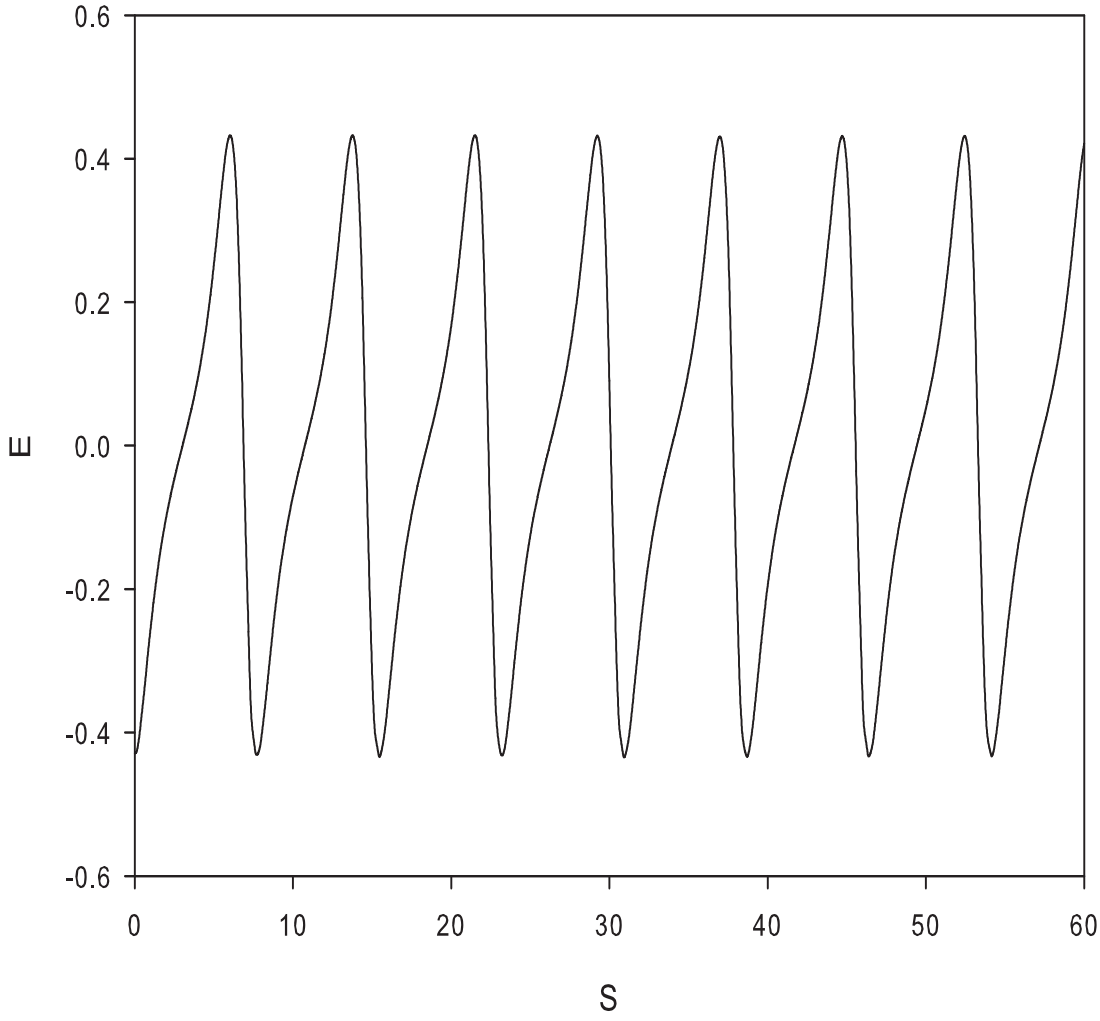

Figure 4.26: Numerical solution of normalized electric field for the parameters $M = 3.5$, $E_0 = 1.5$, $R = 10.0$, $\theta = 2^o$, $\delta_c = \delta_h = 0.0$, $T_c/T_h = 0.0$ and $n_{ec0}/n_0 = n_{pc0}/n_0 = 0.4$. The period of the wave is $T_w = 1.22\tau_c$ (frequency $f_w = 0.82 f_c$).

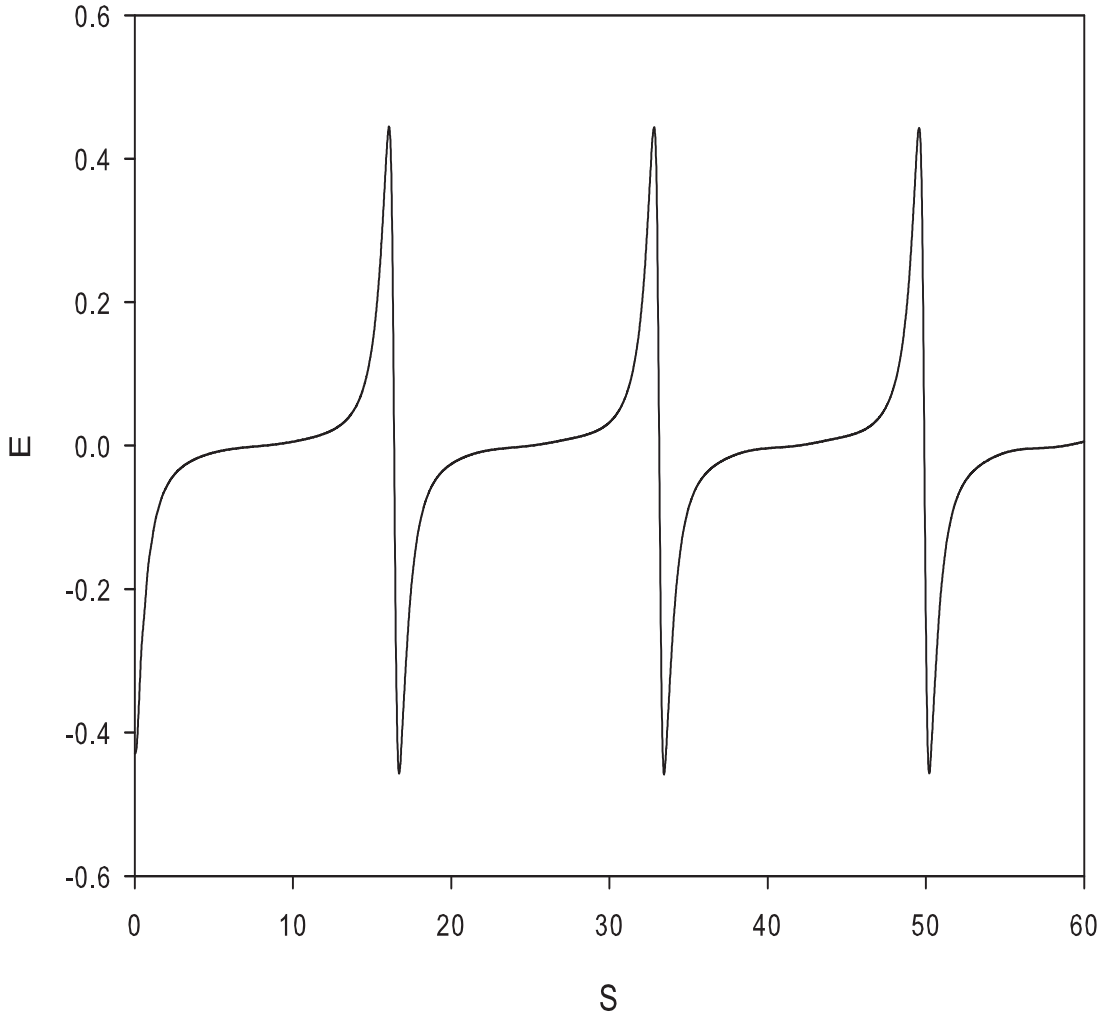

Figure 4.27: Numerical solution of normalized electric field for the parameters $M = 3.5$, $E_0 = 1.5$, $R = 10.0$, $\theta = 2^o$, $\delta_c = \delta_h = 0.0$, $T_c/T_h = 0.0$ and $n_{ec0}/n_0 = n_{pc0}/n_0 = 0.7$. The period of the wave is $T_w = 2.66\tau_c$ (frequency $f_w = 0.38 f_c$).

Effect of the propagation angle on the waves

In figure 4.28, the propagation angle θ relative to the ambient magnetic field $\mathbf{B_0}$ is varied. The fixed parameters are $E_0 = 3.0$, $M = 3.5$, $R = 10.0$, $\delta_c = \delta_h = 0.0$, $n_{ec0}/n_0 = n_{pc0}/n_0 = 0.5$, and $T_c/T_h = 0.0$. The oscillations are of a spiky nature and the periodicity of the wave remains unchanged with a period of $2.75\tau_c$ (frequency f_w=$0.36f_c$), representing an acoustic mode. As the propagation angle increases the wave becomes increasingly more distorted. The double-humped feature in figures $4.28(c) - 4.28(f)$ is similar to a BEN TYPE C (see figure 4a) waveform as observed by Matsumoto *et al.* (1994). The maximum propagation angle that produces a reasonably periodic waveform of this type for the fixed plasma parameters was found to be 30^o, beyond which the waveform was found to be incoherent in structure.

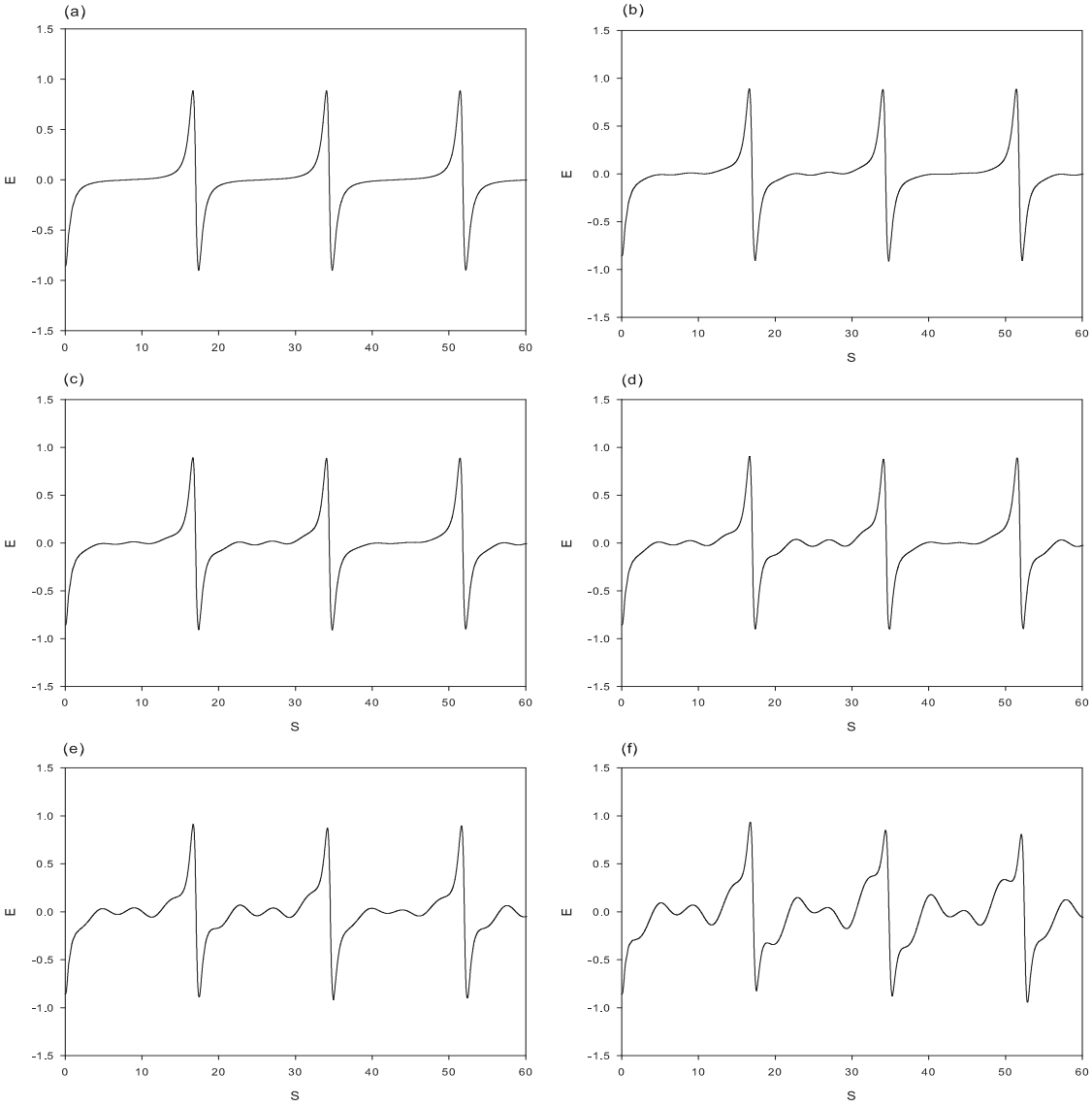

Figure 4.28: Numerical solution of the normalized electric field for different values of the propagation angle $\theta = 2^o$(a), 8^o (b), 10^o (c), 15^o (d), 20^o (e) and 30^o (f). For all curves the fixed parameters are $M = 3.5$, $E_0 = 3.0$, $R = 10.0$, $n_{ec0}/n_0 = n_{pc0}/n_0 = 0.5$, $\delta_c = \delta_h = 0.0$ and $T_c/T_h = 0.0$.

4.3.4 Critical E_0 values for spiky Electrostatic Wave onset

Next we focus on the spiky bipolar structures. Figure 4.29 shows the critical driving electric field amplitudes for the onset of spiky electrostatic waves as a function of the Mach number for various density ratio values. The critical E_0 value is defined as the minimum electric field amplitude for which the wave structure changes from sawtooth to spiky in form. The fixed parameters are $R = 10.0$, $\delta_c = \delta_h = 0.0$, $T_c/T_h = 0.0$, and $\theta = 2^o$. It is noted for a particular density value that as the Mach number increases, a larger driving electric field amplitude is required for the onset of the spiky electrostatic waves. Also as the density of the cold species increases for a fixed Mach number, the critical driving electric field amplitude for the onset of spiky ESWs decreases, which is consistent with the earlier results. On the other hand, for a fixed E_0 value, as the density of the cold species increases, the M-value for the onset of spiky structures also increases.

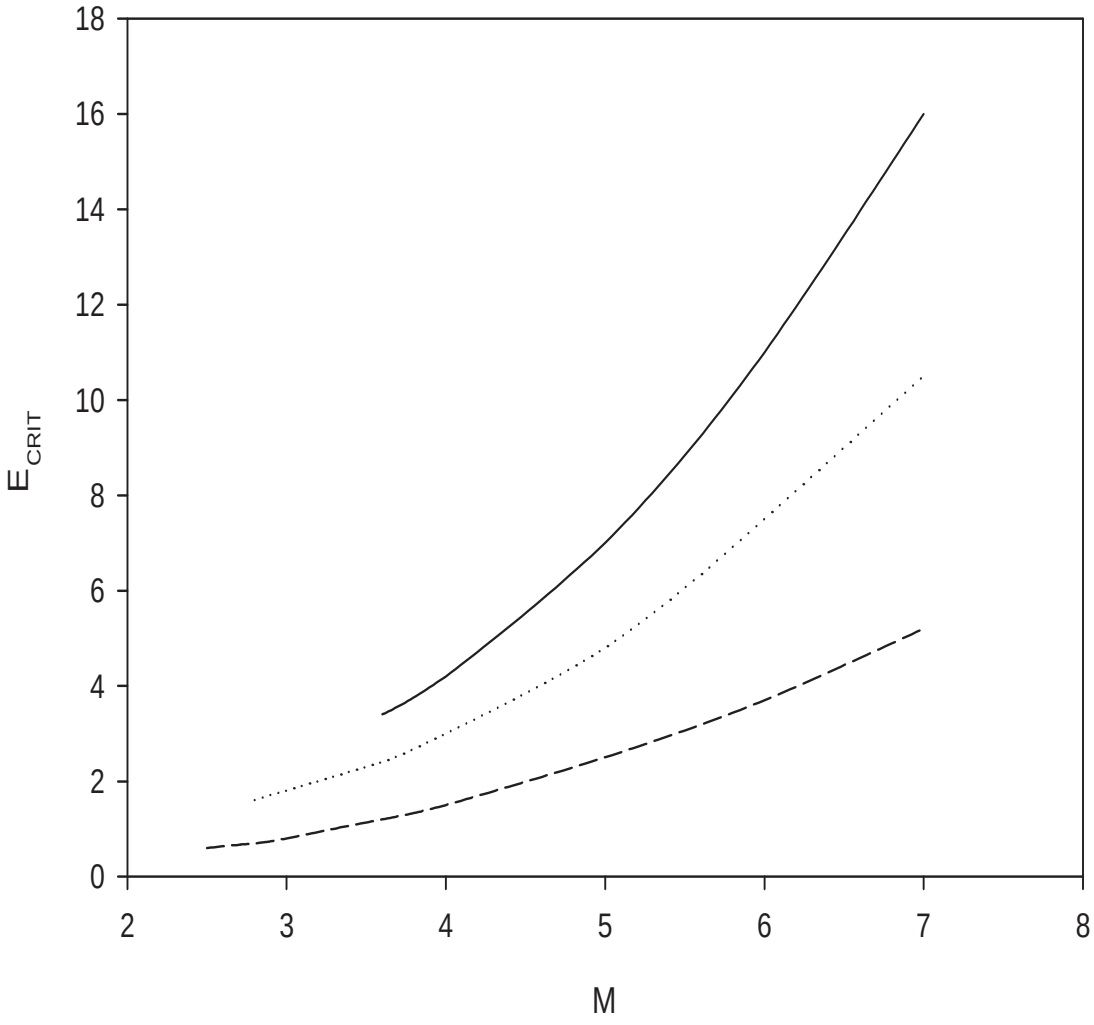

Figure 4.29: Plot of the critical E_0 values for the onset of spiky ESWs as a function of the Mach number for $n_{ec0}/n_0 = n_{pc0}/n_0 = 0.3$ (solid), $n_{ec0}/n_0 = n_{pc0}/n_0 = 0.5$ (dotted) and $n_{ec0}/n_0 = n_{pc0}/n_0 = 0.7$ (dashed). The fixed parameters are $R = 10.0$, $\delta_c = \delta_h = 0.0$, $T_c/T_h = 0.0$, and $\theta = 2^o$.

4.3.5 The Period (T) and Pulse width (w) on the Electrostatic Wave

In figures 4.30 and 4.31 the period and pulse width of the spiky electrostatic wave as a function of the drift velocities for the cold electron and positron components (δ_c) are displayed. For each drift value, the period and the pulse width are determined as defined by Kojima *et al.* (1994, see Figure 4a). These values are plotted as a function of the drift speeds of the cold species, δ_c. The fixed parameters are $M = 3.5$, $E_0 = 3.5$, $R = 10.0$, $n_{ec0}/n_0 = n_{pc0}/n_0 = 0.5$, $\delta_h = 0.0$, $T_c/T_h = 0.0$ and $\theta = 2^o$. As δ_c goes from anti-parallel to parallel flow, the period and pulse width of the ESWs increase.

The effect is opposite for the drift velocities of the hot electron and positron components, i.e as you go from anti-parallel to parallel for the hot drift velocities δ_h, the period and pulse width decrease (figures 4.32 and 4.33).
In their measurements Kojima *et al.* (1994) found that the ratio w/T was a constant for the ESWs, with $w/T = 0.3$. In our studies, we found that the ratio w/T is also a constant, with $w/T \approx 0.96$.

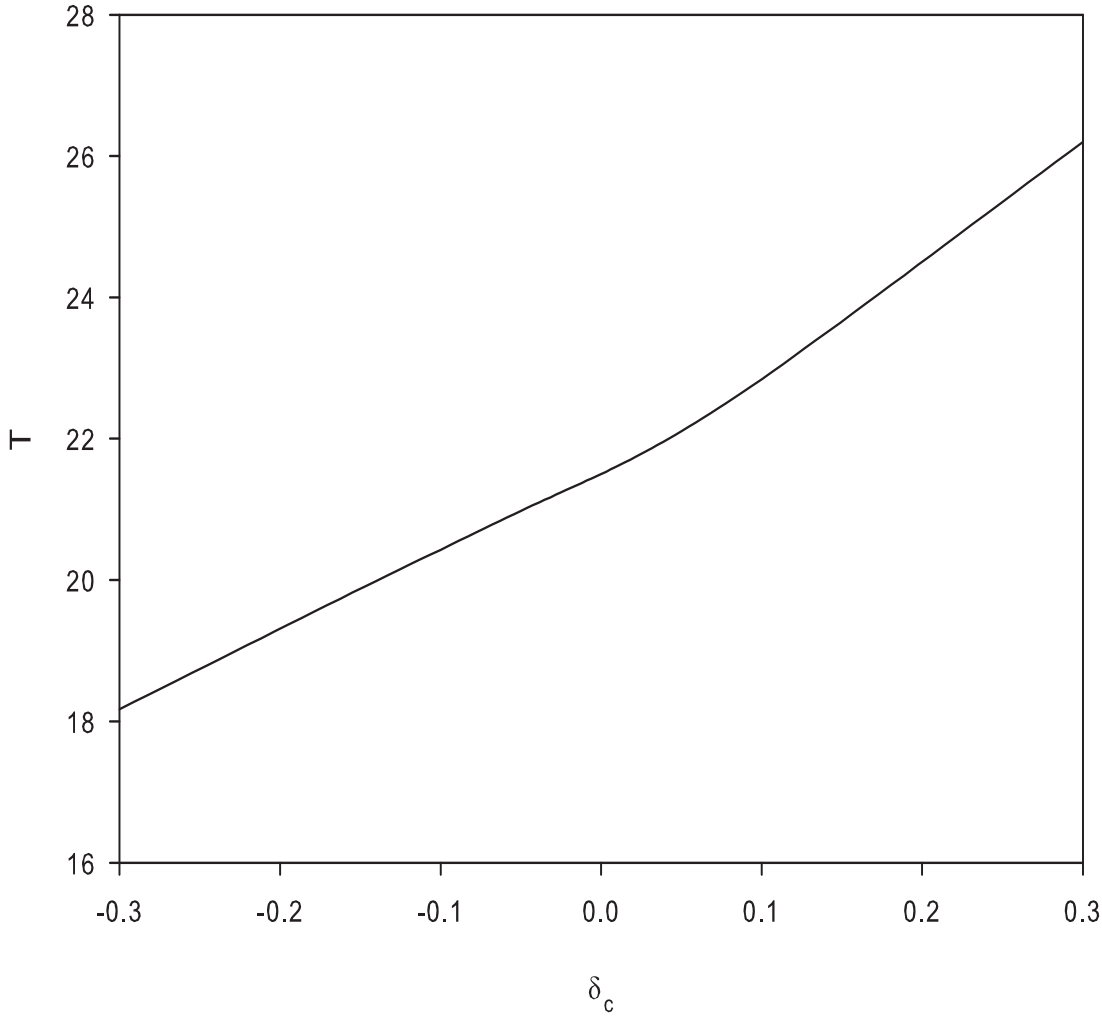

Figure 4.30: Plot of the Period of the ESW as a function of δ_c. The fixed parameters are $M = 3.5$, $E_0 = 3.5$, $R = 10.0$, $n_{ec0}/n_0 = n_{pc0}/n_0 = 0.5$, $\delta_h = 0.0$, $T_c/T_h = 0.0$ and $\theta = 2^o$.

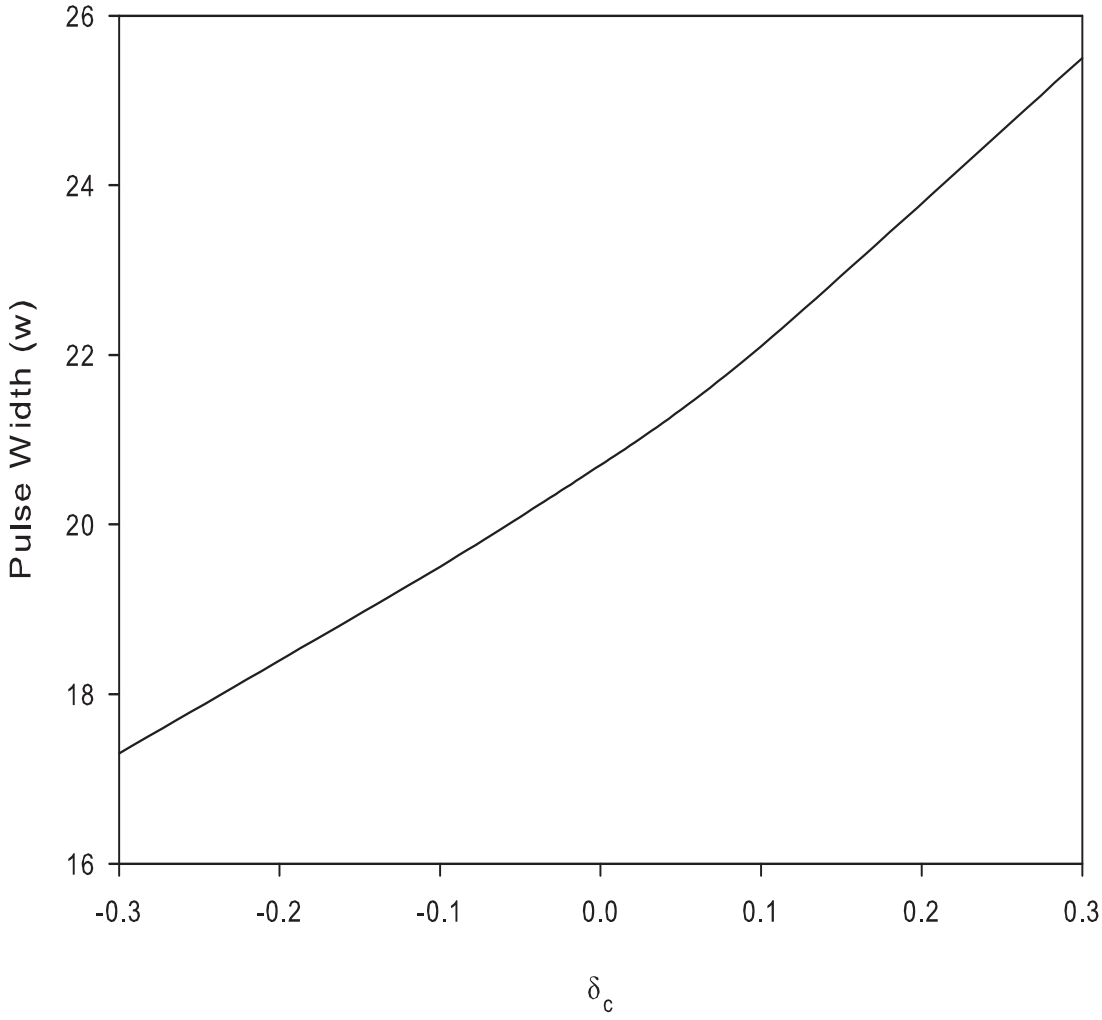

Figure 4.31: Plot of the Pulse width of the ESW as a function of δ_c. The fixed parameters are $M = 3.5$, $E_0 = 3.5$, $R = 10.0$, $n_{ec0}/n_0 = n_{pc0}/n_0 = 0.5$, $\delta_h = 0.0$, $T_c/T_h = 0.0$ and $\theta = 2^o$.

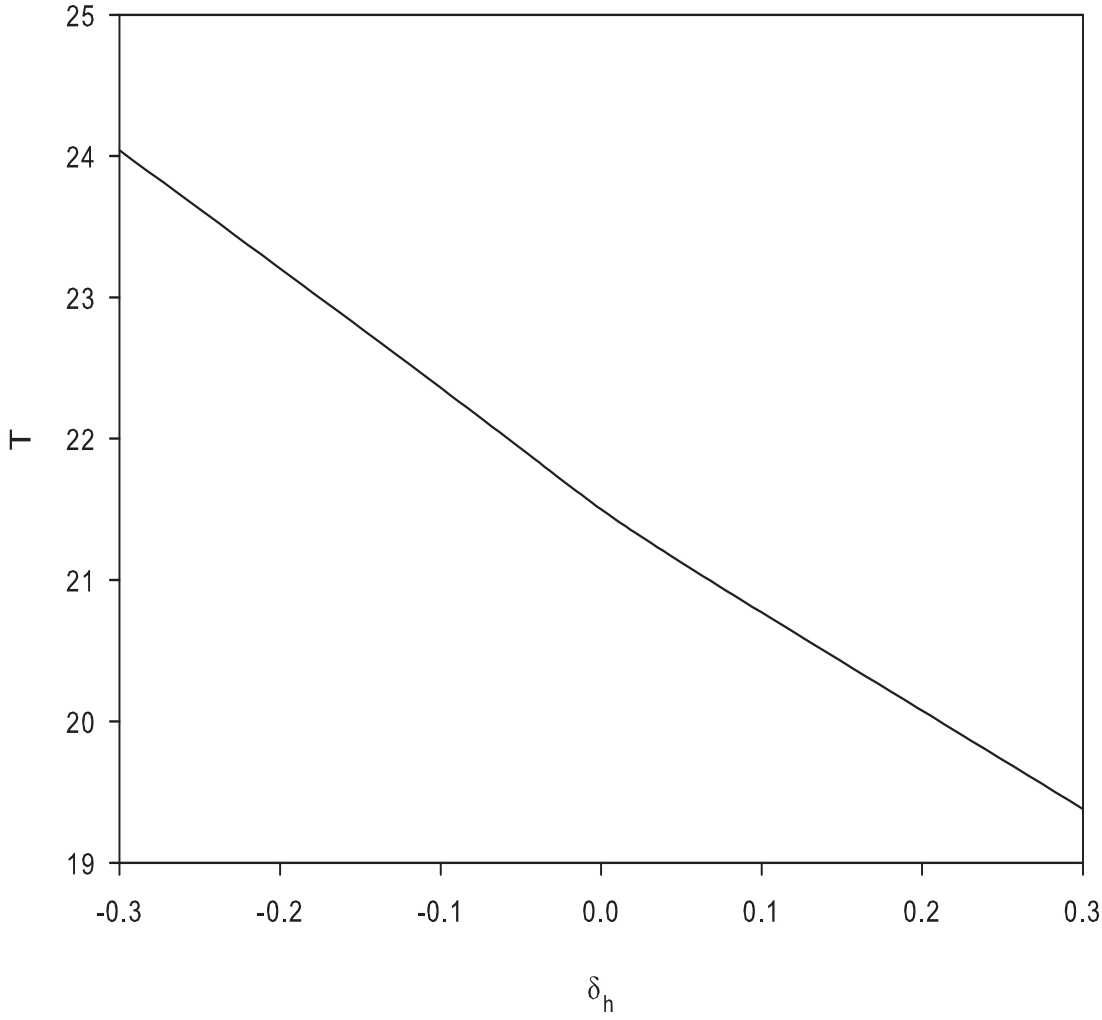

Figure 4.32: Plot of the Period of the ESW as a function of δ_h. The fixed parameters are $M = 3.5$, $E_0 = 3.5$, $R = 10.0$, $n_{ec0}/n_0 = n_{pc0}/n_0 = 0.5$, $\delta_c = 0.0$, $T_c/T_h = 0.0$ and $\theta = 2^o$.

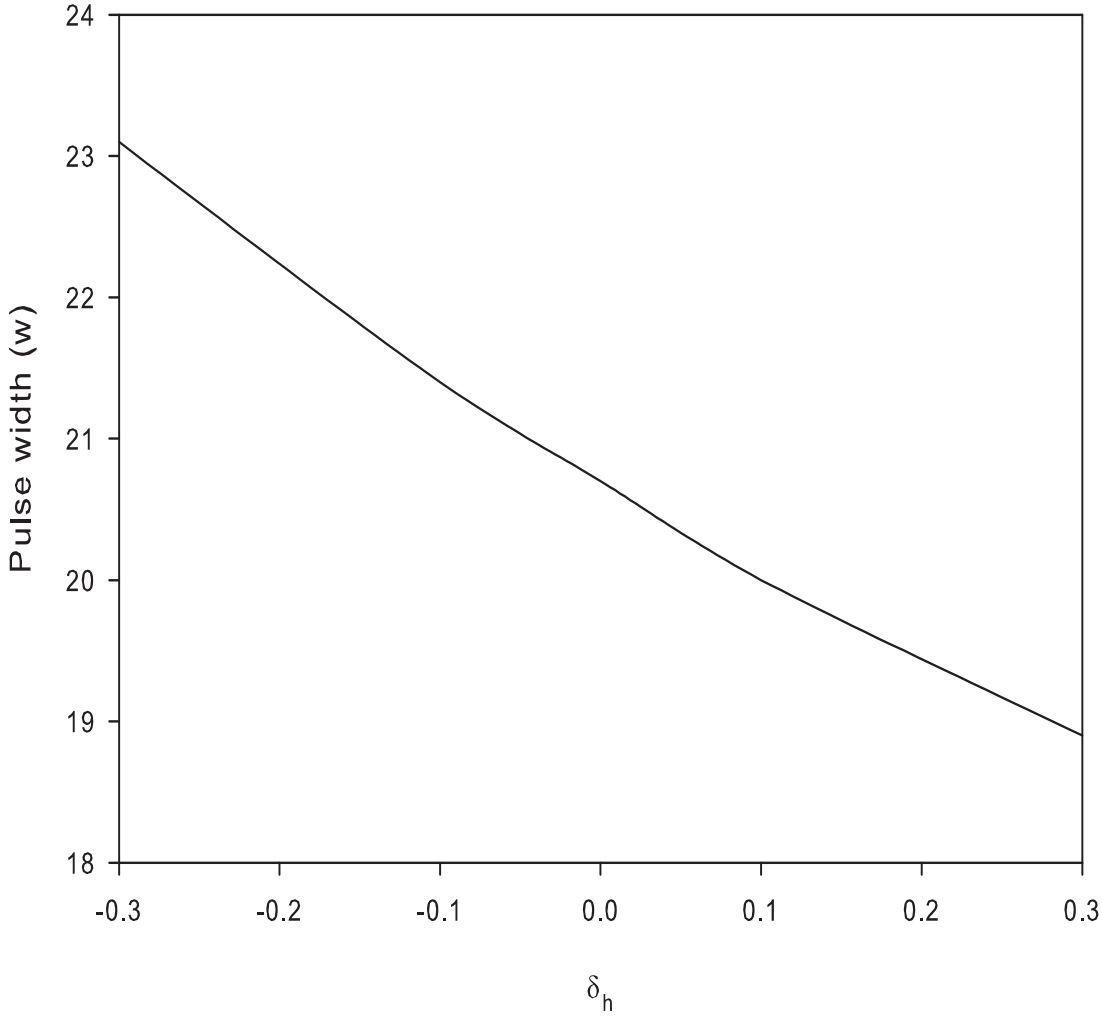

Figure 4.33: Plot of the Pulse width of the ESW as a function of δ_h. The fixed parameters are $M = 3.5$, $E_0 = 3.5$, $R = 10.0$, $n_{ec0}/n_0 = n_{pc0}/n_0 = 0.5$, $\delta_c = 0.0$, $T_c/T_h = 0.0$ and $\theta = 2^o$.

4.4 MODEL 3: Plasma with cool electrons and positrons ($\mathbf{T_c \neq 0}$) and hot electrons and positrons ($\mathbf{T_h \neq 0}$), including the full dynamics for all species

In section 4.3, the model consisted of a cold electron and a cold positron component ($T_c = 0$). Here these components are considered to have a finite temperature ($T_c \neq 0$). Hence the temperature effect within the momentum equation (equation (4.27)) is included and also included is the general equation of state (equation (4.30)) for these two species. The effect of the finite temperature of the cooler species on the electrostatic waves are then examined.

4.4.1 Basic Theory

The model considered here is a homogeneous magnetized, four component, collisionless, electron-positron plasma, consisting of cool electrons (ec) and cool positrons (pc) with equal temperatures T_c and initial densities ($n_{ec0} = n_{pc0}$), and hot electrons (eh) and hot positrons (ph) with equal temperatures T_h and densities ($n_{eh0} = n_{ph0}$). Wave propagation is again taken in the x-direction at an angle θ to the magnetic field $\mathbf{B_0}$, which is assumed to be in the x-z plane.

To determine the dispersion relation for the model, once again the perturbations are considered to vary as $\exp(i(kx-\omega t))$. Replacing $\partial/\partial t$ with $-i\omega$ and $\partial/\partial x$ with ik in equations (4.26) − (4.31), and neglecting the higher order terms and eliminating v_{jy} and v_{jz} for each species, results in,

$$v_{ecx} = \frac{-\frac{ek\phi}{m\omega}(\omega^2 - \Omega^2\cos^2\theta)}{\omega^2 - \Omega^2 - \frac{3k^2v_{tc}^2}{\omega^2}(\omega^2 - \Omega^2\cos^2\theta)} \ , \tag{4.59}$$

$$v_{pcx} = \frac{\frac{ek\phi}{m\omega}(\omega^2 - \Omega^2\cos^2\theta)}{\omega^2 - \Omega^2 - \frac{3k^2v_{tc}^2}{\omega^2}(\omega^2 - \Omega^2\cos^2\theta)} \ , \tag{4.60}$$

$$v_{ehx} = \frac{-\frac{ek\phi}{m\omega}(\omega^2 - \Omega^2\cos^2\theta)}{\omega^2 - \Omega^2 - \frac{3k^2v_{th}^2}{\omega^2}(\omega^2 - \Omega^2\cos^2\theta)} \tag{4.61}$$

and

$$v_{phx} = \frac{\frac{ek\phi}{m\omega}(\omega^2 - \Omega^2\cos^2\theta)}{\omega^2 - \Omega^2 - \frac{3k^2v_{th}^2}{\omega^2}(\omega^2 - \Omega^2\cos^2\theta)} \ . \tag{4.62}$$

In equations (4.59) and (4.60) the contributions from the finite temperature for the cool species are included compared to equations (4.32) and (4.33) in model 2 where T_c is set equal to zero. Substituting these velocities into their respective continuity equations and in turn, substituting the densities into Poisson's equation, the following dispersion relation is derived,

$$\omega^2 = \frac{2\omega_{pc}^2(\omega^2 - \Omega^2\cos^2\theta)}{\omega^2 - \Omega^2 - \frac{3k^2v_{tc}^2}{\omega^2}(\omega^2 - \Omega^2\cos^2\theta)} + \frac{2\omega_{ph}^2(\omega^2 - \Omega^2\cos^2\theta)}{\omega^2 - \Omega^2 - \frac{3k^2v_{th}^2}{\omega^2}(\omega^2 - \Omega^2\cos^2\theta)} \ , \tag{4.63}$$

where $\omega_{pc,ph} = (n_{0j}e^2/\varepsilon_0 m)^{1/2}$ are the plasma frequencies of the cool and hot species respectively. Equation (4.63) is similar in form to that of equation (4) of Moolla *et al.* (2007). Their electron-ion plasma consisted of a cool ion species, a cool electron species and a warm electron species as compared to our model which has a cool electron-positron species and a hot electron-positron species, hence the factor '2' appearing in the numerator for each term. In the limit $T_c = 0$, equation (4.63) reduces to the dispersion relation equation (4.36) of model 2.

In the limit $\omega/k \ll v_{th}$ and $\omega/k \gg v_{tc}$, where $v_{th} = (T_h/m)^{1/2}$ and $v_{tc} = (T_c/m)^{1/2}$ are the thermal velocities of the hot (cool) species, the dispersion relation equation (4.63) becomes,

$$\omega^2 = \frac{2\omega_{pc}^2(\omega^2 - \Omega^2\cos^2\theta)}{\omega^2 - \Omega^2 - 3k^2v_{tc}^2} - \frac{2\omega_{ph}^2\omega^2}{3k^2v_{th}^2} \ . \tag{4.64}$$

Rearranging equation 4.64 one obtains

$$\omega^4 - \omega^2(\Omega^2 + 2\omega_s^2 + 3k^2v_{tc}^2) + 2\omega_s^2\Omega^2\cos^2\theta = 0 \ . \tag{4.65}$$

From equation (4.65)

$$\omega^2 = \frac{1}{2}(\Omega^2 + 2\omega_s^2 + 3k^2v_{tc}^2)\left[1 \pm \sqrt{1 - \frac{(8\omega_s^2\Omega^2\cos^2\theta)}{(\Omega^2 + 2\omega_s^2 + 3k^2v_{tc}^2)^2}}\right] \ . \tag{4.66}$$

Approximating equation (4.66) using the binomial expansion where $(8\omega_s^2\Omega^2\cos^2\theta) \ll (\Omega^2 + 2\omega_s^2 + 3k^2v_{tc}^2)^2$, yields two modes. The positive sign gives the cyclotron mode,

$$\omega_+^2 = (\Omega^2 + 2\omega_s^2 + 3k^2 v_{tc}^2) - \frac{2\omega_s^2 \Omega^2 \cos^2\theta}{\Omega^2 + 2\omega_s^2 + 3k^2 v_{tc}^2} \tag{4.67}$$

and the negative sign gives the acoustic mode,

$$\omega_-^2 = \frac{2\omega_s^2 \Omega^2 \cos^2\theta}{\Omega^2 + 2\omega_s^2 + 3k^2 v_{tc}^2} \ , \tag{4.68}$$

where $\omega_s = \omega_{pc}/(1{+}2/3k^2\lambda_{Dh}^2)^{1/2}$, $\omega_{pc} = (n_{oc}e^2/\varepsilon_0 m)^{1/2}$ and $\lambda_{Dh} = (\varepsilon_0 T_h/n_{oh}e^2)^{1/2}$.

Following the method outlined in the previous sections, in moving to a stationary frame $s = (x - Vt)(\Omega/V)$, the following set of nonlinear first-order differential equations describe the evolution of the system.

$$\frac{\partial \psi}{\partial s} = -E \tag{4.69}$$

$$\frac{\partial E}{\partial s} = R^2 M^2 (n_{pcn} - n_{ecn} + n_{phn} - n_{ehn}) \tag{4.70}$$

$$\frac{\partial n_{ecn}}{\partial s} = \frac{n_{ecn}^3 \left[E + M \sin\theta v_{ecyn} \right]}{\left(\frac{n_{ec0}}{n_0} \right)^2 (M - \delta_c)^2 - 3\frac{T_c}{T_h} p_{ecn} n_{ecn}} \tag{4.71}$$

$$\frac{\partial v_{ecyn}}{\partial s} = \frac{M n_{ecn}}{(M - \delta_c)} \left(\frac{n_0}{n_{ec0}} \right) \left[-\left(M - \frac{(M - \delta_c)}{n_{ecn}} \left(\frac{n_{ec0}}{n_0} \right) \right) \sin\theta + v_{eczn} \cos\theta \right] \tag{4.72}$$

$$\frac{\partial v_{eczn}}{\partial s} = -\left(\frac{n_0}{n_{ec0}} \right) \frac{n_{ecn} v_{ecyn} M \cos\theta}{(M - \delta_c)} \tag{4.73}$$

$$\frac{\partial p_{ecn}}{\partial s} = \frac{3p_{ecn}n_{ecn}^2\Big[E + M\sin\theta v_{ecyn}\Big]}{\left(\frac{n_{ec0}}{n_0}\right)^2(M-\delta_c)^2 - 3\frac{T_c}{T_h}p_{ecn}n_{ecn}} \tag{4.74}$$

$$\frac{\partial n_{pcn}}{\partial s} = \frac{n_{pcn}^3\Big[-E - M\sin\theta v_{pcyn}\Big]}{\left(\frac{n_{pc0}}{n_0}\right)^2(M-\delta_c)^2 - 3\frac{T_c}{T_h}p_{pcn}n_{pcn}} \tag{4.75}$$

$$\frac{\partial v_{pcyn}}{\partial s} = \frac{Mn_{pcn}}{(M-\delta_c)}\left(\frac{n_0}{n_{pc0}}\right)\left[\left(M - \frac{(M-\delta_c)}{n_{pcn}}\left(\frac{n_{pc0}}{n_0}\right)\right)\sin\theta - v_{pczn}\cos\theta\right] \tag{4.76}$$

$$\frac{\partial v_{pczn}}{\partial s} = \left(\frac{n_0}{n_{pc0}}\right)\frac{n_{pcn}v_{pcyn}M\cos\theta}{(M-\delta_c)} \tag{4.77}$$

$$\frac{\partial p_{pcn}}{\partial s} = \frac{3p_{pcn}n_{pcn}^2\Big[-E - M\sin\theta v_{pcyn}\Big]}{\left(\frac{n_{pc0}}{n_0}\right)^2(M-\delta_c)^2 - 3\frac{T_c}{T_h}p_{pcn}n_{pcn}} \tag{4.78}$$

$$\frac{\partial p_{phn}}{\partial s} = \frac{3p_{phn}n_{phn}^2\Big[-E - M\sin\theta v_{phyn}\Big]}{\left(\frac{n_{ph0}}{n_0}\right)^2(M-\delta_h)^2 - 3p_{phn}n_{phn}} \tag{4.79}$$

$$\frac{\partial n_{phn}}{\partial s} = \frac{n_{phn}^3\Big[-E - M\sin\theta v_{phyn}\Big]}{\left(\frac{n_{ph0}}{n_0}\right)^2(M-\delta_h)^2 - 3p_{phn}n_{phn}} \tag{4.80}$$

$$\frac{\partial v_{phyn}}{\partial s} = \frac{Mn_{phn}}{(M-\delta_h)}\left(\frac{n_0}{n_{ph0}}\right)\left[\left(M - \frac{(M-\delta_h)}{n_{phn}}\left(\frac{n_{ph0}}{n_0}\right)\right)\sin\theta - v_{phzn}\cos\theta\right] \tag{4.81}$$

$$\frac{\partial v_{phzn}}{\partial s} = \left(\frac{n_0}{n_{ph0}}\right)\frac{n_{phn}v_{phyn}M\cos\theta}{(M-\delta_h)} \tag{4.82}$$

$$\frac{\partial p_{ehn}}{\partial s} = \frac{3p_{ehn}n_{ehn}^2\Big[E + M\sin\theta v_{ehyn}\Big]}{\left(\frac{n_{eh0}}{n_0}\right)^2(M-\delta_h)^2 - 3p_{ehn}n_{ehn}} \tag{4.83}$$

$$\frac{\partial n_{ehn}}{\partial s} = \frac{n_{ehn}^3\Big[E + M\sin\theta v_{ehyn}\Big]}{\left(\frac{n_{eh0}}{n_0}\right)^2(M-\delta_h)^2 - 3p_{ehn}n_{ehn}} \tag{4.84}$$

$$\frac{\partial v_{ehyn}}{\partial s} = \frac{Mn_{ehn}}{(M-\delta_h)}\left(\frac{n_0}{n_{eh0}}\right)\left[-\left(M - \frac{(M-\delta_h)}{n_{ehn}}\left(\frac{n_{eh0}}{n_0}\right)\right)\sin\theta + v_{ehzn}\cos\theta\right] \tag{4.85}$$

$$\frac{\partial v_{ehzn}}{\partial s} = -\left(\frac{n_0}{n_{eh0}}\right)\frac{n_{ehn}v_{ehyn}M\cos\theta}{(M-\delta_h)} \tag{4.86}$$

In equations (4.69) − (4.86), we recall that the velocities are normalized with respect to the thermal velocity $v_{th} = (T_h/m)^{1/2}$ and the densities with respect to the total density n_0. The equilibrium density of the cool (hot) electrons is n_{ec0} (n_{eh0}), and that of the cool (hot) positrons n_{pc0} (n_{ph0}), with $n_{ec0} + n_{eh0} = n_{pc0} + n_{ph0} = n_0$. $R = \omega_p/\Omega$, where $\omega_p = (n_0e^2/\varepsilon_0 m)^{1/2}$ is the total plasma frequency, $M = V/v_{th}$ is the Mach number and $\delta_{c,h} = v_{0c,0h}/v_{th}$ is the normalized drift velocity of cool (hot) species at s=0.

4.4.2 Numerical Results

Effect of the cool electron and positron temperatures on the waves

Given the detailed analysis of the numerical results presented in the earlier sections, here the focus is solely on the effect of the finite temperature of the cooler species. In figure 4.34 the effect of the cool electron and positron temperature ratio on the electrostatic solitary waves is shown. The fixed parameters are, $E_0 = 3.5$, $M = 3.5$, $R = 10.0$, $\theta = 2^o$, $\delta_c = \delta_h = 0.0$ and $n_{ec0}/n_0 = n_{pc0}/n_0 = 0.5$. It is seen that the periodicity and nonlinearity of the wave increases with an increase in the cool to hot species temperature ratio. The period of the wave increases from $3.42\tau_c$ (frequency f_w=$0.29f_c$) for $T_c/T_h = 0.0$ to $4.02\tau_c$ (frequency f_w=$0.25f_c$) for $T_c/T_h = 0.75$. This behaviour can be correlated to the linear dispersion relation (4.68), where as the temperature of the cooler species increases, ω decreases and hence the period of the wave increases.

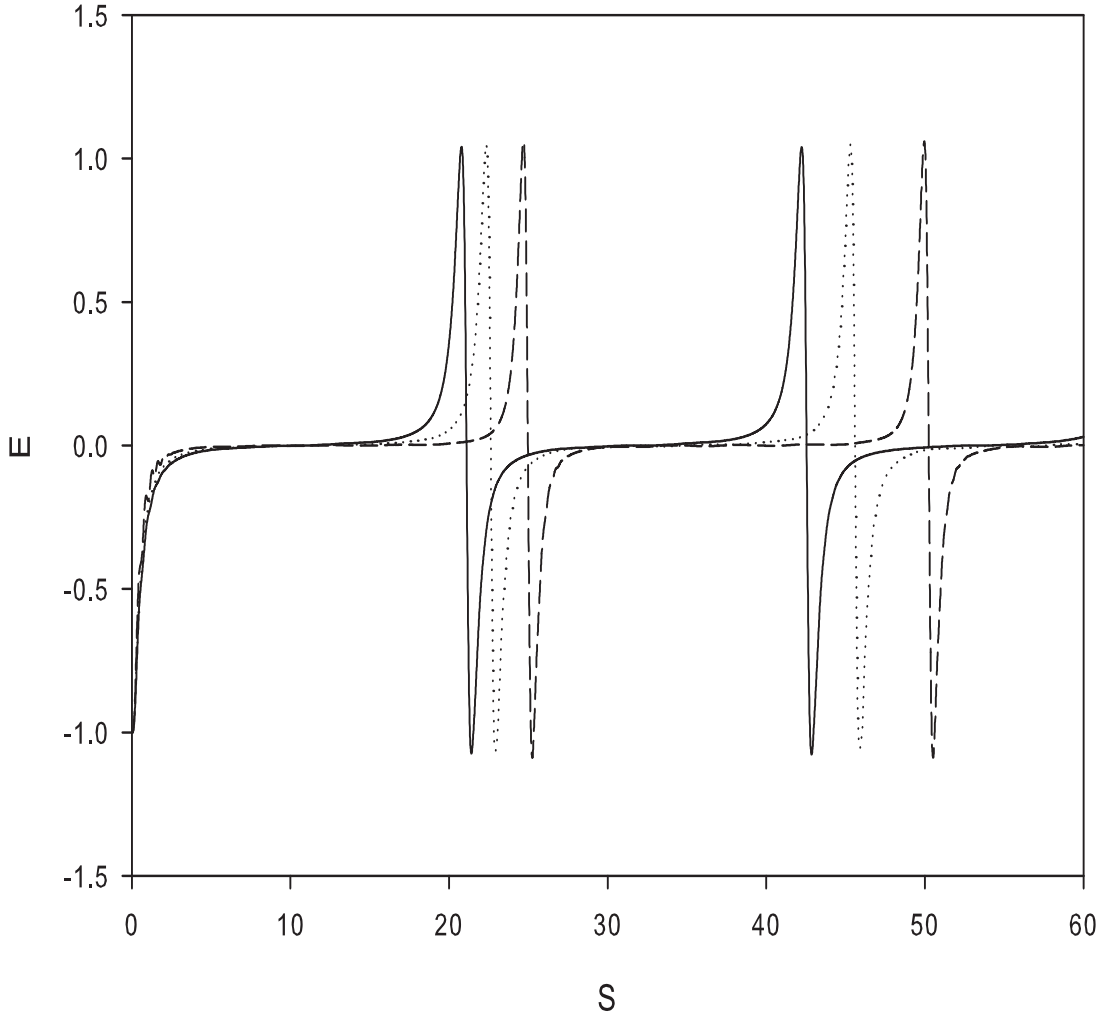

Figure 4.34: Numerical solution of the normalized electric field for the parameters $M = 3.5$, $E_0 = 3.5$, $R = 10.0$, $\theta = 2^o$, $\delta_c = \delta_h = 0.0$, $n_{ec0}/n_0 = n_{pc0}/n_0 = 0.5$ and $T_c/T_h = 0.0$ (solid), 0.5 (dotted), and 0.75 (broken).

4.5 Discussion

In this chapter nonlinear electrostatic waves in a four component electron-positron plasma, following an approach by other authors (e.g. Reddy *et al.*, 2002) in an electron-ion plasma have been studied. Three different plasma models were considered: Model 1 with Boltzmann density distribution for the hot species and fluid equations for the cold species ($T_c = 0$); Model 2 with full dynamics for all four species with $T_c = 0$; and Model 3 which was an extension of Model 2 to allow for finite $T_c \neq 0$. In the models spatial variation is restricted to the x-direction, while the external magnetic field is in the (x, z) plane. In the nonlinear analysis, the associated cyclotron wave and acoustic wave are coupled through the convective derivative terms $v_{jx}\frac{\partial v_{jy}}{\partial x}$ and $v_{jx}\frac{\partial v_{jz}}{\partial x}$ in the momentum equations. These two modes are decoupled in the linear analysis. The spiky waveforms obtained for the electric fields was seen to be similar to those obtained by Reddy *et al.* (2002) and Moolla *et al.* (2007) for an electron-ion plasma. In the study, a transition from linear sinusoidal to sawtooth to spiky waveforms is observed as the amplitude of the driving electric field increases. The results found in this chapter for an electron-positron plasma are very similar to those found by other researchers for electron-ion plasmas. On the other hand, as the Mach number is increased (figures $4.12 - 4.14$) the nonlinearity is suppressed to the point where the bipolar ESWs are no longer excited. For the onset of spiky ESWs, it is noted that as the wave speed increases, a larger driving electric field is required. The period of the waves are affected by the relative

drift of the hot and cold electrons and positrons. Also the nonlinearity of the wave is affected by the density ratio of the electrons and positrons. It is also noted that as the density ratio increases, the critical value for the driving electric field amplitude for the onset of spiky ESWs also decreases and the minimum value required for the wave speed for the onset of spiky ESWs decreases. The ESWs are therefore more easily excited when the cold species dominate. With regard to the structure of the ESWs, the results shows BEN TYPE A ESWs exists for almost parallel propagation, but as the propagation angle increases with respect to the ambient magnetic field $\mathbf{B_0}$, the signature waveform becomes more distorted, representing a BEN TYPE C with its double-humped highly distorted feature. For angles of propagation beyond 30^o the electric field structures lose coherence. The ratio of the pulse widths and periods (w/T) of the electrostatic waves was found to be a constant, which is consistent with experimental observations by Kojima *et al.* (1994). When finite temperature effects are included for the cold species, an increase in the temperature ratio of the cool electrons and positrons causes the broadening out of the waveforms, which vary due to an increase in the wave frequency with T_c.

A comparison of the three models reveals that the assumption of Boltzmann density distribution for the hot species is restrictive in the sense it admits spiky bipolar solutions for comparatively larger values of $R = \omega_p/\Omega(> 100)$, i.e. in weakly magnetized plasmas. On the other hand, models 2 and 3 with full dynamics for all species allows solutions for much lower R-values

(typically $R = 10$).

Chapter 5

Solitary Waves in a Relativistic Electron-Positron Plasma

The studies conducted in the previous chapters were for non-relativistic electron-positron plasmas. Here, nonlinear structures in relativistic electron-positron plasmas are examined.

5.1 Literature Review

The study of relativistic effects in electron-positron plasmas is of importance since it is known that these plasmas exists in pulsars (Beskin *et al.*, 1983; Gurevich and Istomin, 1985), active galactic nuclei (Henri *et al.*, 1993; Hartman *et al.*, 2001) and gamma-ray bursts (Goodman, 1986; Paczyński, 1986; Eichler *et al.*, 1989), where highly energetic charged particles are present. Some of the studies in relativistic electron-positron plasmas will now be high-

lighted. Yu *et al.* (1984) investigated the nonlinear propagation of intense circularly polarized electromagnetic waves in a magnetized electron-positron plasma, where the relativistic and ponderomotive force effects were included. Their analytical investigation determined that sharply spiked potential pulses existed in a strongly magnetized plasma while a smooth pulse was present in a weakly magnetized warm plasma and a moderately spiked pulse in a weakly magnetized cold plasma. Large amplitude solitary Alfvén modes propagating at oblique angles in a magnetized cold relativistic electron-positron plasma have been studied by Verheest and Lakhina (1996). The reductive-perturbation technique was employed to derive the KdV equation and they found that the nonlinearity vanishes for parallel propagation (to the ambient magnetic field), and is strongest at strictly perpendicular propagation. In a further study, Lakhina and Verheest (1997) included the pressure and ultrarelativistic effects. For parallel propagation, in the ultrarelativistive limit, linearly polarized subsonic Alfvén solitons were found to be possible, but supersonic Alfvén solitons did not exist. The Alfvén solitons for perpendicular propagation were found to have a different nature compared to those in cold relativistic plasmas (Verheest and Lakhina, 1996). Lontano *et al.* (2001) investigated the interaction between arbitrary amplitude electromagnetic fields and hot plasmas, and studied the existence of soliton-like electromagnetic distributions in one-dimensional electron-positron plasmas. They found that solitons are possible in overdense plasmas, with the soliton-like structure existing for small temperatures. Ultrarelativistic solitons were also found to exist in hot plasmas.

Ion-acoustics waves in relativistic, three component electron-positron-ion plasmas have recently been of interest. Gill *et al.* (2007) investigated ion-acoustic solitary waves in a weakly relativistic electron-positron-ion plasma using the reductive-perturbation technique to derive the KdV equation. They studied the effect of plasma parameters such as temperature and density ratio of the electrons and positrons and the relativistic factor, on the solitons. These parameters significantly affected the amplitude and width of the solitons. Moreover, a small amplitude study showed that only compressive solitons were possible. An increase in the relativistic effect resulted in an increase in the soliton amplitude. Abdelsalam *et al.* (2008) in their study of ion-acoustic solitary waves in electron-positron-ion plasmas used the Sagdeev pseudo-potential approach and the associated energy-integral equation. They studied arbitrary amplitude soliton profiles as well as the small amplitude profiles using the derived KdV equation. They found that both subsonic and supersonic ion-acoustic solitary waves are possible for low values of the density ratio of positrons to electrons, but only subsonic solitons existed for high density ratios.

The study presented in this chapter is an extension of the work conducted by Bharuthram and Yu (1993), who investigated the existence and properties of finite amplitude electron plasma waves in an unmagnetized electron plasma using the Sagdeev pseudo-potential method. They showed that electrostatic fluctuations can propagate as nonlinear soliton-like structures. Here we investigate the formation of solitons in an unmagnetized, warm, relativistic

plasma, consisting of electrons and positrons through an arbitrary amplitude theory. In addition, small amplitude theory is used to provide an analytical solution. Both species are considered to have a drift velocity and their dynamics are governed by the fluid equations. Soliton profiles are examined as a function of plasma parameters such as the soliton speed, drift velocity and relativistic factor.

5.2 Basic Theory

The model consists of an unmagnetized plasma consisting of relativistic electrons and positrons, with equilibrium densities denoted by n_{e0} and n_{p0}, respectively, and equal temperatures denoted by T.

The dynamics of the system are determined by,
the continuity equations

$$\frac{\partial n_j}{\partial t} + \nabla.(n_j \mathbf{v}_j) = 0 \ , \tag{5.1}$$

and the momentum equations,

$$\frac{\partial \mathbf{P}_j}{\partial t} + (\mathbf{v}_j.\nabla)\mathbf{P}_j = -\frac{T}{n_j}\nabla n_j - \alpha_j e \nabla\phi \ \ , \tag{5.2}$$

where the relativistic momentum $\mathbf{P}_j$ for the j^{th} species is given by

$$\mathbf{P}_j = \frac{m_o \mathbf{v}_j}{(1-\frac{v_j^2}{c^2})^{1/2}} \ , \tag{5.3}$$

where j = e(p) for the electrons (positrons) and $\alpha_j = -1(+1)$ for electrons (positrons). Here n_j, $\mathbf{v}_j$, and T are the densities, fluid velocities and tempera-

tures, respectively. The common rest mass of the electrons and the positrons is $m_o = m_{eo} = m_{po}$, the speed of light is c and ϕ is the electrostatic potential.

The system is closed by the Poisson equation

$$\varepsilon_0 \nabla^2 \phi = e(n_e - n_p) \ . \tag{5.4}$$

5.3 Arbitrary Amplitude Theory

For the study of arbitrary amplitude solitons, equations (5.1) − (5.4) are transformed to a stationary frame moving with velocity V, the phase velocity of the wave, i.e., $\xi = x - Vt$, with wave propagation taken in the x direction. Hence equation (5.1) can be integrated to yield

$$v_j = V\left(1 - \frac{n_o}{n_j}\right) + \frac{n_o v_{j0}}{n_j} \ . \tag{5.5}$$

The plasma is assumed to be undisturbed at $\xi \to \infty$, and therefore the boundary conditions $n_{jo} = n_o$, $v_j = v_{j0}$ and $\phi = 0$ at $\xi \to \infty$.

Substituting equation (5.3) into (5.2) and transforming into the wave equation with the stated boundary conditions at $\xi \to \infty$ yields,

$$\frac{c^2}{\sqrt{1 - \frac{v_e^2}{c^2}}} - \frac{c^2}{\sqrt{1 - \frac{v_{e0}^2}{c^2}}} - \frac{v_e V}{\sqrt{1 - \frac{v_e^2}{c^2}}} + \frac{v_{e0} V}{\sqrt{1 - \frac{v_{e0}^2}{c^2}}} = -v_{t_e}^2 ln\left(\frac{n_e}{n_o}\right) + \frac{e\phi}{m_o} \ , \tag{5.6}$$

$$\frac{c^2}{\sqrt{1-\frac{v_p^2}{c^2}}}-\frac{c^2}{\sqrt{1-\frac{v_{p0}^2}{c^2}}}-\frac{v_pV}{\sqrt{1-\frac{v_p^2}{c^2}}}+\frac{v_{p0}V}{\sqrt{1-\frac{v_{p0}^2}{c^2}}}=-v_{t_p}^2 ln\left(\frac{n_p}{n_o}\right)-\frac{e\phi}{m_o}\ . \quad (5.7)$$

Adding equations (5.6) and (5.7) and using equation (5.5) yields,

$$\begin{aligned} v_{te}^2 lnN_e+\frac{c^2[N_e-\frac{V^2}{c^2}(N_e-1+\frac{v_{e0}}{V})]}{\sqrt{N_e^2-\frac{V^2}{c^2}(N_e-1+\frac{v_{e0}}{V})^2}}-\frac{(c^2-Vv_{e0})}{\sqrt{1-\frac{v_{e0}^2}{c^2}}} \\ =-v_{tp}^2 lnN_p-\frac{c^2[N_p-\frac{V^2}{c^2}(N_p-1+\frac{v_{p0}}{V})]}{\sqrt{N_p^2-\frac{V^2}{c^2}(N_p-1+\frac{v_{p0}}{V})^2}}+\frac{(c^2-Vv_{p0})}{\sqrt{1-\frac{v_{p0}^2}{c^2}}}\ , \end{aligned} \quad (5.8)$$

where $N_e = n_e/n_o$ and $N_p = n_p/n_o$ are the normalized densities of the electrons and positrons respectively.

The Poisson's equation in the wave frame then becomes

$$\left(\frac{e}{m_o}\right)\frac{d^2\phi}{d\xi^2}=\omega_p^2(N_e-N_p)\ , \quad (5.9)$$

where $\omega_p = (n_o e^2/\varepsilon_0 m_o)^{1/2}$ is the plasma frequency.

Defining

$$\phi_e=\frac{e\phi}{m_o}=v_{te}^2 lnN_e+\frac{c^2[N_e-\frac{V^2}{c^2}(N_e-1+\frac{v_{e0}}{V})]}{\sqrt{N_e^2-\frac{V^2}{c^2}(N_e-1+\frac{v_{e0}}{V})^2}}-\frac{(c^2-Vv_{e0})}{\sqrt{1-\frac{v_{e0}^2}{c^2}}} \quad (5.10)$$

and

$$\phi_p = -\frac{e\phi}{m_o} = v_{tp}^2 ln N_p + \frac{c^2[N_p - \frac{V^2}{c^2}(N_p - 1 + \frac{v_{p0}}{V})]}{\sqrt{N_p^2 - \frac{V^2}{c^2}(N_p - 1 + \frac{v_{p0}}{V})^2}} - \frac{(c^2 - V v_{p0})}{\sqrt{1 - \frac{v_{p0}^2}{c^2}}} \ , \quad (5.11)$$

the Poisson's equation (5.9) becomes

$$\frac{d^2\phi_e}{d\xi^2} = \omega_p^2 (N_e - N_p) \ . \quad (5.12)$$

Integrating the above once w.r.t. ξ and solving, one obtains

$$\frac{1}{2}\left(\frac{dN_e}{d\xi}\right)^2 + \ \psi(N_e) = 0 \ , \quad (5.13)$$

where

$$\psi(N_e) = \frac{G(N_e)}{\left(\frac{d\phi_e}{dN_e}\right)^2} \quad (5.14)$$

is the Sagdeev potential, with,

$$-G(N_e) = \omega_p^2 \left[\int_{-\infty}^{\infty} N_e \frac{d\phi_e}{d\xi} d\xi + \int_{-\infty}^{\infty} N_p \frac{d\phi_p}{d\xi} d\xi\right] \ . \quad (5.15)$$

The normalized Sagdeev potential is then found to be

$$\psi(N_e) = \frac{2 - N_e - N_p - c^2M^2\left[\frac{[1-N_e+\frac{v_{e0}}{M}(N_e-2+\frac{v_{e0}}{M})]}{[N_e^2-M^2(N_e-1+\frac{v_{e0}}{M})^2]^{1/2}} + \frac{[1-N_p+\frac{v_{p0}}{M}(N_p-2+\frac{v_{p0}}{M})]}{[N_p^2-M^2(N_p-1+\frac{v_{p0}}{M})^2]^{1/2}}\right]}{\left[\frac{1}{N_e} - \frac{c^2M^2(1-\frac{v_{e0}}{M})^2}{\left(N_e^2-M^2(N_e-1+\frac{v_{e0}}{M})^2\right)^{3/2}}\right]^2}, \tag{5.16}$$

where v_{j0} is normalized with respect to c for the j^{th} species and $M = V/c$ is the normalized soliton speed.

5.3.1 Numerical Results

It is noted that limitations are placed on the range of M values in equation (5.16), i.e $M^2 < N_e^2/(N_e - 1 + \frac{v_{e0}}{M})^2$ and $M^2 < N_p^2/(N_p - 1 + \frac{v_{p0}}{M})^2$. The Sagdeev potential ψ is always zero at $N_e = 1 = N_p$ and $v_{e0} = v_{p0} = 0$ and is evaluated numerically by first determining the positron density values for varying electron density values using equation (5.8). Figure 5.1 shows the typical form of the Sagdeev potential $\psi(Ne)$ for various soliton speeds. For solitons, the Sagdeev potential has to satisfy $|\psi(N_e)| < 1$ for $N_0 < N_e < 1$ for some value N_0, with $d\psi(N_e)/d(N_e) = 0$ at $N_e = 1$ and $d\psi(N_e)/d(N_e) \neq 0$ at $N_e = N_0$. Figure 5.2 shows the corresponding soliton profile after direct numerical integration of equation (5.13) for different soliton speeds. The Runga Kutta code was used for the numerical integration. As the soliton speed M increases it is found that N_0 increases, resulting in solitons with larger amplitudes, as seen in (figure 5.2). Figure 5.3 shows the soliton profile for various c/v_{th} values. As c/v_{th} increases, the soltion amplitude decreases. The soli-

tons become narrower with a corresponding decrease in the half width. The effect of the equal drift velocities of the two species is studied in figure 5.4. An increase in the drift velocities, results in a decrease in the soliton amplitude. In figure 5.5, the electrons and positrons are shown drifting in opposite directions. It is noted that there is a similar trend when compared to the electrons and positrons having equal drifts. Figure 5.6 is an existence diagram showing the soliton amplitudes (N_A) as a function of the normalized soliton speed. The figure was constructed in the following manner. For each value of c/v_{th}, the range of M values for which solitons were possible were established. The figure represents the amplitudes of the solitons as a function of M. For a fixed value of c/v_{th}, no solutions exist to the left (M_{min}) and the right (M_{max}) of the endpoint M-values of the particular curve. It is seen from the figure that as c/v_{th} increases, the range of M for soliton structures to exist decreases. In addition, M_{min} increases with c/v_{th}.

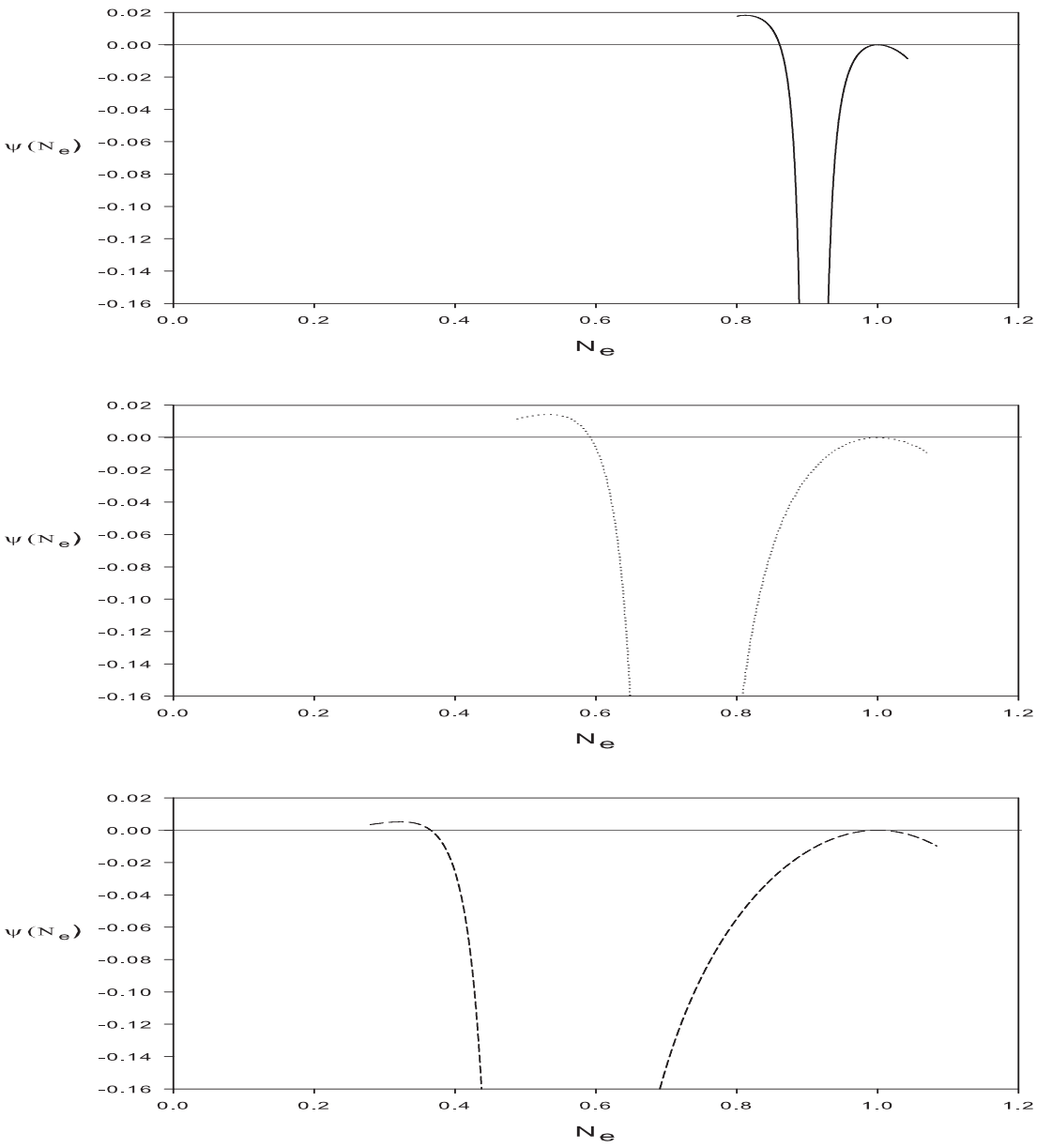

Figure 5.1: The Sagdeev potential for normalized soliton speeds $M = 0.01$ (solid), 0.03 (dotted) and 0.05 (broken). The fixed parameters are $v_{e0}/c = v_{p0}/c = 0.1$ and $c/v_{th} = 10.0$.

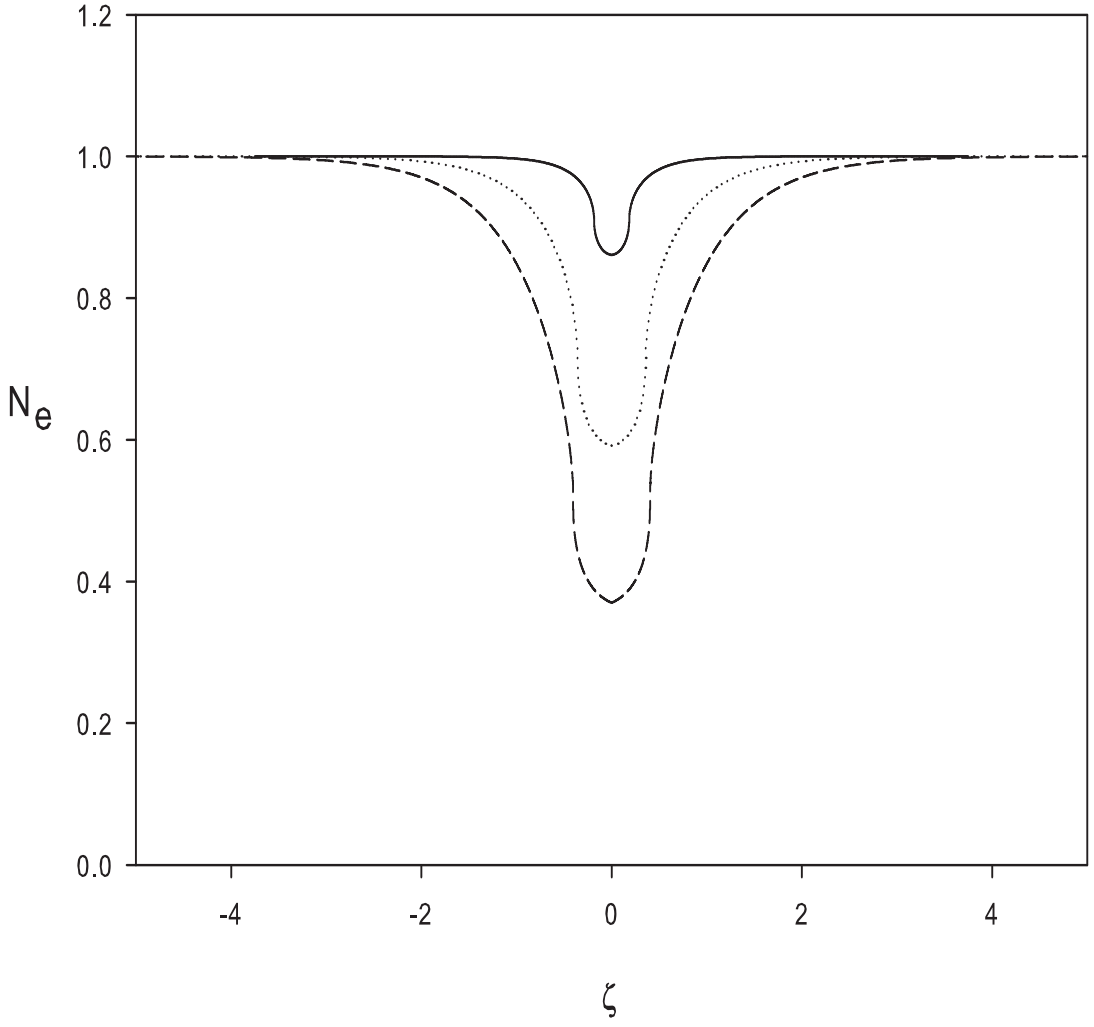

Figure 5.2: Soliton profile for $M = 0.01$ (solid), 0.03 (dotted), 0.05 (broken) with $v_{e0}/c = v_{p0}/c = 0.1$ and $c/v_{th} = 10.0$.

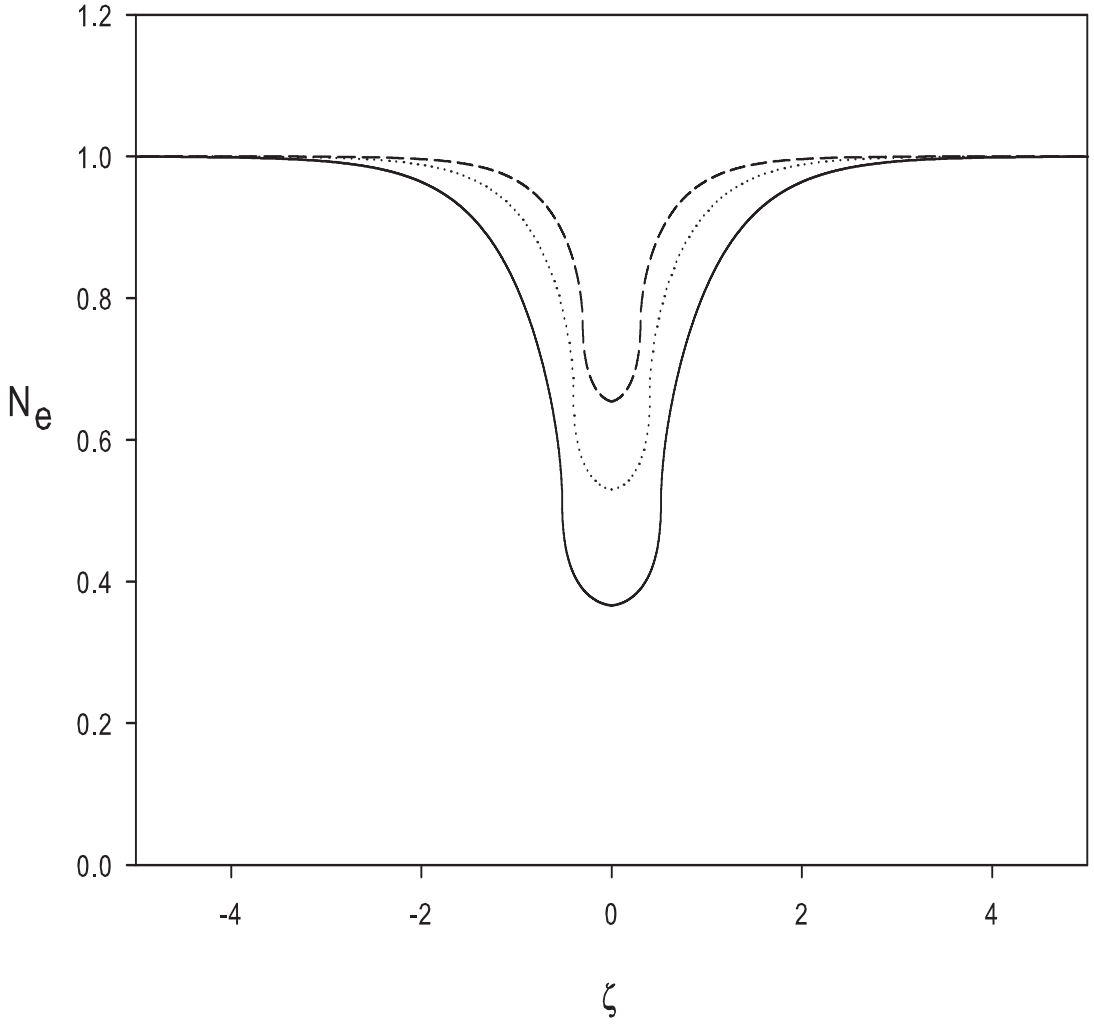

Figure 5.3: Soliton profile for $c/v_{th} = 10.0$ (solid), 13 (dotted), 15 (broken) with normalized soliton speed $M = 0.05$ and $v_{e0}/c = v_{p0}/c = 0.1$.

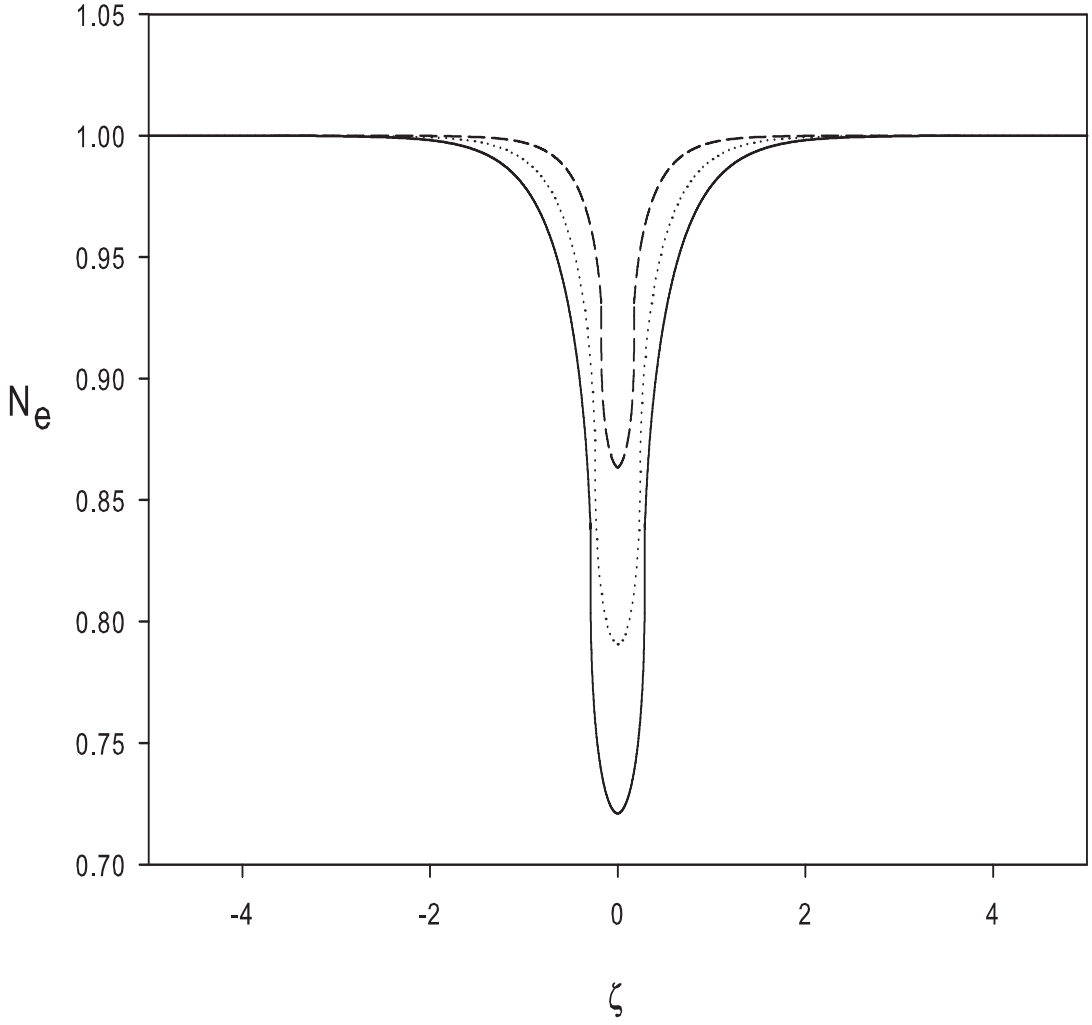

Figure 5.4: Soliton profile for drift velocities values $v_{e0}/c = v_{p0}/c = 0.10$ (solid), $v_{e0}/c = v_{p0}/c = 0.105$ (dotted), $v_{e0}/c = v_{p0}/c = 0.11$ (broken). The fixed parameters are $M = 0.02$ and $c/v_{th} = 10.0$.

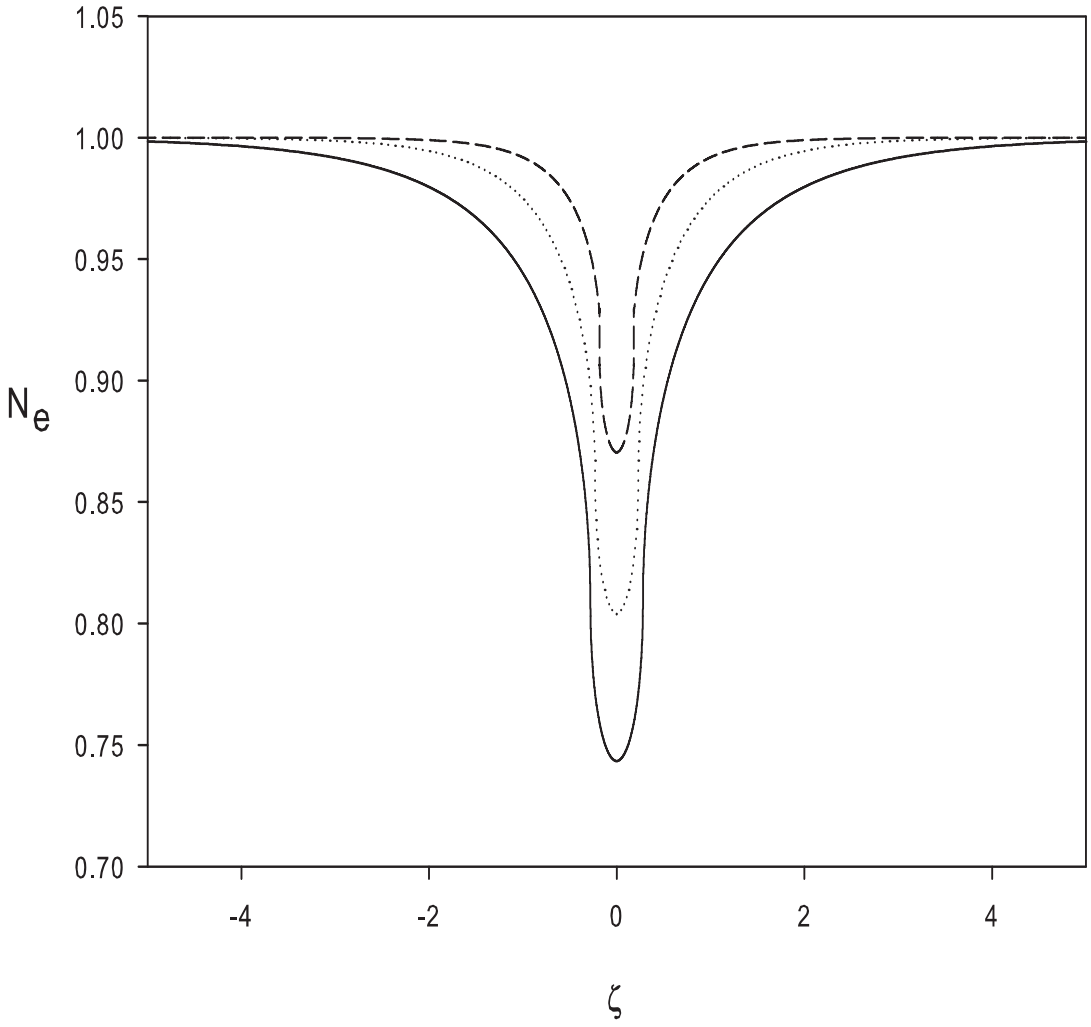

Figure 5.5: Soliton profile for drift velocities values $v_{e0}/c = 0.10$, $v_{p0}/c = -0.10$ (solid), $v_{e0}/c = 0.105$, $v_{p0}/c = -0.105$ (dotted), $v_{e0}/c = 0.11$, $v_{p0}/c = -0.11$ (broken). The fixed parameters are $M = 0.02$ and $c/v_{th} = 10.0$.

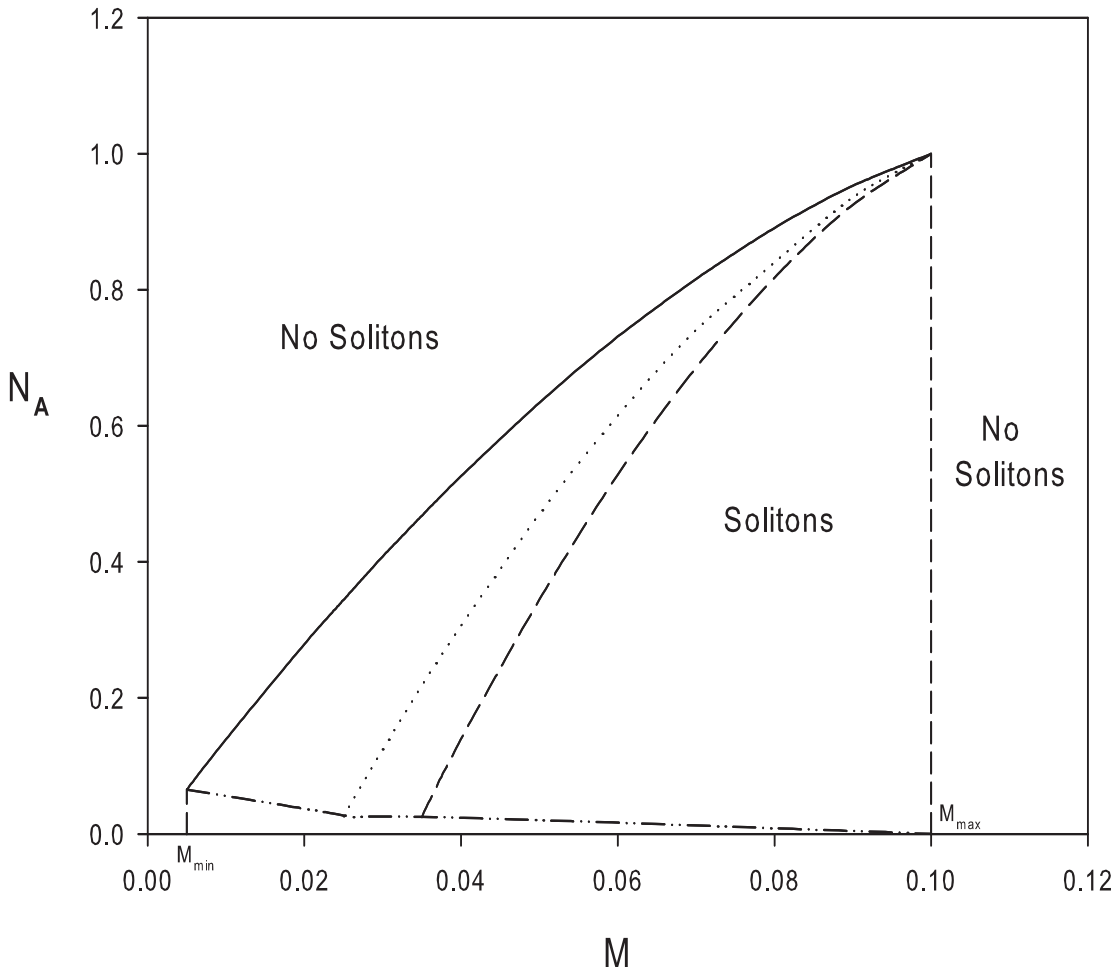

Figure 5.6: The maximum soliton amplitude as a function of the normalized soliton speed for $c/v_{th} = 10.0$ (solid), 13 (dotted) and 15 (broken) with $v_{e0}/c = v_{p0}/c = 0.1$.

5.4 Small Amplitude Theory

Finally, it is briefly shown how an analytical solution for the soliton structure corresponding to the plasma model presented in section 5.3 may be obtained using small amplitude theory. Since an arbitrary amplitude theory (section 5.3) covers all parameter ranges, no attempt is made to numerically compare the results in this section with the previous section. The exercise is merely to seek an analytical expression for the soliton structure.

To study the properties of stationary small amplitude solitary waves, once again equations (5.1) – (5.4) are transformed to a stationary frame moving with velocity V, the phase velocity of the wave, i.e., $\xi = x - Vt$. Substituting the above transformation into equations (5.1) – (5.4), and using the boundary conditions, $v_j = v_{j0}, n_j = 1$, and $\phi = 0$ at $\xi = \infty$, where v_{j0} are the equilibrium drift speeds for the j^{th} species, one obtains

$$n_j = \frac{V - v_{j0}}{V - v_j} \tag{5.17}$$

and

$$-\alpha_j \phi = ln(n_j) + \frac{c^2 - V v_j}{\sqrt{1 - v_j^2/c^2}} - \frac{c^2 - V v_{j0}}{\sqrt{1 - v_{j0}^2/c^2}} \ . \tag{5.18}$$

Proceeding with the small amplitude analysis, the densities $n_j = n_j(\phi)$ are

expanded as follows

$$n_j = n_{j0} + \frac{\partial n_j}{\partial \phi}\phi + \frac{\partial^2 n_j}{\partial \phi^2}\frac{\phi^2}{2} + ... \tag{5.19}$$

Using equations (5.17) and (5.18), one obtains the coefficients

$$\frac{\partial n_j}{\partial \phi} = \frac{-\alpha_j}{1 - \frac{(V - v_{j0})^2}{(1 - v_{j0}^2/c^2)^{3/2}}} \tag{5.20}$$

and

$$\frac{\partial^2 n_j}{\partial \phi^2} = \frac{1 - \frac{3(V - v_{j0})^2(1 - \frac{V v_{j0}}{c^2})}{(1 - v_{j0}^2/c^2)^{5/2}}}{\left[1 - \frac{(V - v_{j0})^2}{(1 - v_{j0}^2/c^2)^{3/2}}\right]^3} \ , \tag{5.21}$$

which have to be read in conjunction with equation (5.17).

Substituting equations (5.20) and (5.21) into equation (5.19), the Poisson's equation (5.4) becomes

$$\frac{\partial^2 \phi}{\partial \xi^2} = (N_1 + P_1)\phi + (N_2 - P_2)\phi^2 \ . \tag{5.22}$$

Integration of equation (5.22), yields,

$$\frac{1}{2}(\frac{d\phi}{d\xi})^2 = (N_1 + P_1)\frac{\phi^2}{2} + (N_2 - P_2)\frac{\phi^3}{6} \ , \tag{5.23}$$

which yields

$$\phi = \phi_0 sech^2\left(\frac{\xi}{W}\right) \ , \tag{5.24}$$

where the soliton amplitude

$$\phi_0 = \frac{3(N_1 + P_1)}{(P_2 - N_2)} \tag{5.25}$$

with

$$N_1 = \frac{1}{1 - \frac{(V - v_{e0})^2}{(1 - v_{e0}^2/c^2)^{3/2}}}, \qquad P_1 = \frac{1}{1 - \frac{(V - v_{p0})^2}{(1 - v_{p0}^2/c^2)^{3/2}}} \tag{5.26}$$

and

$$N_2 = \frac{1 - \frac{3(V - v_{e0})^2 (1 - \frac{V v_{e0}}{c^2})}{(1 - v_{e0}^2/c^2)^{5/2}}}{\left[1 - \frac{(V - v_{e0})^2}{(1 - v_{e0}^2/c^2)^{3/2}}\right]^3}, \qquad P_2 = \frac{1 - \frac{3(V - v_{p0})^2 (1 - \frac{V v_{p0}}{c^2})}{(1 - v_{p0}^2/c^2)^{5/2}}}{\left[1 - \frac{(V - v_{p0})^2}{(1 - v_{p0}^2/c^2)^{3/2}}\right]^3}, \tag{5.27}$$

where the width of the solitons W is given by $W = \frac{2}{\sqrt{N_1 + P_1}}$.

Equation (5.24) shows the localized solution in the form of the well-known square hyperbolic secant for small wave amplitudes (Shukla and Yu, 1978; Lakshmi *et al.*, 1997; Gill *et al.*, 2007). It is noted from equation (5.27) that for zero or equal drift for the two species, $N_2 = P_2$ and consequently the second term in equation (5.23) vanishes, which implies expansions to higher orders in finding an analytical solution. However, if the two species are counter-streaming then the small amplitude solutions are admissible.

5.5 Discussion

In this chapter the existence of both arbitrary and small amplitude solitons in a relativistic electron-positron plasma have been investigated. This model consists of equilibrium electron and positron densities n_{e0} and n_{p0} respectively, and equal electron and positron temperatures denoted by T. The Sagdeev pseudo-potential method is used to derive the energy-integrals for arbitrary amplitude solitons and their profiles studied as functions of plasma parameters. Numerical results are presented showing that the electrostatic fluctuations can propagate as nonlinear soliton-like structures. For our model, an increase in the soliton speed results in an increase in the soliton amplitude. For warmer electron-positron plasmas ((c/v_{th}) decreasing), the results show that the soliton amplitude increases. Increasing c/v_{th} also results in a decrease in the soliton half widths. As the drift velocities increase it is also noted that the soliton amplitude decreases. This trend is the same when the electrons and positrons are drifting in opposite directions. Existence curves for soliton structures show that when c/v_{th} in increased the range of soliton speeds M decreases, with the minimum value of M increasing when c/v_{th} increased. Using small amplitude theory, an analytical expression for the soliton structure is derived. These small amplitude solitary waves in relativistic electron-positron plasmas are shown to exist specifically for counter-streaming species.

Chapter 6

Summary

Several aspects of linear and nonlinear waves in electron-positron plasmas have been studied in this thesis. In Chapter 2, fluid and kinetic theory approaches are used to investigate linear waves in a four-component two temperature electron-positron plasma. Wave propagation is taken oblique to the ambient magnetic field. In the fluid theory model, the hot species are described by the Boltzmann density distribution and the cooler species by the fluid equations with finite temperatures. For purely perpendicular propagation, the results in this study show that there exists only a cyclotron mode with the acoustic mode vanishing ($\omega = 0$). In the short wavelength limit ($k^2\lambda_D^2 \gg 1$), there exists an upper hybrid mode with only the cooler species contributing to the wave dynamics while in the opposite long wavelength limit ($k^2\lambda_D^2 \ll 1$) a cyclotron mode exists with contributions from both the hot and the cooler species. For purely parallel propagation, a constant frequency non-propagating ($\omega = \Omega$) oscillation and an acoustic mode exist. In the long

wavelength limit, for the latter mode both the temperature and density ratios contribute to the dynamics of the wave. In the short wavelength limit, the dispersion relation reduces to the well known Langmuir wave for an electron-positron plasma, as obtained by Zank and Greaves (1995), with contributions only from the cooler species. In the model presented in this thesis, it is found that the linear portions of the dispersion curves have a smaller slope when compared to the corresponding curves for the two species, single temperature model of Zank and Geaves (1995). For small wavenumbers ($k\lambda_D \ll 1$), there is also a sharp rise in the dispersion curves, which is due to the contribution of the second species. It is noted that this is a particular feature of the four component two temperature electron-positron plasma and is not present in the results of Zank and Greaves (1995) in their two component model. Using kinetic theory, the real frequency for the acoustic mode is obtained through appropriate expansions and is found to be in very good agreement with that derived from fluid theory. The modes were also found to be unstable, where the instability is driven by the energy provided by the hot species having a velocity V_{oh} parallel to the ambient magnetic field $\mathbf{B_o}$. However, given that the acoustic mode is a micro-instability arising from resonances in velocity space, Landau damping effects are found to be important for this wave in the kinetic theory approach. As the temperature ratio T_c/T_h increases, the associated Landau damping increases, resulting in the overall growth rate being reduced. An increase in the drift velocity of the hot species (V_{oh}), results in an increase in the growth rate since the free energy required to drive the instability increases. The overall growth rate is enhanced when the

magnetic field strength ($\mathbf{B_o}$) is increased. A possible physical explanation for this behaviour is that the charged particles are more strongly tied to the field lines with increasing $\mathbf{B_o}$ and hence are hindered in moving oblique to the field lines to suppress the instability. Increasing the propagation angle θ relative to the ambient magnetic field results in a decrease in the growth rate.

In chapter 3 the study moved into the nonlinear regime and the existence of solitary waves was investigated. The model considered is the same as that described in chapter 2. Using the reductive perturbation technique, a modified KdV-ZK (mKdV-ZK) equation for nonlinear electrostatic modes was derived and an exact analytical solution was determined for the soliton potential structures. The soliton structures was then studied for different parameters. It was found that propagation at larger angles to the ambient magnetic field enhanced the soliton amplitude. An increase in the cool to hot density ratios (N_c/N_h) resulted in an increase in the soliton amplitude for a fixed temperature. Also, for a fixed density, as the ratio of the cool to hot temperatures (T_c/T_h) decreased, the soliton amplitude increased. These findings have already been published in the Journal of Plasma Physics (Lazarus *et al.*, 2008) and are consistent with similar independent studies published in the literature.

In chapter 4, various four-component electron-positron plasma models were used to explore the existence of nonlinear electric field structures in the form of solitary waves. The objective of the study was to investigate if the elec-

trostatic solitary waves (ESWs) observed (in electron-ion plasmas) in the Broadband Electrostatic Noise (BEN) in different regions of the earth's magnetosphere, could also be a feature of electron-positron plasmas. In Model 1, the hot species are described by the Boltzmann density distribution and the cold species by the fluid equations. Model 2 includes the full dynamics of all species described by the fluid equations, but with $T_c = 0$ for the cold species. All species having finite nonzero temperatures were examined in Model 3. The fixed plasma parameters used in this study are similar to those used in electron-ion plasmas. In solving the set on nonlinear equations, it was found that when the amplitude of the driving electric field was increased, the waveform progressed from a linear sinusoidal to a sawtooth to a highly spiky bipolar structure, similar to earlier studies in electron-ion plasmas. These nonlinear structures arise from the coupling of the acoustic wave and cyclotron wave, which result from the convective derivative terms $v_{jx}(\partial v_{jy}/\partial x)$ and $v_{jx}(\partial v_{jz}/\partial x)$ in the fluid momentum equations. It is seen that an increase in the Mach number causes the nonlinearity of the wave to be suppressed. Hence for larger values of M, a stronger electric field value (E_0) is required in order to generate the spiky bipolar structures. It is also noted that the period of the wave decreases as the Mach number increases. When the cool to hot density ratio is increased the waveform becomes more nonlinear, with increasing periodicity. For larger values of the density ratio with a fixed Mach number, a smaller driving electric field is required to generate the spiky structure. It is also noted that for a fixed E_0 value, as the density of the cold species increases, the M-value required for the onset of the spiky

ESWs increases. The relative drift velocities of the electrons and positrons is found to affect the periodicity of the nonlinear electrostatic waves. The cold electron and positron drift velocities in moving from anti-parallel to parallel to $\mathbf{B_0}$ results in an increase in the pulse width and the period of the spiky structures. This effect is opposite for the hot electron and positron drift velocities where anti-parallel to parallel flow decreases the pulse width and the period of the spiky structure. However, the ratio of the pulse width and the period of the waves (w/T) was calculated to be a constant, consistent with satellite observations by Kojima *et al.* (1994). Increasing the propagation angle with respect to the ambient magnetic field causes the waveform to become distorted, with a transition from a single spike to a double-humped feature. The inclusion of finite temperatures for the cold species is found to broaden the waves, with the periodicity increasing with an increase in the cool to hot temperature ratio. In comparing all three models, it is noted that better enhanced spikes are obtained using model 2 and model 3, where the hot species are described by the fluid equations compared to model 1, where they are described by the Boltzmann density distribution. It is also noted that due to the assumption of the Boltzmann density distribution for the hot species, model 1 is restrictive and the generation of the ESWs are only possible for large values of $R = \omega_p/\Omega$ (=160) compared to model 2 and model 3 where these structures are possible for a much lower value of R (=10), i.e. a more strongly magnetized plasma in comparison to model 1.

In Chapter 5 the focus moved to relativistic plasmas. The existence of both arbitrary and small amplitude solitons in a two component, unmagnetized, warm relativistic electron-positron plasma was investigated. For the arbitrary amplitude studies the Sagdeev pseudo-potential method was adopted. Here, the soliton amplitude was found to increase with an increase in the soliton speed. On the other hand, the soliton amplitude decreased when the drift velocities of the two species were increased, as well as when c/v_{th} was increased, i.e. the thermal velocity v_{th} decreased relative to the speed of light c. It is also noted that as c/v_{th} increased, the range of soliton speeds for soliton structures to exist decreased, with the minimum value of M increasing with c/v_{th}. Next, in a brief study, through an expansion of the Sagdeev potential for small amplitudes, an exact analytical expression was obtained for the nonlinear wave potential, namely, $\phi = \phi_0 sech^2\left(\frac{\xi}{W}\right)$. Here, small amplitude solitons are shown to exist for counter-streaming species.

The above set of studies lends itself to exploring three component electron-positron-ion plasmas. From the recent literature, it is noted that several theoretical studies have been undertaken in electron-positron-ion plasmas in an attempt to model such laboratory plasmas. Therefore it will be of interest to extend the work presented here for pure electron-positron plasmas to include the ion dynamics and study the effect on the waves. Moreover, by including magnetic field perturbations, the entire spectrum of linear and nonlinear electromagnetic waves may be studied.

Appendix A

Derivation of the Kinetic Dispersion Relation

Here we derive the kinetic dispersion relation for the general case where $\mathbf{k} = (k_x, k_y, k_z)$. In doing so, the magnetic field $\mathbf{B_0}$ is taken in the z-direction, i.e. $\mathbf{B} = B_0\hat{z}$.

An isotropic, drifting Maxwellian velocity distribution, with temperatures T_j drifting parallel to the magnetic field, $\mathbf{B_0} = B_0\hat{z}$, with drift velocities V_{oj} is considered (figure A.1).

The equilibrium velocity distribution for the species are given by,

$$f_{\alpha 0} = \frac{n_{\alpha 0}}{(2\pi v_{tj}^2)^{\frac{3}{2}}} \exp\left\{ \frac{-[V_x^2 + V_y^2 + (V_z - V_{oj})^2]}{2v_{tj}^2} \right\}, \tag{A.1}$$

where $j = c(h)$ for the cool (hot) species and $\alpha = ec, pc, eh$ and ph for the cool electrons, cool positrons, hot electrons and hot positrons respectively

and where $v_{tj} = (T_j/m)^{\frac{1}{2}}$ is the thermal velocity of the j^{th} species.

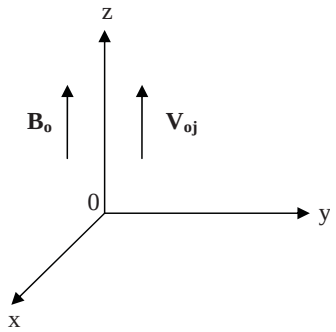

Figure A.1

Introducing the following small perturbations about the equilibrium quantities,

$$f_\alpha = f_{\alpha 0} + f_{\alpha 1}$$
$$\mathbf{E} = \mathbf{E_0} + \mathbf{E_1}$$
$$\mathbf{B} = \mathbf{B_0} + \mathbf{B_1}$$
$$n_\alpha = n_{\alpha 0} + n_{\alpha 1}$$

and linearizing the Vlasov equation

$$\frac{\partial f_\alpha}{\partial t} + \mathbf{V}.\nabla f_\alpha + \frac{q_\alpha}{m}(\mathbf{E} + \mathbf{V} \times \mathbf{B}).\frac{\partial f_\alpha}{\partial \mathbf{V}} = 0, \tag{A.2}$$

yields

$$\frac{\partial f_{\alpha 1}}{\partial t} + \mathbf{V}.\nabla f_{\alpha 1} + \frac{q_\alpha}{m}\mathbf{E}_1.\frac{\partial f_{\alpha 0}}{\partial \mathbf{V}} + \frac{q_\alpha}{m}\Big(\mathbf{E_0} + \mathbf{V} \times \mathbf{B_0}\Big).\frac{\partial f_{\alpha 1}}{\partial \mathbf{V}} = 0, \tag{A.3}$$

where the equation of motion for the electrons and positrons are given by,

$$m\frac{d\mathbf{V}}{dt} = q_\alpha \left\{\mathbf{E} + \mathbf{V} \times \mathbf{B}\right\}. \tag{A.4}$$

For electrostatic modes, $\mathbf{E_1} = -\nabla\phi_1$ since $\mathbf{B_1} = 0$ and $\mathbf{E_0} = 0$. Hence equation (A.3) becomes,

$$\frac{df_{\alpha 1}}{dt} = \frac{q_\alpha}{m}\nabla\phi_1 . \frac{\partial f_{\alpha 0}}{\partial \mathbf{V}}, \tag{A.5}$$

where the operator $\frac{d}{dt} = [\frac{\partial}{\partial t} + \mathbf{V}.\nabla + \frac{q_\alpha}{m}(\mathbf{E_0} + \mathbf{V} \times \mathbf{B_0})\frac{\partial}{\partial \mathbf{V}}]$ is defined as the rate of change following an unperturbed orbit in phase space (Gary *et al.,* 1970).

Integrating along the unperturbed orbits equation (A.5) becomes,

$$f_{\alpha 1}(\mathbf{r}, \mathbf{V}, t) = \frac{q_\alpha}{m}\int_{-\infty}^{t} \nabla\phi_1(\mathbf{r}', \mathbf{t}') . \frac{\partial f_{\alpha 0}(\mathbf{V}')}{\partial \mathbf{V}'} \mathrm{d}t', \tag{A.6}$$

where

$$\mathbf{V}' = \frac{d\mathbf{r}'}{dt'}, \qquad \frac{d\mathbf{V}'}{dt'} = \frac{q_\alpha}{m}\left[\mathbf{V}' \times \mathbf{B_0}\right]$$

and

$$\mathbf{r}'(0) = \mathbf{r}, \qquad \mathbf{V}'(0) = \mathbf{V}.$$

For perturbations that are harmonic in space and time,

$$f_{\alpha 1}(\mathbf{r}, \mathbf{V}, t) = f_{\alpha 1}(\mathbf{V}) \exp\left\{i(\mathbf{k}.\mathbf{r} - \omega t)\right\} \tag{A.7}$$

and

$$\phi_1(\mathbf{r}, t) = \phi_{1k\omega} \exp\left\{i(\mathbf{k}.\mathbf{r} - \omega t)\right\}. \tag{A.8}$$

Assuming that the plasma to be undisturbed at $t = -\infty$, the differentiation of equation (A.1) yields,

$$\frac{\partial f_{\alpha 0}}{\partial \mathbf{V}'} = -\mathbf{V_{eq}} f_{\alpha 0}(\mathbf{V}'), \tag{A.9}$$

where

$$\mathbf{V_{eq}} = \left[\frac{V'_x}{v_{tj}^2}, \frac{V'_y}{v_{tj}^2}, \frac{V'_z - V_{ojz}}{v_{tj}^2}\right].$$

Substitution of equations (A.7)-(A.9) into equation (A.6), with $\nabla\phi_1(\mathbf{r}', \mathbf{t}') = ik\phi_1(\mathbf{r}', \mathbf{t}')$, yields,

$$f_{\alpha 1}(\mathbf{r}, \mathbf{V}, t) = -\frac{iq_\alpha}{m} f_{\alpha 0}(\mathbf{V}') \int_{-\infty}^{t} \mathbf{k}.\mathbf{V_{eq}} \phi(\mathbf{r}', t') \mathrm{d}t'. \tag{A.10}$$

The solution of the equation of motion (A.4) yields,

$$\left.\begin{aligned} V'_x &= V'_\perp \cos(-\Omega t' + \theta) \\ V'_y &= V'_\perp \sin(-\Omega t' + \theta) \\ V'_z &= \text{constant} \end{aligned}\right\} \tag{A.11}$$

where $V'_\perp = \left\{(V'_x)^2 + (V'_y)^2\right\}^{\frac{1}{2}}$ is the velocity perpendicular to the magnetic field lines and $\Omega_\alpha = q_\alpha B_o/m$ are the gyrofrequences of the electrons and positrons. The configuration at $t' = 0$ is illustrated in figure A.2.

Resolving the wave vector $\mathbf{k}$ into components parallel and perpendicular to

$\mathbf{B_0}$ (figure A.3),

$$\mathbf{k} = [k_x, k_y, k_z] = [k_\perp \cos\Psi, k_\perp \sin\Psi, k_z]\,. \tag{A.12}$$

Hence

$$\mathbf{k}.\mathbf{V_{eq}} = \frac{k_\perp V'_\perp}{v_{tj}^2}\cos(\Omega t' + \Psi - \theta) + \frac{k_z(V'_z - V_{ojz})}{v_{tj}^2}. \tag{A.13}$$

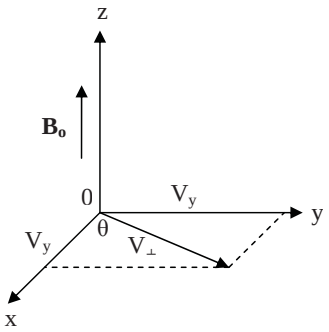

Figure A.2

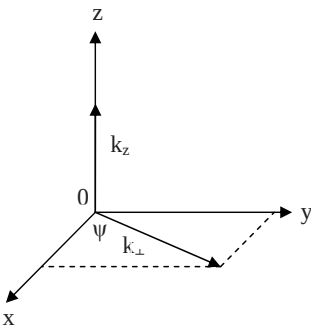

Figure A.3

Using equations (A.7) and (A.13), equation (A.10) becomes,

$$f_{\alpha 1}(\mathbf{r},\mathbf{V},t) = f_{\alpha 1}(\mathbf{V})\exp\{i(\mathbf{k}.\mathbf{r}-\omega t)\} \qquad .$$
$$= -\frac{iq_\alpha}{m} f_{\alpha 0}(V')\left[\frac{k_\perp V'_\perp}{v_{tj}^2}\int_{-\infty}^{t}\phi_1\cos(\Omega t'+\Psi-\theta)dt' + \frac{k_z(V'_z-V_{ojz})}{v_{tj}^2}\int_{-\infty}^{t}\phi_1 dt'\right].$$

Evaluating the above equation at $t=0$ yields

$$f_{\alpha 1}(\mathbf{V}) = -\frac{iq_\alpha}{m} f_{\alpha 0}(\mathbf{V})\phi_{1k\omega}\left[\frac{k_\perp V_\perp}{v_{tj}^2}\int_{-\infty}^{0}\cos(\Omega' t'+\Psi-\theta)\exp\{i(\mathbf{k}.(\mathbf{r}'-\mathbf{r})-\omega t')\}\,dt'\right.$$
$$\left. + \frac{k_z(V_z-V_{ojz})}{v_{tj}^2}\int_{-\infty}^{0}\exp\{i(\mathbf{k}.(\mathbf{r}'-\mathbf{r})-\omega t')\}\,dt'\right]. \tag{A.14}$$

Solving equations (A.11) with $\mathbf{r}'(0)=\mathbf{r}=[x_0,y_0,z_0]$, the approximate orbit equations are

$$\mathbf{r}'-\mathbf{r} = \frac{V'_\perp}{\Omega}\left[-\sin(-\Omega t'+\theta)+\sin\theta\right]\hat{x}$$
$$+\left[\frac{V'_\perp}{\Omega}\left\{\cos(-\Omega t'+\theta)-\cos\theta\right\}\right]\hat{y} + \left[V'_z t'\right]\hat{z}. \tag{A.15}$$

Using equations (A.12) and (A.15), the second integral in equation (A.14) becomes

$$\int_{-\infty}^{0}\exp\left[i\mu\sin(\theta-\Psi)\right]\exp\left[-i\mu\sin(\theta-\Psi-\Omega t')\right]$$
$$\times\exp\left[i(\mathbf{k}.\mathbf{V_{oj}}+k_z(V'_z-V_{ojz})-\omega\right]t'dt', \tag{A.16}$$

where $\mu = \frac{k_\perp V'_\perp}{\Omega}$.

Using the identity (Watson, 1944),

$$\exp(i\mu \sin\beta) = \sum_{p=-\infty}^{\infty} \exp(ip\beta) J_p(\mu), \tag{A.17}$$

where J_p is the ordinary Bessel function of the first kind of order p, equation (A.16) becomes,

$$\sum_{p=-\infty}^{\infty} \sum_{q=-\infty}^{\infty} \left\{ \frac{\exp\left[i(p-q)(\theta-\Psi)\right] J_p(\mu) J_q(\mu)}{i\left[q\Omega + \mathbf{k}.\mathbf{V_{oj}} + k_z(V_z - V_{ojz}) - \omega\right]} \right\}. \tag{A.18}$$

Using the identity

$$\cos\beta = \frac{e^{i\beta} + e^{-i\beta}}{2}, \tag{A.19}$$

the first integral in equation (A.14) can be separated into parts yielding

$$\int_{-\infty}^{0} \left\{ \frac{1}{2} \exp\left[i(\Omega t' + \Psi - \theta)\right] \exp\left[i\left[\mathbf{k}.(\mathbf{r}' - \mathbf{r}) - \omega t'\right]\right] \right\} dt'. \tag{A.20}$$

Using equations (A.16) and (A.17) the first part of equation (A.14) becomes,

$$\frac{1}{2} \sum_{p=-\infty}^{\infty} \sum_{q=-\infty}^{\infty} \frac{\exp\left[i(p-q-1)(\theta-\Psi)\right] J_p(\mu) J_q(\mu)}{i\left[(q+1)\Omega + \mathbf{k}.\mathbf{V_{oj}} + k_z(V_z - V_{ojz}) - \omega\right]} \tag{A.21}$$

Similarly the second part yields

$$\frac{1}{2} \sum_{p=-\infty}^{\infty} \sum_{q=-\infty}^{\infty} \frac{\exp\left[i(p-q+1)(\theta-\Psi)\right] J_p(\mu) J_q(\mu)}{i\left[(q-1)\Omega + \mathbf{k}.\mathbf{V_{oj}} + k_z(V_z - V_{ojz}) - \omega\right]} \tag{A.22}$$

Substituting equations (A.18), (A.21) and (A.22) into equation (A.14) yields,

$$f_{\alpha 1}(\mathbf{V}) = -\frac{q_\alpha}{m} f_{\alpha 0}(\mathbf{V}) \phi_{1k\omega} \left[\frac{k_\perp V_\perp}{2v_{tj}^2} \sum_{p=-\infty}^{\infty} \sum_{q=-\infty}^{\infty} J_p(\mu) J_q(\mu) \times \right.$$

$$\left\{ \frac{\exp\{i(p-q-1)(\theta-\Psi)\}}{(q+1)\Omega + \mathbf{k}.\mathbf{V_{oj}} + k_z(V_z - V_{ojz}) - \omega} + \frac{\exp\{i(p-q+1)(\theta-\Psi)\}}{(q-1)\Omega + \mathbf{k}.\mathbf{V_{oj}} + k_z(V_z - V_{ojz}) - \omega} \right\}$$

$$\left. + k_z \frac{(V_z - V_{ojz})}{v_{tj}^2} \sum_{p=-\infty}^{\infty} \sum_{q=-\infty}^{\infty} \frac{\exp\{i(p-q)(\theta-\Psi)\} J_p(\mu) J_q(\mu)}{q\Omega + \mathbf{k}.\mathbf{V_{oj}} + k_z(V_z - V_{ojz}) - \omega} \right] \qquad \text{(A.23)}$$

The perturbed beam density for the electrons and positrons are given by

$$n_{\alpha 1}(\mathbf{r}, t) = n_{\alpha 1 k\omega} \exp\{i(\mathbf{k}.\mathbf{r} - \omega t)\} = \int f_{\alpha 1}(\mathbf{V}) d^3\mathbf{V} \qquad \text{(A.24)}$$

The integral in equation (A.24) can be evaluated by first transforming to cylindrical coordinates in velocity space with

$$d^3\mathbf{V} = V_\perp dV_\perp dV_z d\theta$$

The triple integral in equation (A.24) can be separated into three parts. Using the expression (A.1) for the equilibrium velocity distribution $f_{\alpha 0}(\mathbf{V})$, the first part yields,

$$-\frac{\pi q_\alpha \phi_{1k\omega} k_\perp n_{\alpha 0}}{T_j (2\pi v_{tj}^2)^{\frac{3}{2}}} \sum_{p=-\infty}^{\infty} \int_0^\infty \left[\int_{-\infty}^{\infty} \frac{\exp\left\{-\frac{(V_z - V_{ojz})^2}{2v_j^2}\right\}}{p\Omega + \mathbf{k}.\mathbf{V_{oj}} + k_z(V_z - V_{ojz}) - \omega} dV_z \right] \times$$

$$\exp\left\{-\frac{V_\perp^2}{2v_{tj}^2}\right\} J_p(\mu) J_{p-1}(\mu) V_\perp^2 dV_\perp, \qquad \text{(A.25)}$$

where we have used $v_{tj}^2 = T_j/m_i$, and the result

$$\int_0^{2\pi} \exp\left[i(p-q-1)\theta\right] d\theta = \begin{cases} 0, & p \neq q+1 \\ 2\pi, & p = q+1. \end{cases} \tag{A.26}$$

Introducing the plasma dispersion function , also known as the Z- function (Fried and Conte 1961)

$$Z(\lambda) = \frac{1}{\sqrt{\pi}} \int_{-\infty}^{\infty} \frac{e^{-x^2}}{x-\lambda} dx$$

for $Im(\lambda) > 0$ or alternatively as

$$Z(\lambda) = 2ie^{-\lambda^2} \int_{-\infty}^{i\lambda} e^{-t^2} dt. \tag{A.27}$$

Expressing the integral in equation (A.25) in terms of the Z-function yields

$$-\frac{\pi q_\alpha \phi_{1k\omega} k_\perp n_{\alpha 0}}{T_j (2\pi v_{tj}^2)^{\frac{3}{2}}} \frac{\sqrt{\pi}}{k_z} \sum_{p=-\infty}^{\infty} \int_0^{\infty} J_p(\mu) J_{p-1}(\mu) Z \left[\frac{\omega - \mathbf{k}.\mathbf{V_{oj}} - p\Omega}{\sqrt{2}k_z v_{tj}}\right] \times \exp\left\{-\frac{V_\perp^2}{2v_{tj}^2}\right\} V_\perp^2 dV_\perp. \tag{A.28}$$

Similarly the second part of the integral in equation (A.24) yields

$$-\frac{\pi q_\alpha \phi_{1k\omega} k_\perp n_{\alpha 0}}{T_j (2\pi v_{tj}^2)^{\frac{3}{2}}} \frac{\sqrt{\pi}}{k_z} \sum_{p=-\infty}^{\infty} \int_0^{\infty} J_p(\mu) J_{p+1}(\mu) Z \left[\frac{\omega - \mathbf{k}.\mathbf{V_{oj}} - p\Omega}{\sqrt{2}k_z v_{tj}}\right] \times \exp\left\{-\frac{V_\perp^2}{2v_{tj}^2}\right\} V_\perp^2 dV_\perp. \tag{A.29}$$

The last part of the integral becomes

$$-\frac{q_\alpha n_{\alpha 0}\phi_{1k\omega}}{T_j v_{tj}^2}\sum_{p=-\infty}^{\infty}\left[1+z_{pj}Z(z_{pj})\right]\exp\left\{-\frac{V_\perp^2}{2v_{tj}^2}\right\}J_p^2(\mu)V_\perp dV_\perp, \qquad \text{(A.30)}$$

where

$$z_{pj}=\frac{\omega-\mathbf{k}.\mathbf{V_{oj}}-p\Omega}{\sqrt{2}k_z v_{tj}}.$$

Combining the results (A.28)-(A.30), yields

$$\begin{aligned} n_{\alpha 1k\omega} = -\frac{q_\alpha n_{\alpha 0}\phi_{1k\omega}}{v_{tj}^2}\Bigg\{ & \frac{1}{T_j\sqrt{2}k_z v_{tj}}\sum_{p=-\infty}^{\infty}\int_0^\infty p\Omega J_p^2(\mu) \\ & Z(z_{pj})\exp\left\{-\frac{V_\perp^2}{2v_{tj}^2}\right\}V_\perp dV_\perp + \\ \frac{1}{T_j}\sum_{p=-\infty}^{\infty}\int_0^\infty & J_p^2(\mu)\left[1+z_{pj}Z(z_{pj})\right]\exp\left\{-\frac{V_\perp^2}{2v_{tj}^2}\right\}V_\perp dV_\perp\Bigg\}, \end{aligned} \qquad \text{(A.31)}$$

where we have used the identity (Watson, 1944),

$$J_{p-1}(\mu)+J_{p+1}(\mu)=\frac{2p}{\mu}J_p(\mu),$$

with $\mu=\frac{k_\perp V_\perp}{\Omega}$.

Using the identity (Watson, 1944),

$$\int_0^\infty J_p^2(\beta x)\exp(-\mu x^2)x dx=\frac{1}{2\mu}\exp(-\frac{\beta^2}{2\mu})I_p(\frac{\beta^2}{2\mu}),$$

where I_p, is the Modified Bessel function of the first kind of order p, equation (A.31) becomes,

$$n_{\alpha 1k\omega} = -\frac{q_\alpha n_{\alpha 0}\phi_{ik\omega}}{T_j}\left\{\frac{1}{\sqrt{2}k_z v_{tj}}\sum_{p=-\infty}^{\infty} p\Omega Z(z_{pj})\exp\left\{-\frac{k_\perp^2 v_{tj}^2}{\Omega^2}\right\} I_p\left\{\frac{k_\perp^2 v_{tj}^2}{\Omega^2}\right\}\right.$$
$$\left. + \sum_{p=-\infty}^{\infty}[1 + z_{pj}Z(z_{pj})]\exp\left\{-\frac{k_\perp^2 v_{tj}^2}{\Omega^2}\right\} I_p\left\{\frac{k_\perp^2 v_{tj}^2}{\Omega^2}\right\}\right\}. \tag{A.32}$$

Letting $\alpha_j = k_\perp^2 v_{tj}^2/\Omega^2$ and $\Gamma_{pj} = e^{-\alpha_j} I_p(\alpha_j)$, equation (A.32) may be written as

$$n_{\alpha 1k\omega} = -\frac{q_\alpha \phi_{1k\omega} n_{\alpha 0}}{T_j}\left\{1 + \frac{\omega - \mathbf{k}.\mathbf{V_{oj}}}{\sqrt{2}k_z v_{tj}}\sum_{p=-\infty}^{\infty} Z(z_{pj})\Gamma_{pj}.\right\} \tag{A.33}$$

Hence for the cool electrons, equation (A.33) can be written as

$$n_{ec1k\omega} = \frac{e\phi_{1k\omega} n_{ec0}}{T_c}\left\{1 + \frac{\omega - \mathbf{k}.\mathbf{V_{oc}}}{\sqrt{2}k_z v_{tc}}\sum_{p=-\infty}^{\infty} Z(z_{pc})\Gamma_{pc}\right\}, \tag{A.34}$$

and for the cool positrons,

$$n_{pc1k\omega} = -\frac{e\phi_{1k\omega} n_{pc0}}{T_c}\left\{1 + \frac{\omega - \mathbf{k}.\mathbf{V_{oc}}}{\sqrt{2}k_z v_{tc}}\sum_{p=-\infty}^{\infty} Z(z_{pc})\Gamma_{pc}\right\}. \tag{A.35}$$

For the hot electrons,

$$n_{eh1k\omega} = \frac{e\phi_{1k\omega} n_{eh0}}{T_h} \left\{ 1 + \frac{\omega - \mathbf{k}.\mathbf{V_{oh}}}{\sqrt{2} k_z v_{th}} \sum_{p=-\infty}^{\infty} Z(z_{ph}) \Gamma_{ph} \right\}, \tag{A.36}$$

and for the hot positrons,

$$n_{ph1k\omega} = -\frac{e\phi_{1k\omega} n_{eh0}}{T_h} \left\{ 1 + \frac{\omega - \mathbf{k}.\mathbf{V_{oh}}}{\sqrt{2} k_z v_{th}} \sum_{p=-\infty}^{\infty} Z(z_{ph}) \Gamma_{ph} \right\}. \tag{A.37}$$

The Poisson's equation,

$$-\varepsilon_0 \nabla^2 \phi = e(n_{ec} - n_{pc} + n_{eh} - n_{ph}) \tag{A.38}$$

in terms of the perturbed quantities may be written as

$$-\varepsilon_0 k^2 \phi_{1k\omega} = e(n_{ec1k\omega} - n_{pc1k\omega} + n_{eh1k\omega} - n_{ph1k\omega}). \tag{A.39}$$

By substituting the density perturbations from equations (A.34)-(A.37), the kinetic dispersion relation becomes,

$$0 = k^2 + \frac{2}{\lambda_{Dc}^2} \left\{ 1 + \frac{\omega - \mathbf{k}.\mathbf{V_{oc}}}{\sqrt{2} k_z v_{tc}} \sum_{p=-\infty}^{\infty} Z(z_{pc}) \Gamma_{pc} \right\} + \frac{2}{\lambda_{Dh}^2} \left\{ 1 + \frac{\omega - \mathbf{k}.\mathbf{V_{oh}}}{\sqrt{2} k_z v_{th}} \sum_{p=-\infty}^{\infty} Z(z_{ph}) \Gamma_{ph} \right\}.$$

where $\lambda_{dj} = (\varepsilon_0 T_j / n_{0j} e^2)^{1/2}$ are the Debye lengths, with $j = c(h)$ for the cool (hot) species and

$$z_{pj} = \frac{\omega - \mathbf{k}.\mathbf{V_{oj}} - p\Omega}{\sqrt{2} k_z v_{tj}}$$

is the argument for the $Z-$ function.

Appendix B

Calculation of Initial Conditions for Model 1

The initial values of v_{phyn} and v_{phzn} are calculated self-consistently.

At $s = 0$, we have point quasi-neutrality. Therefore

$$n_{ecn} + n_{ehn} = n_{pcn} + n_{phn} \tag{B.1}$$

Differentiating the quasi-neutrality condition gives,

$$\frac{\partial n_{ecn}}{\partial s} + \frac{\partial n_{ehn}}{\partial s} = \frac{\partial n_{pcn}}{\partial s} + \frac{\partial n_{phn}}{\partial s} \tag{B.2}$$

Substituting for $n_{eh} = \dfrac{n_{eh0}}{n_0} \exp(\psi)$ and $n_{ph} = \dfrac{n_{ph0}}{n_0} \exp(-\psi)$ into the above and noting that at $s = 0$, $\psi = 0$ and $E = E_0$, yields,

$$\frac{\partial n_{pcn}}{\partial s} = \left(\frac{n_{ph0}}{n_0} + \frac{n_{eh0}}{n_0} \right) E_0 + \frac{\partial n_{ecn}}{\partial s} \tag{B.3}$$

Recalling equations (4.20) and (4.23)

$$\frac{\partial n_{ecn}}{\partial s} \;=\; \frac{n_{ecn}^3}{(M - \delta_c)^2} \left(\frac{n_0}{n_{ec0}} \right)^2 \left[E + M \sin\theta v_{ecyn} \right] \tag{B.4}$$

$$\frac{\partial n_{pcn}}{\partial s} = \frac{n_{pcn}^3}{(M-\delta_c)^2}\left(\frac{n_0}{n_{pc0}}\right)^2\left[-E - M\sin\theta v_{pcyn}\right] \tag{B.5}$$

Substituting equations (B.4)-(B.5) into (B.3) and solving for v_{pcyn0} yields

$$v_{pcyn0} = \frac{E_0 - \left(\frac{n_0}{n_{pc0}}\right)^{-2}\left[\frac{(M-\delta_c)^2 E_0}{n_{pcn}^3}\left(\frac{n_{ph0}}{n_0} + \frac{n_{eh0}}{n_0}\right) - \frac{n_{ecn}^3}{n_{pcn}^3}\left(\frac{n_0}{n_{ec0}}\right)^2\left(E_0 + M\sin\theta v_{ecyn0}\right)\right]}{M\sin\theta} \tag{B.6}$$

To calculate v_{pczn0} equations (4.21) and 4.24) are recalled,

$$\frac{\partial v_{ecyn}}{\partial s} = \frac{M n_{ecn}}{(M-\delta_c)}\left(\frac{n_0}{n_{ec0}}\right)\left[-\left(M - \frac{(M-\delta_c)}{n_{ecn}}\left(\frac{n_{ec0}}{n_0}\right)\right)\sin\theta + v_{eczn}\cos\theta\right] \tag{B.7}$$

$$\frac{\partial v_{pcyn}}{\partial s} = \frac{M n_{pcn}}{(M-\delta_c)}\left(\frac{n_0}{n_{pc0}}\right)\left[\left(M - \frac{(M-\delta_c)}{n_{pcn}}\left(\frac{n_{pc0}}{n_0}\right)\right)\sin\theta - v_{pczn}\cos\theta\right] \tag{B.8}$$

Differentiating equation (B.3) yields

$$\frac{\partial^2 n_{pcn}}{\partial s^2} = -\left(\frac{n_{ph0}}{n_0} - \frac{n_{eh0}}{n_0}\right)E_0^2 + \frac{\partial^2 n_{ecn}}{\partial s^2} \tag{B.9}$$

Now differentiating equations (B.4) and (B.5) and substituting into equation (B.9) and using equations (B.7) and (B.8) yields

$$
\begin{aligned}
v_{phzn0} \;=\; & \frac{3}{M^2 \sin\theta \cos\theta (M-\delta_c)} \left(\frac{n_0}{n_{pc0}}\right)^{-3} \left[\frac{n_{ecn}^5}{n_{pcn}^4} \left(\frac{n_0}{n_{ec0}}\right)^4 \left(E_0 + M \sin\theta v_{ecyn0}\right)^2 \right. \\
& \left. - \; n_{pcn} \left(\frac{n_0}{n_{pc0}}\right)^4 \left(-E_0 - M \sin\theta v_{ecyn0}\right)^2 \right] \\
+ \; & \frac{n_{ecn}^4}{n_{pcn}^4} \left(\frac{n_0}{n_{pc0}}\right)^{-3} \left(\frac{n_0}{n_{ec0}}\right)^3 \left[-M \frac{\sin\theta}{\cos\theta} + \left(\frac{n_{ec0}}{n_0}\right) \frac{(M-\delta_c)\sin\theta}{n_{ecn}\cos\theta} + v_{eczn0} \right] \\
- \; & \frac{(M-\delta_c)^3}{M^2 \sin\theta \cos\theta n_{pcn}^4} \left(\frac{n_0}{n_{pc0}}\right)^{-3} \left(\frac{n_{ph0}}{n_0} - \frac{n_{eh0}}{n_0}\right) E_0^2 \\
+ \; & M \frac{\sin\theta}{\cos\theta} - \left(\frac{n_{pc0}}{n_0}\right) \frac{(M-\delta_c)\sin\theta}{n_{pcn}\cos\theta}
\end{aligned}
\tag{B.10}
$$

Appendix C

Calculation of Initial Conditions for Model 2

The initial values of v_{ehyn} and v_{ehzn} are calculated self-consistently.

At $s = 0$, we have point quasi-neutrality. Therefore

$$n_{ecn} + n_{ehn} = n_{pcn} + n_{phn} \tag{C.1}$$

Differentiating the quasi-neutrality condition gives,

$$\frac{\partial n_{ecn}}{\partial s} + \frac{\partial n_{ehn}}{\partial s} = \frac{\partial n_{pcn}}{\partial s} + \frac{\partial n_{phn}}{\partial s} \tag{C.2}$$

Recalling equations (4.45), (4.48), (4.52) and (4.56),

$$\begin{aligned}
\frac{\partial n_{ecn}}{\partial s} =& \frac{n_{ecn}^3}{(M-\delta_c)^2}\left(\frac{n_0}{n_{ec0}}\right)^2\left[E + M\sin\theta v_{ecyn}\right] \\
\frac{\partial n_{pcn}}{\partial s} =& \frac{n_{pcn}^3}{(M-\delta_c)^2}\left(\frac{n_0}{n_{pc0}}\right)^2\left[-E - M\sin\theta v_{pcyn}\right] \\
\frac{\partial n_{phn}}{\partial s} =& \frac{n_{phn}^3\left[-E - M\sin\theta v_{phyn}\right]}{\left(\frac{n_{ph0}}{n_0}\right)^2(M-\delta_h)^2 - 3p_{phn}n_{phn}}
\end{aligned} \tag{C.3}$$

$$\frac{\partial n_{ehn}}{\partial s} = \frac{n_{ehn}^3 \left[E + M \sin\theta v_{ehyn} \right]}{\left(\frac{n_{eh0}}{n_0} \right)^2 (M - \delta_h)^2 - 3 p_{ehn} n_{ehn}}$$

The following are defined to simplify the calculations,

$$\begin{aligned}
F_1 =& n_{ecn}^3 \left[E + M \sin\theta v_{ecyn} \right] \\
F_2 =& \left(\frac{n_{ec0}}{n_0} \right)^2 M - \delta_c)^2 \\
F_3 =& n_{ehn}^3 \\
F_4 =& \left(\frac{n_{eh0}}{n_0} \right)^2 (M - \delta_h)^2 - 3 p_{ehn} n_{ehn} \\
F_5 =& n_{pcn}^3 \left[-E - M \sin\theta v_{pcyn} \right] \\
F_6 =& \left(\frac{n_{pc0}}{n_0} \right)^2 (M - \delta_c)^2 \\
F_7 =& n_{phn}^3 \left[-E - M \sin\theta v_{phyn} \right] \\
F_8 =& \left(\frac{n_{ph0}}{n_0} \right)^2 (M - \delta_h)^2 - 3 p_{phn} n_{phn}
\end{aligned} \tag{C.4}$$

This implies,

$$\frac{F_1}{F_2} + \frac{F_3}{F_4} \left[E + M \sin\theta v_{ehyn} \right] = \frac{F_5}{F_6} + \frac{F_7}{F_8} \tag{C.5}$$

From the above the initial value of v_{ehyn} is determined to be,

$$v_{ehyn0} = \frac{-E + \left(\frac{F_5}{F_6} + \frac{F_7}{F_8} - \frac{F_1}{F_2} \right) \left(\frac{F_4}{F_3} \right)}{M sin\theta} \tag{C.6}$$

To determine the initial value of v_{ehzn} the quasi-neutrality condition is differentiated twice, i.e.

$$\frac{\partial^2 n_{ecn}}{\partial s^2} + \frac{\partial^2 n_{ehn}}{\partial s^2} = \frac{\partial^2 n_{pcn}}{\partial s^2} + \frac{\partial^2 n_{phn}}{\partial s^2} \tag{C.7}$$

Using the previous definitions, this gives

$$\frac{\partial}{\partial s}\left(\frac{F_1}{F_2}\right) + \frac{\partial}{\partial s}\left(\frac{F_3}{F_4}\right)\left[E + M\sin\theta v_{ehyn}\right] = \frac{\partial}{\partial s}\left(\frac{F_5}{F_6}\right) + \frac{\partial}{\partial s}\left(\frac{F_7}{F_8}\right) \tag{C.8}$$

i.e

$$\frac{F_3}{F_4}\left(M\sin\theta\frac{\partial v_{ehyn}}{\partial s}\right) = \frac{\partial}{\partial s}\left(\frac{F_5}{F_6}\right) + \frac{\partial}{\partial s}\left(\frac{F_7}{F_8}\right) - \frac{\partial}{\partial s}\left(\frac{F_1}{F_2}\right) - \left[E + M\sin\theta v_{ehyn}\right]\frac{\partial}{\partial s}\left(\frac{F_3}{F_4}\right) \tag{C.9}$$

Recalling equations (4.46), (4.49), (4.53) and (4.57)

$$\begin{aligned}
\frac{\partial v_{ecyn}}{\partial s} &= \frac{M n_{ecn}}{(M-\delta_c)}\left(\frac{n_0}{n_{ec0}}\right)\left[-\left(M - \frac{(M-\delta_c)}{n_{ecn}}\left(\frac{n_{ec0}}{n_0}\right)\right)\sin\theta + v_{eczn}\cos\theta\right] \\
\frac{\partial v_{pcyn}}{\partial s} &= \frac{M n_{pcn}}{(M-\delta_c)}\left(\frac{n_0}{n_{pc0}}\right)\left[\left(M - \frac{(M-\delta_c)}{n_{pcn}}\left(\frac{n_{pc0}}{n_0}\right)\right)\sin\theta - v_{pczn}\cos\theta\right] \\
\frac{\partial v_{phyn}}{\partial s} &= \frac{M n_{phn}}{(M-\delta_h)}\left(\frac{n_0}{n_{ph0}}\right)\left[\left(M - \frac{(M-\delta_h)}{n_{phn}}\left(\frac{n_{ph0}}{n_0}\right)\right)\sin\theta - v_{phzn}\cos\theta\right] \\
\frac{\partial v_{ehyn}}{\partial s} &= \frac{M n_{ehn}}{(M-\delta_h)}\left(\frac{n_0}{n_{eh0}}\right)\left[-\left(M - \frac{(M-\delta_h)}{n_{ehn}}\left(\frac{n_{eh0}}{n_0}\right)\right)\sin\theta + v_{ehzn}\cos\theta\right]
\end{aligned} \tag{C.10}$$

Substituting for $\frac{\partial v_{ecyn}}{\partial s}$, $\frac{\partial v_{pcyn}}{\partial s}$, $\frac{\partial v_{phyn}}{\partial s}$, $\frac{\partial v_{ehyn}}{\partial s}$ and performing the differentiation of equation (C.9), the initial value for v_{ehzn} is:

$$v_{ehzn0} = \left[M - \left(\frac{n_{eh0}}{n_0}\right)\frac{(M-\delta_h)}{n_{ehn}}\right]\frac{sin\theta}{cos\theta} + \frac{F_4}{F_5}\left(\frac{n_{eh0}}{n_0}\right)\frac{(M-\delta_h)}{M^2 sin\theta cos\theta n_{ehn}}$$

$$\times\left[\frac{\partial}{\partial s}\left(\frac{F_5}{F_6}\right) + \frac{\partial}{\partial s}\left(\frac{F_7}{F_8}\right) - \frac{\partial}{\partial s}\left(\frac{F_1}{F_2}\right) - \left(E + M\sin\theta v_{ehyn0}\right)\frac{\partial}{\partial s}\left(\frac{F_3}{F_4}\right)\right] \tag{C.11}$$

Appendix D

Calculation of Initial Conditions for Model 3

To calculate the initial values of v_{echn} and v_{eczn}, self-consistently the same procedure in Appendix C is followed, with the cool electron and position temperatures included.

At $s = 0$, we have point quasi-neutrality. Therefore

$$n_{ecn} + n_{ehn} = n_{pcn} + n_{phn} \tag{D.1}$$

Differentiating the quasi-neutrality condition gives,

$$\frac{\partial n_{ecn}}{\partial s} + \frac{\partial n_{ehn}}{\partial s} = \frac{\partial n_{pcn}}{\partial s} + \frac{\partial n_{phn}}{\partial s} \tag{D.2}$$

Recalling equations (4.72), (4.76), (4.81) and (4.85),

$$\frac{\partial n_{ecn}}{\partial s} = \frac{n_{ecn}^3 \left[E + M \sin\theta v_{ecyn} \right]}{\left(\frac{n_{ec0}}{n_0} \right)^2 (M - \delta_c)^2 - 3 \frac{T_c}{T_h} p_{ecn} n_{ecn}}$$

$$
\begin{aligned}
\frac{\partial n_{pcn}}{\partial s} =& \frac{n_{pcn}^3\Big[-E - M\sin\theta v_{pcyn}\Big]}{\left(\frac{n_{pc0}}{n_0}\right)^2(M-\delta_c)^2 - 3\frac{T_c}{T_h}p_{pcn}n_{pcn}} \\
\frac{\partial n_{phn}}{\partial s} =& \frac{n_{phn}^3\Big[-E - M\sin\theta v_{phyn}\Big]}{\left(\frac{n_{ph0}}{n_0}\right)^2(M-\delta_h)^2 - 3p_{phn}n_{phn}} \\
\frac{\partial n_{ehn}}{\partial s} =& \frac{n_{ehn}^3\Big[E + M\sin\theta v_{ehyn}\Big]}{\left(\frac{n_{eh0}}{n_0}\right)^2(M-\delta_h)^2 - 3p_{ehn}n_{ehn}}
\end{aligned}
\tag{D.3}
$$

Using the following definitions,

$$
\begin{aligned}
G_1 =& n_{ecn}^3\Big[E + M\sin\theta v_{ecyn}\Big] \\
G_2 =& \left(\frac{n_{ec0}}{n_0}\right)^2(M-\delta_c)^2 - 3\frac{T_c}{T_h}p_{ecn}n_{ecn} \\
G_3 =& n_{ehn}^3 \\
G_4 =& \left(\frac{n_{eh0}}{n_0}\right)^2(M-\delta_h)^2 - 3p_{ehn}n_{ehn} \\
G_5 =& n_{pcn}^3\Big[-E - M\sin\theta v_{pcyn}\Big] \\
G_6 =& \left(\frac{n_{pc0}}{n_0}\right)^2(M-\delta_c)^2 - 3\frac{T_c}{T_h}p_{pcn}n_{pcn} \\
G_7 =& n_{phn}^3\Big[-E - M\sin\theta v_{phyn}\Big] \\
G_8 =& \left(\frac{n_{ph0}}{n_0}\right)^2(M-\delta_h)^2 - 3p_{phn}n_{phn}
\end{aligned}
\tag{D.4}
$$

Hence v_{ehyn} can be determined.

Differentiating the quasi-neutrality twice yields,

$$\frac{\partial^2 n_{ecn}}{\partial s^2} + \frac{\partial^2 n_{ehn}}{\partial s^2} = \frac{\partial^2 n_{pcn}}{\partial s^2} + \frac{\partial^2 n_{phn}}{\partial s^2} \tag{D.5}$$

Recalling equations (4.73), (4.77), (4.82) and (4.86) we have,

$$\begin{aligned}
\frac{\partial v_{ecyn}}{\partial s} =& \frac{M n_{ecn}}{(M-\delta_c)} \left(\frac{n_0}{n_{ec0}}\right) \left[-\left(M - \frac{(M-\delta_c)}{n_{ecn}} \left(\frac{n_{ec0}}{n_0}\right)\right) \sin\theta + v_{eczn} \cos\theta \right] \\
\frac{\partial v_{pcyn}}{\partial s} =& \frac{M n_{pcn}}{(M-\delta_c)} \left(\frac{n_0}{n_{pc0}}\right) \left[\left(M - \frac{(M-\delta_c)}{n_{pcn}} \left(\frac{n_{pc0}}{n_0}\right)\right) \sin\theta - v_{pczn} \cos\theta \right] \\
\frac{\partial v_{phyn}}{\partial s} =& \frac{M n_{phn}}{(M-\delta_h)} \left(\frac{n_0}{n_{ph0}}\right) \left[\left(M - \frac{(M-\delta_h)}{n_{phn}} \left(\frac{n_{ph0}}{n_0}\right)\right) \sin\theta - v_{phzn} \cos\theta \right] \\
\frac{\partial v_{ehyn}}{\partial s} =& \frac{M n_{ehn}}{(M-\delta_h)} \left(\frac{n_0}{n_{eh0}}\right) \left[-\left(M - \frac{(M-\delta_h)}{n_{ehn}} \left(\frac{n_{eh0}}{n_0}\right)\right) \sin\theta + v_{ehzn} \cos\theta \right]
\end{aligned} \tag{D.6}$$

Following the process in Appendix C, the initial value of v_{ehzn} is calculated.

Appendix E

PUBLISHED

PAPER

J. Plasma Physics (2008), *vol.* 74, *part* 4, *pp.* 519–529.
doi:10.1017/S0022377807006836 Printed in the United Kingdom

Modified Korteweg–de Vries–Zakharov–Kuznetsov solitons in symmetric two-temperature electron–positron plasmas

I. J. LAZARUS[1,3], R. BHARUTHRAM[2] and M. A. HELLBERG[3]

[1] Department of Physics, Durban University of Technology, Durban, South Africa (lazarusi@dut.ac.za)

[2] Faculty of Science, University of Witwatersrand, Johannesburg, South Africa (ramesh.bharuthram@wits.ac.za)

[3] School of Physics, University of KwaZulu-Natal, Durban, South Africa

(Received 8 July 2007 and in revised form 3 August 2007, first published online 16 November 2007)

Abstract. Solitary waves are investigated in a magnetized electron–positron plasma consisting of equal hot and cool components of each species. The hot components have a Boltzmann distribution and the cool components are described by the fluid equations. A modified Korteweg–de Vries–Zakharov–Kuznetsov equation governing the oblique propagation of nonlinear electrostatic modes is derived using the reductive-perturbation technique. Soliton amplitudes are studied as a function of plasma parameters such as the particle number densities and the temperatures. Such results may be of relevance to the magnetosphere of pulsars.

1. Introduction

Electron–positron plasmas play a significant role in the understanding of the early universe (Rees 1983), active galactic nuclei (Miller and Witta 1987), gamma ray bursts (GRBs; see Piran (2004)), pulsar magnetospheres (Goldreich and Julian 1969; Michel 1982) and in the Solar atmosphere (Tandberg and Emslie 1988). In the case of pulsars, for instance, high-energy particles are accelerated along the pulsar magnetic field and they emit curvature photons, which in turn generate new electron–positron pairs (Beskin et al. 1983).

Many investigations into electron–positron plasma behaviour have focused on the relativistic regime. However, it is plausible that non-relativistic astrophysical electron–positron plasmas may exist, given the effect of cooling by cyclotron emission (Bhattacharyya et al. 2003). Electron–positron laboratory plasmas are useful for simulating astrophysical plasmas and studying fundamental electron–positron behaviour. Owing to the progress in pure positron production (Boehmer 1994; Greaves et al. 1994), it is now possible to perform experiments on a variety of electron–positron pair plasmas (Greaves and Surko 1995; Liang et al. 1998; Wilks et al. 2005).

New generation laser–plasma systems, where lasers can reach much higher intensities, also make it possible to model astrophysical plasma conditions in a laboratory environment (Remington 2005). These laser–plasma systems have been suggested

as sources of high-intensity radiation, where particles are accelerated to relativistic velocities. Such systems could therefore form the basis of electron–positron pair creation (Alkofer et al. 2001; Ringwald 2001; Roberts et al. 2002). As pair plasmas give rise to radiowave emission, with large energy scales, pulsar atmospheres are likely to host other quantum electrodynamical effects as well, such as vacuum nonlinearities in the form of photon–photon scattering (Marklund and Shukla 2006). More recently, laboratory experiments have been carried out on an alternative form of pair plasma, namely fullerene pair plasmas (Oohara et al. 2005).

Pair plasmas are characterized as fully ionized gases with particles of equal and opposite charge and having equal mass. The equality in masses means that only one frequency scale exists and hence, owing to the symmetry, the analysis is simplified. The nonlinear behaviour of waves propagating in electron–positron plasmas has been investigated in a number of studies. For instance, Gedalin et al. (1985) investigated nonlinear wave conversions in electron–positron plasmas in a very strong magnetic field. They showed that the nonlinear Landau damping phenomena related to Čerenkov resonances as well as cyclotron resonances, causes large frequency shifts. Stenflo et al. (1985) studied the nonlinear propagation of field-aligned circularly polarized electromagnetic waves in an electron–positron plasma. They discussed the modulational instabilities and wave localization and showed that a new class of cusped solitons are possible. Owing to multidimensional effects, Yu et al. (1986) showed that a new class of nonlinear structures, namely the travelling Alfvén vortex, can also exist in strongly magnetized electron–positron plasmas. Bharuthram (1992) investigated the existence of double layers in an unmagnetized electron–positron plasma. This asymmetric model consisted of hot and cool electrons and hot positrons, all of which were assumed to be Boltzmann-distributed, while the cold positrons, treated as very cold, were described by the fluid equations. Pillay and Bharuthram (1992) then investigated the possibility of large-amplitude solitons where both the cold electrons and positrons, which are strictly cold, were now described by the fluid equations. Verheest et al. (1996), considered an unmagnetized symmetric two-temperature electron–positron plasma with equal electron and positron densities of the cool species at temperature T_{c}, and similarly equal densities of the two hot species at temperature T_{h}. They described the two hot species with the Boltzmann distribution and treated the two cool species as fluids. The Sagdeev potential method was used to explore the existence and properties of nonlinear, arbitrary amplitude electrostatic potential structures. The Boltzmann assumption was shown to impose upper limits on the density and temperature of the cool species, and hence only small amplitude soliton structures were found to be possible. Misra and Chowdhury (2003) investigated the nonlinear interaction of electromagnetic pulses in an electron–positron plasma and showed that the electromagnetic wave envelope is governed by a coupled Schrödinger equation which also possesses solitary wave-like solutions.

We also note that nonlinear low-frequency structures have been studied in electron–ion plasmas. For instance, in one of the earlier studies, Shukla and Yu (1978) investigated a two-component magnetized electron–ion plasma. They found that finite-amplitude ion-acoustic solitary waves propagate obliquely to an external magnetic field. More recently, these structures have been studied in three-component plasmas consisting of electrons, ions and positrons. Popel et al. (1995) showed that the presence of positrons in an unmagnetized plasma, in the supersonic region, decreased the amplitude of the usual ion-acoustic soliton in electron–ion

plasmas. It is interesting to note that in a magnetized electron–positron–ion plasma, and in the subsonic region, the presence of positrons increased the ion-acoustic soliton amplitude (Mahmood et al. 2003).

In this paper, we investigate the properties of nonlinear electron–positron solitons in a magnetized, two-temperature, electron–positron plasma, allowing for propagation at oblique angles to the magnetic field. The symmetric four-component, two-temperature pair plasma, formed by the mixing of two simple pair plasmas with different temperatures, could exist on a timescale shorter than the thermalization time. Using the reductive-perturbation technique, we derive a modified Korteweg–de Vries–Zakharov–Kuznetsov (mKdV-ZK) equation for solitary structures, and study the soliton structure as a function of the plasma parameters.

The paper is structured as follows. In Sec. 2, the basic equations for the electron–positron plasma are presented. Section 3 provides an analytical derivation of the mKdV-ZK equation. In Sec. 4, we present the numerical results and discuss the limitations of the model. A summary of our findings is presented in Sec. 5.

2. Theory

We consider a homogeneous magnetized, four-component electron–positron plasma, consisting of cool electrons and positrons with equal temperatures and equilibrium densities denoted by $T_{\rm c}$ and $N_{\rm c}$, respectively, and hot electrons and positrons with equal temperatures and equilibrium densities denoted by $T_{\rm h}$ and $N_{\rm h}$, respectively. We note that the electron distribution function may be made up of a number of distribution functions with different characteristics, e.g. having different values of $n_\alpha(\mathbf{x},t)$, $\mathbf{u}_\alpha(\mathbf{x},t)$, $T_\alpha(\mathbf{x},t)$, etc. Thus, for instance, the electrons may be made up of two 'subspecies' of electrons, primary and secondary, generated by different mechanisms and with different temperatures. On a timescale that is short compared with the electron thermalization time, the distribution function could then be bi-Maxwellian, with two different temperatures. Wave propagation is at an angle θ to the ambient magnetic field $\mathbf{B}_0$, which is taken in the x-direction.

Charge neutrality at equilibrium requires for each species that

$$N_{\rm c} + N_{\rm h} = N_0. \tag{1}$$

In our model the hot isothermal species have a Boltzmann distribution given by

$$n_{\rm eh} = N_{\rm h} \exp\left(\frac{e\phi}{\kappa T_{\rm h}}\right) \tag{2}$$

$$n_{\rm ph} = N_{\rm h} \exp\left(\frac{-e\phi}{\kappa T_{\rm h}}\right), \tag{3}$$

where $n_{\rm eh}$ ($n_{\rm ph}$) is the density of the hot electrons (positrons) and ϕ is the electrostatic potential.

The dynamics of the cooler adiabatic species, denoted by the running subscript α are governed by the fluid equations, namely:

- the continuity equations

$$\frac{\partial n_\alpha}{\partial t} + \boldsymbol{\nabla}\cdot(n_\alpha \mathbf{u}_\alpha) = 0; \tag{4}$$

- the equations of motion

$$\frac{\partial \mathbf{u}_\alpha}{\partial t} + \mathbf{u}_\alpha \cdot \nabla \mathbf{u}_\alpha + \frac{1}{n_\alpha m_\alpha} \nabla p_\alpha = -\frac{q_\alpha}{m_\alpha} \nabla \phi + \Omega_\alpha \mathbf{u}_\alpha \times \mathbf{e}_x ; \tag{5}$$

- the adiabatic pressure equations

$$\frac{\partial p_\alpha}{\partial t} + \mathbf{u}_\alpha \cdot \nabla p_\alpha + \gamma_\alpha p_\alpha \nabla \cdot \mathbf{u}_\alpha = 0. \tag{6}$$

The system is closed by the Poisson equation

$$\varepsilon_0 \nabla^2 \phi + \sum_\alpha n_\alpha q_\alpha + \sum_\beta N_\beta q_\beta \exp\left[\frac{-q_\beta \phi}{\kappa T_\beta}\right] = 0, \tag{7}$$

where n_α, $\mathbf{u}_\alpha$ and p_α are the densities, fluid velocities and pressures, respectively, of the cooler species. Here q_α (q_β) are the charges of the cool (hot) species and $m = m_\mathrm{e} = m_\mathrm{p}$ is the common mass of the electrons and the positrons. The adiabatic compression indices are denoted by γ_α and the gyrofrequencies by $\Omega_\alpha = q_\alpha B_0/m$.

Linearization of (2)–(7) yields the following dispersion relation for electron–positron plasmas

$$\sum_\alpha \frac{\omega_{\mathrm{p}\alpha}^2 \left(k^2 \hat{\omega}_\alpha^2 - k_\parallel^2 \Omega_\alpha^2\right)}{\hat{\omega}_\alpha^4 - \hat{\omega}_\alpha^2 \left(k^2 v_{\mathrm{T}\alpha}^2 + \Omega_\alpha^2\right) + k_\parallel^2 v_{\mathrm{T}\alpha}^2 \Omega_\alpha^2} = k^2 + \sum_\beta \frac{1}{\lambda_{\mathrm{D}\beta}^2}. \tag{8}$$

We note that this is similar in form to the dispersion relation for linear modes obtained by Verheest et al. (2002) for multi-fluid plasmas.

Here, the plasma frequencies $\omega_{\mathrm{p}\alpha}$, the Debye lengths $\lambda_{\mathrm{D}\beta}$ and thermal velocities $v_{\mathrm{T}\alpha}$ for the species α are defined as $\omega_{\mathrm{p}\alpha}^2 = N_\alpha q_\alpha^2/\varepsilon_0 m$, $\lambda_{\mathrm{D}\beta}^2 = \varepsilon_0 \kappa T_\beta / N_\beta q_\beta^2$ and $v_{\mathrm{T}\alpha}^2 = \gamma_\alpha P_\alpha / N_\alpha m$, respectively. The Doppler-shifted wave frequencies are defined as $\widehat{\omega}_\alpha = \omega - k_\parallel U_\alpha$, where $k_\parallel$ is the component of the wavenumber parallel to the direction of the static magnetic field.

Assuming strongly magnetized particles, and using $\omega^2 \ll (k_\parallel^2/k^2)\Omega^2$, $\omega/k \gg v_{\mathrm{Tc}}$ and $\Omega \gg \omega \gg k v_{\mathrm{Tc}}$, we obtain from the general expression, (8) the appropriate phase velocity for oblique propagation as

$$\frac{\omega}{k} = \frac{k_\parallel}{k} \left[\left(\frac{N_\mathrm{c}}{N_\mathrm{h}}\right)\left(\frac{\kappa T_\mathrm{h}}{m}\right)\right]^{\frac{1}{2}}. \tag{9}$$

This expression is analogous in form to that of the electron-acoustic wave in an unmagnetized electron–ion plasma (Gary and Tokar 1985) with the $(k_\parallel/k)$ factor reflecting the effect of the magnetic field. We note that at parallel propagation the dispersion relation reduces to

$$\sum_\alpha \frac{\omega_{p\alpha}^2}{\hat{\omega}_\alpha^2 - k^2 v_{\mathrm{T}\alpha}^2} = 1 + \sum_\beta \frac{1}{k^2 \lambda_{\mathrm{D}\beta}^2} = 1 + \frac{2}{k^2 \lambda_\mathrm{D}^2}, \tag{10}$$

where $\lambda_\mathrm{D}^2 = \varepsilon_0 \kappa T_\mathrm{h}/N_\mathrm{h} e^2$, which for the unmagnetized form of our two-temperature electron–positron model yields

$$\frac{\omega^2}{k^2} = \frac{2\omega_{\mathrm{pc}}^2 \lambda_{\mathrm{dh}}^2}{2 + k^2 \lambda_{\mathrm{dh}}^2} + \frac{3}{2} v_{\mathrm{Tc}}^2. \tag{11}$$

3. Nonlinear modes

We introduce the stretched co-ordinates,

$$\rho = \epsilon^{\frac{1}{2}}(x - Vt), \quad \eta = \epsilon^{\frac{1}{2}} y, \quad \zeta = \epsilon^{\frac{1}{2}} z, \quad \tau = \epsilon^{\frac{3}{2}} t, \tag{12}$$

and expand the fluid velocity, density, pressure and electrical potential by the small parameter ϵ as

$$\begin{aligned} u_{\alpha x} &= U_{\alpha 0} + \epsilon^{\frac{1}{2}} u_{1\alpha x} + \epsilon u_{2\alpha x} + \epsilon^{\frac{3}{2}} u_{3\alpha x} + \cdots \\ u_{\alpha y} &= \epsilon u_{1\alpha y} + \epsilon^{\frac{3}{2}} u_{2\alpha y} + \epsilon^2 u_{3\alpha y} + \cdots \\ u_{\alpha z} &= \epsilon u_{1\alpha z} + \epsilon^{\frac{3}{2}} u_{2\alpha z} + \epsilon^2 u_{3\alpha z} + \cdots \\ n_\alpha &= N_{\alpha 0} + \epsilon^{\frac{1}{2}} n_{1\alpha} + \epsilon n_{2\alpha} + \epsilon^{\frac{3}{2}} n_{3\alpha} + \cdots \\ p_\alpha &= P_{\alpha 0} + \epsilon^{\frac{1}{2}} p_{1\alpha} + \epsilon p_{2\alpha} + \epsilon^{\frac{3}{2}} p_{3\alpha} + \cdots \\ \phi &= \epsilon^{\frac{1}{2}} \phi_1 + \epsilon \phi_2 + \epsilon^{\frac{3}{2}} \phi_3 + \cdots . \end{aligned} \tag{13}$$

Using (12) and (14) and taking (7) to order $\epsilon^{\frac{1}{2}}$ and (4)–(6) to order ϵ and solving, we obtain

$$n_{1\alpha} = \left(\frac{N_{\alpha 0}^2 q_\alpha}{m N_{\alpha 0} (V - U_{\alpha 0})^2 - \gamma_\alpha P_{\alpha 0}} \right) \phi_1 . \tag{14}$$

Substituting for $n_{1\alpha}$ into (7), we obtain

$$\sum_\alpha \frac{\omega_{\mathrm{p}\alpha}^2}{(V - U_{\alpha 0})^2 - v_{\mathrm{T}\alpha}^2} - \sum_\beta \frac{1}{\lambda_{\mathrm{D}\beta}^2} = 0. \tag{15}$$

The phase velocity V can be determined from the above equation.

Taking (7) to order ϵ and (4)–(6) to order $\epsilon^{\frac{3}{2}}$ and then substituting for $n_{2\alpha}$ into Poisson's equation, we then have

$$\mathscr{D}\phi_2 + B\phi_1^2 = 0 \tag{16}$$

where

$$\mathscr{D} = \sum_\alpha \frac{\omega_{\mathrm{p}\alpha}^2}{\left[(V - U_{\alpha 0})^2 - v_{\mathrm{T}\alpha}^2\right]} - \sum_\beta \frac{1}{\lambda_{\mathrm{D}\beta}^2} \tag{17}$$

and

$$B = \sum_\alpha \frac{\omega_{\mathrm{p}\alpha}^2 q_\alpha \left[3(V - U_{\alpha 0})^2 + (\gamma_\alpha - 2) v_{\mathrm{T}\alpha}^2\right]}{2m\left[(V - U_{\alpha 0})^2 - v_{\mathrm{T}\alpha}^2\right]^3} + \frac{1}{2} \sum_\beta \frac{q_\beta}{\lambda_{\mathrm{D}\beta}^2 \kappa T_\beta}. \tag{18}$$

We note that this expression for B differs slightly from that of Verheest et al. (2002). In fact, having carried out the calculation *ab initio*, we point out that (18) is a correction of the equivalent equation given by Verheest et al. (2002). From (15), $\mathscr{D} = 0$, hence the first term in (16) vanishes, which implies either $B = 0$ or $\phi_1 = 0$. For our electron–positron model, one can easily show that $B = 0$ if the cool electrons and positrons have equal drifts. Then $\phi_1 \neq 0$, which will naturally lead to a mKdV-ZK type of equation for ϕ_1.

Taking Poisson's equation to order $\epsilon^{\frac{3}{2}}$ and the continuity, momentum and pressure equations to order ϵ^2, we obtain the mKdV-ZK equation (Verheest et al. 2002)

$$\frac{\partial \phi_1}{\partial \tau} + a\frac{\partial^3 \phi_1}{\partial \rho^3} + c\ \phi_1^2 \frac{\partial \phi_1}{\partial \rho} + d\frac{\partial}{\partial \rho}\left(\frac{\partial^2 \phi_1}{\partial \eta^2} + \frac{\partial^2 \phi_1}{\partial \zeta^2}\right) = 0. \tag{19}$$

where the coefficients a, c and d are given by

$$a = \frac{1}{A}, \quad c = \frac{C}{A}, \quad d = \frac{D}{A},$$

with

$$A = 2\sum_{\alpha} \frac{\omega_{\mathrm{p}\alpha}^2 (V - U_{\alpha 0})}{\left[(V - U_{\alpha 0})^2 - v_{\mathrm{T}\alpha}^2\right]^2}, \tag{20}$$

$$C = \frac{1}{2}\sum_{\alpha} \frac{\omega_{\mathrm{p}\alpha}^2 q_\alpha^2 \left[15(V - U_{\alpha 0})^4 + E_1 (V - U_{\alpha 0})^2 v_{\mathrm{T}\alpha}^2 + E_2 v_{\mathrm{T}\alpha}^4\right]}{m^2 \left[(V - U_{\alpha 0})^2 - v_{\mathrm{T}\alpha}^2\right]^5} - \frac{1}{2}\sum_{\beta} \frac{q_\beta}{\lambda_{\mathrm{D}\beta}^2 \kappa^2 T_\beta^2}, \tag{21}$$

$$D = 1 + \sum_{\alpha} \frac{\omega_{\mathrm{p}\alpha}^2 (V - U_{\alpha 0})^4}{\Omega_\alpha^2 \left[(V - U_{\alpha 0})^2 - v_{\mathrm{T}\alpha}^2\right]^2}, \tag{22}$$

where

$$E_1 = \gamma_\alpha^2 + 13\gamma_\alpha - 18 \quad \text{and} \quad E_2 = 2\gamma_\alpha^2 - 7\gamma_\alpha + 6.$$

We seek a one-soliton planar solution propagating at an angle θ to the static magnetic field. For stationary nonlinear solutions we have the running phase argument

$$\sigma = \rho\ \cos\theta + \eta\ \sin\theta\cos\psi + \zeta\ \sin\theta\sin\psi - M\tau, \tag{23}$$

where ψ is the second angle in spherical co-ordinates.

Then the mKdV-ZK equation reduces to

$$(c\ \cos\theta\ \phi_1^2 - M)\partial_\sigma \phi_1 + \alpha \partial_\sigma^3 \phi_1 = 0, \tag{24}$$

where $\alpha = (a\ \cos^2\theta + d\ \sin^2\theta)\cos\theta$.

Using the standard technique (Nicholson 1983) to solve (24), we obtain

$$\phi_1 = \sqrt{\frac{6M}{c\cos\theta}}\,\mathrm{sech}(\mu\sigma), \tag{25}$$

where

$$\mu^2 = \frac{M}{(a\cos^2\theta + d\sin^2\theta)\cos\theta}. \tag{26}$$

We normalize the electrostatic potential ϕ, by T_h/e, the fluid speeds u_α by the thermal velocity $v_\mathrm{th} = (T_\mathrm{h}/m)^{1/2}$, the particle density by the equilibrium plasma density N_0, the spatial length by $\lambda_\mathrm{D} = (\varepsilon_0 T_\mathrm{h}/N_\mathrm{h} e^2)^{1/2}$ and the time by $\omega_\mathrm{ph}^{-1} = (N_\mathrm{h} e^2/\varepsilon_0 m)^{-1/2}$.

Using $\widehat{\ }$ to indicate normalized variables, it follows that the normalized electrostatic potential (25) becomes

$$\widehat{\phi} = \phi_m\ \mathrm{sech}(\widehat{\mu}\widehat{\sigma}), \tag{27}$$

where the normalized soliton amplitude is given explicitly by

$$\phi_m = \left[\frac{6(N_c/N_h)^{\frac{7}{2}}[1+(T_c/T_h)(N_c/N_h)^{-1}]^{\frac{1}{2}}\widehat{M}}{[F+E_2(T_c/T_h)^2-(N_c/N_h)^4]\cos\theta}\right]^{\frac{1}{2}}, \tag{28}$$

and

$$\mu^2 = \left[\frac{\widehat{M}}{([(N_c/N_h)+(T_c/T_h)(N_c/N_h)^{-2}]^{-\frac{1}{2}}+(2/\Lambda^2)[N_c/N_h+T_c/T_h]^{\frac{3}{2}}\sin^2\theta)\cos\theta}\right], \tag{29}$$

where

$$F = 15\left(\frac{N_c}{N_h}\right)^2\left[1+\left(\frac{T_c}{T_h}\right)\left(\frac{N_c}{N_h}\right)^{-1}\right]^2$$
$$+E_1\left(\frac{T_c}{T_h}\right)\left(\frac{N_c}{N_h}\right)\left[1+\left(\frac{T_c}{T_h}\right)\left(\frac{N_c}{N_h}\right)^{-1}\right] \quad \text{and} \quad \Lambda^2 = \frac{\Omega^2}{\omega_{ph}^2}.$$

4. Numerical results and limitations

4.1. Limitations of the model

The calculation is based on a reductive perturbation expansion, and thus is valid only for small normalized soliton amplitude, where the 'natural' normalization energy is associated with $T_{eff} = N_0T_cT_h/(N_cT_h + N_hT_c)$. The hot species are assumed to have a Boltzmann distribution, and the cool species behave adiabatically and are governed by the fluid equations. This implies that there are two further limits imposed on our model. For the cool species, we ensure that the thermal velocity is much less than the phase velocity of the fluctuation, i.e. $v_{tc} \ll v_{ph}$, and the Boltzmann assumption requires that the thermal velocity of the hot species is much larger than the phase velocity, i.e. $v_{ph} \ll v_{th}$. Hence, the model can only be applied if $v_{tc} \ll v_{ph} \ll v_{th}$. Using expression (9) for v_{ph}, this becomes

$$\sqrt{\frac{T_c}{T_h}} \ll \frac{k_\parallel}{k}\sqrt{\frac{N_c}{N_h}} \ll 1. \tag{30}$$

This means that upper limits are imposed on both the temperature ratio (T_c/T_h) and the particle density ratio (N_c/N_h).

4.2. Numerical results

In this section we carry out a parameter study of the soliton dependence on plasma variables as some of the features are not transparent from (27)–(29). Figure 1 shows the typical soliton potential profile as a function of the propagation angle θ. For simplicity we set $U_{\alpha 0} = 0$ for all species. For each angle θ, the profile has a maximum at $\sigma = 0$ (as may be seen also from (27)). As θ is increased, the amplitude increases and the half-width decreases, the effect being more significant for larger propagation angles. The former follows from the $1/\sqrt{\cos\theta}$ dependence of (28), the latter from the $1/[(G + H\sin^2\theta)\cos\theta]$ behaviour of (29). Here G and H are functions of the density ratio, the temperature ratio and the gyrofrequency. Figure 2 is a plot of the soliton amplitude as a function of θ. The graph shows

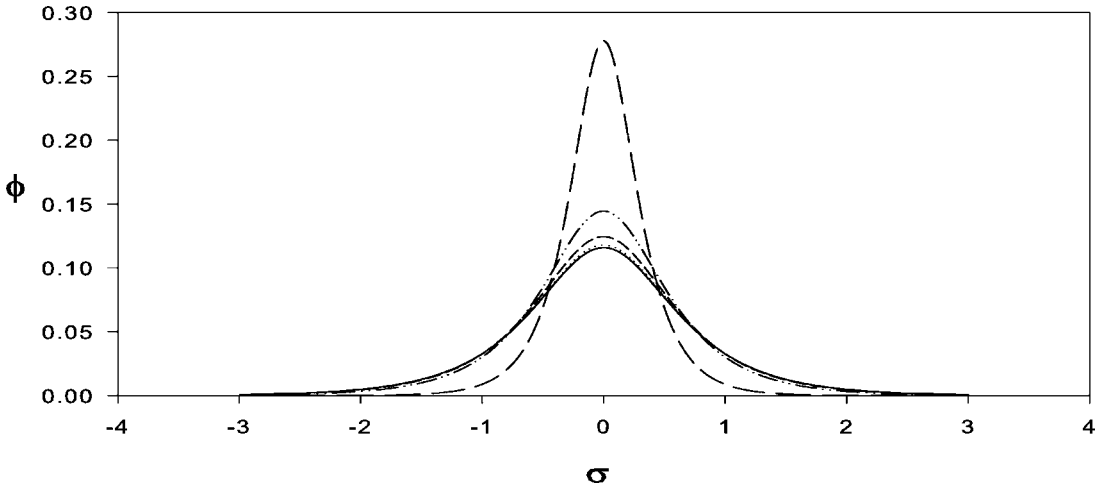

Figure 1. The soliton profile ϕ for different angles of propagation θ. The curves correspond to $\theta = 0^\circ$ (——), 15° (· · · · · ·), 30° (— — —), 50° (–·–) and 80° (– – –). The fixed plasma parameters are the normalized Mach number $M = 1.2$, $T_c/T_h = 0.01$, $N_c/N_h = 1/9$ and $\gamma_\alpha = 3$.

that the soliton amplitude increases monotonically with θ, as may also be deduced from the behaviour observed in Fig. 1. We note that the approximation used in the derivation may restrict validity to $k_\parallel < k_\perp$, which implies that our results are more relevant for larger angles of propagation (small $k_\parallel$). Figure 3 shows the variation of the soliton amplitude with the equilibrium density ratio N_c/N_h, for various temperature ratios T_c/T_h. N_c (N_h) are the equilibrium densities of the cool (hot) electron and positron species. It is seen that as the ratio of the cool to hot equilibrium densities is increased, the soliton amplitude increases. Although a large range of solitons is shown to be possible, the limits imposed by our model demand that $(k_\parallel/k)\sqrt{N_c/N_h} \ll 1$, i.e. $N_c/N_h < 0.25$ for $\theta = 15^\circ$.

This is similar to the results of Verheest et al. (1996), where solitons were found to be possible for low values of the density ratio and are of small amplitude ($\phi_m < 0.2$). For a fixed N_c/N_h, the amplitude ϕ_m is larger for smaller values of the ratio of the cool to hot temperatures. This is clearer in Fig. 4, where it is seen that ϕ_m decreases as the temperature ratio increases for a chosen density ratio. We note that as the temperature ratio decreases, the plasma moves further away from a state of thermodynamic equilibrium, thereby making it easier to generate nonlinear soliton structures with a corresponding larger amplitude.

5. Conclusion

In this paper we have investigated the existence of solitary waves in a magnetized four-component two-temperature electron–positron plasma propagating obliquely to the ambient magnetic field $\mathbf{B}_0$. This model is symmetric with equal equilibrium densities N_h and N_c, and temperatures T_h and T_c, for the hot and cool electrons and positrons respectively. The hot species are described by the Boltzmann density distribution and the cooler species by the fluid equations with finite temperatures.

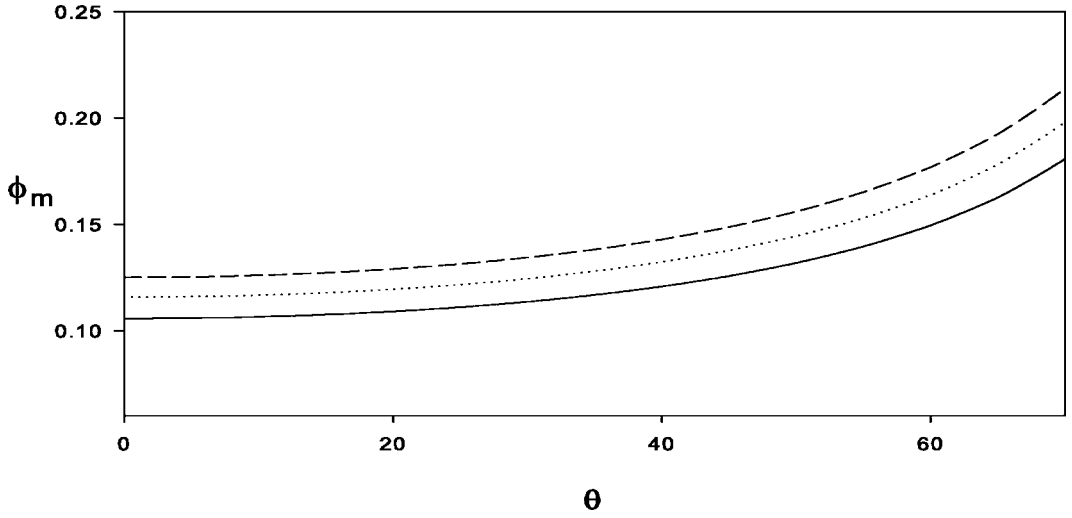

Figure 2. The variation of the soliton amplitude ϕ_m as a function of the propagation angle θ for different normalized Mach numbers $M = 1.0$ (——), 1.2 (· · · · ·) and 1.4 (— — —). The fixed plasma parameters are $N_c/N_h = 1/9$, $T_c/T_h = 0.01$ and $\gamma_\alpha = 3$.

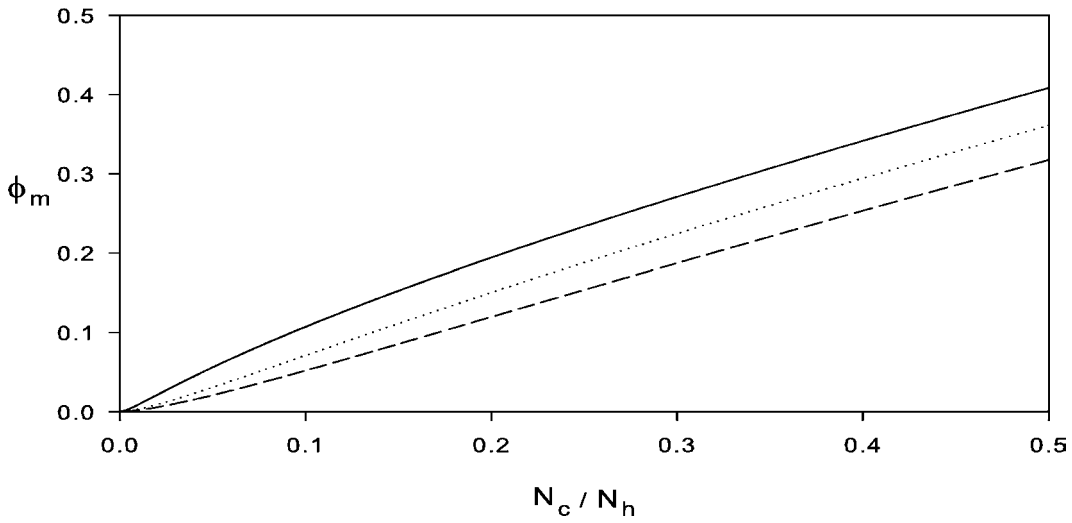

Figure 3. The variation of the soliton amplitude ϕ_m as a function of N_c/N_h. The curves correspond to the temperature ratio $T_c/T_h = 0.01$ (——), 0.05 (· · · · ·) and 0.1 (— — —). The fixed plasma parameters are $M = 1.2$, $\theta = 15^\circ$ and $\gamma_\alpha = 3$.

The reductive perturbation technique was used to derive the mKdV-ZK equation for nonlinear electrostatic modes. An exact analytical solution was determined for the soliton potential structures. Owing to the symmetry of the model, double layers are not possible. Double layers can only be found if there is an asymmetry in the system. Numerical results are presented showing that the soliton amplitudes

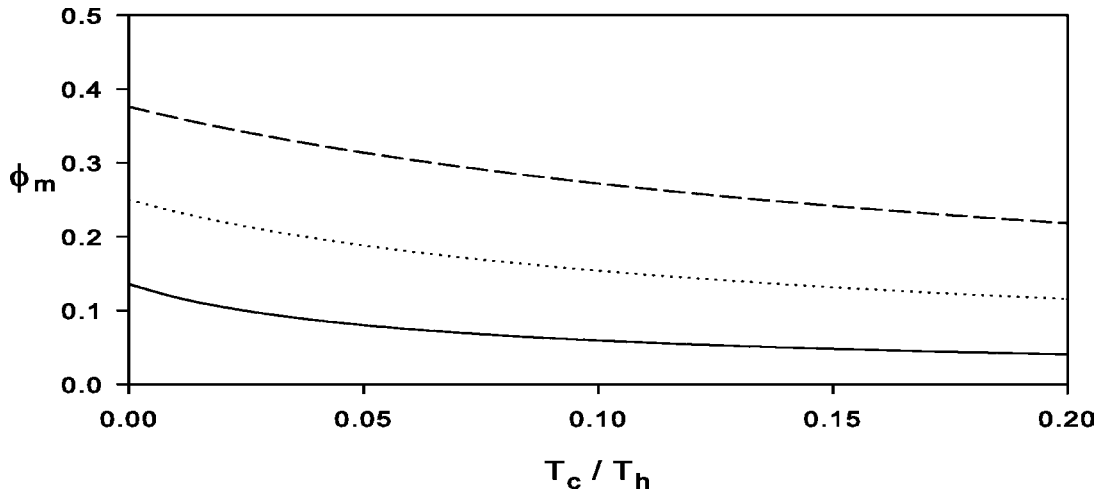

Figure 4. The variation of the soliton amplitude ϕ_m as a function of T_c/T_h. The curves correspond to $N_c/N_h = 0.11$ (——), 0.25 (· · · · · ·) and 0.43 (— — —). The fixed plasma parameters are $M = 1.2$, $\theta = 15^\circ$ and $\gamma_\alpha = 3$.

are functions of plasma parameters such as the propagation angle θ, N_c/N_h and T_c/T_h. Owing to our use of the reductive perturbation approach and the limitations imposed by the model, i.e. $v_{tc} \ll \omega/k \ll v_{th}$, only small-amplitude solitons can be considered. Propagation at larger angles to $\mathbf{B}_0$ are found to enhance the soliton amplitude. As N_c/N_h, the ratio of the cool to hot species, was increased, the soliton amplitude increased. The soliton amplitude also increases as the plasma moves away from a state of thermal equilibrium, i.e. as T_c/T_h is decreased. Given that we have presented a non-relativistic analysis, our results could be of relevance to astrophysical electron–positron plasmas produced through cooling by cyclotron emission, and in laboratory experiments, arising from pair production by ultra-intense laser pulses (Liang et al. 1998) or in beam-generated electron–positron plasmas (Greaves and Surko 1995). Finally, we wish to emphasize the difference between our work and that of Verheest et al. (2002). The latter paper sets up a general formalism, which is in principle applicable to acoustic solitons in a wide variety of multi-species plasmas. Verheest et al. then apply it to a number of examples of Korteweg–de Vries–Zakharov–Kuznetsov cases, but do not consider an electron–positron plasma or discuss examples of mKdV-ZK solitons.

References

[1] Alkofer, R., Hecht, M. B., Roberts, C. D., Schmidt, S. M. and Vinnik, D. V. 2001 *Phys. Rev. Lett.* **87**, 193902.

[2] Beskin, V. S., Gurevich, A. V. and Istomin, Ya. N. 1983 *Sov. Phys.–JETP* **58**, 235.

[3] Bhattacharyya, R., Janaki, M. S. and Dasgupta, B. 2003 *Phys. Lett.* A **315**, 120.

[4] Bharuthram, R. 1992 *Astrophys. Space Sci.* **189**, 213.

[5] Boehmer, H. 1994 *Slow Positron Beam Techniques for Solids and Surfaces (AIP Conf. Proc., 303)* (ed. E. Ottewitte and A. Weiss). New York: American Institute of Physics, p. 442.

[6] Gary, S. P. and Tokar, R. L. 1985 *Phys. Fluids* **28**, 2439.

[7] Gedalin, M. E., Lominadze, J. G., Stenflo, L. and Tsytovich, V. N. 1985 *Astrophys. Space Sci.* **108**, 393.

[8] Goldreich, P. and Julian, W. H. 1969 *Astrophys. J.* **157**, 869.

[9] Greaves, R. G., Tinkle, M. D. and Surko, C. M. 1994 *Phys. Plasmas* **1**, 1439.

[10] Greaves, R. G. and Surko, C. M. 1995 *Phys. Rev. Lett.* **75**, 3846.

[11] Liang, E. P., Wilks, S. C. and Tabak, M. 1998 *Phys. Rev. Lett.* **81**, 4887.

[12] Mahmood, S., Mustaq, A. and Saleem, H. 2003 *New J. Phys.* **5**, 28.

[13] Marklund, M. and Shukla, P. K. 2006 *Rev. Mod. Phys.* **78**, 591.

[14] Michel, F. C. 1982 *Rev. Mod. Phys.* **54**, 1.

[15] Miller, H. R. and Witta, P. J. 1987 *Active Galactic Nuclei*. Berlin: Springer, p. 202.

[16] Misra, A. P. and Chowdhury, A. R. 2003 *Chaos, Solitons and Fractals* **15**, 801.

[17] Nicholson, D. R. 1983 *Introduction to Plasma Theory*. New York: Wiley, p. 173.

[18] Oohara, W., Date, D. and Hatakeyama, R. 2005 *Phys. Rev. Lett.* **95**, 175003.

[19] Pillay, R. and Bharuthram, R. 1992 *Astrophys. Space Sci.* **198**, 85–93.

[20] Piran, T. 2004 *Rev. Mod. Phys.* **76**, 1143.

[21] Popel, S. I., Vladimirov, S. V. and Shukla, P. K. 1995 *Phys. Plasmas* **2**, 716.

[22] Rees, M. J. 1983 *The Very Early Universe* (ed. G. W. Gibbons, S. W. Hawking and S. Siklas). Cambridge: Cambridge University Press.

[23] Remington, B. A. 2005 *Plasma Phys. Control. Fusion* **47**, A191.

[24] Ringwald, A. 2001 *Phys. Lett.* B **510**, 107.

[25] Roberts, C. D., Schmidt, S. M. and Vinnik, D. V. 2002 *Phys. Rev. Lett.* **89**, 153901.

[26] Shukla, P. K. and Yu, M. Y. 1978 *J. Math. Phys.* **19**, 2506.

[27] Stenflo, L., Shukla, P. K. and Yu, M. Y. 1985 *Astrophys. Space Sci.* **117**, 303.

[28] Tandberg, E. H. and Emslie, A. G. 1988 *The Physics of Solar Flares*. Cambridge: Cambridge University Press, p. 124.

[29] Verheest, F., Hellberg, M. A., Gray, G. J. and Mace, R. L. 1996 *Astrophys. Space Sci.* **239**, 125.

[30] Verheest, F., Mace, R. L., Pillay, S. R. and Hellberg, M. A. 2002 *J. Phys. A: Math. Gen.* **35**, 795.

[31] Wilks, S. C., Chen, H., Liang, E., Patel, P., Price, D., Remington, B., Shepherd, R., Tabak, M. and Kruer, W. L. 2005 *Astrophys. Space Sci.* **298**, 347.

[32] Yu, M. Y., Shukla, P. K. and Stenflo, L. 1986 *Astrophys. J.* **309**, L63.

Appendix F

COMPUTER PROGRAMS

```
C      ROOTFINDER.FOR     FIND POSITIVE ROOTS OF FOURTH ORDER POLYNOMIAL
C      FOR VARIOUS PARAMETERS - ANGLES,DENSITIES, TEMPERATURE RATIO THTC.
C      R=W/WP, KLAMDA=K*LAMDA, TCTH=TC/TH
C      N0C=N0C/N0, N0H=N0H/N0 (N0=N0C+N0H UNNORMALIZED DENSITY)
C      W NORMALIZED BY : LAMDA_D2 = Th/4PI N0 E2

       PROGRAM ROOTFINDER
       IMPLICIT NONE
       INTEGER I
       REAL*8 A,B,C,P1,P2,ROOT1,ROOT2,N0C,N0H,TCTH
       REAL*8 R,R2,THETA,KLAMDA,KLAMDA2
       REAL*8 N1,N2,N3,NUM,DEN,PI,S,ANG
*****************************************************************
C       INITIAL VALUES
*****************************************************************
       PI=3.1415927D0
       N0C=0.5D0
       N0H=1.0D0-N0C
       TCTH=0.001D0
       R=0.333D0

       THETA=(60.0d0/180.0d0)*pi

       R2=R**2
       KLAMDA=0.0D0

       OPEN(25,FILE='ROOT1.DAT')
       OPEN(26,FILE='ROOT2.DAT')
c*****************************************************************
        DO I=1,301
         KLAMDA2=KLAMDA*KLAMDA
         NUM=KLAMDA2*N0C/N0H
         DEN=1.0D0+(0.5D0*KLAMDA2)/N0H
         A=1.0D0
         B=-(1.0D0/R2+3.0D0*KLAMDA2*TCTH+NUM/DEN)
         C=((COS(THETA)**2)/R2)*(3.0D0*KLAMDA2*TCTH+NUM/DEN)
         P1=(-B+SQRT(B**2-4.0D0*A*C))/(2.0D0*A)
         P2=(-B-SQRT(B**2-4.0D0*A*C))/(2.0D0*A)
         ROOT1=SQRT(P1)
         ROOT2=SQRT(P2)
         write(6,*) KLAMDA,ROOT2
         write(25,*) KLAMDA,ROOT1
         write(26,*) KLAMDA,ROOT2
         KLAMDA=KLAMDA+0.1D0

       ENDDO

       END
```

```
theta = 0.0 Degree;
TCTH = 0.01;
V0H = 0.5;
V0C = 0.0;
N0C = 0.1;
R = 0.333;
N0H = 1 - N0C;
KZ = K Cos[theta];
KZ2 = KZ KZ;
KZ3 = KZ2 KZ;
K2 = K K;
KPERP = K Sin[theta];
KPERP2 = KPERP KPERP;
ALPHAH = KPERP2 R2;
ALPHAC = KPERP2 TCTH R2;
ZPH = (ω - KZ V0H - (P / R)) / (√2 KZ);
ZPC = (ω - KZ V0C - (P / R)) / (√2 KZ √TCTH);
Z0C2 = (((N0C / TCTH)) / ( 2.0 N0H + K2) + 1.5);

stream = OpenWrite["e:/ian/Kinetic Disp/kineticgraphs/kparr/approxRealKZ.dat",
   FormatType → OutputForm];
stmp = OpenWrite["e:/ian/Kinetic Disp/kineticgraphs/kparr/approxGammaKZ.dat",
   FormatType → OutputForm];
OutputStream["c:/ian/Kinectic Disp/approxRealO2.dat", 119];
OutputStream["c:/ian/Kinectic Disp/approxGammaO2.dat", 120];

Do[
  KZ = K Cos[theta];
  W = Sqrt[ 2.0 N0C KZ2 / (2.0 N0H + K2) + 3.0 KZ2 TCTH];
  G = ( W^4 Sqrt[π / 8] / (KZ3 (1 + (6.0 KZ2 TCTH) / (W^2))) )
     ( ( ( -1.0 ( 1.0 / TCTH) )^(3.0 / 2.0) ) Exp[-1.0 Z0C2] + ( N0H / N0C) ( KZ V0H / W - 1.0)
        (Sum[BesselI[0, KPERP^2 R^2] Exp[-KPERP^2 R^2], {P, 0, 0} ]) );
  Print[K, " ", W, " ", G];
  Write[stream, K, "     ", W];
  Write[stmp, K, "     ", G],
  {K, 0.01, 5.0, 0.01}];
Close[stream]
Close[stmp]

datare = Import["e:/ian/Kinetic Disp/kineticgraphs/kparr/approxRealKZ.dat", "List"];
datarep = Partition[datare, 2]
datare1 = Import["e:/ian/Kinetic Disp/kineticgraphs/kparr/approxGammaKZ.dat", "List"];
datarep1 = Partition[datare1, 2]
ListPlot[datarep, PlotJoined → True]
ListPlot[datarep1, PlotJoined → True]
```

```
ZFUN[ζ_] := i √π Exp[-ζ^2] (1 + Erf[i ζ]);
TCTH = 0.001;
V0C = 0.0;
V0H = 0.5;
R = 0.333;
R2 = R R;
theta = 45.0 Degree;
N0C = 0.1;
N0H = 1.0 - N0C;
KPERP = k Sin[theta];
KPERP2 = KPERP KPERP;
kz = k Cos[theta];
ALPHAH = KPERP2 R2;
ALPHAC = KPERP2 TCTH R2;
ZPH = (ω - kz V0H - (P / R)) / (√2 kz);
ZPC = (ω - kz V0C - (P / R)) / (√2 kz √TCTH);
rootguess = 0.0033 + 0.00033 I;

stream = OpenWrite["e:/ian/Kinetic Disp/kineticgraphs/kparr/GdrRealnewkz45DEG.dat",
  FormatType → OutputForm]
stmp = OpenWrite["e:/ian/Kinetic Disp/kineticgraphs/kparr/GdrGammanewkz45DEG.dat",
  FormatType → OutputForm]

Do[DD[k_, ω_] := k^2 + (2.0 N0C / TCTH)
    (1.0 + ((ω - kz V0C) / (√2.0 kz √TCTH)) (Sum[BesselI[P, KPERP^2 TCTH R^2] Exp[
          -KPERP^2 TCTH R^2] ZFUN[(ω - kz V0C - (P / R)) / (√2 kz √TCTH)], {P, -5, 5}]))
   + (2.0 N0H) (1.0 + ((ω - kz V0H) / (√2.0 kz)) (Sum[BesselI[P, KPERP^2 R^2]
        Exp[-KPERP^2 R^2] ZFUN[(ω - kz V0H - (P / R)) / (√2 kz)], {P, -5, 5}]));
 roott = ω /. FindRoot[DD[k, ω] == 0, {ω, rootguess}, MaxIterations → 250,
    AccuracyGoal → 5, WorkingPrecision → 10];
 omegaa = NumberForm[Re[roott], ExponentFunction → (If[-90 < # < 90, Null, #] &)];
 gamman = NumberForm[Im[roott], ExponentFunction -> (If[-90 < # < 90, Null, #] &)];
 rootguess = roott;
 Print[k, "   ", omegaa, "   ", gamman];
 Write[stream, k, "   ", omegaa];
 Write[stmp, k, "   ", gamman],
 {k, 0.01, 5.0, 0.01}]
Close[stream]
Close[stmp]
datare = Import[
   "c:/ian/Kinetic Disp/kineticgraphs/dentcth/GdrRealnoc0.05tcth=0.01.dat", "List"];
dataim = Import["c:/ian/Kinetic Disp/kineticgraphs/dentcth/
     GdrGammanoc0.05tcth=0.01.dat", "List"];
datarep = Partition[datare, 2];
dataimp = Partition[dataim, 2];
ListPlot[datarep, PlotJoined → True]
ListPlot[dataimp, PlotJoined → True]
```

```
      PROGRAM PHIvsSIGMA
        IMPLICIT NONE
        INTEGER i
        REAL*8 A1,A2,B1,B2,M,NCNH,TCTH,OM,D1,D2,D3,D4
        REAL*8 TH,PHI,DEN,NUM,AMP,MU,ANGLE,S,C,X
C     **********PARAMETERS**********
      B1=30.0d0
      B2=3.0d0
      M=1.2d0
      OM=1.0d0
      TCTH=0.01d0
      NCNH=0.1d0/0.9d0
      A1=SQRT(NCNH)
      A2=SQRT(1.0d0+TCTH/NCNH)
      TH=80.0d0
c
c     ****************************
c
      open(25,file="C:\PHD\DATA\PvsSIG\80DEM1.2.dat",status="unknown")
      do i=1,600
        X=-3.0d0+i*0.01d0
        D1=15.0d0*(A1**4)*(A2**4)+B1*TCTH*(A1**2)*(A2**2)+B2*(TCTH**2)
        D2=A1**8
        NUM=6.0d0*M*(A1**7)*A2
        DEN=(D1-D2)*COS(TH*3.141592654/180)
        AMP=sqrt(NUM/DEN)
        D3=(A1/A2)+(2/(OM)**2)*(A1**3)*(A2**3)*(SIN(TH*3.14159/180)**2)
        D4= COS(TH*3.141592654/180)
        MU=(M/(D3*D4))
        PHI=AMP*(1/COSH(((MU)**0.5)*X))
      write(25,*) X,PHI
      enddo
        endfile(25)
        close(25)
        end
```

```
      PROGRAM PHIMvsNc
C     PROGRAM FOR THE MAXIMUM SOLITON AMPLITUDE AS A FUNCTION OF THE
C     DENSITY ROTIO NC/NH FOR VARIOUS TEMPERATURE RATIOS TC/TH
        IMPLICIT NONE
        INTEGER i
        REAL*8 A1,A2,B1,B2,M,TCTH,OM,D1,D2
        REAL*8 TH,DEN,NUM,AMP,NH,NC,NCNH
C     **********PARAMETERS**********
      B1=30.0d0
      B2=3.0d0
      M=1.2d0
      OM=1.0d0
      TCTH=0.1d0
      TH=15.0d0
c
c     ****************************
c
      open(25,file="C:\PHD\DATA\NCNH\t1T15M12.dat",status="unknown")
      do i=1,700
        NC=i*0.001d0
        NH=1-NC
        NCNH=NC/NH
        A1=SQRT(NC/NH)
        A2=SQRT(1.0d0+TCTH/(NC/NH))
        D1=15.0d0*(A1**4)*(A2**4)+B1*TCTH*(A1**2)*(A2**2)+B2*(TCTH**2)
        D2=A1**8
        NUM=6.0d0*M*(A1**7)*A2
        DEN=(D1-D2)*COS(TH*3.141592654/180)
        AMP=sqrt(NUM/DEN)

      write(25,*) NC,AMP

      enddo
        endfile(25)
        close(25)
        end
```

```
      PROGRAM PHIMvsTCTH
C     PROGRAM FOR THE MAXIMUM SOLITON AMPLITUDE AS A FUNCTION OF THE
C     TEMPERATURE RATIO FOR VARIOUS DENSITY RATIOS NC/NH
        IMPLICIT NONE
        INTEGER i
        REAL*8 A1,A2,B1,B2,M,TCTH,OM,D1,D2
        REAL*8 TH,DEN,NUM,AMP,NCNH
C     **********PARAMETERS**********
      B1=30.0d0
      B2=3.0d0
      M=1.4d0
      OM=1.0d0
      TCTH=0.0001d0
      NCNH=0.3d0/0.7d0
      TH=15.0d0
c
c     ****************************
c
      open(25,file="C:\ian\DATA\TCTH\tcN37T15M12.dat",status="unknown")
      do i=0,100
        TCTH=i*0.01
        A1=SQRT(NCNH)
        A2=SQRT(1.0d0+TCTH/(NCNH))
        D1=15.0d0*(A1**4)*(A2**4)+B1*TCTH*(A1**2)*(A2**2)+B2*(TCTH**2)
        D2=A1**8
        NUM=6.0d0*M*(A1**7)*A2
        DEN=(D1-D2)*COS(TH*3.141592654/180)
        AMP=sqrt(NUM/DEN)

      write(25,*) TCTH,AMP

      enddo
        endfile(25)
        close(25)
        end
```

```
        PROGRAM MODEL1
c       PROGRAM MAIN4.FOR: Boltzmann electrons and positrons and cool fluid
c               electrons and positrons (-E).Using cosh,sinh
        IMPLICIT NONE
        external derivs
        external rk4
        INTEGER i,n,NMAX
        REAL*8 h,x,dydx(8),y(8),yout(8),M,theta,E0,M2
        REAL*8 delta,MST,MCT,R,NONEC,NONPC,INVMMD2
        REAL*8 pi,ST,CT,MMD,NONEC2,NONPC2,INVNONEC2,INVNONPC2
        REAL*8 MMD2,INVMMD,INVNONEC,INVNONPC,necn,npcn
        REAL*8 INVNONPC3,NONEC3,NONEC4,NONPC4,NOHNO
        REAL*8 TERMA,TERMB,TERMC,TERMD,TERME,TERMF
        REAL*8 TERMG,TERMH,TERMI,TERMJ,TERMK,TERML
        REAL*8 TERMM,TERMN,A1,A2,TERMBB,nphno,nehno,necno,npcno
        common /plasma/M,theta,R,delta,necno,npcno,nehno,nphno
        pi=3.1415927d0
        h=0.015d0
        n=8
        x=0.0d0
c     **********PARAMETERS**********
        M=1.6d0
        delta=0.02d0
        theta=(2.0d0/180.0d0)*pi
        E0=0.8d0
        R=160.0d0
        necno=0.73d0
        npcno=necno
        nehno=1.0d0-necno
        nphno=nehno
c     ****************************
c     psi=y(1)
c     E=y(2)
c     necn=y(3)
c     vecyn=y(4)
c     veczn=y(5)
c     npcn=y(6)
c     vpcyn=y(7)
c     vpczn=y(8)
c************************************************
       MMD=(M-delta)
       MMD2=MMD**2
       INVMMD=1.0d0/MMD
       INVMMD2=1.0d0/MMD2
       nonec=1.0d0/necno
       nonpc=1.0d0/npcno
       NONEC2=NONEC**2
       NONPC2=NONPC**2
       NONEC3=NONEC*NONEC2
       NONEC4=NONEC2*NONEC2
       NONPC4=NONPC2*NONPC2
       INVNONEC=(1.0d0/NONEC)
       INVNONPC=(1.0d0/NONPC)
       INVNONEC2=INVNONEC**2
       INVNONPC2=INVNONPC**2
       INVNONPC3=INVNONPC*INVNONPC2
```

```
        ST=sin(theta)
        CT=cos(theta)
        MST=M*ST
        MCT=M*CT

        y(1)=0.0d0

        y(2)=E0

        y(3)=necno

        y(4)=0.01d0

        y(5)=0.01d0

        y(6)=npcno


        TERMA=(INVNONPC2*NONEC2*(y(3))**3)/((y(6))**3)
        TERMB=y(2)+MST*y(4)
        TERMBB=((nehno+nphno)*INVNONPC2*MMD2*(y(2)))/((y(6))**3)

        y(7)=(-y(2)+TERMBB-(TERMA*TERMB))/MST

        TERMC=(3.0d0*INVNONPC3)/(M*M*ST*CT*MMD)
        TERMD=(y(2)+MST*y(4))**2
        TERME=(((NONEC4*((y(3))**5))/((y(6))**4)))*TERMD
        TERMF=(-y(2)-MST*y(7))**2
        TERMG=NONPC4*y(6)*TERMF
        TERMH=TERMC*(TERME-TERMG)
        TERMI=-1.0d0*(MST/CT)+(MMD*INVNONEC*ST)/(CT*y(3))+y(5)
        TERMJ=(((INVNONPC3*NONEC3*((y(3))**4))/((y(6))**4)))*TERMI
        TERMK=MST/CT-(MMD*INVNONPC*ST)/(CT*y(6))
        TERML=(INVNONPC3*MMD2*MMD)/(M2*ST*CT*(y(6)**4))
        TERMM=TERML*(NPHNO-NEHNO)*y(2)*y(2)

        y(8)=TERMH+TERMJ+TERMK-TERMM

c     Let's loop here

        open(25,file="ian1.dat",status="unknown")
        write(25,*) x,-y(2)/M
        write(6,*) x,-y(2)/M
          do i=1,6000
          call derivs(x,y,dydx)
          call rk4(y,dydx,n,x,h,yout,derivs)
          y(1)=yout(1)
          y(2)=yout(2)
          y(3)=yout(3)
          y(4)=yout(4)
          y(5)=yout(5)
          y(6)=yout(6)
          y(7)=yout(7)
          y(8)=yout(8)
          x=x+h
          write(25,*) x,-yout(2)/M
          write(6,*) x,-y(2)/M
```

```
          enddo
        endfile(25)
        close(25)
        end


        SUBROUTINE derivs(x,y,dydx)
c       Subroutine expressing the differential equations for Model 1 with -E
        IMPLICIT NONE
        REAL*8 x,dydx(8),y(8),theta,M,R
        REAL*8 ST,CT,MST,MCT,NONEC,NONPC,A1,A2
        REAL*8 R2,M2,MMD,MMD2,NONEC2,NONPC2,NOHNO
        REAL*8 INVMMD,INVMMD2,INVNONEC,INVNONPC,TERM1,TERM2
        REAL*8 delta,necn3,npcn3,nphno,nehno,necno,npcno
        REAL*8 N1,N2,N3,N4,N5,N6,LIM
        common /plasma/M,theta,R,delta,necno,npcno,nehno,nphno
c        x=x
c     psi=y(1)
c     E=y(2)
c     necn=y(3)
c     vecyn=y(4)
c     veczn=y(5)
c     npcn=y(6)
c     vpcyn=y(7)
c     vpczn=y(8)

        A1=nphno*(cosh(y(1))-sinh(y(1)))
        A2=nehno*(cosh(y(1))+sinh(y(1)))
        R2=R**2
        M2=M**2
        ST=sin(theta)
        CT=cos(theta)
        MST=M*ST
        MCT=M*CT
        MMD=M-delta
        MMD2=MMD**2
        nonec=1.0d0/necno
        nonpc=1.0d0/npcno
        NONEC2=NONEC**2
        NONPC2=NONPC**2
        INVNONEC=(1.0d0/NONEC)
        INVNONPC=(1.0d0/NONPC)
        INVMMD=(1.0d0/MMD)
        INVMMD2=INVMMD**2
        TERM1=(M-(MMD*INVNONEC)/(y(3)))
        TERM2=(M-(MMD*INVNONPC)/(y(6)))
        necn3=y(3)**3
        npcn3=y(6)**3
        N1=NONEC2*INVMMD2
        N2=INVMMD*M*NONEC
        N3=INVMMD*MCT*NONEC
        N4=NONPC2*INVMMD2
        N5=INVMMD*M*NONPC
        N6=INVMMD*MCT*NONPC

c     ******************** Runge-Kutte form ******************
        dydx(1)=-1.0d0*y(2)
```

```
  dydx(2)=R2*M2*(y(6)-y(3)+A1-A2)

  dydx(3)=necn3*N1*(y(2)+MST*y(4))

  dydx(4)=y(3)*N2*(-1.0d0*ST*TERM1+CT*y(5))

  dydx(5)=-y(3)*N3*y(4)

  dydx(6)=npcn3*N4*(-y(2)-MST*y(7))

  dydx(7)=y(6)*N5*(ST*TERM2-CT*y(8))

  dydx(8)=y(6)*N6*y(7)

  END

SUBROUTINE rk4(y,dydx,n,x,h,yout,derivs)
  IMPLICIT NONE
  INTEGER n,NMAX
  REAL*8 h,x,dydx(n),y(n),yout(n)
  EXTERNAL derivs
  PARAMETER (NMAX=50)
  INTEGER i
  REAL*8 h6,hh,xh,dym(NMAX),yt(NMAX),dyt(NMAX)
  hh=h*0.5d0
  h6=h/6.0d0
  xh=x+hh
  do i=1,n
    yt(i)=y(i)+hh*dydx(i)
enddo
  call derivs(xh,yt,dyt)
  do i=1,n
     yt(i)=y(i)+hh*dyt(i)
enddo
  call derivs(xh,yt,dym)
  do i=1,n
    yt(i)=y(i)+h*dym(i)
    dym(i)=dyt(i)+dym(i)
enddo
  call derivs(x+h,yt,dyt)
  do i=1,n
      yout(i)=y(i)+h6*(dydx(i)+dyt(i)+2.0d0*dym(i))
enddo
  return
  END
```

```
        PROGRAM MODEL2andMODEL3
c       PROGRAM FullDynamics5.for. Cool electrons and positrons and Hot
c       electrons and positrons - All Fluid. d(psi)/d(s)=-E.
        IMPLICIT NONE
        external derivs
        external rk4
        INTEGER i,n,NMAX
        REAL*8 h,x,dydx(18),y(18),yout(18),M,M2,theta,E0,TCTH
        REAL*8 deltaC,deltaH,MST,MCT,R,NONEC,NONPC,NONEH,NONPH
        REAL*8 pi,ST,CT,MMDC,MMDH,NONEC2,NONPC2,NONEH2,NONPH2
        REAL*8 NECNO2,NPCNO2,NEHNO2,NPHNO2,MMDC2,MMDH2,NECN,NPCN
        REAL*8 NONEC3,NONEC4,NONPC4,NOHNO,INVMMDC,INVMMDH
        REAL*8 INVMMDC2,INVMMDH2,TERMZ1,TERMZ2,TERMZ21,TERMZ22
        REAL*8 DF1F2,DF3F4,DF5F6,DF7F8,DF1,DF2,DF3,DF4,DF5,DF6
        REAL*8 DF7,DF8,DF11,DF121,DF122,  DF71,DF721,DF722,DF51
        REAL*8 DF521,DF522,nphno,nehno,necno,npcno
        REAL*8 F1,F2,F3,F4,F5,F6,F7,F8
        common /pl/M,theta,R,deltaC,deltaH,necno,npcno,nehno,nphno,TCTH
        pi=3.1415927d0
        h=0.15D0
        n=18
        x=0.0d0
c     **********PARAMETERS**********
        M=3.5d0
        deltaC=0.0d0
        deltaH=0.0d0
        TCTH=0.0d0
        theta=(2.0d0/180.0d0)*pi
        E0=3.0d0
        R=10.0d0
        necno=0.5d0
        npcno=necno
        nehno=1.00d0-necno
        nphno=nehno
c     ****************************
c     psi=y(1)
c     E=-y(2)
C     COLD ELECTRONS
c     necn=y(3)
c     vecyn=y(4)
c     veczn=y(5)
c     pecn=y(6)
c     COLD POSITRONS
c     npcn=y(7)
c     vpcyn=y(8)
c     vpczn=y(9)
c     ppcn=y(10)
C     HOT POSITRONS
c     pphn=y(11)
c     nphn=y(12)
c     vphyn=y(13)
c     vphzn=y(14)
c     HOT ELECTRONS
c     pehn=y(15)
c     nehn=y(16)
c     vehyn=y(17)
c     vehzn=y(18)
```

```
c************************************************
       MMDC=(M-deltaC)
       MMDH=(M-deltaH)
       MMDC2=MMDC**2
       MMDH2=MMDH**2
       INVMMDC=1.0d0/MMDC
       INVMMDH=1.0d0/MMDH
       INVMMDC2=1.0d0/MMDC2
       INVMMDH2=1.0d0/MMDH2
       NONEC=1.0d0/NECNO
       NONPC=1.0d0/NPCNO
       NONEH=1.0d0/NEHNO
       NONPH=1.0d0/NPHNO
       NONEC2=NONEC**2
       NONPC2=NONPC**2
       NONEC3=NONEC*NONEC2
       NONEC4=NONEC2*NONEC2
       NONPC4=NONPC2*NONPC2
       NECNO2=NECNO**2
       NPCNO2=NPCNO**2
       NEHNO2=NEHNO**2
       NPHNO2=NPHNO**2
       M2=M*M
       ST=dsin(theta)
       CT=dcos(theta)
       MST=M*ST
       MCT=M*CT
c
        y(1)=0.0d0
        y(2)=E0
        y(3)=necno
        y(4)=0.01d0
        y(5)=0.01d0
        y(6)=necno*TCTH
        y(7)=npcno
        y(8)=0.01d0
        y(9)=0.01d0
        y(10)=npcno*TCTH
        y(11)=nphno
        y(12)=nphno
        y(13)=0.01d0
        y(14)=0.01d0
        y(15)=nehno
        y(16)=nehno

        F1=(y(3)**3)*(y(2)+MST*y(4))
        F2=NECNO2*MMDC2-3.0d0*TCTH*y(6)*y(3)
        F3=y(16)**3
        F4=NEHNO2*MMDH2-3.0d0*y(15)*y(16)
        F5=(y(7)**3)*(-y(2)-MST*y(8))
        F6=NPCNO2*MMDC2-3.0d0*TCTH*y(10)*y(7)
        F7=(y(12)**3)*(-y(2)-MST*y(13))
        F8=NPHNO2*MMDH2-3.0D0*y(11)*y(12)
 c
        y(17)=(-y(2)+(F5/F6+F7/F8-F1/F2)*(F4/F3))/MST
 c
        DF11=3.0d0*(y(3)**5)*((y(2)+MST*y(4))**2)/F2
```

```
        DF121=(M2*ST*(y(3)**4)*NONEC)/MMDC
        DF122=(-M+(MMDC*NECNO)/y(3))*ST+y(5)*CT
        DF1=DF11+DF121*DF122
        DF2=-12.0d0*TCTH*y(6)*F1/F2
        DF1F2=(F2*DF1-F1*DF2)/(F2**2)
        DF71=3.0d0*(y(12)**5)*((-y(2)-MST*y(13))**2)/F8
        DF721=(M2*ST*(y(12)**4)*NONPH)/MMDH
        DF722=(M-(MMDH*NPHNO)/y(12))*ST-y(14)*CT
        DF7=DF71-DF721*DF722
        DF8=-12.0d0*y(11)*F7/F8
        DF7F8=(F8*DF7-F7*DF8)/(F8**2)
        DF51=(3.0D0*y(7)**5)*((-y(2)-MST*y(8))**2)/F6
        DF521=(M2*ST*(y(7)**4)*NONPC)/MMDC
        DF522=(M-(MMDC*NPCNO)/y(7))*ST-y(9)*CT
        DF5=DF51-DF521*DF522
        DF6=-12.0d0*TCTH*y(10)*F5/F6
        DF5F6=(F6*DF5-F5*DF6)/(F6**2)
        DF3=(3.0d0*y(16)**5)*(y(2)+MST*y(17))/F4
        DF4=(-12.0d0*y(15)*F3*(y(2)+MST*y(17)))/F4
        DF3F4=(F4*DF3-F3*DF4)/(F4**2)
C
        TERMZ1=(M-(MMDH*NEHNO)/y(16))*(ST/CT)
        TERMZ21=(F4*NEHNO*MMDH)/(F3*M2*ST*CT*y(16))
        TERMZ22=y(2)+MST*y(17)
        TERMZ2=TERMZ21*(DF5F6+DF7F8-DF1F2-TERMZ22*DF3F4)
c
        y(18)=TERMZ1+TERMZ2
c
c     Let's loop here
c
       open(25,file="c:\ian\GRAPHS\ANG\TANG=35.dat",status="unknown")
        write(25,*) x,-y(2)/M
        write(6,*) x,-y(2)/M
          do i=1,1200
          call derivs(x,y,dydx)
          call rk4(y,dydx,n,x,h,yout,derivs)
          y(1)=yout(1)
          y(2)=yout(2)
          y(3)=yout(3)
          y(4)=yout(4)
          y(5)=yout(5)
          y(6)=yout(6)
          y(7)=yout(7)
          y(8)=yout(8)
          y(9)=yout(9)
          y(10)=yout(10)
          y(11)=yout(11)
          y(12)=yout(12)
          y(13)=yout(13)
          y(14)=yout(14)
          y(15)=yout(15)
          y(16)=yout(16)
          y(17)=yout(17)
          y(18)=yout(18)
          x=x+h
          write(25,*) x,-yout(2)/M
          write(6,*) x,-y(2)/M
```

```
          enddo
        endfile(25)
        close(25)
        end
C*************************************************************************
        SUBROUTINE derivs(x,y,dydx)
c       Subroutine expressing the differential equations for Model 2 with +E
        IMPLICIT NONE
        REAL*8 x,dydx(18),y(18),theta,M,R,R2,M2
        REAL*8 ST,CT,MST,MCT,NONEC,NONPC,NONEH,NONPH
        REAL*8 NONEC2,NONPC2,NECNO2,NPCNO2,NEHNO2,NPHNO2
        REAL*8 NONEH2,NONPH2,MMDC,MMDH,MMDC2,MMDH2
        REAL*8 INVMMDC,INVMMDH,INVMMDC2,INVMMDH2
        REAL*8 TERM1,TERM2,TERM3,TERM4
        REAL*8 deltaC,deltaH,necn3,npcn3,nphno,nehno,necno,npcno
        REAL*8 N1,N2,N3,N4,N5,N6,N7,N8,F1,F2,F3,F4,F5,F6,F7,F8,TCTH
       common /pl/M,theta,R,deltaC,deltaH,necno,npcno,nehno,nphno,TCTH
c         x=x
C*************************************************************************
c     psi=y(1)
c     E=y(2)
c     necn=y(3)
c     vecyn=y(4)
c     veczn=y(5)
c     pecn=y(6)
c     npcn=y(7)
c     vpcyn=y(8)
c     vpczn=y(9)
c     ppcn=y(10)
C     HOT POSITRONS
c     pphn=y(11)
c     nphn=y(12)
c     vphyn=y(13)
c     vphzn=y(14)
c     HOT ELECTRONS
c     pehn=y(15)
c     nehn=y(16)
c     vehyn=y(17)
C*************************************************************************
        R2=R**2
        M2=M**2
        ST=dsin(theta)
        CT=dcos(theta)
        MST=M*ST
        MCT=M*CT
        MMDC=M-deltaC
        MMDH=M-deltaH
        MMDC2=MMDC**2
        MMDH2=MMDH**2
        NONEC=1.0d0/NECNO
        NONPC=1.0d0/NPCNO
        NONEH=1.0d0/NEHNO
        NONPH=1.0d0/NPHNO
        NONEC2=NONEC**2
        NONPC2=NONPC**2
        NONEH2=NONEH**2
        NONPH2=NONPH**2
```

```
        NECNO2=NECNO**2
        NPCNO2=NPCNO**2
        NEHNO2=NEHNO**2
        NPHNO2=NPHNO**2
        INVMMDC=(1.0d0/MMDC)
        INVMMDC2=INVMMDC**2
        INVMMDH=(1.0d0/MMDH)
        INVMMDH2=INVMMDH**2
C
        TERM1=M-((MMDC*NECNO)/(y(3)))
        TERM2=M-((MMDH*NEHNO)/(y(16)))
        TERM3=M-((MMDC*NPCNO)/(y(7)))
        TERM4=M-((MMDH*NPHNO)/(y(12)))
C
        F1=(y(3)**3)*(y(2)+MST*y(4))
        F2=NECNO2*MMDC2-3.0d0*TCTH*y(6)*y(3)
        F3=(y(16)**3)
        F4=NEHNO2*MMDH2-3.0d0*y(15)*y(16)
        F5=(y(7)**3)*(-y(2)-MST*y(8))
        F6=NPCNO2*MMDC2-3.0d0*TCTH*y(10)*y(7)
        F7=(y(12)**3)*(-y(2)-MST*y(13))
        F8=NPHNO2*MMDH2-3.0d0*y(11)*y(12)
        N1=INVMMDC*M*NONEC
        N2=INVMMDC*MCT*NONEC
        N3=INVMMDH*M*NONEH
        N4=INVMMDH*MCT*NONEH
        N5=INVMMDC*M*NONPC
        N6=INVMMDC*MCT*NONPC
        N7=INVMMDH*M*NONPH
        N8=INVMMDH*MCT*NONPH
C
c     ******************** Runge-Kutte form ******************
        dydx(1)=-y(2)

        dydx(2)=1.0d0*R2*M2*(y(7)-y(3)+y(12)-y(16))

C     Cold Electrons (necn,vecyn,veczn,pecn)

        dydx(3)=(F1/F2)

        dydx(4)=y(3)*N1*(-ST*TERM1+CT*y(5))

        dydx(5)=-y(3)*N2*y(4)

        dydx(6)=3.0d0*y(6)*(y(3)**2)*(y(2)+MST*y(4))/F2

C     Cold Positrons (npcn,vpcyn,vpczn,ppcn)

        dydx(7)=(F5/F6)

        dydx(8)=y(7)*N5*(ST*TERM3-CT*y(9))

        dydx(9)=y(7)*N6*y(8)

        dydx(10)=3.0d0*y(10)*(y(7)**2)*(-y(2)-MST*y(8))/F6

C     Hot Positrons (pphn,nphn,vphyn,vphzn)
```

```
        dydx(11)=3.0d0*y(11)*(y(12)**2)*(-y(2)-MST*y(13))/F8

        dydx(12)=F7/F8

        dydx(13)=y(12)*N7*(ST*TERM4-CT*y(14))

        dydx(14)=y(12)*N8*y(13)

C     Hot Electrons (pchn,nchn,vchyn,vchzn)

        dydx(15)=3.0d0*y(15)*(y(16)**2)*(y(2)+MST*y(17))/F4

        dydx(16)=F3*(y(2)+MST*y(17))/F4

        dydx(17)=y(16)*N3*(-ST*TERM2+CT*y(18))

        dydx(18)=-y(16)*N4*y(17)

      END

C*************************************************************************

      SUBROUTINE rk4(y,dydx,n,x,h,yout,derivs)
        IMPLICIT NONE
        INTEGER n,NMAX
        REAL*8 h,x,dydx(n),y(n),yout(n)
        EXTERNAL derivs
        PARAMETER (NMAX=50)
        INTEGER i
        REAL*8 h6,hh,xh,dym(NMAX),yt(NMAX),dyt(NMAX)
        hh=h*0.5d0
        h6=h/6.0d0
        xh=x+hh
        do i=1,n
          yt(i)=y(i)+hh*dydx(i)
      enddo
        call derivs(xh,yt,dyt)
        do i=1,n
           yt(i)=y(i)+hh*dyt(i)
      enddo
        call derivs(xh,yt,dym)
        do i=1,n
          yt(i)=y(i)+h*dym(i)
          dym(i)=dyt(i)+dym(i)
      enddo
        call derivs(x+h,yt,dyt)
        do i=1,n
          yout(i)=y(i)+h6*(dydx(i)+dyt(i)+2.0d0*dym(i))
      enddo
        return
        END
```

```
       PROGRAM SAGDEEV
c      SAGDEEV-NEW.FOR Calculates the Sagdeev Potential for a Relativistic
c      Electron-Positron Plasma
c      IMPLICIT NONE
       EXTERNAL NEWTON
       INTEGER i
       REAL*8 SI,M,M2,C,C2,N1,N2,NPO,F,N11,N21,N3,N4
       REAL*8 D1,D2,D3,DEN,NUM,NE,G,VEO,VPO,VEO2,VPO2
       COMMON/PLASMA/M,M2,C,C2,VEO,VPO,VEO2,VPO2
C      **********PARAMETERS**********
      M=0.05d0
      C=10.0d0
      VEO=0.1D0
      VPO=0.1D0
      M2=M*M
      C2=C*C
      VEO2=VEO*VEO
      VPO2=VPO*VPO
      NE=0.28d0
C
C     ****************************
C
      open(25,file="out.dat")
        do i=1,1280d0
        CALL NEWTON(NE,NPO)
        N11=(VEO/(M))*(NE-2.0d0+VEO/(M))
        N21=(VPO/(M))*(NPO-2.0d0+VPO/(M))
        N1=(1.0d0-NE+N11)/(SQRT(NE*NE-M2*(NE-1+VEO/(M))**2))
        N2=(1.0d0-NPO+N21)/(SQRT(NPO*NPO-M2*(NPO-1+VPO/(M))**2))
        N3=(M*C2*VEO-VEO2*C2)/(SQRT(1.0d0-(VEO2)))
        N4=(M*C2*VPO-VPO2*C2)/(SQRT(1.0d0-(VPO2)))
        D1=1.0d0/NE
        D2=C2*M2*(1.0d0-VEO/(M))**2.0d0
        D3=(NE*NE-M2*(NE-1+VEO/(M))**2)**(3.0D0/2.0D0)
        NUM=2.0d0-NPO-NE-C2*M2*(N1+N2)-N3-N4
        DEN=(D1-(D2/D3))**2.0d0
        SI=NUM/DEN
        write(25,*) NE,SI
        write(6,*) NE,SI
         write(26,*) NE,NPO,F
         NE=0.001d0+NE
        enddo
        endfile(25)
        close(25)
        end

C     TO CALCULATE NPO FOR VARIOUS NE VALUES USING NEWTON_RAPHSON
       SUBROUTINE NEWTON(NE,NPO)
       IMPLICIT NONE
       INTEGER i
       REAL*8 F,G,M,NE
       REAL*8 C2,M2,E,NP1
       REAL*8 F1,F2,F3,G1,G2,G3,A11,A12
       REAL*8 A,A1,A2,A3,NPO,DELTA,C,VEO,VPO,VEO2,VPO2
       COMMON/PLASMA/M,M2,C,C2,VEO,VPO,VEO2,VPO2
C      **********PARAMETERS**********
       NPO=1.0d0
```

```
       E=dexp(1.0d0)
C
C     ****************************
C
      do i=1,50
        A11=(C2-M*C2*VPO)/SQRT(1.0D0-VPO2)
        A12=(C2-M*C2*VEO)/SQRT(1.0D0-VEO2)
        A1=A11+A12-(log(NE))/(log(E))
        A2=C2*(NE-M2*(NE-1.0d0+VEO/(M)))
        A3=SQRT(NE*NE-M2*(NE-1+VEO/(M))**2.0d0)
        A=A1-(A2/A3)
        F1=(log(NPO))/(log(E))
        F2=C2*(NPO-M2*(NPO-1.0d0+VPO/(M)))
        F3=SQRT(NPO*NPO-M2*(NPO-1.0d0+VPO/(M))**2.0d0)
        F=F1+(F2/F3)-A
        G1=SQRT(NPO*NPO-M2*(NPO-1+VPO/(M))**2.0d0)
        G2=(C2*(1.0d0-M2))
        G3=C2*(NPO-M2*(NPO-1.0d0+VPO/(M)))**2.0d0
        G=(1.0d0/NPO)+(G1*G2-(G3/G1))/(G1*G1)
        NP1=NPO -(F/G)
        DELTA=ABS(NP1-NPO)
        IF (DELTA<0.000000000001) goto 10
        NPO=NP1
      Enddo
C     endfile(25)
C     close(25)
10    END
```

```
c     PROGRAM TO DETERMINE THE SOLITON PROFILE FOR A RELATIVISTIC
c     ELECTRON-POSITRON PLASMA
       PROGRAM TEST
       IMPLICIT NONE
       external derivs
       EXTERNAL NEWTON
       external rk4
       INTEGER i,n
       REAL*8 h,x,dydx(1),y(1),yout(1)
       REAL*8 M,C,M2,C2,NE,G,F,NPO,N11,N21,N3,N4
       REAL*8 SI,NUM,DEN,N1,N2,D1,D2,D3,VEO,VPO,VEO2,VPO2
       COMMON/PLASMA/M,M2,C,C2,VEO,VPO,VEO2,VPO2,SI
       h=0.001d0
       n=1
       x=-0.001d0
c     **********PARAMETERS*****
         M=0.02d0
         C=11.0d0
         C2=C*C
         M2=M*M
         VEO=0.10D0
         VPO=0.10D0
         VEO2=VEO*VEO
         VPO2=VPO*VPO
c     ************************

         y(1)=0.8319D0

c     Let's loop here

       open(25,file="sag1.dat")
       open(26,file="sag2.dat")
       write(25,*) x,y(1)
       write(26,*) -1.0d0*x, y(1)
       do i=1,5000D0
       NE=Y(1)
       CALL NEWTON(NE,NPO,F,G)
       N11=(VEO/(M))*(NE-2+VEO/(M))
       N21=(VPO/(M))*(NPO-2+VPO/(M))
       N1=(1.0d0-NE+N11)/(SQRT(NE*NE-M2*(NE-1+VEO/(M))**2))
       N2=(1.0d0-NPO+N21)/(SQRT(NPO*NPO-M2*(NPO-1+VPO/(M))**2))
       N3=(M*C2*VEO-VEO2*C2)/(SQRT(1-(VEO2)))
       N4=(M*C2*VPO-VPO2*C2)/(SQRT(1-(VPO2)))
       D1=1.0d0/NE
       D2=C2*M2*(1.0d0-(VEO/(M)))**2
       D3=(NE*NE-M2*(NE-1+VEO/(M))**2)**(3.0d0/2.0d0)
       NUM=2.0d0-NPO-NE-C2*M2*(N1+N2)-N3-N4
       DEN=(D1-(D2/D3))**2
       SI=NUM/DEN
      call derivs(x,y,dydx)
      call rk4(y,dydx,n,x,h,yout,derivs)
      y(1)=yout(1)
      x=x+h
      write(6,*) x,yout(1)
      write(25,*) x,yout(1)
      write(26,*) -1.0d0*x, yout(1)
```

```
       enddo
       endfile(25)
       endfile(26)
       close(25)
       close(26)
       end
c*******************************************************************************
c
C      SUBROUTINE TO CALCULATE NPO FOR VARIOUS NE VALUES USING NEWTON_RAPHSON
       SUBROUTINE NEWTON(NE,NPO,F,G)
       IMPLICIT NONE
       INTEGER i
       REAL*8 F,G,M,NE,NP,SI
       REAL*8 C2,M2,E,NP1
       REAL*8 F1,F2,F3,G1,G2,G3,g4,G5,A11,A12
       REAL*8 A,A1,A2,A3,NPO,DELTA,C,VEO,VPO,VEO2,VPO2
       COMMON/PLASMA/M,M2,C,C2,VEO,VPO,VEO2,VPO2,SI
C      **********PARAMETERS**********
       NPO=1.0d0
       E=dexp(1.0d0)
C
C     ****************************
C
c        open(25,file="g:\ian\RELWAVES\NEWTON.dat",status="unknown")
        do i=1,50
        A11=(C2-M*C2*VPO)/SQRT(1.0D0-VPO2)
        A12=(C2-M*C2*VEO)/SQRT(1.0D0-VEO2)
        A1=A11+A12-(log(NE))/(log(E))
        A2=C2*(NE-M2*(NE-1.0d0+VEO/(M)))
        A3=SQRT(NE*NE-M2*(NE-1+VEO/(M))**2)
        A=A1-A2/A3
        F1=(log(NPO))/(log(E))
        F2=C2*(NPO-M2*(NPO-1.0d0+VPO/(M)))
        F3=SQRT(NPO*NPO-M2*(NPO-1+VPO/(M))**2)
        F=F1+(F2/F3)-A
        G1=SQRT(NPO*NPO-M2*(NPO-1+VPO/(M))**2)
        G2=(C2*(1.0d0-M2))
        G3=C2*(NPO-M2*(NPO-1+VPO/(M)))**2
        G=(1/NPO)+(G1*G2-(G3/G1))/(G1*G1)
        NP1=NPO-(F/G)
        DELTA=ABS(NP1-NPO)
        IF (DELTA<0.000000000001) goto 10
c       write(25,*)NPO,NP1,F,G
        NPO=NP1
      Enddo
C     endfile(25)
C     close(25)
10    END
c*******************************************************************************
c
       SUBROUTINE derivs(x,y,dydx)
        IMPLICIT NONE
        REAL*8 x,dydx(1),y(1),SI,NPO
        REAL*8 M,C,M2,C2,NUM,DEN,VEO,VPO,VEO2,VPO2
        REAL*8 N1,N2,D1,D2,D3,SAG,NP,NE
        COMMON/PLASMA/M,M2,C,C2,VEO,VPO,VEO2,VPO2,SI
        x=x
```

```
        M2=M**2
        C2=C**2

c************************ Runge-Kutte form ******************
        SAG=-2.0d0*(SI)
        dydx(1)=dsqrt(SAG)
       END
c*************************************************************************
c
      SUBROUTINE rk4(y,dydx,n,x,h,yout,derivs)
        IMPLICIT NONE
        INTEGER n,NMAX
        REAL*8 h,x,dydx(n),y(n),yout(n)
        EXTERNAL derivs
        PARAMETER (NMAX=50)
        INTEGER i
        REAL*8 h6,hh,xh,dym(NMAX),yt(NMAX),dyt(NMAX)
        hh=h*0.5d0
        h6=h/6.0d0
        xh=x+hh
        do i=1,n
          yt(i)=y(i)+hh*dydx(i)
      enddo
        call derivs(xh,yt,dyt)
        do i=1,n
           yt(i)=y(i)+hh*dyt(i)
      enddo
        call derivs(xh,yt,dym)
        do i=1,n
          yt(i)=y(i)+h*dym(i)
          dym(i)=dyt(i)+dym(i)
      enddo
        call derivs(x+h,yt,dyt)
        do i=1,n
            yout(i)=y(i)+h6*(dydx(i)+dyt(i)+2.0d0*dym(i))
      enddo
        return
        END
```

References

- Abdelsalm U M, Moslem W M and Shukla P K 2008 *'Ion-acoustic solitary waves in a dense pair-ion plasma containing degenerate electrons and positrons'*, *Phys. Lett. A* **372**, *4057*

- Alkofer R, Hecht M B, Roberts C D, Schmidt S M, Vinnik D V 2001 *'Pair Creation and an X-Ray Free Electron Laser'*, *Phys. Rev. Lett.* **87**, *193902*

- Andre M, Koskinen H, Gustafsson G and Lundin R 1987 *'Ion waves and upgoing ion beams observed by the Viking satellite'*, *Geophys. Res. Lett.* **14**, *463*

- Ashour-Abdalla M and Okuda H 1986a *'Theory and simulations of broadband electrostatic noise in the geomagnetic tail'*, *J. Geophys. Res.* **91**, *6833*

- Bale S D, Kellogg, Larson D E, Lin R P, Goetz K and Leppng R P 1998 *'Bipolar electrostatic structures in the transition region: Evidence of electron phase space holes'*, *Geophys. Res. Lett.* **25**, *2929*

- Beskin V S, Gurevich A V and Istomin Ya. N 1983 *'Electrodynamics of pulsar magnetospheres'*, *Soviet Phys. JETP* **58**, *235*

- Beskin V S, Gurevich A V and Istomin Ya. N 1993 *'Physics of the Pulsar Magnetosphere'*, (Cambridge University Press, Cambridge), 96

- Bhattacharyya R, Janaki M S, Dasgupta B 2003 *'Relaxation in electron-positron plasma: a possibility'*, *Physics letters A* **315**, *120*

- Bharuthram R 1992 *'Arbitrary Amplitude Double Layers in a Multi-Species Electron-Positron Plasma'*, *Astrophys. Space Sci.* **189**, *213*

- Bharuthram R and Pather T 1996 *'The kinetic dust-acoustic instability in a magnetized dusty plasma'*, *Planet. Space Sci.* **44**, *137*

- Bharuthram R, Reddy R V, Lakhina G S, and Singh N 2002 *'Low Frequency Nonlinear Waves in the Auroral Plasma'*, *Physica Scripta* **98**, *137*

- Bharuthram R and Shukla P K 1988 *'Nonlinear Properties of Electron Acoustic Wave Turbulence in the Geomagnetic Tail'*, *Astrophys. Space Sci.* **149**, *127*

- Bharuthram R and Yu M Y 1993 *'Relativistic Electron Plasma Waves'*, *Astrophys. Space Sci.* **207**, *197*

- Boehmer H 1994 *'Formation of electron-positron plasmas in the laboratory'*, edited by Ottewitte E and Weiss A, AIP Conf. Proc. No 303 (AIP, New York), p.422

- Bounds S R, Pfaff R F, Knowlton S F, Mozer F S, Temerin M A, Kletzing C A 1999 *'Solitary potential structures associated with ion and electron beams near 1 R_E altitude'*, *J. Geophys. Res.* **104**, *28709*

- Cattell C A, Neiman C, Dombeck J, Crumley J, Wygant J R, Kletzing C A, Peterson W K, Mozer F S and Andre M 2003 *'Large amplitude solitary waves in and near the Earth's magnetosphere, magnetopause and bow shock: Polar and Cluster observations'*, *Nonlinear Proc. Geophys.* **10**, *13*

- Cattell C A, Crumley J, Dombeck J, Wygant J R and Mozer F S 2002 *'Polar observations of solitary waves at the Earth's magnetopause'*, *Geophys. Res. Lett.* **29**, *2001GL01400469-1*

- Cattell C A, Dombeck J, Wygant J R, Hudson M K, Mozer F S, Temerin M A, Peterson W K, Kletzing C A, Russell C T and Pfaff R F 1999 *'Comparisons of Polar satellite observations of solitary wave velocities in the plasma sheet boundary and the high altitude cusp to those in the auroral zone'*, *Geophys. Res. Lett.* **26**, *425*

- Cattell C A, Crumley J, Dombeck J, Lysak R, Kletzing C, Peterson W K and Collin H 2001b *'Polar Observations of Solitary Waves At High And Low Altitudes And Comparison To Theory'*, *Adv. Space Res.* **28**, *1631*

- Choi C R, Ryu C M, Lee N C and Lee D Y 2005 *'Ion acoustic solitary waves in a dusty plasma obliquely propagating to an external magnetic field'*, *Phys. Plasmas* **12**, *022304*

- Deng X H, Tang R X, Matsumoto H, Pickett J S, Fazakerley A N, Kojima H, Baumjohann W, Coates A, Nakamura R, Gurnett D A and

Liu Z X 2006 *'Observations of electrostatic solitary waves associated with reconnection by GEOTAIL and CLUSTER'*, *Adv. Space Res.* **37**, *1373*

- Eichler D, Livio M, Piran T and Schramm D N 1989 *'Nucleosynthesis, Neutrino bursts, and Gamma-Rays from Coalescing Neutron Stars'*, *Nature* **340**, *126*

- Ergun R E, Carlson C W, McFadden J P, Mozer F S, Delroy, G T, Peria W, Chaston, C C, Temerin M, Elphic R, Strangeway R, Pfaff R, Cattell C A, Klumpar D, Shelley E, Peterson W, Moebius E, and Kistler L 1998 *'FAST satellite observations of large-amplitude solitary wave structures'*, *Geophys. Res. Lett.* **25**, *2041*

- Esfandyari-Kalejahi A, Kourakis I and Shukla P K 2006 *'Oblique modulation of electrostatic modes and envelope excitations in pair-ion and electron-positron plasmas'*, *Phys. Plasmas* **13**, *122310*

- Farid T, Mamun A A, Shukla P K and Mirza A M 2001 *'Nonlinear electrostatic waves in a magnetized dust-ion plasma'*, *Phys. Plasmas* **8**, *1529*

- Fishman G J, Paciesas W S, Meegan C A and Wilson R B 1986 *'Observation of a strong gamma-ray burst on the spacelab 2 mission'*, *Adv. Space Res.* **6**, *23*

- Fonseca R A, Silva L O, Tonge J W, Mori W B and Dawson J M 2003

'Three-dimensional Weibel instability in astrophysical scenarios', *Phys. Plasmas* **10**, *1979*

- Franz J R, Kintner P M and Pichett J S 1998 *'POLAR Observations of Coherent Electric Field Structures'*, *Geophys. Res. Lett.* **25**, *1277*

- Fried B D and Conte S D 1961 *'The Plasma Dispersion Function'*, Academic Press, New York

- Gary S P and Sanderson J J 1970 *'Longitudinal waves in a perpendicular collisionless plasma shock'*, *J. Plasma Phys.* **4**, *739*

- Gary S P and Tokar R L 1985 *'The electron acoustic Mode'*, *Phys. Fluids* **28**, *2439*

- Gedalin M E, Lominadze J G, Stenflo L, Tsytovich V N 1985 *'Nonlinear Wave Conversion in Electron-Positron Plasmas'*, *Astrophys. Space Sci.* **108**, *393*

- Ghosh S S and Lakhina G S 2004 *'Anomalous width variation of rarefactive ion acoustic solitary waves in the context of auroral plasmas'*, *Nonlinear Proc. Geophys.* **11**, *219*

- Gill T S, Singh A, Kaur H, Saini N S and Bala P 2007 *'Ion-acoustic solitons in weakly relativistic plasma containing electron-positron and ion'*, *Phys. Lett. A* **361**, *364*

- Goldreich P and Julian W H 1969 *'Pulsar Electrodynamics'*, *ApJ* **157, 869**

- Goodman J 1986 *'Are gamma-ray bursts optically thick?'*, *ApJ* **308**, *L47*

- Grabbe C L and Eastman T E 1984 *'Generation of broadband electrostatic noise by ion-beam instabilities in the magnetotail'*, *J. Geophys. Res.* **89**, *3865 and 3977*

- Grabbe C L 1985 *'New results on the generation of broadband electrostatic waves in the magnetotail'*, *Geophys. Res. Lett.* **12**, *483*

- Greaves R G, Tinkle M D, Surko C M 1994 *'Creation and uses of positron plasmas'*, *Phys. Plasmas* **1**, *1439*

- Greaves R G and Surko C M 1995 *'An Electron-Positron Beam-Plasma Experiment'*, *Phys. Rev. Lett.* **75**, *3846*

- Greenstadt E W and Fredricks R W 1979 *'Shock systems in collisionless space plasmas'*, *Solar System Plasma Physics*, ed. by Lanzerotti L J, Kennel C F and Parker E N, 3, North-Holland, Amsterdam **3**

- Gurevich A V and Istomin Ya N 1985 *''*, *Soviet Phys. JETP* **62**, *1*

- Hartman R C *et al.* 2001 'Day-Scale Variability of 3C 279 and Searches for Correlations in Gamma-Ray, X-Ray, and Optical Bands', *ApJ* **558**, *583*

- Henri G, Pelletier G and Roland J 1993 *'Gamma-ray emission of active galactic nuclei as a signature of relativistic electron-positron beams'*, *ApJ* **404**, *L41*

- Hurley K, Cline T, Frontera F, Dal Fiume D, Orlandini M, Costa E, Piro L and Feroci M 1998 *'Ulysses/BeppoSAX Observations of Cosmic Gamma-Ray Bursts'*, *Nuc. Phys. B (Proc. Suppl.)* **69/1-3**, *660*

- Huba J D, Gladd N T and Papadopoulos K, 1978 *'Lower-hybrid-drift wave turbulence in the distant magnetotail'*, *J. Geophys. Res.* **83**, *5217*

- Iwamoto N 1993 *'Collective modes in nonrelativistic electron-positron plasmas'*, *Phys. Rev. E* **47**, *604*

- Klebesadel R W, Strong I B and Olson R A 1973 *'Observations of Gamma-Ray Bursts of Cosmic Origin'*, *ApJ* **182**, *L85*

- Kojima H, Ohtsuka K, Matsumoto H,Omura Y, Anderson R R, Saito Y, Mukai T, Kokubun S and Yamamoto T 1999 *'Plasma Waves in Slow-Mode Shocks Observed by GEOTAIL Spacescraft'*, *Adv. Space Res.* **24**, *51*

- Kojima H, Matsumoto H, Miyatake T, Nagano I, Fujita A, Frank L A, Mukai T, Paterson W R, Saito Y, Machida S and Anderson R R, 1994 *'Relation between electrostatic solitary waves and hot plasma flow in the plasma sheet boundary layer: GEOTAIL Observations'*, *Geophys. Res. Lett.* **21**, *2919*

- Kourakis I, Esfandyari-Kalejahi A, Mehdipoor M and Shukla P K 2006 *'Modulated electrostatic modes in pair plasmas: Modulational stability profile and envelope excitations'*, *Phys. Plasmas* **13**, *052117*

- Lakhina G S and Verheest F 1997 *'Alfvénic Solitons in Ultrarelativistic Electron-Positron Plasmas'*, *Astrophys. Space Sci.* **253**, *97*

- Lattimer J M and Schramm D N 1976 *'The tidal disruption of neutron stars by black holes in close binaries'*, *ApJ* **210**, *549*

- Lazarus I J, Bharuthram R, Hellberg M A 2008 *'Modified Korteweg-de Vries-Zakharov-Kuznetsov solitons in symmetric two-temperature electron-positron plasmas'*, *J. Plasma Physics* **74**, *519*

- Lee L C and Kan J R 1981 *'Nonlinear ion-acoustic waves and solitons in a magnetized plasma'*, *Phys. Fluids* **24**, *430*

- Liang E P, Wilks S C, Tabak M 1998 *'Pair Production by Ultraintense Lasers'*, *Phys. Rev. Lett.* **81**, *4887*

- Lominadze J G, Machabeli G Z and Usov V V 1983 *'Theory of NP 0532 pulsar radiation and the nature of the activity of the Crab Nebula'*, *Astrophys. Space Sci.* **90**, *19*

- Lontano M, Bulanov S and Koga J 2001 *'One-dimensional electromagnetic solitons in a hot electron-positron plasma'*, *Phys. Plasmas* **8**, *5113*

- Mace R L and Hellberg M A 1993 *'Electron-acoustic and cyclotron-sound instabilities driven by field-aligned hot-electron streaming'*, *J. Geophys. Res.* **98**, *5881*

- MacFadyen A I and Woosley S E 1999 *'Collapsars - Gamma-Ray Bursts and Explosions in "Failed Supernovae"'*, *ApJ* **524**, *262*

- Machabeli G Z, Osmanov Z N and Mahajan S M 2005 *'Parametric mechanism of the rotation energy pumping by a relativistic plasma'*, *Phys. Plasmas* **12**, *062901*

- Mahmood S, Mustaq A and Saleem H 2003 *'Ion acoustic solitary wave in homogeneous magnetized electron-positron-ion plasmas'*, *New J. Phys.* **5**, *28*

- Mangeney A, Salem C, Lacombe C, Bougeret J L, Perche C, Manning R, Kellogg P J, Goetz K, Monson S J, Bosqued J M 1999 *'WIND observations of coherent electrostatic waves in the solar wind'*, *Ann. Geophysicae* **17**, *307*

- Marklund M and Shukla P K 2006 *'Nonlinear collective effects in photon-photon and photon-plasma interactions'*, *Rev. Mod. Phys.* **78**, *591*

- Matsumoto H, Kojima H, Miyatake T, Omura Y, Okada M, Nagano I, and Tsutsui M 1994 *'Electrostatic Solitary Waves (ESW) in the magnetotail: BEN wave forms observed by GEOTAIL*, *Geophys. Res. Lett.* **21**, *2915*

- Matsumoto H, Kojima H, Kasaba Y, Miyake T, Anderson R R and Mukai T 1997 *'Plasma Waves in the Upstream and Bow Shock Regions Observed by GEOTAIL'*, *Adv. Space Res.* **20**, *683*

- Matsumoto H, Frank L A, Omura Y, Kojima H, Paterson W R, Tsutsui M, Anderson R R, Horiyama S, Kokubun S and Yamamoto T 1999 *'Generation mechanism of ESW based on GEOTAIL plasma wave observation, plasma observation and particle simulation'*, *Geophys. Res. Lett.* **26**, *421*

- Matsukiyo S and Hada T 2003 *'Parametric instabilities of circularly polarized Alfvén waves in a relativistic electron-positron plasma'*, *Phys. Rev. E* **67**, *046406*

- Metzger M R, Djorgovski S G, Kulkarni S R, Steidel C C , Adelberger K L, Frail D A, Costa E and Frontera F 1997 *'Spectral constraints on the redshift of the optical conterpart to the γ-ray burst of 8 May 1997'*, *Nature* **387**, *878*

- Michel F C 1982 *'Theory of pulsar magnetospheres'*, *Rev. Mod. Phys.* **54**, *1*

- Miller H R and Witta P J 1987 *'Active Galactic Nuclei'* (Springer-Verlag, Berlin), p.202

- Misra A P and Chowdhury A R 2003 *'Nonlinear interaction of electromagnetic pulses with an electron-positron plasma-a coupled NLS equation'*, *Chaos, Solitons and Fractals* **15**, *801*

- Mofiz U A, de Angelis U and Forlani A 1985 *'Solitons in weakly nonlinear electron-positron plasmas and pulsar microstructure'*, *Phys. Rev. A* **31**, *951*

- Moolla S, Bharuthram R, Singh S V and Lakhina G S 2003 *'Nonlinear high-frequency waves in the magnetosphere'*, *Pramana J.Phys.* **61**, *1209*

- Moolla S, Bharuthram R, Singh S V, Lakhina G S and Reddy R V 2007 *'An Explanation for high-frequency broadband electrostatic noise in the Earth's magnetosphere'*, *J. Geophys. Res.* **112**, *A07214*

- Mozer F S, Ergun R, Temerin M, Cattell C A, Dombeck J, and Wygant J R 1997 *'New Features of Time Domain Electric-Field Structures in the Auroral Acceleration Region'*, *Phys. Rev. Lett* **79**, *1281*

- Nicholson D R 1983 *'Introduction to Plasma Theory'* (John Wiley, USA), p.173

- Nishikawa K I, Hardee P E, Hededal C B and Fishman G J 2006 *'ACCELERATION MECHANICS IN RELATIVISTIC SHOCKS BY THE WEIBEL INSTABILITY'*, *ApJ* **642**, *1267*

- Omidi N 1985 *'Broadband electrostatic noise produced by ion beams in the earth's magnetotail'*, *J. Geophys. Res.* **90**, *12330*

- Omura Y, Kojima H and Matsumoto H 1994 *'Computer simulation of Electrostatic Solitary Waves: A nonlinear model of broadband electrostatic noise'*, *Geophys. Res. Lett.* **21**, *2923*

- Oohara W, Date D, Hatakeyama R 2005 *'Electrostatic Waves in a Paired Fullerene-Ion Plasma'*, *Phys. Rev. Lett.* **95**, *175003*

- Paczyński B 1986 *'Gamma-ray bursters at cosmological distances'*, *ApJ.* **308**, *L43*

- van Paradijs J 1998 *'Optical Afterglows of Gamma-Ray Bursts'*, *Nuc. Phys. B (Proc. Suppl.)* **69/1-3**, *668*

- Paul W 1990 *'Electromagnetic traps for charged and neutral particles'*, *Rev. Mod. Phys.* **62**, *531*

- Pillay R and Bharuthram R 1992 *'Large Amplitude Solitons in a Multi-Species Electron-Positron Plasma'*, *Astrophys. Space Sci.* **198**, *85-93*

- Piran T 2005 *'The physics of gamma-ray bursts'*, *Rev. Mod. Phys.* **76**, *1143*

- Piran T 1999 *'Gamma-Ray Bursts and the Fireball Model'*, *Physics Reports* **314**, *575*

- Popel S I, Vladimirov S V, Shukla P K, 1995 *'Ion-acoustic solitons in electron-positron-ion plasmas'Phys. Plasmas* **2**, *716*

- Press W H, Teukolsky S A, Vetterling W T and Flannery B P, 1996 Numerical Receipes *in Fortran 90 - 'The Art of Parallel Scientific Computing'* **2**, *702-704, 731, 740, 1297, 1308*

- Reddy R V, Lakhina G S, Singh N, and Bharuthram R 2002 *'Spiky parallel electrostatic ion cyclotron and ion acoustic waves'*, *Nonlinear Proc. Geophys.* **9**, *25*

- Reddy R V, Singh S V, Lakhina G S and Bharuthram R 2005 *'Electrostatic Ion Cyclotron and Ion Acoustic waves in Auroral Plasma'*, *Proceedings of ISSS* **7**, *26*

- Reddy R V, Singh S V, Lakhina G S and Bharuthram R 2006 *'Parallel electric field structures associated with the low-frequency oscillations in the auroral plasma'*, *Earth Planets Space* **58**, *1227*

- Rees M J 1983 *'The Very Early Universe'*, edited by Gibbons G W, Hawking S W and Siklas S (Cambridge University Press, Cambridge)

- Remington B A 2005 *'High energy density laboratory astrophysics'*, *Plasma Phys. Controlled Fusion* **47**, *A191*

- Ringwald A 2001 *'Pair Production from Vacuum at the Focus of an X-Ray Free Electron Laser'*, *Phys. Lett. B* **510**, *107*

- Roberts C D, Schmidt S M, Vinnik D V 2002 *'Quantum Effects with an X-Ray Free-Electron Laser'*, *Phys. Rev. Lett.* **89**, *153901*

- Rosenberg M 1993 *'Ion- and dust-acoustic instabilities in dusty plasmas'*, *Planet. Space Sci.* **41**, *229*

- Ruderman M A and Sutherland P G 1975 *'Theory of pulsars: polar gaps, sparks, and coherent microwave radiation'*, *ApJ* **196**, *51*

- Sakurai K *'Solar-Flare Particles'* edited by Oda M, Nishimura J and Sakarai K, pp. 271 (Terra Scientific Publishing Company (TERRAPUB), Tokoyo, 1988

- Share G H and Murphy R J '*in Stars as Suns: Activity, Evolution and Planets*', ASP Conf. Series 219, ed. Benz A and Dupree A, 133 (2004); Share G H, Murphy R J, Smith D M, Schwartz R A and Lin R P (2004), *ApJ* **615**, *L169*

- Scarf F L, Fredricks R W, Frank L A, Russel C T, Coleman P J, Jr. and Neugebauer M 1970 *'Dircet correlation of large amplitude waves with suprathermal protons in the upstream solar wind'*, *J. Geophys. Res.* **75**, *7316*

- Schriver D and Ashour-Abdalla M 1987 *'Generation of high-frequency broadband electrostatic noise: The role of cold electrons'*, *J. Geophys. Res.* **92**, *5807*

- Schriver D and Ashour-Abdalla M 1989 *'Broadband electrostatic noise due to field-aligned currents'*, *Geophys. Res. Lett.* **16**, *899*

- Shukla P K and Yu M Y 1978 *'Exact solitary ion acoustic waves in a magnetoplasma'*, *J. Math. Phys.* **19**, *2506*

- Shukla N and Shukla P K 2007 *'A new purely growing instability in a strongly magnetized nonuniform pair plasma'*, *Phys. Lett. A* **367**, *120*

- Singh S V and Lakhina G S 2001 *'Generation of electron-acoustic waves in the magnetosphere'*, *Planetary and Space Science* **49**, *107*

- Stewart G A and Laing E W 1992 *'Wave propagation in equal-mass plasmas'*, *J. Plasma Phys.* **47**, *295*

- Sturrock P A 1971 *'A Model of Pulsars'*, *ApJ* **164**, *529*

- Szpigel S, Durães F O and Steffens F M 2007 'Contribution from drell-Yan Processes to the Emission Spectrum in Solar Flares', *Brazilian J. Phys.* **37**, *52*

- Stenflo L, Shukla P K and Yu M Y 1985 *'Nonlinear Propagation of Electromagnetic Waves in Magnetized Electron-Positron Plasmas'*, *Astrophys. Space Sci.* **117**, *303*

- Tagare S G, Singh S V, Reddy R V and Lakhina G S 2004 *'Electron acoustic solitons in the Earth's magnetotail'*, *Nonlinear Proc. Geophys.* **11**, *215*

- Tandberg E H and Emslie A G 1988 *'The Physics of Solar Flares'* (Cambridge University Press, Cambridge), p.124

- Temerin M A, Cerny K, Lotko W and Mozer F S 1982 *'Observations of double layers and solitary waves in the auroral plasma'*, *Phys. Rev. Lett.* **48**, *1175*

- Temerin M, Woldorff M and Mozer F S 1979 *'Nonlinear Steepening of the Electrostatic Ion Cyclotron Wave'*, *Phys. Rev. Lett.* **43**, *1941*

- Tsurutani B T, Arballo J K, Lakhina G S, Ho C M, Buti B, Pickett J S and Gurnett D A 1998 *'Plasma Waves in the Dayside Polar Cap Boundary Layer: Bipolar and Monopolar Electric Pulses and Wistler Mode Waves'*, *Geophys. Res. Lett.* **25**, *4117*

- Verheest F, Hellberg M A, Gray G J and Mace R L 1996 *'Electrostatic Solitons in Multispecies Electron-Positron Plasmas'*, *Astrophys. Space Sci.* **239**, *125*

- Verheest F and Lakhina G S 1996 *'Oblique Solitary Alfvén Modes in Relativistic Electron-Positron Plasmas'*, *Astrophys. Space Sci.* **240**, *215*

- Verheest F, Mace R L, Pillay S R, Hellberg M A, 2002 *'Unified derivation of Korteweg-de Vries-Zakharov-Kuznetsov equations in multispecies plasmas'*, *J.Phys.A:Math. Gen.* **35**, *795*

- Wilks S C, Chen H, Liang E, Patel P, Price D, Remington B, Shepherd R, Tabak M and Kruer W L 2005 *'Electron-Positron Plasmas Created by Ultra-Intense Laser Pulses Interacting with Solid Targets'*, *Astrophys. Space Sci.* **298**, *347*

- Yu M Y, Shukla P K and Rao N N 1984 *'Strong Electromagmetic Waves in a Magnetized Relativistic Electron-Positron Plasma'*, *Astrophys. Space Sci.* **107**, *327*

- Yu M Y, Shukla P K and Stenflo L 1986 *'Alfven Vortices in a Strongly Magnetized Electron-Positron Plasma'*, *ApJ* **309**, *L63*

- Watson G A 1944 *'Treatise on the Theory of Bessel Functions'*, Cambridge Press, 2nd Edition

- Woosley S E 1993 *'Gamma-ray bursts from stellar mass accretion disks around black holes'*, *ApJ* **405**, *273*

- Woosley S E and Zhang W 2004 *'The Collapsar Model, Supernovae, and X-Ray Flashes'*, *Third Rome Workshop on Gamma-Ray Bursts in the Afterglow Era, ASP Conference Series* **312**, *273*

- Zank G P and Greaves R G 1995 *'Linear and nonlinear modes in non-relativistic electron-positron plasmas'*, *Phys. Rev. E* **51**, *6079*